

'The next time I teach a topic course in chaos (which I seem to do every year, at student request), I am going to use this book as the primary text. I like the idea of using the study of one application (the pendulum) to present as many topics and processes as appropriate; other applications and their models can be related to that problem. And, of course, having all the computer programs to do the graphics for experiments and exercises is very helpful.'

David C. Arney, *The UMAP Journal*

The previous edition of this text was the first to provide a quantitative introduction to chaos and nonlinear dynamics at undergraduate level. It was widely praised for the clarity of the writing and for the unique and effective way in which the authors presented the basic ideas. These same qualities characterize this revised and expanded second edition.

Interest in chaotic dynamics has grown explosively in recent years. Applications to practically every scientific field have had far-reaching impact. As in the first edition, the authors present all the main features of chaotic dynamics using the damped, driven pendulum as the primary model. A special feature is the inclusion of both analytic and computer exercises with which the reader may expand upon the many numerical simulations included in the book. This allows learning through participation, without the extensive scientific background demanded by more advanced books.

This second edition includes additional material on the analysis and characterization of chaotic data, and applications of chaos. Experimental data from a chaotic pendulum are analyzed using methods of nonlinear time series analysis. With the help of new computer programs provided in the book (and also available from one of the authors on an optional diskette), readers and students can learn about these methods and use them to characterize their own data. The second edition also explains methods for short-term prediction and control. Spatio-temporal chaos is now introduced with examples from fluid dynamics, crystal growth, and other areas. The number of references has more than doubled; solutions are included to selected exercises.

This new edition of *Chaotic dynamics* can be used as a text for a unit on chaos for physics and engineering students at the second- and third-year level. Such a unit would fit very well into modern physics and classical mechanics courses.

Baker/Gollub

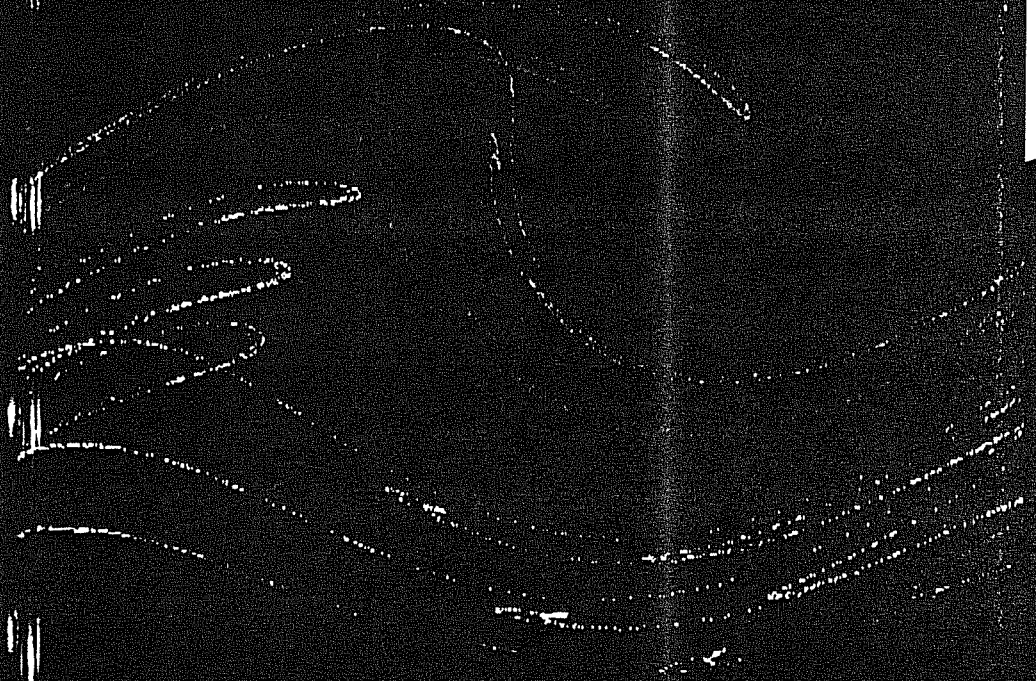
*Chaotic Dynamics*

CAMBRIDGE

# *Chaotic Dynamics*

SECOND EDITION

an introduction



G. L. Baker and J. P. Gollub

ISBN 0-521-47685-2



9 780521 476850

CAMBRIDGE  
UNIVERSITY PRESS

---

# Contents

---

Published by the Press Syndicate of the University of Cambridge  
The Pitt Building, Trumpington Street, Cambridge CB2 1RP  
40 West 20th Street, New York, NY 10011-4211, USA  
10 Stamford Road, Oakleigh, Melbourne 3166, Australia

© Cambridge University Press 1990, 1996

First published 1990  
Reprinted 1990 (with corrections), 1991 (twice), 1992, 1994  
Second edition 1996

Printed in the United States of America

A catalogue record for this book is available from the British Library

Library of Congress cataloguing in publication data

Baker, Gregory L.  
Chaotic dynamics: an introduction / Gregory L. Baker and Jerry P. Gollub.  
— 2nd ed.  
p. cm.  
ISBN 0-521-47106-0. —ISBN 0-521-47685-2 (pbk.)  
I. Pendulum. 2. Chaotic behavior in systems. I. Gollub, J. P., 1944— .  
II. Title.  
QA862.P4B35 1996  
003'.85—dc20 95-9059 CIP.

ISBN 0 521 47106 0 hardback  
ISBN 0 521 47685 2 paperback

	<i>page</i>
<i>Preface</i>	xi
<i>Acknowledgments</i>	xiv
<b>CHAPTER ONE</b> <b>Introduction</b>	1
<b>CHAPTER TWO</b> <b>Some helpful tools</b>	7
2.1 Phase space	7
2.2 Poincaré section	21
2.3 Spectral analysis of time series	27
Problems	35
<b>CHAPTER THREE</b> <b>Visualization of the pendulum's dynamics</b>	39
3.1 Sensitivity to initial conditions	41
3.2 Phase diagrams and Poincaré sections	43
3.3 Time series and power spectra	59
3.4 Basins of attraction	59
3.5 Bifurcation diagrams	66
Problems and simulations	72
<b>CHAPTER FOUR</b> <b>Toward an understanding of chaos</b>	74
4.1 The logistic map	76
4.1.1 Period doubling	77
4.1.2 The periodic windows	81
4.1.3 Lyapunov exponents	84
4.1.4 Entropy	86
4.1.5 Stretching and folding	88
4.2 The circle map	89
4.3 The horseshoe map	96

4.4 Application to the pendulum	100
Problems	105
<b>CHAPTER FIVE The characterization of chaotic attractors</b>	109
5.1 Dimension	110
5.2 Lyapunov exponents	119
5.3 Lyapunov exponents and dimension	123
5.4 Information change and Lyapunov exponents	126
Problems	129
<b>CHAPTER SIX Experimental characterization, prediction, and modification of chaotic states</b>	133
6.1 Characterization of chaotic states	133
6.1.1 Experiment and simulation	135
6.1.2 Reconstruction of the attractor	137
6.1.3 Time-delay coordinates	139
6.1.4 Choosing the time delay	143
6.1.5 Embedding dimension and attractor dimension	145
6.1.6 Lyapunov exponents	150
6.1.7 Summary	152
6.2 Prediction of chaotic states	152
6.2.1 Method of analogues	153
6.2.2 Linear approximation method	156
6.3 Modification of chaotic states	159
6.4 Conclusion	163
Problems	164
<b>CHAPTER SEVEN Chaos broadly applied</b>	166
7.1 Chaos in lasers	166
7.2 Chaotic chemical reactions	168
7.3 Chaos in fluid dynamics	170
7.4 Spatio-temporal chaos in fluids	172
7.4.1 Spatio-temporal chaos in thermal convection	173
7.4.2 Spatio-temporal chaos on a rotating fluid film	176
7.5 Spatio-temporal intermittency in model equations	178
7.6 Strong turbulence	179
7.7 Chaotic mixing in fluids	180
7.8 Complex dynamics of interfacial growth: artificial snowflakes	181
7.9 Chaos in earthquake dynamics	184
7.10 Chaos and quantum physics	185

7.11 Foundations of statistical mechanics	187
7.12 Conclusion	189
<i>Further reading</i>	190
<i>Appendix A Numerical integration – Runge–Kutta method</i>	193
<i>Appendix B Computer program listings</i>	196
<i>Appendix C Solutions to selected problems</i>	242
<i>References</i>	246
<i>Index</i>	253
<i>Diskette order information</i>	256

---

# Preface

---

The remarkable fact that determinism does not imply either regular behavior or predictability has had a major impact on many fields of science, engineering, and mathematics. The discovery of chaos changes our understanding of the foundations of physics, and has many practical applications as well. This subject sheds new light on the workings of lasers, fluids, mechanical structures, chemical reactions, earthquakes, neural networks, and biological rhythms.

Interest in chaos (or more generally, nonlinear dynamics) grew rapidly after 1963, when Lorenz published his numerical work on a simplified model of convection and discussed its implications for weather prediction. The research literature has exploded, and many books on chaotic dynamics have appeared. The first edition of this book was the first work aimed at a level at once more accessible than graduate texts, and yet more suitable for nonspecialists, including undergraduates in science, than various popular books on chaos. It has been used by scientists and students wishing to have a true introduction, and as a text or text supplement for courses in mathematics, physics, and engineering. These include short courses on chaos, classical mechanics, or modern physics. Some of the material can be included in an introductory course in physics, engineering, or differential equations.

*Chaotic dynamics: an introduction* introduces chaotic dynamics through the study of the driven pendulum, a simple system whose nonlinear properties are often ignored in teaching mathematics and physics. It is written at a level accessible to sophomore/junior level undergraduate students of mathematics or physics. It has been found to be quite readable for secondary and college teachers, or anyone with a few

courses in college mathematics and physics. Unlike various popularizations, this work is intended to help the reader develop a deep understanding of chaotic dynamics and to provide the experience and pleasure of participation through analytic and computer exercises. The following background is assumed: elementary multivariable calculus, linear differential equations, and introductory physics. We have included a heuristic treatment of Fourier analysis. Since many of the exercises are numerical, some programming experience is desirable.

This *second edition* is significantly expanded to take advantage of recent developments.

We have included a new chapter (Chapter 6) in which we introduce methods of characterizing experimental data and testing it for chaotic behavior. For this purpose we employ data from a chaotic pendulum provided by J.A. Blackburn. A careful comparison of experimental and numerical data is an important feature of this chapter. We then go on to describe methods of making short-term prediction for chaotic systems, and again test these ideas on the same experimental data. The chapter concludes with an introductory treatment of methods for modifying and controlling chaotic states.

Chapter 7, 'Chaos broadly applied', contains considerable new material. Recognizing that chaotic systems often involve spatially varying fields, we consider several examples of spatio-temporal chaos, which often involves many degrees of freedom. Other new applications include chaotic mixing and earthquake dynamics.

Throughout the book, we have made many smaller additions and corrections, often at the suggestion of readers. Some problems have been added, along with listings of new programs for data analysis. The number of references has been doubled.

A menu-driven runtime software package, called CHAOS II, is available at modest cost. Hardware requirements and information for ordering the software are given at the end of the book. Several new programs have been added to the original version, along with a file containing the experimental data used as an example in the text.

Since this book is not a research review, but rather a focused introduction to the basic phenomena, we have emphasized accessibility rather than completeness. For example, Hamiltonian dynamical systems are generally beyond the level of this book, though they are important in many fields. In selecting citations and references, we have included those that we judged to provide useful additional information, but these are

not exhaustive and cannot provide a balanced assessment of the scholarship of the many scientists and mathematicians who have contributed to the subject.

Gregory L. Baker  
Bryn Athyn, Pennsylvania

Jerry P. Gollub  
Haverford, Pennsylvania

# Acknowledgments

Many people provided important ideas and help with this second edition. We especially appreciate the experimental (not numerical!) data provided by James Blackburn from his elegant driven pendulum. We are also indebted to the following colleagues for helpful discussions: Al Albano, Reggie Brown, Charles Ebert, Eric Kostelich, Justin Odhner, Roger Rollins, Ira Schwartz, Herschel Snodgrass, John Starrett, Steve Strogatz, Harry Swinney, and James Yorke.

We wish to thank James Blackburn for permission to publish the pendulum diagram in Figure 6.2, Harry Swinney for permission to reprint the phase portrait shown in Figure 7.2, John Wiley and Sons for permission to reprint the phase portrait in Figure 7.5, Guenter Ahlers for permission to reprint the patterns in Figure 7.6 and Julio Ottino for permission to reprint the mixing diagrams in Figure 7.9. GLB thanks Nancy Mitzen for library assistance, and the Research Committee of the College of the Academy of the New Church for financial support. JPG acknowledges the financial support of the National Science Foundation programs in condensed matter physics and fluid dynamics.

Finally, we would like to thank our wives, Margaret Baker and Diane Nissen, for their understanding and support.

# Introduction

The irregular and unpredictable time evolution of many nonlinear systems has been dubbed ‘chaos.’ It occurs in mechanical oscillators such as pendula or vibrating objects, in rotating or heated fluids, in laser cavities, and in some chemical reactions. Its central characteristic is that the system does not repeat its past behavior (even approximately). Periodic and chaotic behavior are contrasted in Figure 1.1. Yet, despite their lack of regularity, chaotic dynamical systems follow deterministic equations such as those derived from Newton’s second law.

The unique character of chaotic dynamics may be seen most clearly by imagining the system to be started twice, but from slightly different initial conditions. We can think of this small initial difference as resulting from measurement error, for example. For nonchaotic systems this uncertainty leads only to an error in prediction that grows *linearly* with time. For chaotic systems, on the other hand, the error grows *exponentially* in time, so that the state of the system is essentially unknown after a very short time. This phenomenon, which occurs only when the governing equations are nonlinear, is known as *sensitivity to initial conditions*. Henri Poincaré (1854–1912), a prominent mathematician and theoretical astronomer who studied dynamical systems, was the first to recognize this phenomenon. He described it as follows: ‘...it may happen that small differences in the initial conditions produce very great ones in the final phenomena. A small error in the former will produce an enormous error in the latter. Prediction becomes impossible, and we have the fortuitous phenomenon’ (Poincaré, 1913).

If prediction becomes impossible, it is evident that a chaotic system can resemble a stochastic system (a system subject to random external forces). However, the source of the irregularity is quite different. For

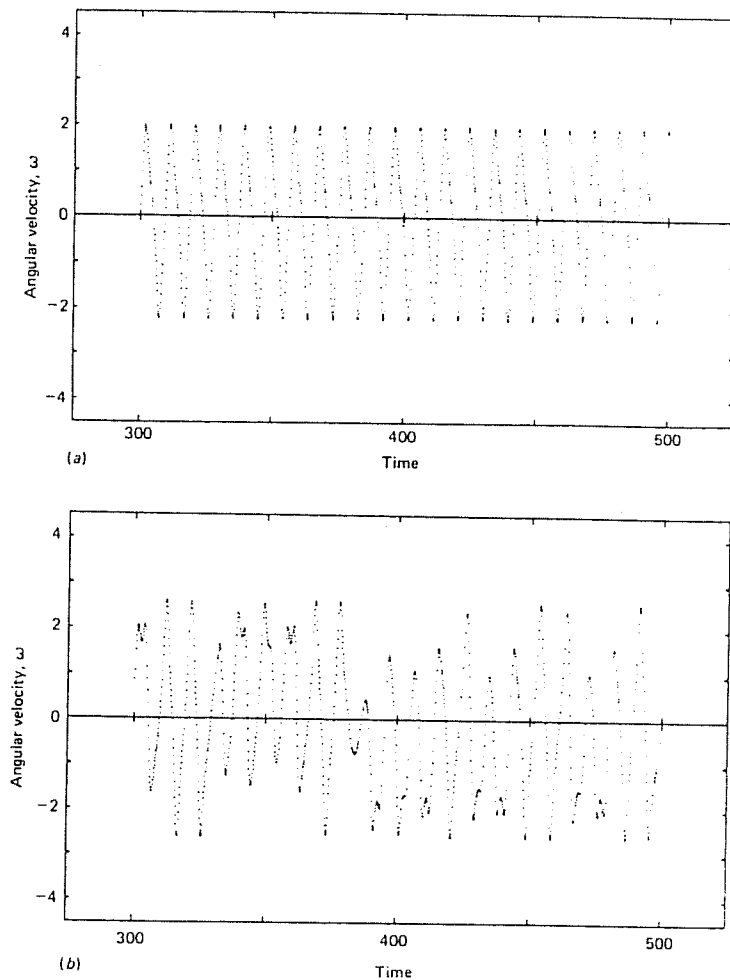


Fig. 1.1 The damped, driven pendulum can exhibit both periodic and chaotic motions. Here, the angular velocity is shown as a function of time for the two cases.

chaos, the irregularity is part of the intrinsic dynamics of the system, not unpredictable outside influences.

Chaotic motion is not a rare phenomenon. Consider a dynamical system described by a set of first order differential equations. Necessary conditions for chaotic motion are that (a) the system has at least three independent dynamical variables, and (b) the equations of motion contain a nonlinear term that couples several of the variables. The equations can often be expressed in the form:

$$\left. \begin{aligned} dx_1/dt &= F_1(x_1, x_2, \dots, x_n), \\ dx_2/dt &= F_2(x_1, x_2, \dots, x_n), \\ &\vdots \\ dx_n/dt &= F_n(x_1, x_2, \dots, x_n), \end{aligned} \right\} \quad (1.1)$$

where  $n$  must be at least 3. Two examples of appropriate nonlinear equations are:

$$\left. \begin{aligned} dx_1/dt &= \alpha x_1 + \beta x_2 + \gamma x_1 x_2 + \dots + \delta x_n, \\ dx_1/dt &= \alpha x_1 + \beta x_2 + \gamma \sin x_2 + \dots + \delta x_n \end{aligned} \right\} \quad (1.2)$$

where  $\alpha, \beta, \gamma, \delta$  are constants. In each case the nonlinear term couples both  $x_1$  and  $x_2$ . Systems such as these are often chaotic for some choices of the constants.

The fact that only three variables are required for chaos was surprising when first discovered. We shall see that three-space is sufficient to allow for (a) divergence of trajectories, (b) confinement of the motion to a finite region of the phase space of the dynamical variables, and (c) uniqueness of the trajectory. The nonlinearity condition is perhaps less surprising. Solutions to linear differential equations can always be expressed as a linear superposition of periodic functions, once initial transients have decayed. The effect of a nonlinear term is often to render a periodic solution unstable for certain parameter choices. While these conditions do not guarantee chaos, they do make its existence possible.

The nonlinearity condition has probably been responsible for the late historical development of the study of chaotic systems. Despite the fact that chaotic systems are deterministic and are described by many of the long-known classical equations of physics, the development of the subject itself is more recent. This circumstance may arise from the fact that, with the exception of some first order equations, nonlinear differential equations are either difficult or impossible to solve analytically. Although it is sometimes possible to use linearized approximations, the solution of nonlinear differential equations generally requires numerical methods whose practical implementation demands the use of a digital computer. The first numerical study to detect chaos in a nonlinear dynamical system was that of Lorenz's model of convective fluid flow (Lorenz, 1963). Similarly, the majority of the diagrams in this book are based upon the use of numerical methods on a personal computer to solve nonlinear equations.

From these general comments on chaotic systems, we turn to the physical system that is the focus of this work – the damped, driven pendulum. The choice of the pendulum as a model system has strong

historical precedent in physics. Galileo postulated the constancy of period for small amplitude oscillations of the pendulum from observations of swaying lamps in the cathedral at Pisa in 1581 (Robinson, 1921). He took up the problem of the relationship between the period and pendulum length in his famous *Dialogue on the Two Principal World Systems* in 1632, and in 1637 he suggested that the square of the period was proportional to the length of the pendulum for small oscillation amplitudes (Dugas, 1958). The pendulum also served as a primary timing mechanism for clocks and as a method of measuring variations in the earth's gravitational field. As a pedagogical device the pendulum has long been a standard mechanical example in introductory physics and classical mechanics courses. Now, 400 years after Galileo's initial work, the pendulum has again become an object of research as a chaotic system. The references scattered throughout this work attest to its popularity.

The damped, sinusoidally driven pendulum of mass  $m$  (or weight  $W$ ) and length  $l$  is described by the following equation of motion:

$$ml^2 \frac{d^2\theta}{dt^2} + \gamma \frac{d\theta}{dt} + W \sin \theta = A \cos(\omega_D t). \quad (1.3)$$

This equation expresses Newton's second law with the various terms on the left representing acceleration, damping, and gravitation. The angular velocity of the forcing,  $\omega_D$ , may be different from the natural frequency of the pendulum. In order to minimize the number of adjustable parameters the equation may be rewritten in dimensionless form as:

$$\frac{d^2\theta}{dt^2} + (1/q) \frac{d\theta}{dt} + \sin\theta = g \cos(\omega_D t) \quad (1.4)$$

where  $q$  is the damping or quality parameter,  $g$  is the forcing amplitude, *not to be confused with the gravitational acceleration*, and  $\omega_D$  is the drive frequency. The low-amplitude natural angular frequency of the pendulum is unity, and time is regarded as dimensionless. (This particular notation follows that used by Gwinn and Westervelt. See, for example, Gwinn and Westervelt (1986).) This equation satisfies the necessary conditions for chaos when it is written as a set of first order equations:

$$\left. \begin{aligned} \frac{d\omega}{dt} &= -(1/q)\omega - \sin\theta + g \cos\phi, \\ \frac{d\theta}{dt} &= \omega, \\ \frac{d\phi}{dt} &= \omega_D. \end{aligned} \right\} \quad (1.5)$$

The variable  $\phi$  is introduced as the phase of the drive term. The

necessary three variables  $(\omega, \theta, \phi)$  are evident, and the  $\sin\theta$  and  $g \cos\phi$  terms are clearly nonlinear. Whether the motion is chaotic depends upon the values of the parameters  $g$ ,  $\omega_D$ , and  $q$ . For some values the pendulum locks onto the driving force, oscillating in a periodic motion whose frequency is the driving frequency, possibly with some harmonics or subharmonics. But for other choices of the parameters the pendulum motion is chaotic. One may view the chaos as resulting from a subtle interplay between the tendency of the pendulum to oscillate at its 'natural' frequency and the action of the forcing term. The transitions between nonchaotic and chaotic states, due to changes in the parameters, occur in several ways and depend delicately upon the values of the parameters.

A variety of analytic and computational tools may be used in the study of chaotic systems. In Chapter 2 several of these are discussed. The pendulum's phase space and its properties are described, together with the conceptual device known as the Poincaré section. Then, since Fourier spectra are an indicator of chaotic motion, some elements of Fourier analysis are outlined. Chapter 3 is a description of the application of these and other techniques to the pendulum.

The driven pendulum would seem to be one of the simplest physical systems. Yet its behavior is rich and complex. The study of its motion can be facilitated by simple mathematical models formulated as difference equations, that provide a discrete *mapping* of the system from one state to another. Mappings have the advantage of being conceptually simple and numerically efficient, and they may be used as paradigms for various aspects of the pendulum motion. Chapter 4 contains discussions of three such maps, the logistic map, the circle map, and the horseshoe map. We use them to provide insight into the behavior of the pendulum.

Chapter 5 is concerned with the geometric structure of the *attractor* that describes the chaotic pendulum. The attractor, and its Poincaré section, are *fractal* structures with noninteger dimensionality. Various approaches to the calculation of fractal dimension are described. Another geometric feature is the exponential divergence of the chaotic trajectories on the attractor. The rate of this divergence is characterized by Lyapunov exponents. The calculation of these exponents and their relation to (a) the fractal dimension, (b) the dissipative nature of the pendulum, and (c) the duration of predictable behavior are also discussed.

Up to this point the presentation is focused on the fundamental ideas of chaotic dynamics. In Chapter 6 we discuss the relationship between these ideas and the analysis of experimental data. The developing methodology for characterization of nonlinear dynamical behavior in

experimental phenomena is complex. In this chapter we describe some of these methods and apply them to experimental data from a physical pendulum. The results of this study are then compared to those from the numerical simulations developed earlier in the book. The experimental data are also used to illustrate the possibility of prediction of chaotic data. Finally, we illustrate, through numerical simulation, the control of unstable dynamical states, in an otherwise chaotic pendulum.

Chapter 7 concludes the book with a brief survey of chaotic behavior in physical systems, including lasers, chemical reactions, fluids, crystal growth, and earthquakes. We emphasize the extension of chaotic dynamics to spatially extended systems having many degrees of freedom. Finally, the application of chaotic dynamics to quantum systems, and the connection between chaos and irreversibility are also discussed briefly.

Two appendices present numerical aspects of this book. Appendix A is a description of the Runge-Kutta algorithm used to solve the pendulum differential equation. Appendix B provides brief descriptions and listings of the computer programs used throughout the text, and in the computer exercises given at the end of several of the chapters. The listings utilize the language True BASIC™, but they are adaptable to any compiled BASIC or other high level language. (Interpreted BASIC, which is typically delivered with current microcomputers, is too slow for most of these simulations. The exceptions are the mappings in Chapter 4.) A third appendix, C, provides solutions to selected problems.

# 2

## Some helpful tools

In this chapter we discuss three mathematical constructs that are generally useful in the study of dynamical systems: phase space, the Poincaré section, and power spectra. Phase space is the mathematical space of the dynamical variables of a system. The Poincaré section is a ‘snapshot’ of the motion in the phase space, taken at regular time intervals. The power spectrum is computed using Fourier analysis to display the frequency composition of the time variation of the dynamical variables.

### 2.1 Phase space

The phase space of a dynamical system is a mathematical space with orthogonal coordinate directions representing each of the variables needed to specify the instantaneous state of the system. For example, the state of a particle moving in one dimension is specified by its position ( $x$ ) and velocity ( $v$ ); hence its phase space is a plane. On the other hand, a particle moving in three dimensions would have a six-dimensional phase space with three position and three velocity directions. A phase space may be constructed in several different ways. For example, momenta can be used instead of velocities.

Let us focus the discussion on the pendulum and begin with the familiar simple pendulum in the small amplitude approximation where the restoring term,  $\sin\theta$ , is taken as  $\theta$ . (Recall that the equations are written in dimensionless form for simplicity, with time measured in units of the inverse of the natural frequency.) The equation of motion is

$$\frac{d^2\theta}{dt^2} + \theta = 0. \quad (2.1)$$

With the addition of the angular velocity variable,  $\omega \equiv d\theta/dt$ , this linear, second order equation can be reduced to two first order equations:

$$d\omega/dt = -\theta$$

and

$$d\theta/dt = \omega.$$

In this way each dynamical variable has its own first order differential equation. Without loss of generality, the initial conditions can be chosen so that the solution becomes

$$\theta = a_i \cos t \text{ and } \omega = a_i \sin t$$

where  $\{a_i\}$  represents the possible amplitudes of the motion. This solution set gives the parametric curves for  $\omega$  and  $\theta$ , and one can eliminate the time parameter to give a two-dimensional representation for differing values of  $a_i$ . This diagram, shown in Figure 2.1, is the appropriate *phase space diagram* (in this case a phase plane diagram). Each value of  $a_i$  yields a closed orbit of fixed energy. The energy increases with the square of the radius  $a_i$ . The orbit is usually called a *phase trajectory*.

An important feature of the trajectory is that two trajectories corresponding to similar energies will pass very close to each other, but the orbits will not cross each other. This *noncrossing* property derives from the fact that past and future states of a deterministic mechanical

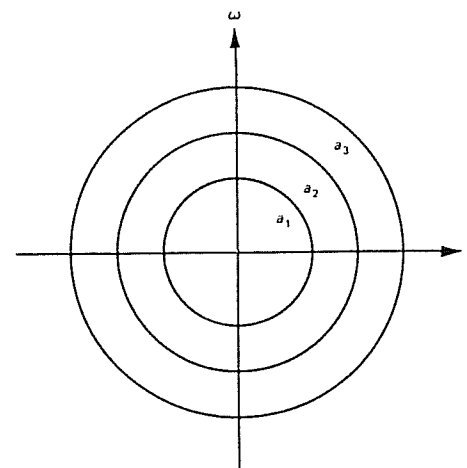


Fig. 2.1 Phase diagram of the linear pendulum. The angular velocity,  $\omega$ , and the angular displacement,  $\theta$ , are the coordinate axes.

system are uniquely prescribed by the system state at a given time. A crossing of trajectories at time  $t$  would introduce ambiguity into past and future states, thereby rendering the system indeterminate. Such indeterminacy would contradict the assumed uniqueness of the trajectory. Figure 2.2 shows the indeterminacy of trajectories emanating from a hypothetical crossing.

Another important feature of the phase space of *conservative* (constant energy) systems is the *preservation of areas*. This means that all the points found in a given area of phase space at one time move in such a way that at a later time the area occupied by these points remains the same. This feature is illustrated in Figure 2.3 and in Examples 2.1 and 2.2.

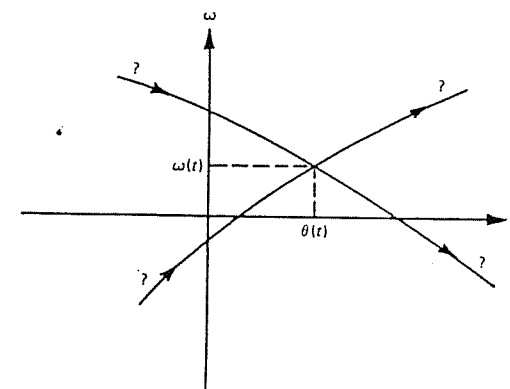


Fig. 2.2 The noncrossing property of phase trajectories. Crossing of trajectories violates uniqueness of trajectories in a deterministic dynamical system.

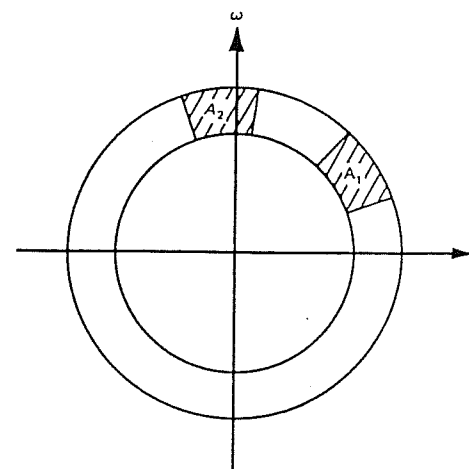


Fig. 2.3 Preservation of phase space area.

**Example 2.1**

For the linear oscillator  $d^2\theta/dt^2 + \theta = 0$ , consider the evolution of the area  $A_1$  as shown in Figure 2.4 during one quarter of the period. Since the system is energy conserving,  $A_1$  should remain constant. Because of the circular symmetry, preservation of the area can be shown by proving that every point in  $A_1$  rotates (at a constant radius) through the same angle in the quarter period. The energy conserving feature ensures that each point rotates at a constant radius because the energy of the oscillator is proportional to the square of the radius. For the rotation angle we note that since  $\theta = a\cos \omega t$  and  $\omega = a\sin \omega t$ , the polar angle of a given point is

$$\alpha(t) = \tan^{-1}(\tan t) = t. \quad (2.2)$$

Therefore at  $t = t_0 + \pi/2$ ,  $\alpha(t_0 + \pi/2) = t_0 + \pi/2$ . But since  $\alpha(t)$  was arbitrary, all points rotate by  $\pi/2$  in one quarter period, and the area is preserved.

**Example 2.2**

As another example of area preservation consider the very simple motion of a constant velocity rotor. The two first order equations become

$$d\omega/dt = 0$$

and

$$d\theta/dt = \omega_0.$$

The corresponding phase trajectories are just horizontal lines with differing angular velocities, as shown in Figure 2.5. The linear dependence of  $\theta$  on  $\omega_0$  ensures that an initial rectangle of points transforms to a parallelogram with a constant base and height, thereby maintaining the original area.

Example 2.2 also raises the question of boundaries on the phase plane coordinates. In contrast to the linearized pendulum whose finite motion allowed both  $\theta$  and  $\omega$  to be bounded conveniently in phase space, the angular coordinate  $\theta$  for the rotor can increase (positively or negatively) without bound. Yet physically  $\theta$  is periodic. Therefore the phase

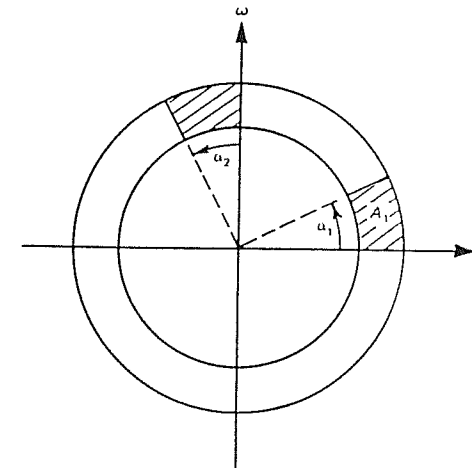


Fig. 2.4 Evolution of the linear oscillator described in Example 2.1.

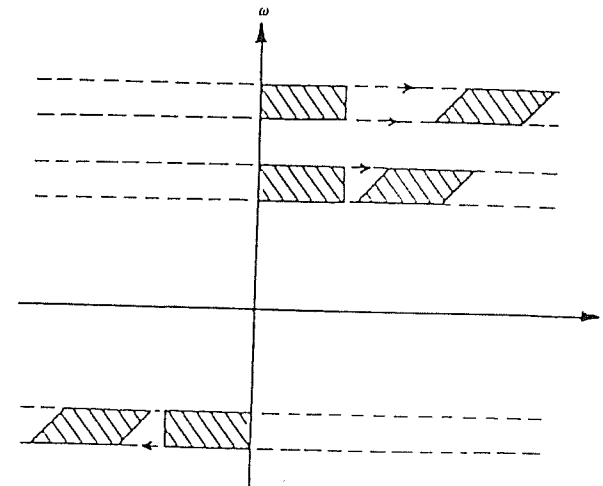


Fig. 2.5 Phase space diagram of a constant velocity rotor.

diagram is also made periodic by imposing *periodic boundary conditions* on  $\theta$  as illustrated in Figure 2.6. The  $\theta$  axis can be limited to  $[-\pi, \pi]$ , and the two edges of this domain are regarded as identical. As the rotor goes around in the positive  $\theta$  direction, its phase representation disappears off the right edge of the phase diagram and immediately reappears on the left side. Similar periodic boundary conditions can also be usefully

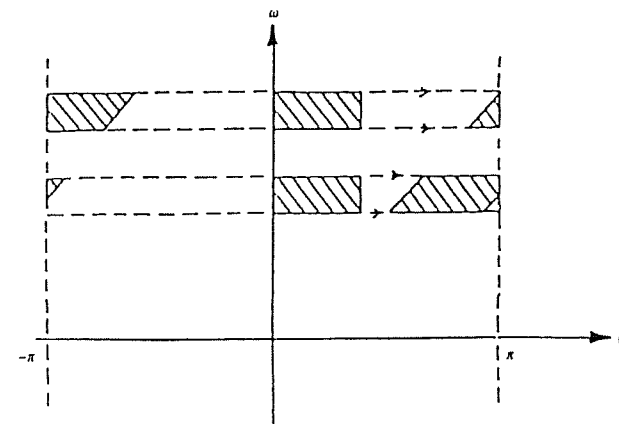


Fig. 2.6 Phase space diagram of the rotor with periodic boundary conditions. Phase points moving to the right disappear at  $\theta = \pi$  and then reappear at  $\theta = -\pi$ .

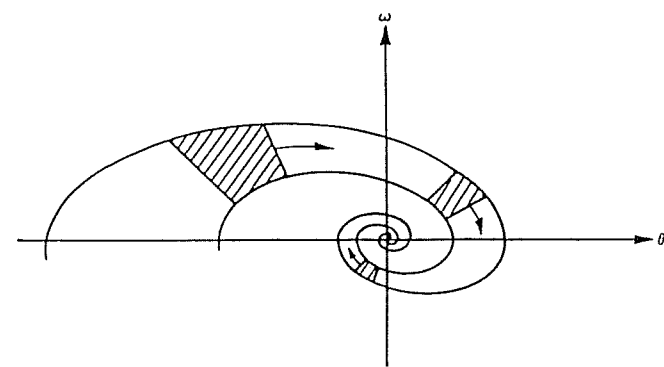


Fig. 2.7 Phase space diagram of the dissipative linear pendulum. Phase area is not preserved.

applied to the forced pendulum whose motion passes through the vertical direction.

The property of area preservation, or volume preservation in a higher-dimensional space, is a general feature of conservative systems. This property leads to a classification of dynamical systems into two categories – *conservative* or *dissipative* – depending upon whether the phase volumes stay constant or contract, respectively. For example, the linearized undamped pendulum conserves energy, and its trajectories preserve phase area. On the other hand, the trajectories of the linearized damped pendulum,

$$\frac{d^2\theta}{dt^2} + \frac{d\theta}{dt} + \theta = 0, \quad (2.3)$$

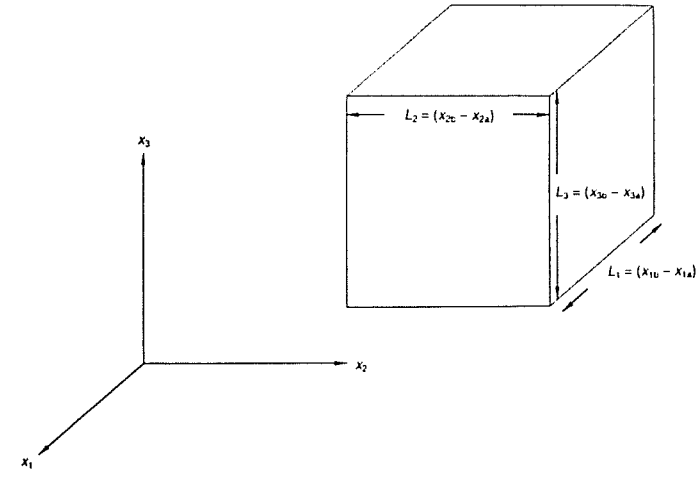


Fig. 2.8 Evolution of a volume in three-dimensional phase space.

decay to a single point:  $\omega = 0 = \theta$ . This area contraction is illustrated in Figure 2.7. Such a point is called an *attractor*, because a finite set of initial coordinates  $(\theta, \omega)$  converge to it. Obviously phase area is *not* preserved and the system is said to be dissipative.

Using these phase space characteristics we can develop a method for determining from the equations of motion whether a system is conservative or dissipative. The development of the method is easiest to understand in three space dimensions; thus we assume phase coordinates  $x_1, x_2, x_3$ , as in Figure 2.8. The equations of motion of the system can be written in terms of the phase 'velocity' components,

$$\left. \begin{aligned} \frac{dx_1}{dt} &= F_1(x_1, x_2, x_3), \\ \frac{dx_2}{dt} &= F_2(x_1, x_2, x_3), \\ \frac{dx_3}{dt} &= F_3(x_1, x_2, x_3). \end{aligned} \right\} \quad (2.4)$$

Now consider a set of phase points contained in a small 'box' in phase space of volume  $V$  with sides of lengths  $L_1, L_2$ , and  $L_3$ , as shown in Figure 2.8. In a short time  $dt$  this box will evolve to a slightly different one with volume  $V + dV$ . The length  $L_j$  is given by the difference in phase coordinates,  $(x_{jb} - x_{ja})$ . All lengths are small quantities.

The volume of the 'box' is given by

$$\begin{aligned} V &= L_1 L_2 L_3 \\ &= (x_{1b} - x_{1a})(x_{2b} - x_{2a})(x_{3b} - x_{3a}). \end{aligned}$$

Then, using the product rule for differentiation, the rate of change of volume becomes

$$\frac{dV}{dt} = L_2 L_3 (\dot{x}_{1b} - \dot{x}_{1a}) + L_1 L_3 (\dot{x}_{2b} - \dot{x}_{2a}) + L_1 L_2 (\dot{x}_{3b} - \dot{x}_{3a}), \quad (2.5)$$

where  $\dot{x}$  indicates  $dx/dt$ . This expression can be rewritten, using equation (2.4), as

$$\frac{dV}{dt} = L_2 L_3 [F_1(x_{1b}, x_{2a}, x_{3a}) - F_1(x_{1a}, x_{2a}, x_{3a})] + 2 \text{ similar terms.}$$

Next we approximate with a Taylor series, for example,

$$F_1(x_{1b}, x_{2a}, x_{3a}) \approx F_1(x_{1a}, x_{2a}, x_{3a}) + \frac{\partial F_1(x_{1a}, x_{2a}, x_{3a})}{\partial x_1} (x_{1b} - x_{1a}). \quad (2.6)$$

Then the rate of change of volume is

$$\begin{aligned} \frac{dV}{dt} &= L_2 L_3 [F_1(x_{1a}, x_{2a}, x_{3a}) + \frac{\partial F_1}{\partial x_1} (x_{1b} - x_{1a}) \\ &\quad - F_1(x_{1a}, x_{2a}, x_{3a})] + 2 \text{ similar terms} \\ &= L_2 L_3 \frac{\partial F_1}{\partial x_1} (x_{1b} - x_{1a}) + 2 \text{ similar terms.} \end{aligned}$$

Finally, the logarithmic rate of volume change is compactly expressed as

$$\frac{1}{V} \frac{dV}{dt} = \nabla \cdot \mathbf{F}. \quad (2.7)$$

The logarithmic derivative is therefore independent of the particular volume chosen, and depends only on  $\nabla \cdot \mathbf{F}$ . If this quantity is zero, the system is termed *conservative*, whereas if the divergence of phase velocity is negative the system is *dissipative*. The kinematic properties of the flux in phase space for a conservative system are analogous to the flow of an incompressible fluid in hydrodynamics. (The term *Hamiltonian* is sometimes used in connection with phase volume preserving systems. Many dynamical systems obey Hamilton's equations of motion and such systems are called *Hamiltonian* systems. These systems preserve volume in phase space, according to Liouville's theorem, and therefore Hamiltonian systems are a subset of the set of conservative systems. See Helleman (1983).)

### Example 2.3

Let us write both of our example pendula in the phase velocity form and determine their phase space preservation characteristics by this method

(i)  $\frac{d^2\theta}{dt^2} + \theta = 0$  (undamped) becomes

$$d\theta/dt = \omega \text{ and } d\omega/dt = -\theta.$$

Therefore  $\mathbf{F} = (\omega, -\theta)$  and  $\nabla \cdot \mathbf{F} = \partial\omega/\partial\theta + \partial(-\theta)/\partial\omega = 0$ , indicating that phase area is preserved.

(ii)  $\frac{d^2\theta}{dt^2} + d\theta/dt + \theta = 0$  (damped) becomes

$$d\theta/dt = \omega \text{ and } d\omega/dt = -\omega - \theta.$$

Therefore  $\mathbf{F} = (\omega, -\omega - \theta)$  and  $\nabla \cdot \mathbf{F} = \partial\omega/\partial\theta + \partial(-\omega - \theta)/\partial\omega = -1$ , indicating that phase area diminishes in time and the system is, as expected, dissipative.

These two examples show how easily the divergence criterion may be applied. For the driven pendulum, the equation:

$$\frac{d^2\theta}{dt^2} + (d\theta/dt)/q + \sin\theta = g\cos(\omega_D t)$$

is converted to a set of first order equations:

$$d\omega/dt = -\omega/q - \sin\theta + g\cos\phi,$$

$$d\theta/dt = \omega,$$

$$d\phi/dt = \omega_D.$$

Then the right sides form the components of the three-dimensional vector  $\mathbf{F}$ . It is left as an exercise for the reader to show that  $\nabla \cdot \mathbf{F} = -1/q$  and that, therefore, the system is dissipative.

We have looked at phase diagrams for the damped and undamped linearized pendula. Let us now introduce the full nonlinear restoring torque,  $\sin\theta$ . Figure 2.9 shows the phase plane for the undamped pendulum:

$$\frac{d^2\theta}{dt^2} + \sin\theta = 0. \quad (2.8)$$

For small values of  $d\theta/dt$  and  $\theta$ , the diagram appears similar to that of the pendulum in the linear approximation, but as  $\theta$  approaches  $\pm\pi$  – a pendulum swing that would go all around the circle – the picture changes. At  $(\pm\pi, 0)$  the slope develops a discontinuity. The largest of the closed trajectories bounds the region where the motion is oscillatory (or vibrational). On the open trajectory of higher angular velocity, the

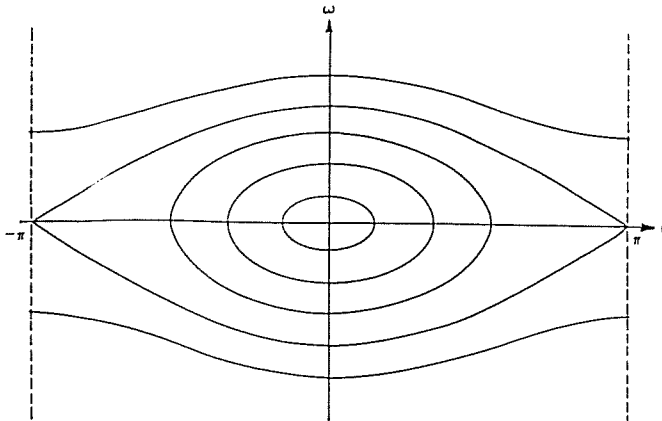


Fig. 2.9 Phase diagram of the nonlinear pendulum. The restoring force term contains  $\sin\theta$ .

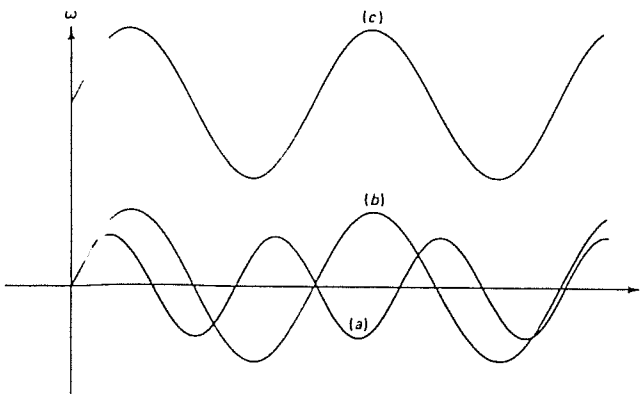


Fig. 2.10 Angular velocity time series. In contrast to the linearized pendulum, the period of the motion for the nonlinear pendulum increases with increasing amplitude. Curves (a) and (b) show oscillatory motions of differing amplitudes. Curve (c) shows the pendulum with sufficient energy to exhibit both rotary and oscillatory motions.

pendulum goes completely around the circle, and its motion is a rotation modulated by oscillation. The average angular velocity becomes nonzero. (One might compare this to a direct current electrical signal modulated by an alternating current signal.) The corresponding time series of these motions are shown in Figure 2.10.

Consider now the addition of a damping term so that the equation becomes

$$\frac{d^2\theta}{dt^2} + \frac{d\theta}{dt} + \sin\theta = 0. \quad (2.9)$$

Typical trajectories are shown in Figure 2.11. As indicated previously, the damping term results in an attractor at the origin where  $\sin\theta \approx 0$ . Now, however, further attractors are added at  $\theta = \pm n\pi$ ,  $\omega = 0$ . This can

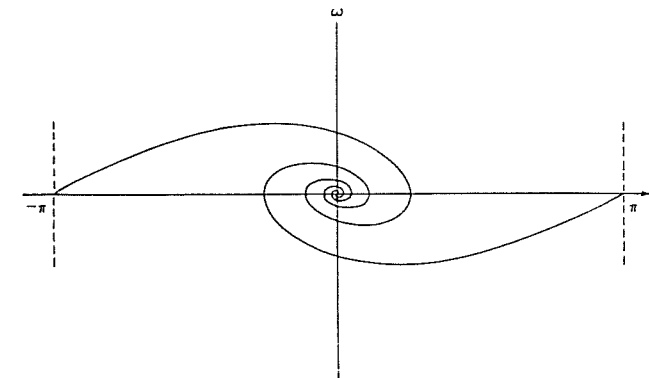


Fig. 2.11 Pair of phase space trajectories for the damped pendulum.

be seen by setting the phase velocity equal to zero and solving for the stationary values of  $\theta$  and  $\omega$ ; that is,

$$\left. \begin{aligned} \frac{d\theta}{dt} &= \omega = 0, \\ \frac{d\omega}{dt} &= -\omega - \sin\theta = 0. \end{aligned} \right\} \quad (2.10)$$

While these attractors are points where the phase velocity goes to zero, questions arise as to the stability of these points. Will the trajectories tend to go back to these critical points if slightly perturbed? Will the stability depend upon the direction of the perturbation? These questions can be answered by looking carefully at the critical points. A useful technique for examining dynamical behavior near critical points involves the assumption that the system will not deviate substantially from linear behavior *near the critical points*. Then each of the nonlinear terms in the differential equations is given a linear approximation near the critical points. This method was developed by Poincaré in 1914 (Hayashi, 1964).

For the case of the damped pendulum,

$$\left. \begin{aligned} \frac{d\theta}{dt} &= \omega, \\ \frac{d\omega}{dt} &= -\omega - (\theta - n\pi), \end{aligned} \right\} \quad (2.11)$$

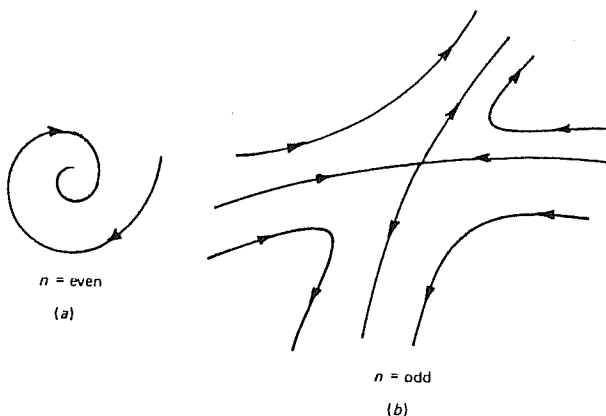
it is easy to see (Problem 2.6) that near  $\theta = \pm n\pi$ , where  $n$  is even, the linear approximation is

$$\left. \begin{aligned} \frac{d\theta}{dt} &= \omega, \\ \frac{d\omega}{dt} &= -\omega - (\theta - n\pi), \end{aligned} \right\} \quad (2.12)$$

and when  $n$  is odd the linear approximation becomes

$$\left. \begin{aligned} \frac{d\theta}{dt} &= \omega, \\ \frac{d\omega}{dt} &= -\omega + (\theta - n\pi). \end{aligned} \right\} \quad (2.13)$$

**Fig. 2.12** Critical points in phase space: (a) focal point; (b) saddle point. In (b) the trajectories going to the saddle point are stable whereas the trajectories coming from the saddle point are unstable.



In each case  $\theta$  is transformed to a value centered at the critical point such that  $\theta \rightarrow \Delta\theta = \theta - n\pi$  and therefore the linearized phase plane equations are

$$\begin{aligned} n = \text{even}; \quad d\Delta\theta/dt &= \omega, & n = \text{odd}; \quad d\Delta\theta/dt &= \omega, \\ &d\omega/dt = -\omega - \Delta\theta, & &d\omega/dt = -\omega + \Delta\theta. \end{aligned} \quad \left. \right\} (2.14)$$

Following the usual method for solving sets of first order linear differential equations, trial solutions of the form  $\Delta\theta = Ae^{\lambda t}$  and  $\omega = Be^{\lambda t}$  may be substituted into the equations; this yields two pairs of homogeneous algebraic equations. The condition for a nontrivial solution is the vanishing of the determinant of the coefficients of  $A$  and  $B$ . This condition produces quadratic characteristic equations in  $\lambda$  for each case:

$$\lambda^2 + \lambda + 1 = 0: n = \text{even}, \quad \lambda^2 + \lambda - 1 = 0: n = \text{odd}. \quad (2.15)$$

For the  $n = \text{even}$  case, the  $\lambda$  values are complex conjugates with negative real parts. This implies that both  $\Delta\theta$  and  $\omega$  will spiral inward toward the equilibrium point attractor, which is called a *focus*. This case is shown in Figure 2.12(a). On the other hand, the  $n = \text{odd}$  condition produces two real values of  $\lambda$ , one positive and one negative. In this case the stable phase trajectories move toward the critical point in one direction (negative exponent), but the unstable trajectories move away from it in another direction (positive exponent). This kind of critical point is called a *saddle point* and is shown in Figure 2.12(b). The respective directions are obtained by determining the  $A$  and  $B$  coefficients appropriate to each  $\lambda$  value. Note how the unstable trajectory directions correspond to the only possible directions for the pendulum, located momentarily at the saddle point. The details of the solution are left as an exercise (Problem

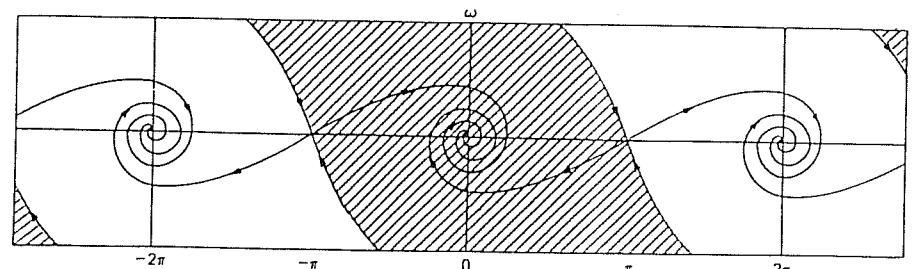


**Fig. 2.13** Phase space diagram of the damped pendulum. Alternate shaded and unshaded regions are basins of attraction. All points within a particular basin are attracted to the focal point within the basin.

2.7). Putting all this information together, the phase diagram for the damped pendulum can be drawn as in Figure 2.13.

This phase diagram suggests yet another property of trajectories in phase space. As drawn in Figure 2.13, the phase space is divided into alternating regions as indicated by the shading. Inside each region all the trajectories will eventually spiral to the enclosed focal point. Each region is the set of all initial conditions  $(\omega, \theta)$  of trajectories that will eventually converge on a specific attractor – in this case a focal point. Such regions are called *basins of attraction*. Furthermore, each of the diagonal curves (Figure 2.13) dividing one basin from another is called a *separatrix*. The arrows on the separatrix (and elsewhere) indicate the flow of the trajectories, toward and away from the saddle points. We will see (Chapter 3) that one characteristic of chaos is the partial dissolution of the separatrix as the basins start to merge.

While most of the discussion so far has focused on the phase *plane*, it is important to realize that the phase space construction need not be confined to two dimensions. A previously introduced equation set,

$$\begin{aligned} dx_1/dt &= F_1(x_1, x_2, x_3), \\ dx_2/dt &= F_2(x_1, x_2, x_3), \\ dx_3/dt &= F_3(x_1, x_2, x_3), \end{aligned} \quad \left. \right\} (2.16)$$

would define a three-dimensional phase space. We may use this set of equations to illustrate some further properties of phase space. We have already described the divergence method for determining if the above system is conservative. Further, it is evident that the equations are not explicitly time-dependent. The equation set is then called *autonomous*

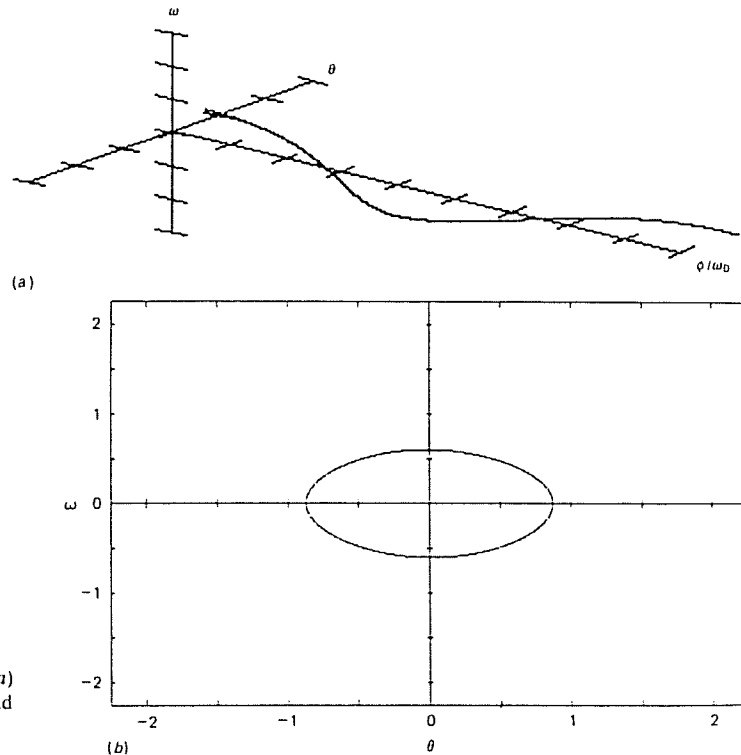


Fig. 2.14 Phase diagrams for the moderately-driven pendulum,  $g = 0.5$ : (a) three dimensions, and (b) two dimensions ( $q = 2$ ).

and describes a time-independent flow in phase space, similar to a set of stream lines in a fluid. In fact, the vector  $\mathbf{F}$  is called a *flow*. Autonomous systems also obey the noncrossing property described earlier. However, a projection of a higher-dimensional space onto a plane might show apparent crossings which do not represent actual intersections.

The autonomous property is sufficiently useful that it is often desirable to convert a time variable to some other variable in order to make a nonautonomous system into an autonomous system. For example, the variable  $\phi$  is introduced in the driven pendulum equations at  $d\phi/dt = \omega_0$  so that the system's dynamical variables become  $\theta$ ,  $\omega$ , and  $\phi$ . This is convenient since the explicit time dependence enters as a *periodic* term,  $g\cos(\omega_0 t)$ , and therefore  $\phi$  can be a periodic variable. Then in a three-dimensional phase space, both  $\theta$  and  $\phi$  can be given periodic boundary conditions such as  $\theta \in [-\pi, \pi]$  and  $\phi \in [0, 2\pi]$ . In Figure 2.14(a) and (b), a moderately-driven pendulum system is illustrated in both three- and

two-dimensional phase spaces. The two-dimensional diagram is a projection of the three-dimensional diagram. These diagrams show the state of the pendulum after the initial transient effects have disappeared and after the system has evolved to a steady state. The resulting closed orbit is an *attractor* in the same sense as the point is an attractor for the dissipative, nondriven pendulum. This attractor is obviously one-dimensional and is called a *limit cycle*.

The motion of the pendulum illustrated in Figure 2.14 is a simple oscillation. As the drive amplitude increases, more complex motions occur, both periodic and chaotic. Some examples of more complex periodic motions are illustrated in Figure 2.15, for various drive amplitudes ( $g$ ). The path in real space and the corresponding phase plane diagram are shown in each case. The orbits involve a superposition of oscillation and complete rotation.

## 2.2 Poincaré section

A Poincaré section is a device invented by Henri Poincaré as a means of simplifying phase space diagrams of complicated systems. It is constructed by viewing the phase space diagram stroboscopically in such a way that the motion is observed periodically. For the driven pendulum, the strobe period is the period of the forcing.

In order to make this idea more concrete let us refer to the moderately driven pendulum whose attractor was shown in Figure 2.14(a). The Poincaré method consists of cutting or sectioning the spiral attractor at regular intervals and looking at these sections along the  $\phi$  axis through the  $(\theta, \omega)$  plane. If this sectioning is done at intervals corresponding to the forcing motion, then the stroboscopic pictures all show one point. The motion always comes back to the same  $(\theta, \omega)$  coordinates as  $\phi$  is increased by  $2\pi$ . Figure 2.16 illustrates the result. This strobe diagram is called a *Poincaré section* as the graph is 'cut' periodically.

The Poincaré section can provide information about the ratio of the strobe frequency,  $\omega_s$ , to the natural frequency of the dynamical motion,  $\omega_0$ . For example, if a motion whose natural frequency was equal to 1 were strobed at a frequency equal to 2, the Poincaré section would have two points. In general, if the natural frequency of the motion,  $\omega_0$ , is equal to  $(p/q)\omega_s$ , where  $p/q$  is rational, then there are  $q$  points, and the order of their appearance is such that, as a given point appears on the circle, the next  $[q - (p + 1)]$  positions are skipped. All of the  $q$  points, however, are

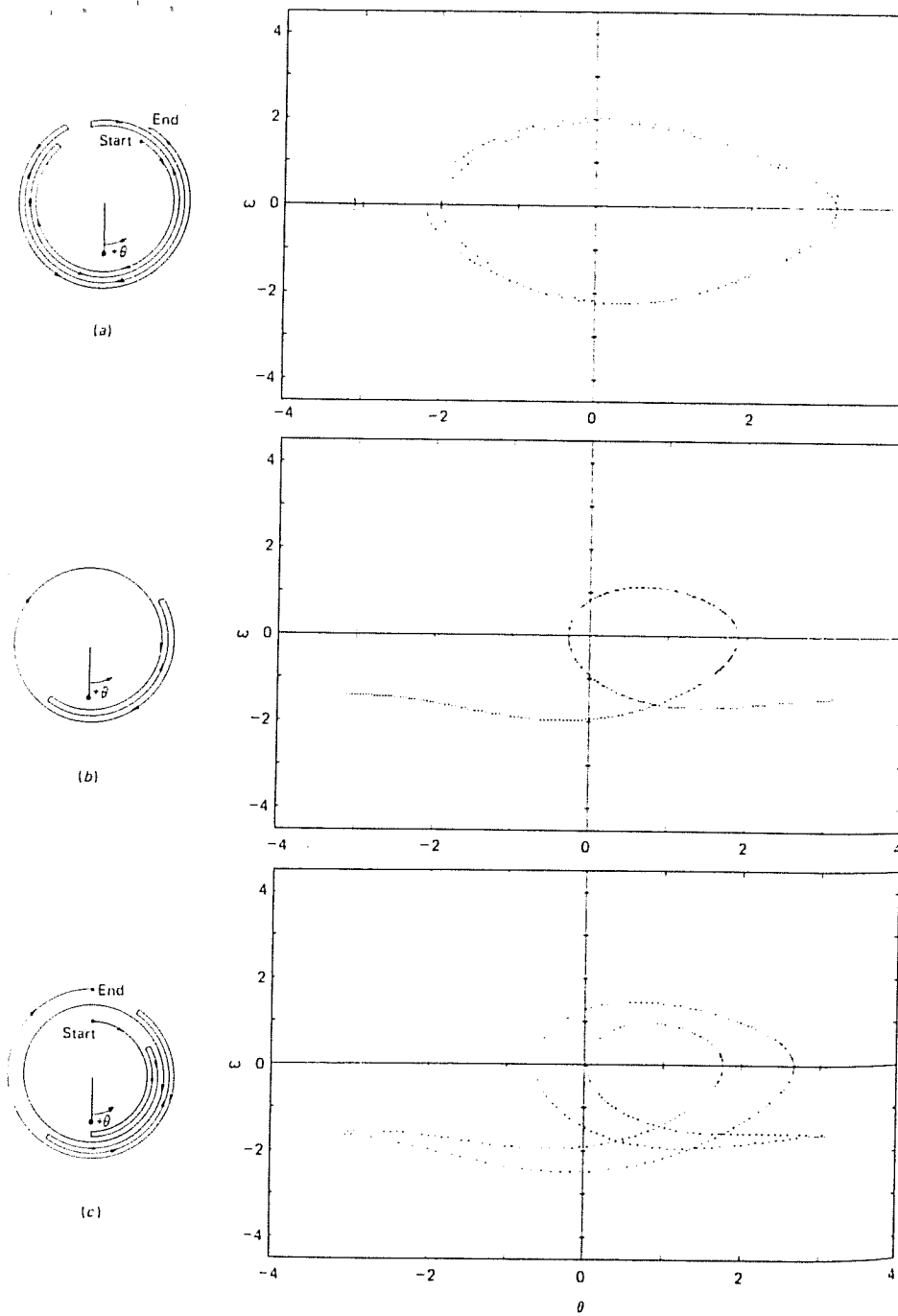


Fig. 2.15 Steady state phase diagram and sketch of the corresponding pendulum motion for different drive amplitudes. All motions are periodic and one complete cycle is shown in each case. The direction of the arrow depends on the initial conditions. (a)  $g = 1.07$ ; (b)  $g = 1.35$ ; (c)  $g = 1.45$ . ( $q = 2$ ).

eventually filled in. Figure 2.17 illustrates the situation where, for example, when  $\omega_0 = \frac{4}{5}\omega_s$ , there are five points and  $5 - (4 + 1) = 0$  positions are skipped as the points go counterclockwise around the circle. These strobe points provide the coordinate values for  $\theta$  and  $\omega$  on the Poincaré plot, and the numbering of the points represents their order of appearance.

If the pendulum goes all the way around, then  $\omega$  has a direct current component as well, and the pattern of dots is not centered on the origin. Since the mixture of rotation and oscillation may lead to a nonzero average displacement  $\langle\theta\rangle$ , the offset will generally be asymmetric. Furthermore, if the relation between the strobe frequency and the pendulum frequency is irrational (incommensurate), then the strobe points will never repeat and the points will gradually fill in a circle on the Poincaré section. Finally, if the system becomes dissipative – in the pendulum case by the addition of a damping term – then the points on the Poincaré section will move toward the appropriate attractor. These ideas are illustrated in Figure 2.18.

For a dynamical system with a periodic forcing term, the Poincaré section provides a simplification of the phase diagram while retaining the essential features of the dynamics. Therefore it is ideally suited to the driven pendulum. In Figure 2.19, some of the periodic motions illustrated by phase diagrams in Figure 2.15 are shown as Poincaré sections. For the periodic motions, the appearance of these sections is quite simple. But in Chapter 3, where the chaotic behavior of the pendulum is described, the simplification of phase space provided by the Poincaré section is shown to be very important for an understanding of the

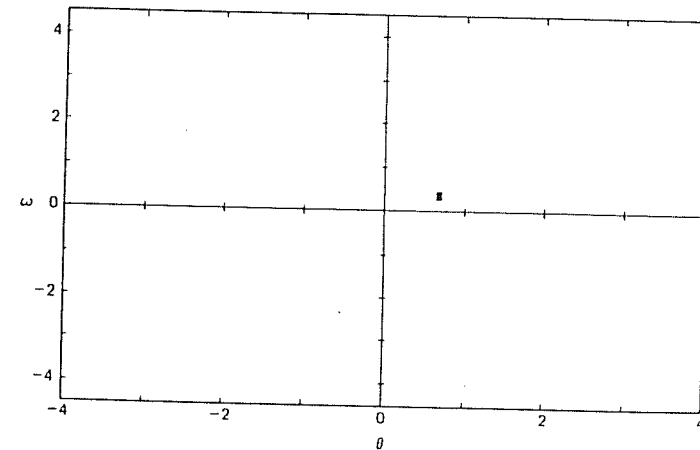


Fig. 2.16 Poincaré section of the linearized pendulum ( $g = 0.5$ ,  $q = 2$ ,  $\phi = 0$ ).

Fig. 2.17 Relationship of strobe frequency to dynamical motion frequency. The positioning and order of points on a Poincaré section is shown for different ratios of strobe ( $\omega_0$ ) and motion ( $\omega_s$ ) frequencies. (a)  $\omega_0 = \frac{4}{5}\omega_s$ ; (b)  $\omega_0 = \frac{3}{5}\omega_s$ ; (c)  $\omega_0 = \frac{2}{3}\omega_s$ .

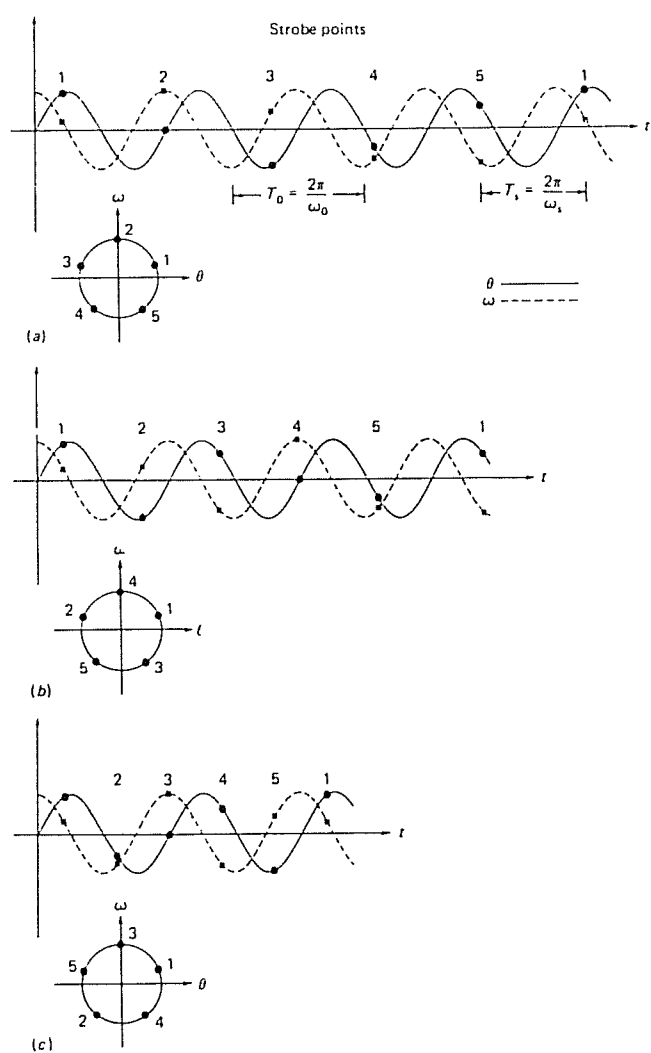


Fig. 2.18 Poincaré sections of different motions. (a) Combined oscillatory and rotational motion whose frequency is a rational fraction of the strobe frequency. (b) Oscillatory motion whose frequency is incommensurate with the strobe frequency. (c) Dissipative motion.

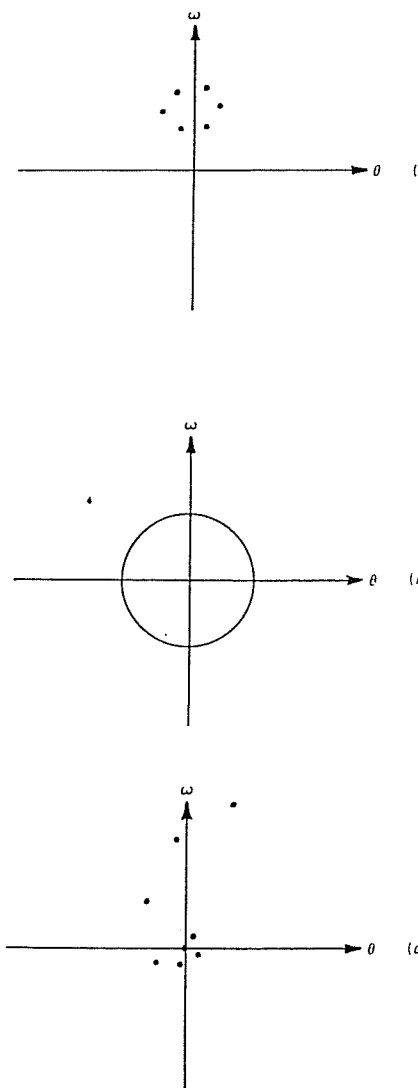
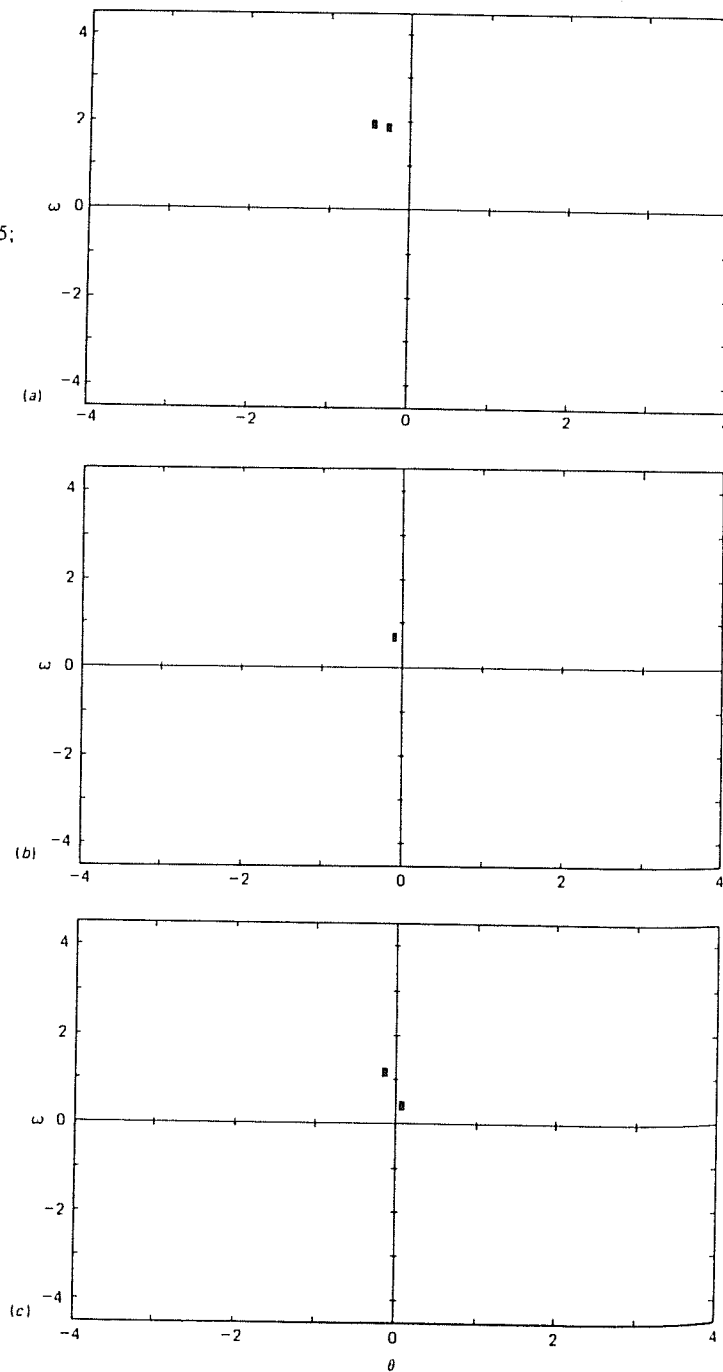


Fig. 2.19 Poincaré sections of motion illustrated in Figure 2.15. The section is taken at  $\phi = 0$  ( $q = 2$ ). (a)  $g = 1.07$ ; (b)  $g = 1.35$ ; (c)  $g = 1.45$ .



physics. One useful tool for the study of chaos is the observation of the distribution of points on a computer-generated Poincaré section.

### 2.3 Spectral analysis of time series

The time evolution of a dynamical system is represented by the time variation  $f(t)$  or (when sampled at regular intervals) *time series* of its dynamical variables. Any function  $f(t)$  may be usefully represented as a superposition of periodic components. The determination of their relative strengths is called *spectral analysis*.

Depending upon the nature of the function,  $f(t)$ , we may represent it in two different but related ways. If  $f(t)$  is periodic, then the spectrum may be expressed as a linear combination of oscillations whose frequencies are *integer multiples* of a basic frequency. This linear combination is called a *Fourier series*. However, it is more likely that  $f(t)$  is not periodic, and the spectrum must then be expressed in terms of oscillations with a continuum of frequencies. Such a spectral representation is called the *Fourier transform* of  $f(t)$ . This representation is especially useful for chaotic dynamics. Because the Fourier transform is in general a complex-valued function, it is often preferable to define a real-valued function which is the modulus squared of the transform. This real function is called the *power spectrum* of  $f(t)$ . One familiar but crude example of the power spectrum is the LED display of an electronic graphics equalizer. The moving bars on the display indicate the instantaneous electronic power in each of the sections of the audio frequency spectrum.

In this section we review the main features of the Fourier series and then give the Fourier transform method as the limiting case of the Fourier series when the periodicity of  $f(t)$  becomes infinitely large, that is, when  $f(t)$  ceases to be periodic.

If the function is periodic such that  $f(t) = f(t + nT)$  – with  $n$  being a positive or negative integer and  $T$  being the basic periodicity – then, as noted above, the frequencies of the various spectral components are all integer multiples of the basic frequency,  $1/T = \omega_0/2\pi$ . The *Fourier series* representation of  $f(t)$  may be written compactly in complex notation:

$$f(t) = \sum_{n=-\infty}^{\infty} a_n e^{in\omega_0 t}, \quad (2.17)$$

where the  $a_n$  are the amplitudes of the components of frequency  $n\omega_0$ .

These amplitudes may be determined from the calculation:

$$a_n = \frac{\omega_0}{2\pi} \int_{-\pi/\omega_0}^{\pi/\omega_0} f(t) e^{-in\omega_0 t} dt. \quad (2.18)$$

(See, for example, Kaplan (1973). An example of a periodic time series often found in electronics is the 'sawtooth' function, shown in Figure 2.20.

#### Example 2.4

The time series of the 'sawtooth' function is  $f(t) = t : t \in (-T/2, T/2)$  where  $T = 2\pi/\omega_0$ . (The pattern is repeated.)

It is left as an exercise to show that

- $a_n = 0$  for  $n = 0$ ;
- $a_n = 1/n\omega_0$  for  $n = \text{odd integer}$ ; and
- $a_n = -1/n\omega_0$  for  $n = \text{even integer}$ .

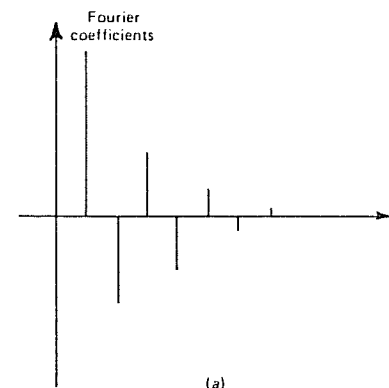
Substitution of these results back into the Fourier series expression and manipulation of the ensuing complex expressions leads to the result:

$$f(t) = \frac{2}{\omega_0} [\sin(\omega_0 t) - \frac{1}{2}\sin(2\omega_0 t) + \frac{1}{3}\sin(3\omega_0 t) - \dots].$$

Note that the coefficients  $1, -\frac{1}{2}, \frac{1}{3}$ , and so forth, are not the same as the  $a_n$  but are combinations of pairs of  $a_n$ . Figure 2.20(a) shows a bar chart of the coefficients. The original function  $f(t)$  and the resultant of the first two frequency components are shown as an approximation to  $f(t)$  in Figure 2.20(b).

The *Fourier transform* is an extension of the Fourier series in that the basic periodicity  $T$  of  $f(t)$  is allowed to become infinitely large. This condition implies that  $f(t)$  need no longer be periodic. In this circumstance the spacing between the frequency components becomes infinitesimal. The discrete spectrum of frequency components becomes a continuum of spectral densities as shown. Therefore, a given component  $a_n$  converts to  $a(\omega)\delta\omega$  where  $\delta\omega$  is a small interval of frequency and  $a(\omega)$  is the frequency-dependent amplitude or *Fourier transform*. The practical advantage of the transform is that it can be used to analyze a function about whose properties we are totally ignorant. It often yields surprising and illuminating information.

One may think of the transition from the Fourier series to the Fourier



(a)

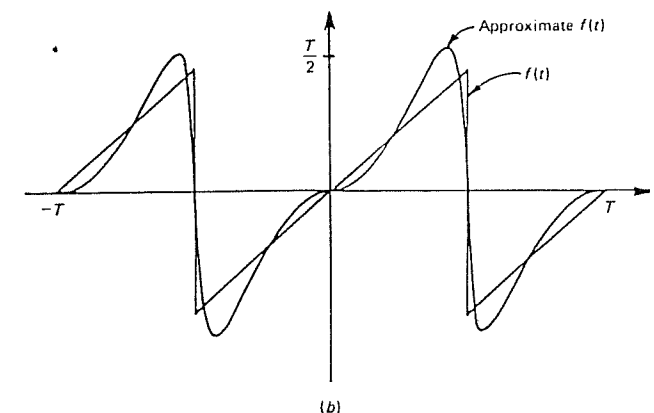


Fig. 2.20 Fourier spectrum of a sawtooth waveform. (a) Fourier coefficients. (b) Sawtooth,  $f(t)$ , together with an approximation of  $f(t)$  using the two largest components of the Fourier spectrum.

transform in terms of the following set of transformations:

$$T \rightarrow \infty$$

$$n\omega_0 \rightarrow \omega,$$

$\omega$  being a continuous variable, and

$$a_n \rightarrow a(\omega)d\omega.$$

Taking the appropriate limits leads to the following conversions:

$$f(t) = \sum_{n=-\infty}^{\infty} a_n e^{in\omega_0 t} \text{ becomes } f(t) = \int_{-\infty}^{\infty} a(\omega) d\omega e^{i\omega t} \quad (2.19)$$

and

$$a_n = \frac{\omega_0}{2\pi} \int_{-\infty}^{\infty} f(t) e^{-i\omega_0 t} dt \text{ becomes } a(\omega) d\omega = \frac{d\omega}{2\pi} \int_{-\infty}^{\infty} f(t) e^{-i\omega t} dt. \quad (2.20)$$

The two right hand expressions lead to reciprocal expressions for the Fourier transform,

$$a(\omega) = \frac{1}{2\pi} \int_{-\infty}^{\infty} f(t) e^{-i\omega t} dt, \quad (2.21)$$

and the original function,

$$f(t) = \int_{-\infty}^{\infty} a(\omega) e^{i\omega t} d\omega. \quad (2.22)$$

As noted earlier, the Fourier transform  $a(\omega)$  often turns out to be complex, and it is useful to define a real-valued function, the *power spectrum*, as

$$S(\omega) = |a(\omega)|^2. \quad (2.23)$$

One might compare this definition with the relation between wave amplitude and wave energy. The power spectrum is the quantity typically calculated in experimental or numerical work.

Let us consider two examples that can be solved analytically.

#### Example 2.5

Let  $f(t)$  be a decaying, oscillating function

$$f(t) = \begin{cases} e^{-\gamma t} e^{i\omega_0 t}, & t \in [0, \infty) \\ 0 & , t \in (-\infty, 0] \end{cases}$$

as shown in Figure 2.21(a). The function has a natural frequency  $\omega_0$ . It could represent a dissipative, tuned electrical circuit, for example. Calculation of the integral for  $a(\omega)$  leads to

$$a(\omega) = \frac{1}{2\pi[\gamma + i(\omega - \omega_0)]}$$

and then

$$S(\omega) = \frac{1}{4\pi^2[\gamma^2 + (\omega - \omega_0)^2]}.$$

This function is called a *Lorentzian* and is shown in Figure 2.21(b).  $S(\omega)$  is symmetric about the dominant 'natural' frequency,  $\omega_0$ , but because of the damping parameter  $\gamma$ , it has a finite width.

#### 2.3 Spectral analysis of time series

If  $\gamma \rightarrow 0$ , then  $S(\omega)$  becomes very sharp (approaching a delta function) with all the power then concentrated in the  $\omega_0$  component.

There is generally a reciprocal relationship between the width of  $f(t)$  and the width of its Fourier transform (or  $S(\omega)$ ). In Example 2.5, the width of  $f(t)$  associated with the decaying exponential envelope is  $\Delta t = 1/\gamma$ , whereas the width of the Lorentzian  $a(\omega)$  is  $\Delta\omega = \gamma$ . The product of the complementary widths is a constant of order unity. As  $f(t)$  sharpens in the time domain,  $a(\omega)$  broadens in the frequency domain, and vice versa.

#### Example 2.6

Let  $f(t)$  be a wave modulated by a *Gaussian* curve:

$$f(t) = e^{-t^2/2\sigma^2} e^{i\omega_0 t}, \quad t \in (-\infty, +\infty),$$

as illustrated in Figure 2.22(a). Calculation of the integral  $a(\omega)$  leads to

$$S(\omega) = e^{-(\omega - \omega_0)^2/\sigma^2},$$

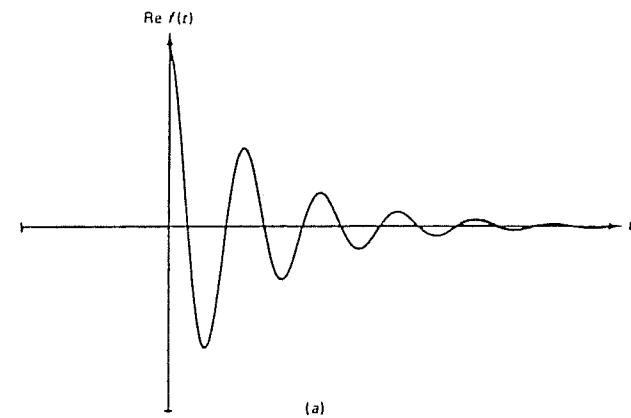
which is Gaussian as shown in Figure 2.22(b). It may be shown (Problem 2.13) that the width of  $f(t)$  is about  $\Delta t = \sigma$ , and the width of  $S(\omega)$  is about  $\Delta\omega = 1/(\sqrt{2}\sigma)$ , the same reciprocal relationship between the widths holding as in Example 2.5.

#### Example 2.7

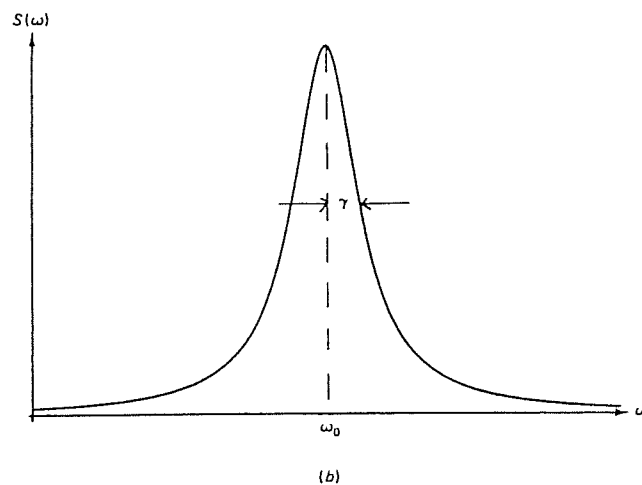
Let  $f(t)$  be a linear superposition of two oscillations, with frequencies of  $f_1 = 2$  and  $f_2 = 3$ , with amplitudes of  $A_1 = 2$  and  $A_2 = 1$ , respectively, as illustrated in Figure 2.23(a). The corresponding power spectrum shown in Figure 2.23(b) was obtained numerically, and one easily observes the 4:1 ratio of the spectral intensities.

#### Example 2.8

Various types of electrical noise are easily represented by their power spectra. For example, Johnson noise which results from thermal agitation in electric circuits is frequency-independent or 'white' (in analogy with white light). On the other hand, ' $1/f$ ' noise, which is common in resistors and solid state devices, has a spectrum varying as  $f^{-1}$  (or another power) at low frequencies (Malmstadt, Enke, and Crouch, 1981). These two types are illustrated in Figure 2.24.



(a)

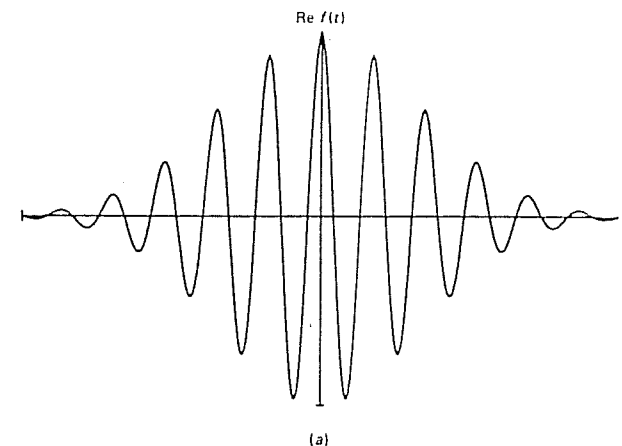


(b)

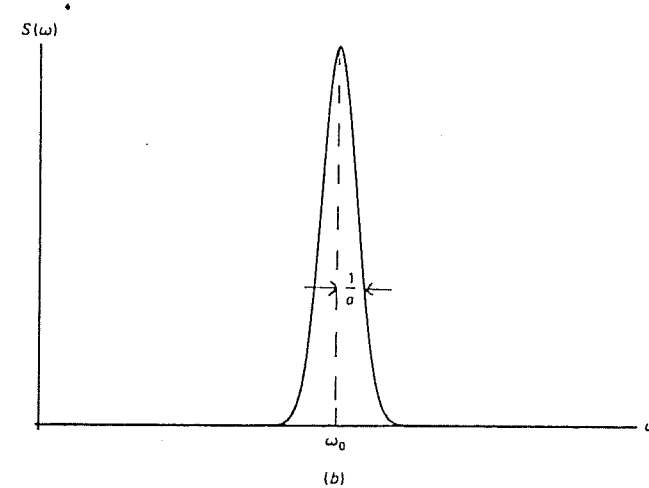
Fig. 2.21 (a) The real part of the decaying exponential time series of Example 2.5.  
 (b) Power spectrum.

Fourier analysis is an interesting subject and the reader who wishes to study it further may find helpful the treatment in Kaplan (1973). Occasionally a brief discussion in the context of quantum physics is provided in the modern physics sections of the introductory physics texts. See, for example, Orear (1979).

Analytical calculation of the Fourier transform can become very



(a)



(b)

Fig. 2.22 (a) The real part of the Gaussian time series of Example 2.6. (b) Power spectrum.

difficult if the time variation is at all complicated, but numerical methods are straightforward. At first glance, it appears that the appropriate algorithms would involve numerical integration. However, a distinctly different and very efficient approach may be taken when the data are discrete or digitized. The algorithm is called the *fast Fourier transform* (FFT) and was reinvented by J.W. Cooley and J.W. Tukey in 1964. (The method had originally been discovered in 1942 and utilized with hand calculators.) It takes advantage of certain symmetry properties in the

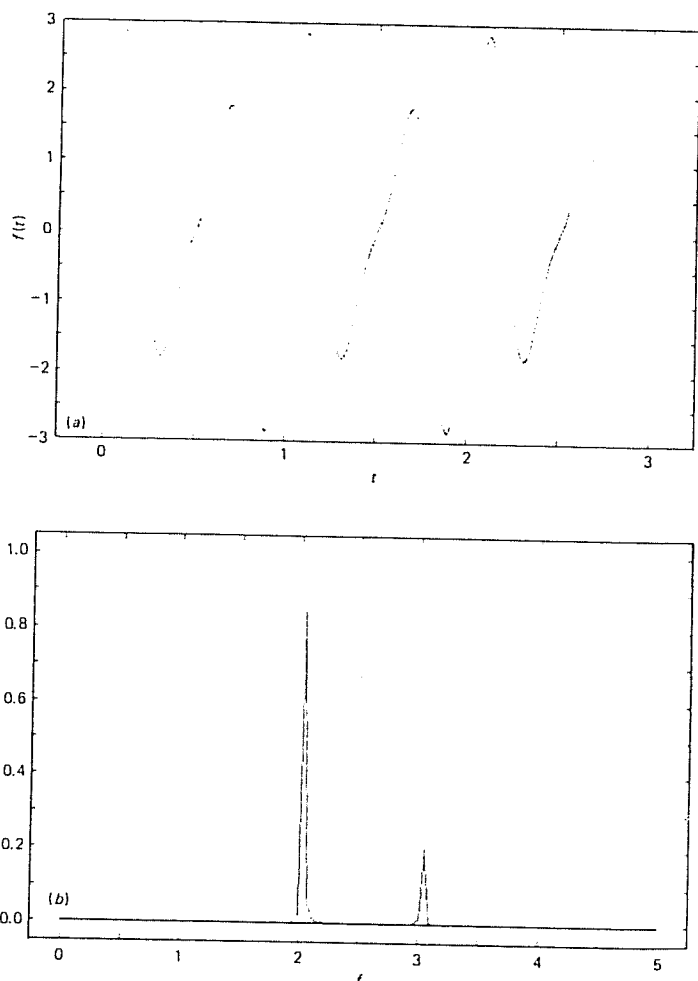


Fig. 2.23 (a) Two component time series.  
(b) Power spectrum.

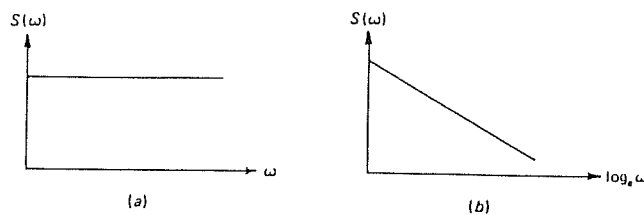


Fig. 2.24 Power spectra of noise time series. (a) White noise. (b)  $1/f$  noise.

trigonometric functions at their points of evaluation, in order to achieve an increase in speed over more conventional methods. If  $N$  is the number of data points in the time variation of a signal, then conventional algorithms would require about  $N^2$  computer operations, whereas the FFT requires about  $N \log_2 N$  operations. For a 1000 point transform this means a reduction by a factor of about 100, and larger samples lead to even more significant gains. A short introduction is provided in Higgins (1976) and a listing in BASIC is given in Appendix B. (A more comprehensive treatment is available in Press *et al.* (1986), Chapter 12.)

With this background of mathematical tools now available, we may, in Chapter 3, concentrate more fully on the driven, damped pendulum.

### Problems

- 2.1 For the linearized undamped pendulum show that the solutions,  $\omega = A \sin t$  and  $\theta = A \cos t$ , lead to circular trajectories in the phase plane.
- 2.2 Show that one possible solution to the linearized damped pendulum:  $d^2\theta/dt^2 + d\theta/dt + \theta = 0$  is  $\theta = A e^{-\lambda t} \cos(\omega_0 t)$ . Show that  $\lambda = \frac{1}{2}$  and  $\omega_0 = \sqrt{3}/2$ .
- 2.3 A particle falls a distance  $x(t)$  in a gravitational field, with velocity  $v(t)$ . The system of equations is  

$$\begin{aligned} dx/dt &= v, \\ dv/dt &= g. \end{aligned}$$

Show that the phase area is conserved. If a friction force,  $-kv$ , is added to the acceleration equation show that the phase area shrinks.
- 2.4 Hénon and Heiles studied stellar orbits in a galaxy using a two-dimensional model with a potential  $V(x,y) = \frac{1}{2}(x^2 + y^2) + x^2y - \frac{1}{3}y^3$ . This leads to a system of equations for the four-dimensional phase space of  

$$\begin{aligned} dp_x/dt &= -x - 2xy, \\ dp_y/dt &= -y - x^2 + y^2, \\ dx/dt &= p_x, \\ dy/dt &= p_y. \end{aligned}$$

Is this system dissipative?
- 2.5 One of the simplest sets of nonlinear equations that exhibits chaos

is due to Rossler (1976):

$$\begin{aligned} \frac{dx}{dt} &= -y - z, \\ \frac{dy}{dt} &= x + ay, \\ \frac{dz}{dt} &= b + xz - cz, \end{aligned}$$

where  $a = b = 0.2$  and  $c = 5.7$ . Show that for small  $x$  the system is dissipative.

- 2.6 Lorenz developed the following system of equations to describe the interrelations of temperature variation and convective motion

$$\begin{aligned} \frac{dx}{dt} &= -\sigma x + \sigma y, \\ \frac{dy}{dt} &= -xz + rx - y, \\ \frac{dz}{dt} &= xy - bz, \end{aligned}$$

where  $\sigma, r, b$  are positive constants. Prove that the system is dissipative.

- 2.7 Show that the system  $\frac{d^2\theta}{dt^2} + \frac{d\theta}{dt} + \sin\theta = 0$  linearizes to  $\frac{d^2\theta}{dt^2} + \frac{d\theta}{dt} + (\theta - n\pi) = 0$  near  $\theta = n\pi$  when  $n$  is even, and to  $\frac{d^2\theta}{dt^2} + \frac{d\theta}{dt} - (\theta - n\pi) = 0$  near  $\theta = n\pi$  when  $n$  is odd. In general one would use a Taylor's series expansion – can this case be treated more intuitively?

- 2.8 Find the general solution to  $\frac{d^2\theta}{dt^2} + \frac{d\theta}{dt} - (\theta - n\pi) = 0$  when  $n$  is odd.

- 2.9 Consider the nonlinear second order differential equation of Problem 2.7 written as two first order equations:

$$\begin{aligned} \frac{d\omega}{dt} &= -\omega - \sin\theta, \\ \frac{d\theta}{dt} &= \omega. \end{aligned}$$

The special points  $\theta = n\pi$  and  $\omega = 0$  are called *critical points* or *fixed points* because the time derivatives of  $\theta$  and  $\omega$  are zero at these points. Such points may be stable or unstable. Discuss the stability of the pendulum's motion near these points. Distinguish between odd and even values of  $n$ .

- 2.10 Find the fixed points of the Lorenz system as given in Problem 2.6 by setting the time derivatives equal to zero. Assume that  $\sigma > 0$ ,  $r > 1$ , and  $b > 0$ . The trajectory of this system orbits chaotically about the two fixed points producing a pattern that resembles a butterfly. (See Chapter 6.)

- 2.11 Find the fixed points of the Rossler systems (Problem 2.5).

- 2.12 Apply the procedure of linearization to the Lorenz system as outlined in the text for the pendulum. That is, linearize each nonlinear term in the Lorenz equations with a first order Taylor

series expansion near a fixed point  $(x_0, y_0, z_0)$ . The resulting set of linear differential equations are soluble.

- 2.13 Linearize the nonlinear Rossler equations (Problem 2.5) about a fixed point  $(x_0, y_0, z_0)$

- 2.14 Following the rationale of Figure 2.17 develop the Poincaré plot for

$$(i) \omega = \frac{2}{3}\omega_s \text{ and } (ii) \omega = \frac{1}{3}\omega_s.$$

- 2.15 (a) Find the power spectrum of the 'square' wave packet:

$$f(t) = \begin{cases} a & t \in [0, \pi/2] \\ 0 & \text{for all other values of } t. \end{cases}$$

$$(b) \text{Show that the average power is } f(t)^2 = a^2,$$

- 2.16 Prove the formula given in the text for the Fourier series amplitudes,  $a_n$ .

- 2.17 Develop the results for  $a_n$  in Example 2.4.

- 2.18 Do the calculation of  $S(\omega)$  for the decaying exponential wave to obtain the Lorentzian curve.

- 2.19 Calculate the width of the Gaussian power spectrum.

The following problems require the use of a computer. Listings provided in Appendix B may be helpful, although they were primarily developed for the driven, damped pendulum, and therefore have to be modified for these exercises.

- 2.20 Write a program which will display trajectories in phase space for the undamped, linearized pendulum. The program should require a set of initial  $(\theta, \omega)$  coordinates as input. Remember to keep  $\theta$  reasonably small so that  $\sin\theta \approx \theta$ .

- 2.21 Write a program which will display trajectories in phase space for the damped, linearized pendulum. Use the equation

$$\frac{d^2\theta}{dt^2} + \gamma \frac{d\theta}{dt} + \omega_0^2 \theta = 0.$$

- 2.22 Modify the program described in Problem 2.21 so that the term in  $\theta$  becomes  $\omega_0^2 \sin\theta$  and try various inputs. In this case you should modify the display of the  $\theta$  coordinate so that its boundary conditions become periodic, as outlined in the chapter.

- 2.23 Modify the program described in Problem 2.20 so that the input will be a set of initial coordinates which will form an initial area. The program should then demonstrate the motion of the given area in phase space.

- 2.24 Modify the program described in Problem 2.21 to follow the evolution of a block of initial coordinates. The development of this

- phase space should illustrate a dissipative system.
- 2.25 Develop a program to illustrate Poincaré sections similar to those shown in Figure 2.17. Use the linearized version of the pendulum.
  - 2.26 In Appendix B the program called EXPFFT computes the power spectrum of a linear combination of periodic components. Use this program to look at  $f(t) = \sin(2\pi f_0 t)$ . Use a Nyquist frequency of 1 and sample 32 points for  $f_0 = \frac{1}{8}$ . Try different numbers of points and different Nyquist frequencies. (The Nyquist frequency is the maximum frequency shown by the spectrum.) Try to determine the relationships which involve the number of points, the Nyquist frequency, and the resolution in frequency of the power spectrum.
  - 2.27 Modify the above program to display the power spectrum of the function  $e^{-t}$  on  $[0, \infty)$ . Experiment with a variety of conditions (Nyquist frequency, number of points, etc.) in your program.

## 3

# Visualization of the pendulum's dynamics

Using the tools described in Chapter 2, we are now in a position to discuss the main features of the motion of the driven pendulum. The equations of motion may be written as:

$$\left. \begin{aligned} d\omega/dt &= -\omega/q - \sin\theta + g\cos\phi, \\ d\theta/dt &= \omega, \\ d\phi/dt &= \omega_D. \end{aligned} \right\} \quad (3.1)$$

Since the system has three variables, its trajectory resides in a phase space of three dimensions, the minimum for chaotic behavior. In this chapter, we present and discuss a variety of computer simulations in order to characterize the dynamics of the pendulum. To allow compact illustration, values of  $\theta$  and  $\phi$  outside the range  $(0, 2\pi)$  are plotted at the equivalent point within that range.

The differential equations contain three adjustable parameters: the driving force amplitude  $g$ , the damping factor  $q$ , and the angular drive frequency  $\omega_D$ . One could define a three-dimensional parameter space in which each point represents a particular choice of the parameters  $(g, q, \omega_D)$ . However, a full exploration of the behavior as a function of all three parameters would be a forbidding task. Instead, we fix  $\omega_D$ , choose a few values of  $q$ , and let  $g$  vary sufficiently to obtain a wide variety of dynamical behavior. As an aid to making appropriate parameter choices, we note that a constant torque of unity is just sufficient to keep

the pendulum stationary at  $\theta = \pi/2$ . Therefore forcing amplitudes in the region  $g \approx 1$  are used. Furthermore, the undamped pendulum of small amplitude has a 'natural' angular frequency equal to 1 in our units. Interesting dynamics occur when the forcing-term amplitude is of order unity and the drive frequency  $\omega_D$  is near (but not equal to) 1. Part of the rich variety of dynamical behaviour comes from the interplay between the 'natural' frequency and the drive frequency. One set of parameters containing intervals of chaotic dynamics consists of  $q = 2$ ,  $\omega_D = 2/3$ , and  $0.5 \leq g \leq 1.5$  (Gwinn and Westervelt, 1985).

It is important that the reader develop an understanding of the physical content of the equations and diagrams. One way to accomplish this is to use a computer animation of the pendulum motion. The program in Appendix B entitled MOTION is one version of such a simulation. By running this program or a similar one, the reader can observe the pendulum's behavior for a variety of conditions (especially different values of  $g$ ). Figure 3.1 shows a 'multiple exposure snapshot' of that animation. We encourage the reader to utilize the simulation frequently while reading this chapter. For some parameter values the motion appears to be periodic, while for others it is chaotic. In some cases the pendulum is nearly periodic for substantial intervals, with intervening irregular intervals; the net effect is that the motion is chaotic.

We are concerned here with the long-term behavior of the pendulum rather than the initial transients, which can be different. Therefore, the animation should be allowed to go through 20 or 30 drive cycles before one considers the motion to have converged to its long-term or

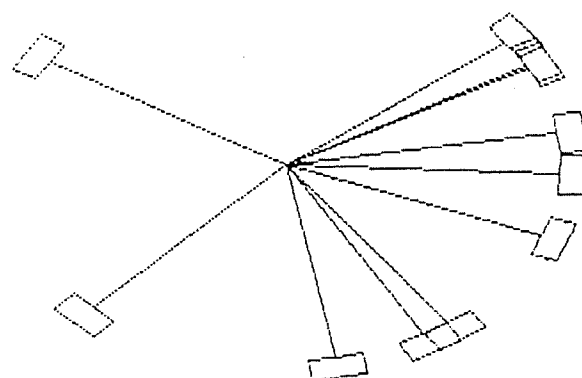


Fig. 3.1 A multiple exposure of the pendulum animation.

statistically stationary state. We will sometimes refer to the long-term behavior as the 'steady state', though the motion need not be time-independent.

Finally, the sensitivity of chaotic trajectories raises an interesting question about the use of computer simulations for the solution of unstable, nonlinear systems. Throughout this book we use numerical methods to generate chaotic orbits over very long periods of time. Yet these computations have their own sources of error; (a) the small inaccuracies introduced by the numerical methods used for integration of the equations, and (b) the finite number of significant figures used by the computer. In view of sensitivity to initial conditions we might think that these errors would multiply rapidly and that our computations would completely misrepresent the dynamics of the chaotic pendulum. Surprisingly, this is not a big problem and the fact that researchers with many different computers produce very similar geometric patterns from the same equations suggests that factors other than sensitivity to initial conditions are involved in this question. We explain this apparent paradox in Chapter 5.

### 3.1 Sensitivity to initial conditions

The fundamental characteristic of a chaotic physical system is its sensitivity to the initial state. Sensitivity means that if two identical mechanical systems are started at initial conditions  $x$  and  $x + \epsilon$  respectively, where  $\epsilon$  is a very small quantity, their dynamical states will diverge from each other very quickly in phase space, their separation increasing exponentially on the average. This phenomenon is illustrated for the pendulum in Figure 3.2(a). Phase trajectories of a chaotic pendulum, originating at two neighboring points, diverge markedly in less than one forcing period.

Sensitivity may also be illustrated by observing the phase space evolution of a block of pendulum states. (Figures 2.3 and 2.7 display unforced pendula in the undamped and damped cases, respectively.) Figure 3.2(b) shows the evolution of a block of initial phase points for the chaotic pendulum. After one half of a forcing period, the initial rectangular block has become long, thin, and curved. Because the system is dissipative, the area of the block shrinks with increasing time. Yet the set of phase points stretches along certain directions and contracts along other directions. The directions of divergence and shrinkage are different

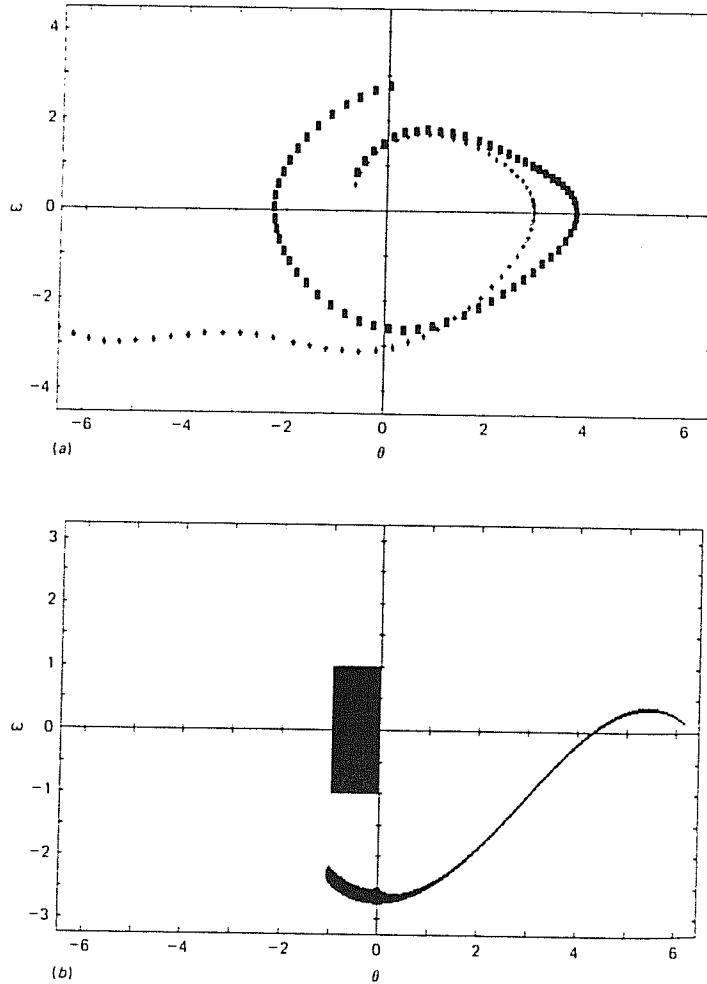


Fig. 3.2 Sensitivity to initial conditions. In (a) two phase trajectories, with neighboring initial points near the origin, evolve during one drive cycle ( $g = 1.5$ ,  $q = 4$ ). In (b) the phase points of trajectories from a block of initial points,  $-0.5 < \theta < 0$  and  $-0.5 < \omega < 0.5$ , are shown after one half of a drive cycle. (The diagram may be regarded as a projection of the three-dimensional phase trajectories onto the  $(\theta, \omega)$  plane.)

at different points in phase space. The net effect is that two closely spaced points are later found quite far apart.

The exponential divergence of adjacent phase points has a further consequence for the chaotic attractor. In order that the trajectories of two adjacent phase points remain bounded without intersecting, they must fold back on themselves, producing a three-dimensional chaotic attractor with many layers (actually an infinite number). A quantitative discussion of exponential divergence and the resulting geometrical complexity of the attractor is given in Chapters 4 and 5.

### 3.2 Phase diagrams and Poincaré sections

We now use the geometrical tools of Chapter 2 to characterize the driven pendulum at a variety of driving force amplitudes  $g$ . The other parameters are held fixed at  $\omega_D = 2/3$  and  $q = 2$ , though the effect of changing them is also interesting. (These parameters are pure numbers since the pendulum equation was made dimensionless.)

We begin by examining the trajectories in the three-dimensional space  $(\theta, \omega, \phi)$ , as shown in Figure 3.3. The first case is periodic, since the trajectory retraces its path exactly. The situations in Figures 3.3(b) and (c) are clearly more complicated, but it is difficult to tell exactly what has happened from this diagram. Finally, Figure 3.3(d) is a chaotic state, and the diagram is so complex as to be nearly useless as a way of characterizing the dynamics.

Clearly, a better method of displaying the dynamics is needed. Two-dimensional phase projections and Poincaré sections turn out to be helpful, and these are shown in Figure 3.4. The value of  $g$  for each pair of diagrams is given in the caption. The upper parts of Figure 3.4 show projections of the trajectories onto the  $(\theta, \omega)$  phase plane. In this space, periodic motion appears as a closed orbit. Of course, the projected orbits can appear to cross, and this occurs in the more complicated cases shown.

The lower parts of Figure 3.4 are the Poincaré sections, which are simply slices across the  $\phi$  axis of the three-dimensional attractor. Periodic orbits ((a), (b), (d), (e), (f)) appear as a finite number of dots (enlarged for clarity), while chaotic orbits ((c), (g)) form complicated sets containing an infinite number of points. We shall return to an examination of their structure shortly.

The shape of the Poincaré sections varies with the phase at which they are taken. Sections for different values of  $\phi$  are shown in Figure 3.5, and

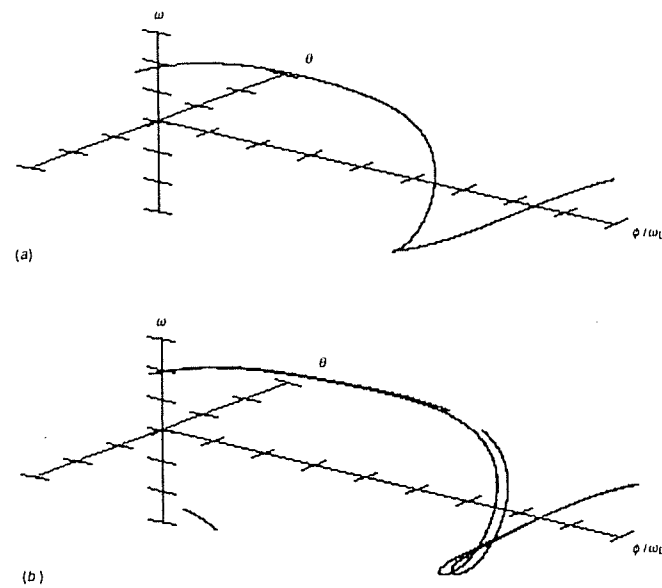


Fig. 3.3 Three-dimensional phase portraits for several values of driving force strength and  $q=2$ . (a)  $g=0.9$ ; (b)  $g=1.07$ ; (c)  $g=1.47$ ; (d)  $g=1.5$ . This last case is chaotic.

the aggregate of these shapes is similar to the full attractor of Figure 3.3(d). As  $\phi$  is increased, the attractors become stretched and folded repetitively, much like the kneading of dough. Evidence of this stretching and folding process may be seen in the fact that the sections contain a number of layers.

Actually, the structure of the attractors is much more complicated than is apparent from the sequence of Poincaré sections in Figure 3.5. This may be illustrated by looking at a small part of one of the sections, greatly magnified, as shown in Figure 3.6. The three parts of this diagram show the attractor at different scales of magnification. (The different scales are obtained simply by changing the window for the graph. Each graph is abstracted from a set of about 10 000 points.) The stretching and folding processes lead to a cascade of scales: the attractor consists of an infinite number of layers. The fine structure, when magnified, resembles the gross structure. This property is called *self-similarity*.

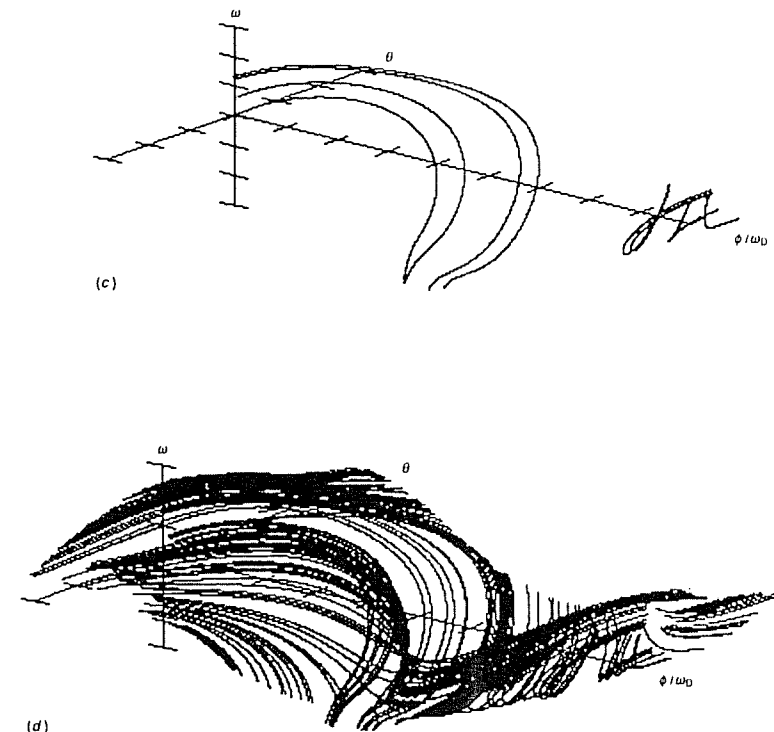
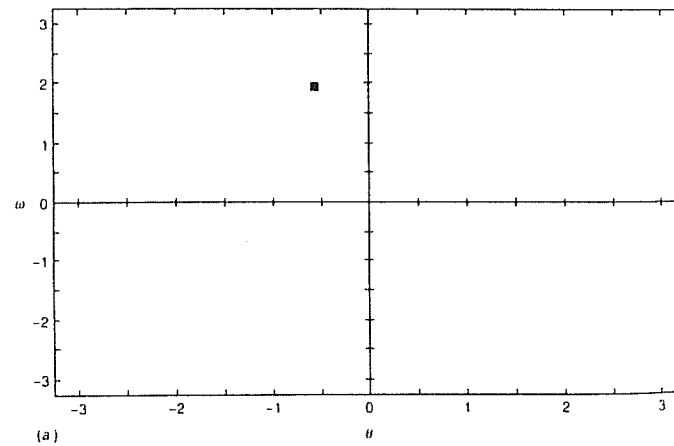
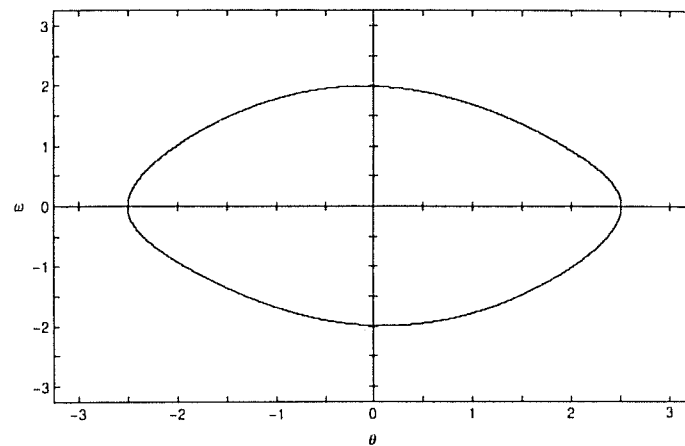


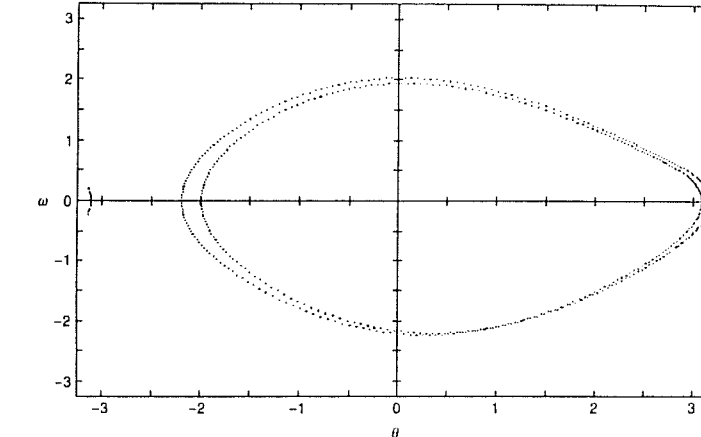
Fig. 3.3 *cont.*

These simulations of the chaotic attractor and its Poincaré sections reveal a hierarchical structure that is uncharacteristic of ordinary compact geometrical objects. In Chapter 5 the chaotic attractor and corresponding Poincaré sections are discussed as *fractals* – mathematical sets of noninteger dimension. While the periodic attractor is one-dimensional (Figures 3.3(a), (b), and (c)) and its Poincaré section is zero-dimensional (a few points), chaotic attractors are more complex, and their dimension is a fraction greater than two (see Chapter 5). Attractors having noninteger dimension are called *strange attractors*.

Finally, in Figure 3.7, we show several chaotic Poincaré sections corresponding to different values of the damping coefficient  $q$ . The layers of the attractor are more widely spaced as the damping decreases (or  $q$  increases).



(a)



(b)

Fig. 3.4 Phase plane (above) and Poincaré sections (below) for several values of driving force amplitude and  $q=2$ . In some cases the dots of the Poincaré sections have been enlarged for clarity. (a)  $g=0.9$ ; (b)  $g=1.07$ , and a period doubling is apparent; (c)  $g=1.15$ , and the system is chaotic; (d)  $g=1.35$ , and the system is periodic again; (e)  $g=1.45$ , and another period doubling has occurred; (f)  $g=1.47$ , and a second period doubling is apparent; (g)  $g=1.50$ , another chaotic state.

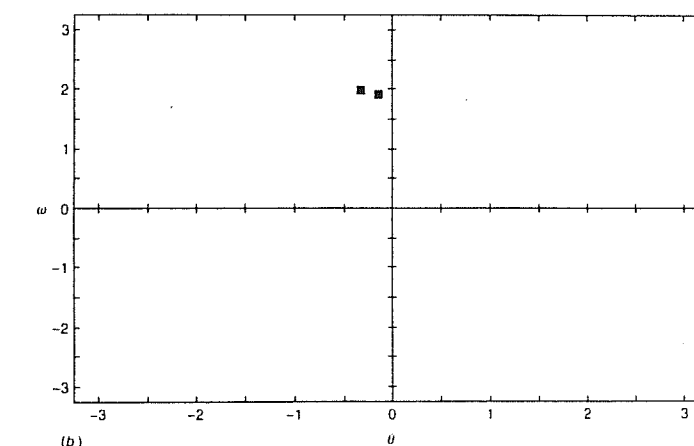


Fig. 3.4 cont.

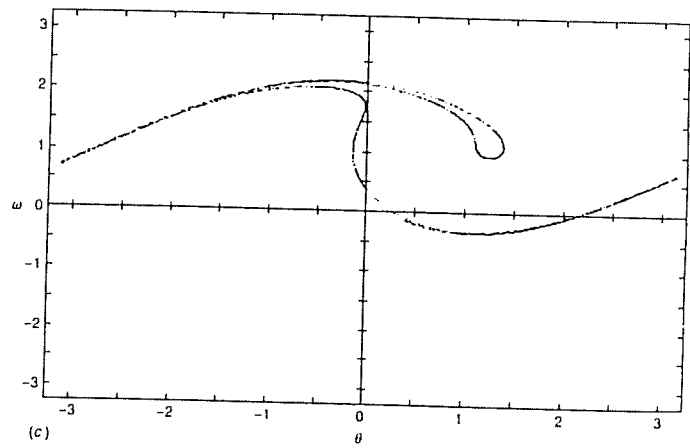
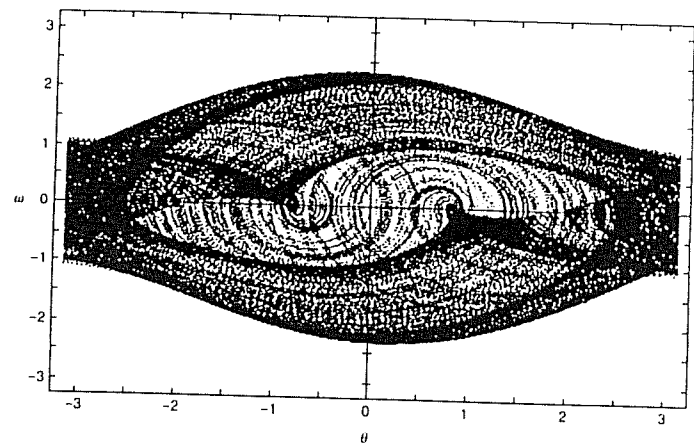


Fig. 3.4 *cont.*

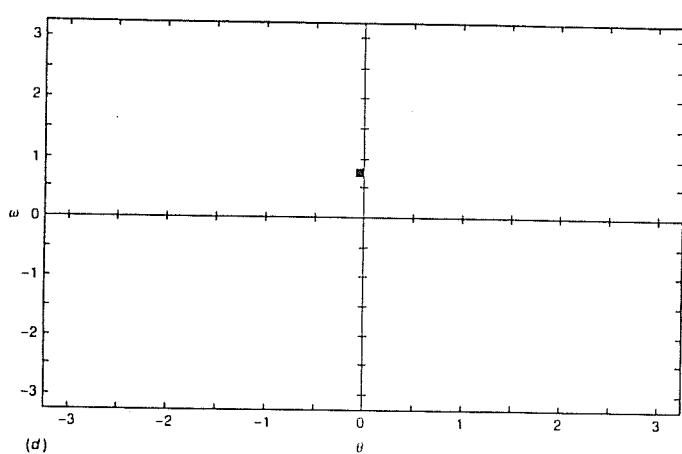
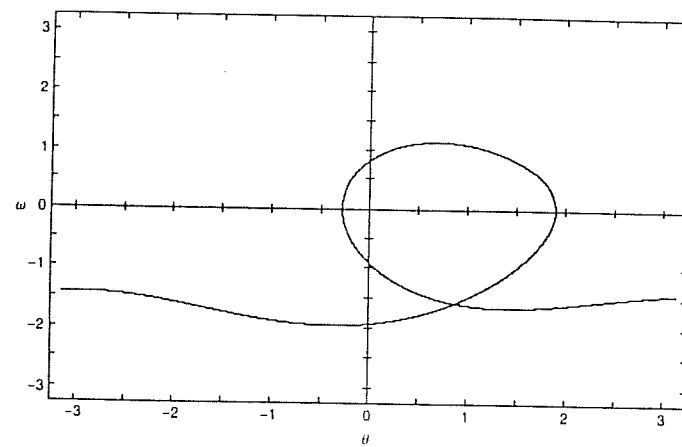
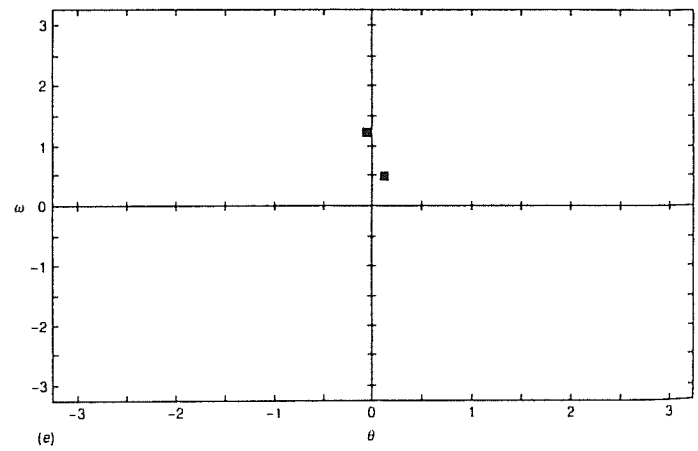
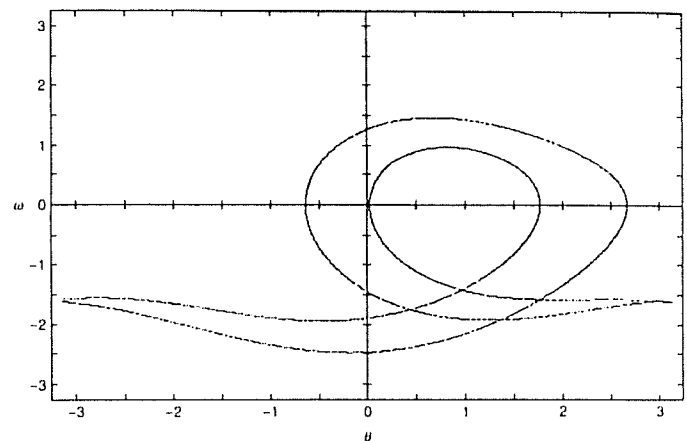
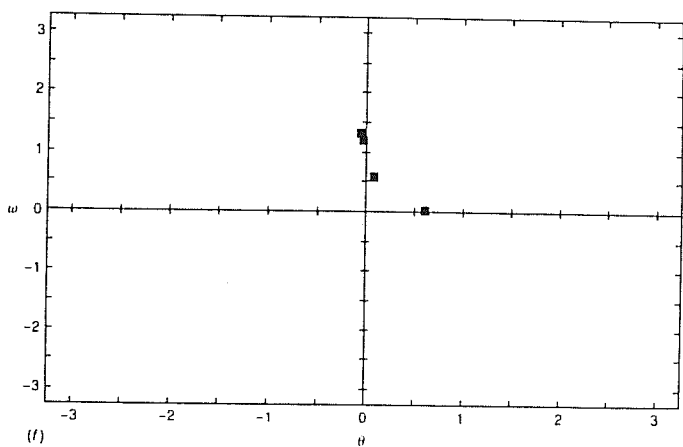
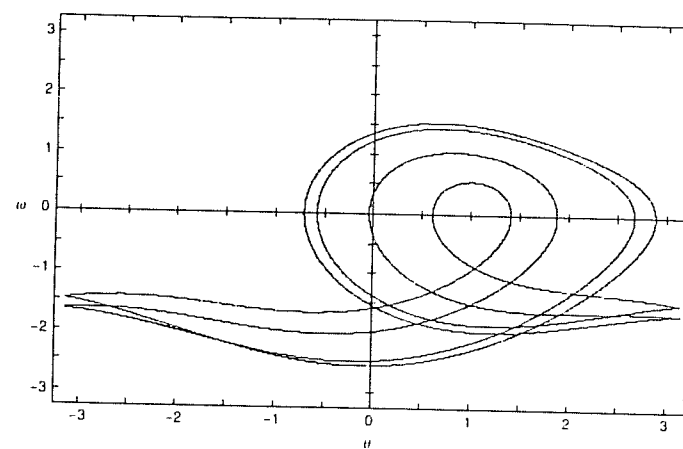


Fig. 3.4 *cont.*

Fig. 3.4 *cont.*Fig. 3.4 *cont.*

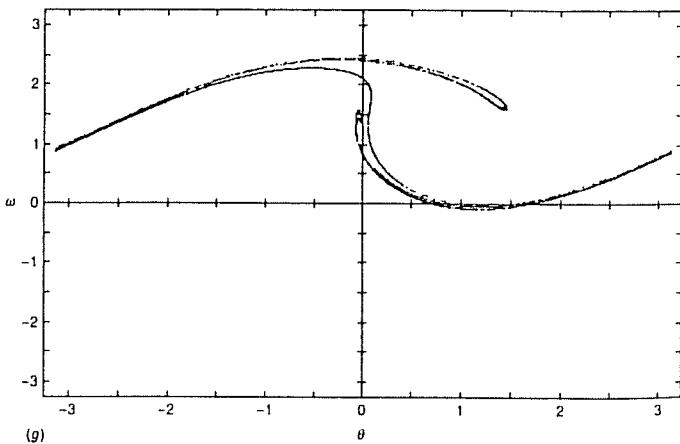
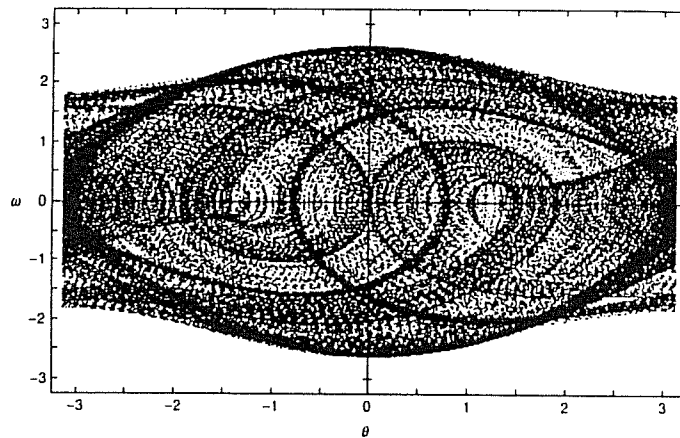
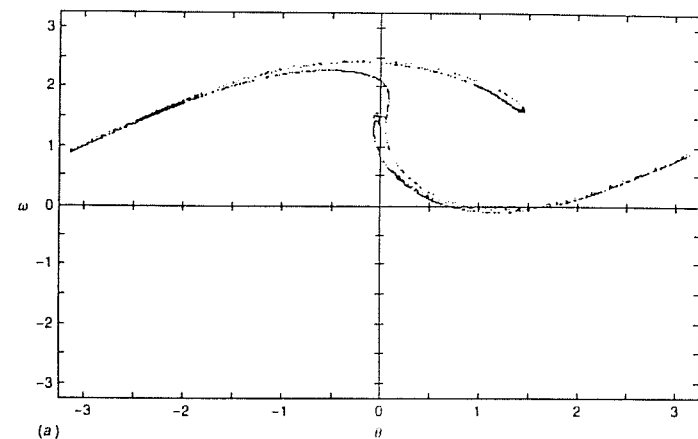
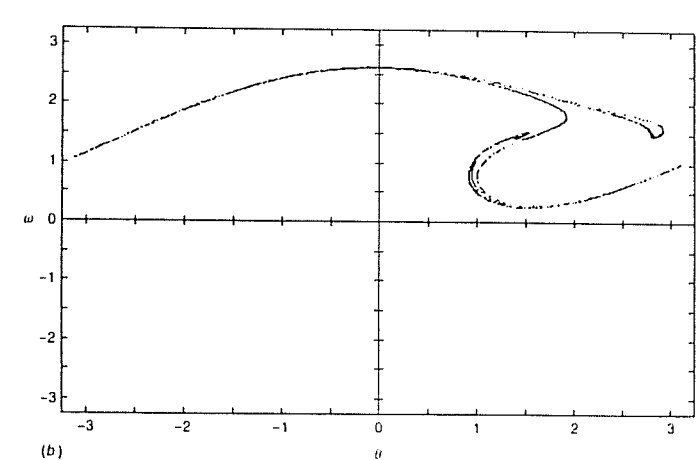


Fig. 3.4 *cont.*

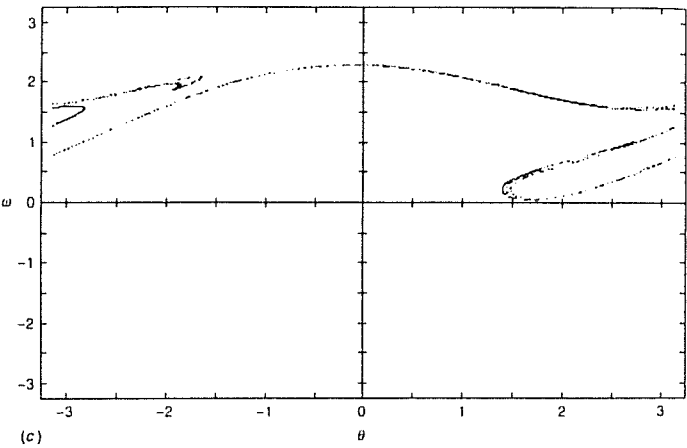


(a)

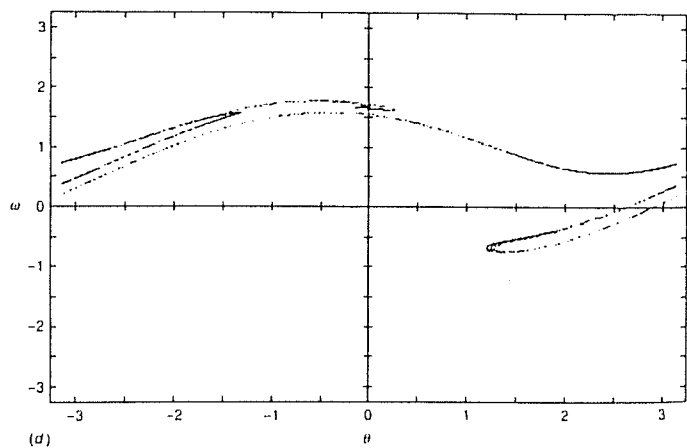


(b)

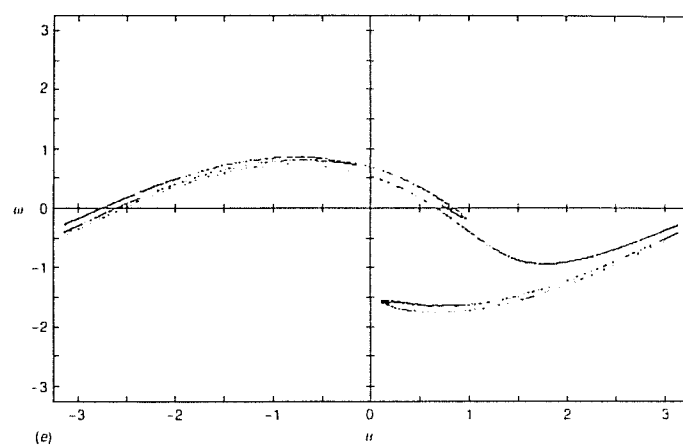
Fig. 3.5 Poincaré sections taken at incremented values of  $\phi$ , the phase of the forcing term.  $\Delta\phi = 2\pi/10$ . At  $\phi = \pi$  the section is anti-symmetric to the  $\phi = 0$  case.  $g = 1.5$ ,  $q = 2$ . (a)  $\phi = 0.0$ , (b)  $\phi = 0.628319$ , (c)  $\phi = 1.25664$ , (d)  $\phi = 1.88496$ , (e)  $\phi = 2.51327$ , (f)  $\phi = 3.14159$ .



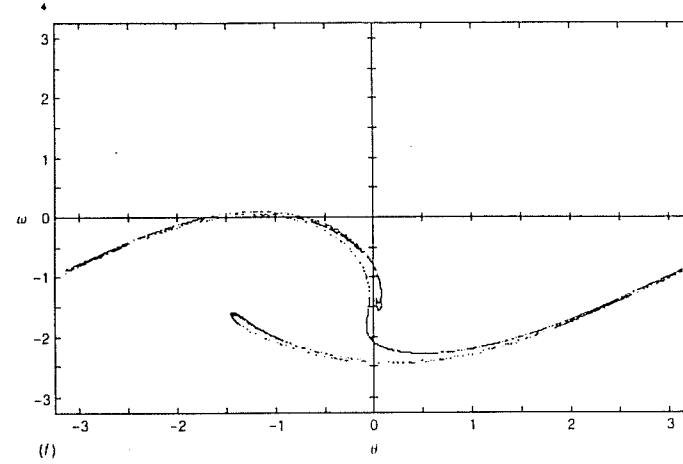
(c)



(d)

Fig. 3.5 *cont.*

(e)



(f)

Fig. 3.5 *cont.*

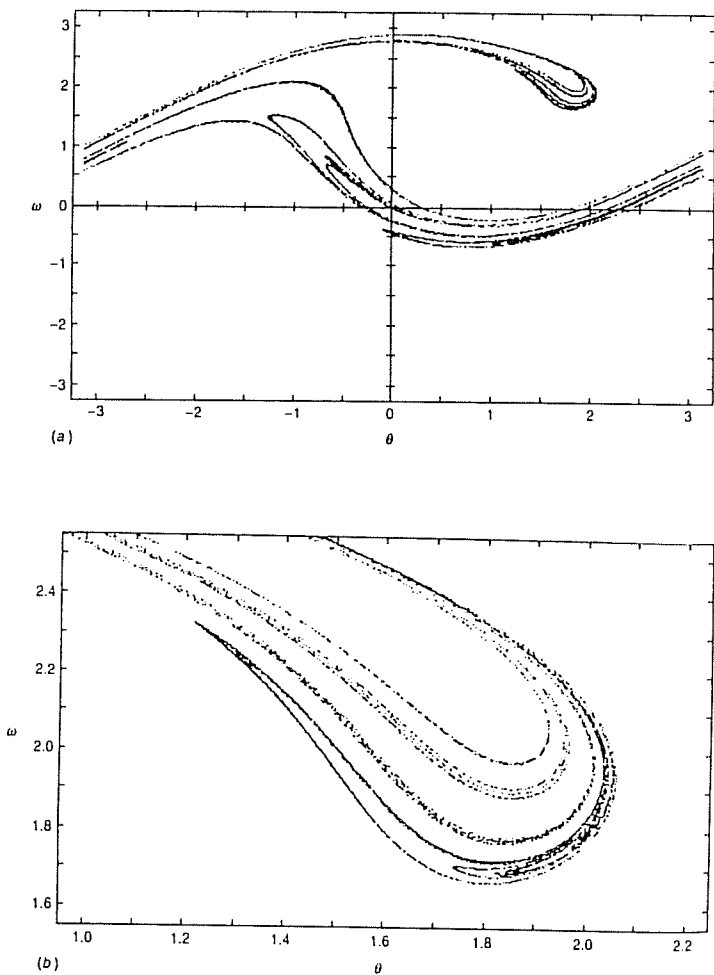


Fig. 3.6 (a)–(c) Attractor in the Poincaré section for  $q=4$  and  $g=1.5$  viewed at different magnifications, thus revealing the self-similar structure caused by the folding and stretching of phase volume.

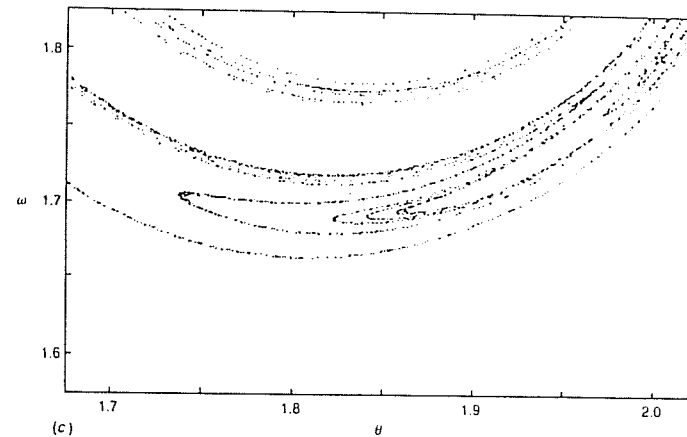


Fig. 3.6 *cont.*

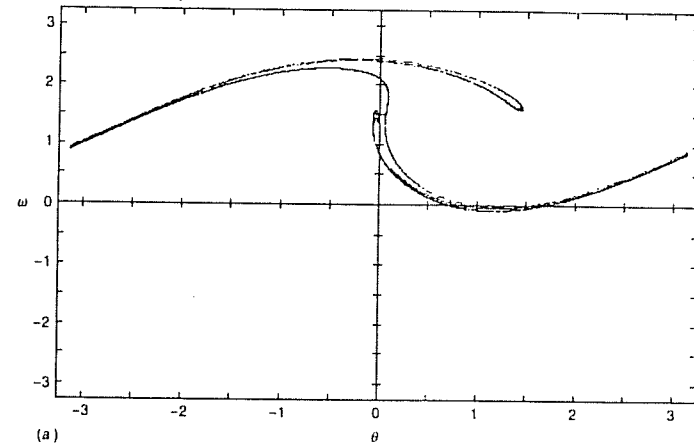


Fig. 3.7 Attractors in the Poincaré section for chaotic states of pendula with different amounts of damping ( $g=1.5$ ): (a)  $q=2$ , (b)  $q=2.8$ , (c)  $q=4$ .

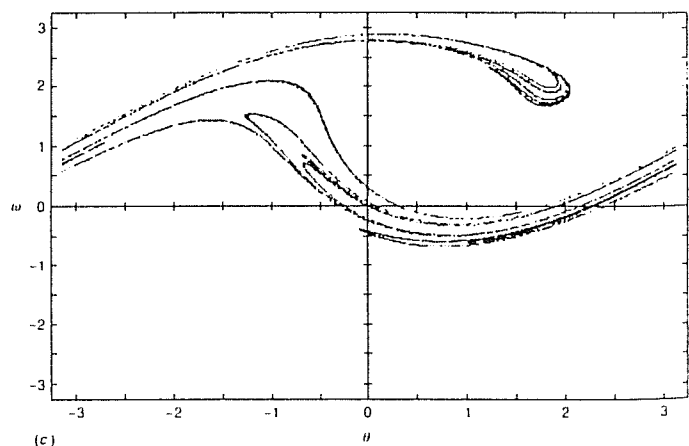
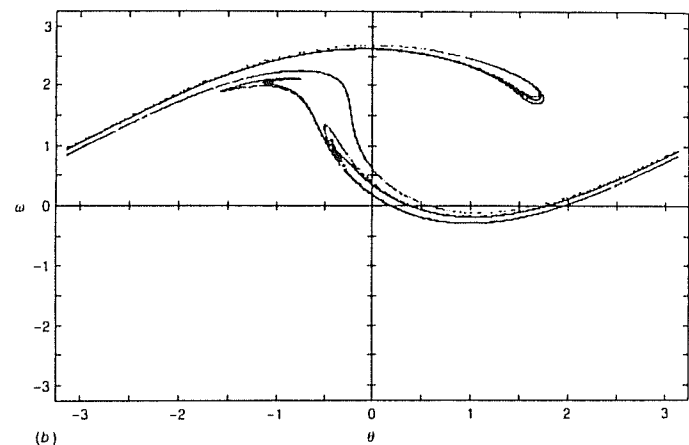


Fig. 3.7 cont.

### 3.3 Time series and power spectra

In Chapter 2 the power spectrum was introduced as a representation of the relative abundance of different frequencies in a given time series. Figure 3.8 shows a time series and power spectrum for the angular velocity  $\omega$  at a drive amplitude of  $g=0.95$ . The time series in Figure 3.8(a) shows a periodic oscillation. The corresponding power spectrum (Figure 3.8(b)) exhibits a strong peak at the drive frequency,  $1/(3\pi)$  together with some higher frequency harmonics. The harmonics are not unexpected since the phase space pattern is asymmetric. Logarithmic plots are used to highlight components with low power levels – an important feature of chaotic spectra.

In Figure 3.9 a corresponding set of diagrams is given for a chaotic state at  $g=1.5$ . The time series is obviously irregular. The power spectrum is broadband, and contains substantial power at low frequencies. A sharp component at  $\omega_D/2\pi$  is also present. Though a broad spectrum does not guarantee sensitivity to initial conditions, it is, in practice, a reliable indicator of chaos.

This book is primarily concerned with dynamical systems defined by sets of differential equations. However, it is worth noting that power spectra are also very useful for the analysis of experimental data. Measurements typically include time series of some dynamical variable, and the corresponding power spectrum can be readily analyzed to determine the state of the system. (See, for example, Gollub and Benson (1980) and Iansiti *et al.* (1985).)

Another useful technique for distinguishing chaotic and nonchaotic motions is the calculation of *Lyapunov exponents*, which are quantitative measures of the evolution of neighboring phase trajectories. As with Fourier analysis, the method is applicable to both numerical and experimental data; we describe it in Chapter 5.

### 3.4 Basins of attraction

Figure 2.13 showed the phase portrait of the damped *unforced* pendulum. Each of the point attractors at  $\theta=2n\pi$  ( $n=\text{integer}$ ) is encompassed by a region called a *basin of attraction*. All the points  $(\theta, \omega)$  in the basin converge on the enclosed point attractor. The boundary between two basins of attraction is called the *separatrix*. For the case cited, the

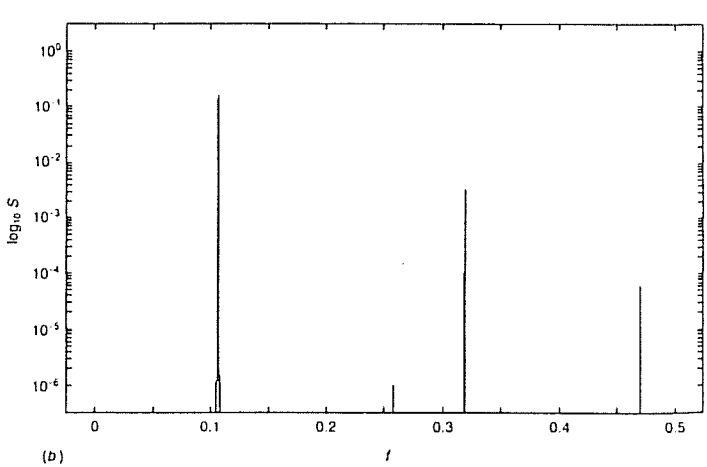
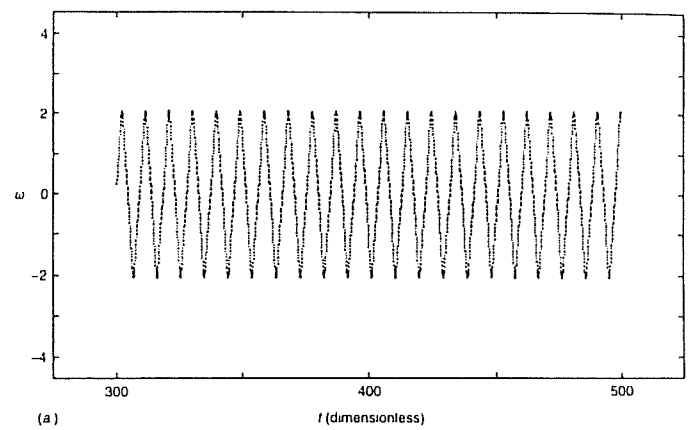


Fig. 3.8 (a) Time series and (b) power spectrum of angular velocity,  $\omega$ , for periodic motion at  $g=0.95$ .

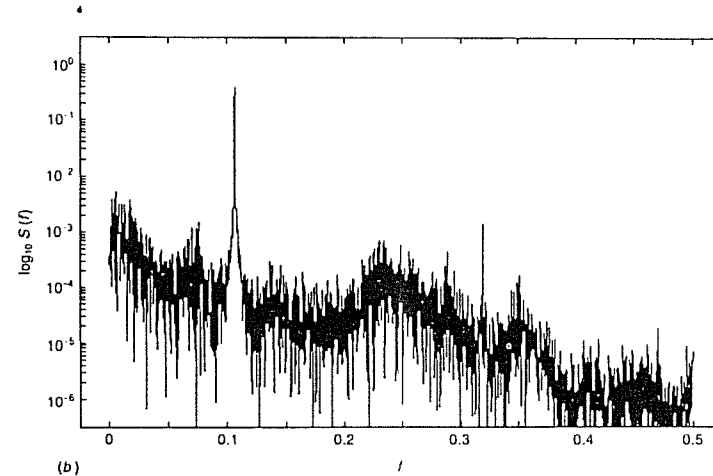
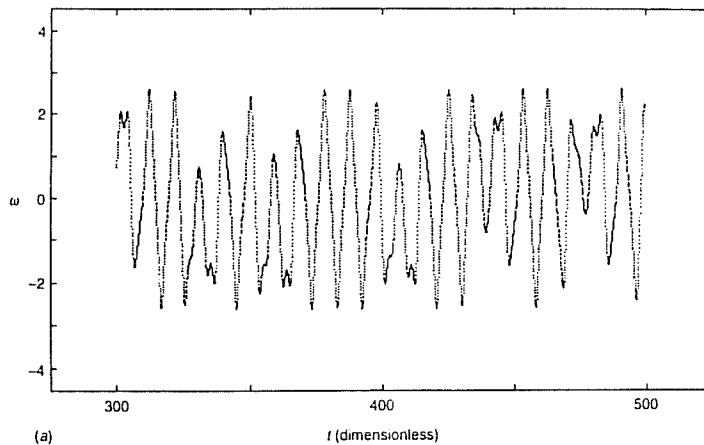


Fig. 3.9 (a) Time series and (b) power spectrum of angular velocity for chaotic motion at  $g=1.5$ . The peak is located at the drive frequency.

separatrix is a line defined by the stable phase trajectory going to the saddle point as shown in Figure 2.13.

In order to determine basins of attraction for the *forced* pendulum numerically, it is necessary to take advantage of some property that differs from one basin to another. For example (Gwynn and Westervelt, 1985), one can use the fact that, in the region  $g > 1.3$ , there are two stable rotary modes with average components of angular velocity close to  $\pm \omega_D$  for the different basins. The phase portraits of these modes are shown in Figures 3.10(a) and (b).

The basins of attraction are obtained by taking each pair  $(\theta, \omega)$  of initial conditions on a grid and calculating the trajectory of that pair over many cycles. To eliminate transient effects, the first 30 cycles are discarded; and the velocity is then averaged over the remaining cycles. The two basins of attraction are distinguished by the *sign* of  $\langle \omega \rangle$  and, for positive  $\langle \omega \rangle$  a circle is put at the corresponding location of the initial condition. Figure 3.11 shows the basins of attraction for  $g = 1.3$ , a periodic state.

On a large scale the basins of attraction of Figure 3.11 bear some resemblance to those of the undriven pendulum, but the basin boundaries appear fuzzy. In fact, careful studies (Gwynn and Westervelt, 1986) have shown the boundaries to be fractals (see Chapter 5); that is, the basins are interwoven near the boundaries. If the initial phase space coordinates of a trajectory near the boundary are not specified precisely, the basin of attraction for the trajectory is uncertain. This uncertainty is related to the fractal dimension of the boundary.

Further insight may be gained by looking at the basins of attraction with the Poincaré section superposed (Gwynn and Westervelt, 1985). This type of diagram may be generated by insertion of the Poincaré algorithm into the basin of attraction program. For a nonchaotic state one finds that each piece of the Poincaré section is unambiguously inside a single basin of attraction, as in the case  $g = 1.47$ . (See Figure 3.12(a) where the Poincaré attractor consists of eight points, four from each of the two sets of initial conditions.) For  $g = 1.48$ , Figure 3.12(b), the attractors spread out, reaching toward the basin boundaries. Finally, in the chaotic state for  $g = 1.5$ , the basin structure breaks up, and the previously separate attractors corresponding to two different initial conditions join together to form a single attractor consisting of an infinite number of lines, as shown in Figure 3.12(c).

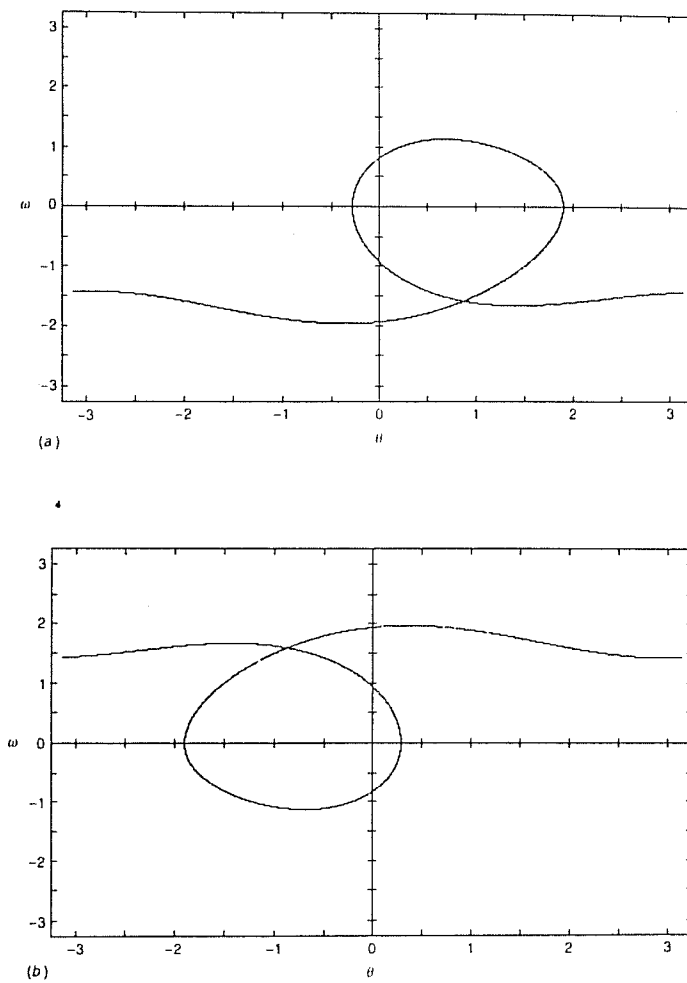


Fig. 3.10 Phase plane for  $g = 1.35$  and  $q = 2$  showing positive and negative drifting states for different initial conditions: (a)  $\theta_0 = 0, \omega_0 = 0$ ; (b)  $\theta_0 = 0, \omega_0 = 2.3$ .

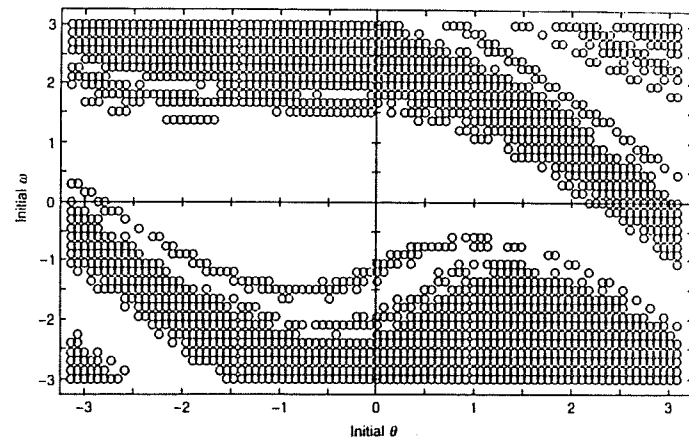
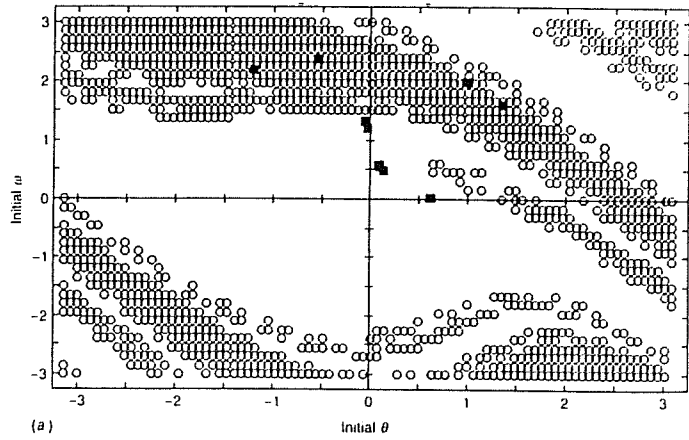
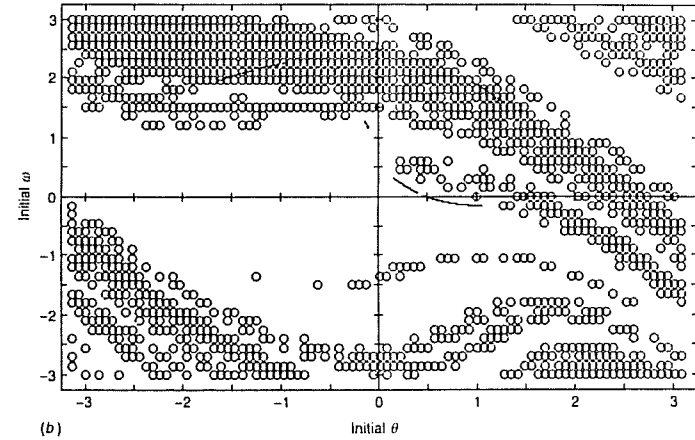


Fig. 3.11 Basin of attraction for  $g = 1.3$ , a state of periodic motion. The circles indicate positive drift of the angular velocity. The blank regions correspond to negative average angular velocity. The basins are intertwined.

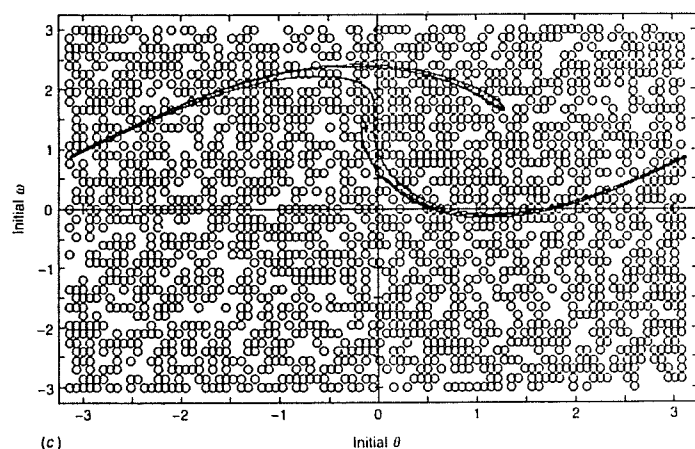


(a)

Fig. 3.12 Basins of attraction with the superposed Poincaré sections. The open circles indicate a positive average  $\langle \omega \rangle$ . (a) The Poincaré section consists of small clusters of points when  $g = 1.47$ . (b) The attractors have spread toward the basin boundaries for  $g = 1.48$ . (c) The separate attractors corresponding to two different initial conditions merge and the basins lose their identities at the onset of chaos. Here,  $g = 1.5$ . In each case  $q = 2$ .



(b)



(c)

Fig. 3.12 *cont.*

### 3.5 Bifurcation diagrams

Phase diagrams, Poincaré sections, time series, and power spectra provide information about the dynamics of the pendulum for specific values of the parameters  $g$ ,  $q$ , and  $\omega_D$ . The dynamics may also be viewed more globally over a range of parameter values, thereby allowing simultaneous comparison of periodic and chaotic behavior. The bifurcation diagram provides a summary of the essential dynamics and is therefore a useful method of acquiring this overview.

For some values of the parameters, a pendulum will have only one long-term motion, while for other slightly different choices, two or more motions may be possible. If several of them are stable, the actual behavior will depend on initial conditions. In dynamics a change in the number of solutions to a differential equation as a parameter is varied is called a *bifurcation*.

For the pendulum, bifurcations can be easily detected by examining a graph of  $\omega$  (at a fixed phase in the drive cycle) versus the drive amplitude  $g$ . Several examples of these graphs, called *bifurcation diagrams*, are shown in Figure 3.13. The interpretation is relatively straightforward. If the pendulum is lightly driven and the motion is periodic with the same period as the drive frequency,  $\omega_D$ , then the angular velocity  $\omega$  has one value at a given time (point of constant phase) during the drive cycle. If the parameter  $g$  is increased sufficiently, further components of longer period are added to the motion, and one observes more than one value of  $\omega$  at the given phase. The system has undergone a bifurcation.

For the diagrams shown in Figure 3.13,  $\omega$  is taken at the *beginning* of the drive cycle ( $\phi = 0$ ). The system is allowed to come to a steady state by omitting the first 30 drive cycles. The figure shows the next 30 drive cycles. Suppose first that the pendulum is lightly driven (say  $g = 0.9$ ), as in Figure 3.13(a). Its motion is an oscillation at the forcing frequency. The phase trajectory is a limit cycle that is symmetric about the origin; the corresponding Poincaré section shows a fixed point. The angular velocity takes only a single value in the bifurcation diagram.

If the driving force is slightly increased to about 1.025, then the phase trajectory loses its symmetry about the origin and has two different shapes (Figure 3.14) depending on the choice of initial conditions. This two-valuedness appears in Figure 3.13(a) as a splitting. But note that the pendulum's motion still is oscillatory, with a main frequency  $\omega_D$  and possibly some higher frequency harmonic content. Each set of initial conditions produces only one value of  $\omega$  in the bifurcation diagram. One such branch is shown in Figure 3.13(b).

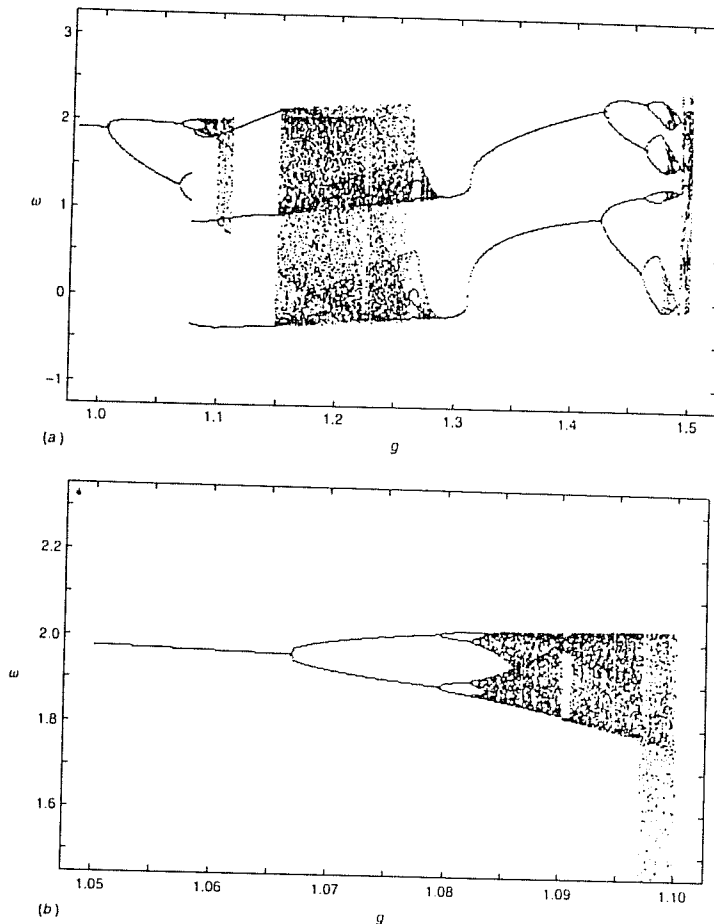


Fig. 3.13 (a) Bifurcation diagrams showing the long-term values of the angular velocity  $\omega$  at the beginning of each drive cycle, plotted against the forcing amplitude  $g$ . (b) and (c) Expansions of parts of (a). The other parameters are  $g = 2$  and  $\omega_D = \frac{2}{3}$ .

If the driving amplitude is increased to approximately 1.07, the periodicity of the pendulum doubles, and it now has frequency components at  $\omega_D$  and  $\omega_D/2$ . Observation of the animation for a given set of initial conditions shows two slightly different oscillatory motions offrequency  $\omega_D$  whose combination has a frequency of  $\omega_D/2$ . The motion is sketched in Figure 2.15(a). This effect is called *period doubling*. It

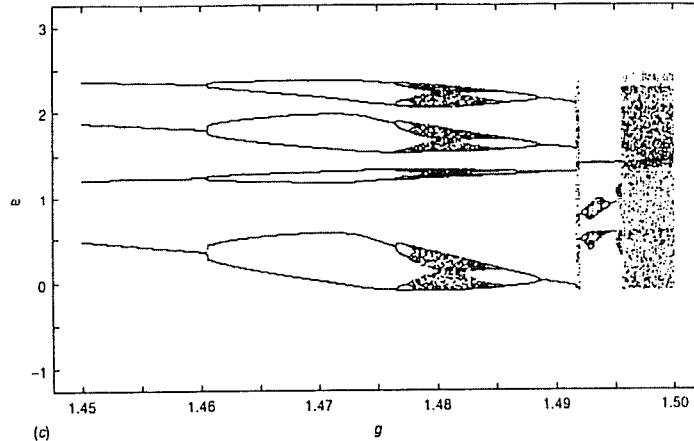


Fig. 3.13 cont.

causes the system to cycle between two values of  $\omega$  (at the beginning of the drive cycle) for each set of initial conditions. This change is evident in the bifurcation diagram of Figure 3.13(a). Given the two-valuedness resulting from the two asymmetric attractors, a total of four values of  $\omega$  may occur at  $\phi=0$ .

The bifurcation diagram is very complex. For certain ranges of the parameter  $g$ , the angular velocity takes on an infinite number of values, though there are also many holes; these states are chaotic. It is also interesting to see that within the chaotic regions there are small intervals in which the motion abruptly becomes periodic again (for example,  $g \sim 1.12$ ). Beyond the large chaotic region occupying much of the interval  $1.08 < g < 1.28$ , a wide interval of periodic motion appears again, centered at  $g = 1.35$ . Study of the animation in this region shows a rotary motion with a small, superposed oscillation. Depending upon the initial conditions, the rotary motion has either a positive or negative average angular velocity. (See Figure 3.3(e)). This two-valuedness is evident in the bifurcation diagram.

Beyond  $g = 1.43$ , a new *subharmonic cascade* occurs. At  $g = 1.45$  (see Figure 3.13(c)) the Poincaré section consists of two points, and at  $g = 1.47$  four points (for a given set of initial conditions). In the region around  $g = 1.48$  there are four densely occupied bands of  $\omega$ . The motion is chaotic and  $\omega$  takes different values in a regular cycling around the

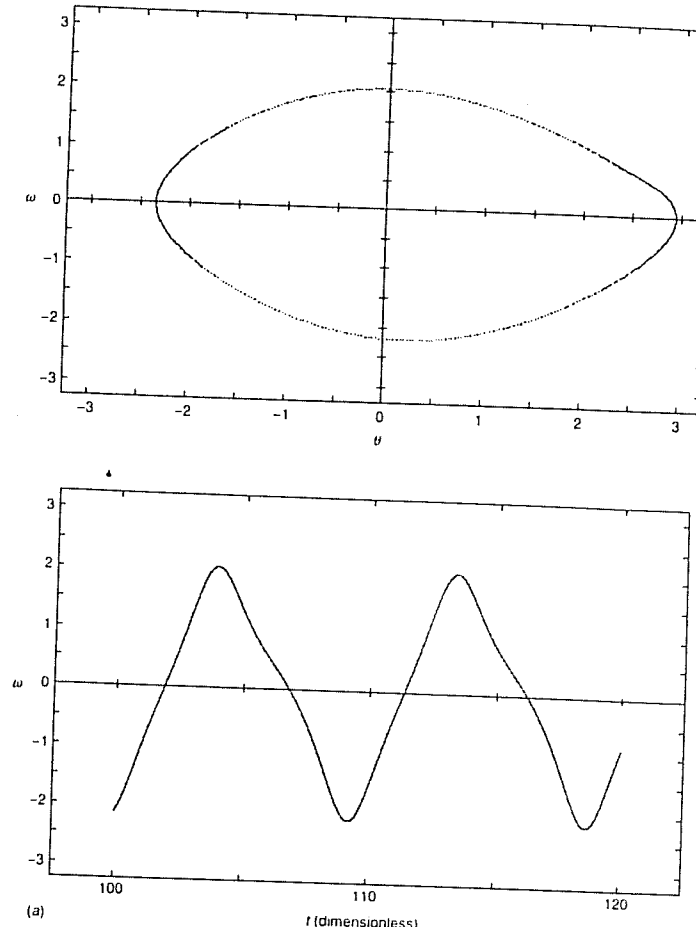
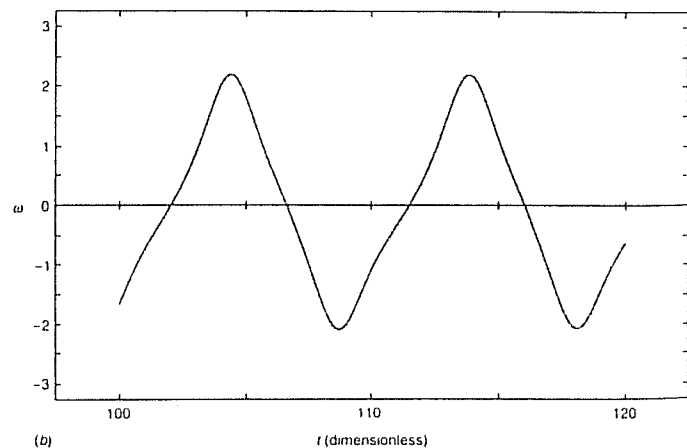
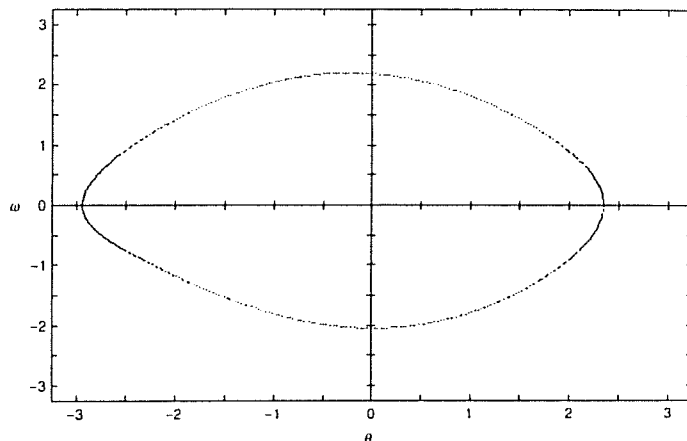


Fig. 3.14 Phase diagrams (above) and the velocity time series (below) showing two periodic trajectories (a), (b), which develop from different sets of initial conditions.  $g = 1.025$ ,  $q = 2$ ,  $\omega_D = \frac{2}{3}$ .

bands. A narrow periodic interval occurs for  $1.487 < g < 1.493$ , followed by chaotic motion for higher  $g$ .

The bifurcation sequences observed as a function of  $g$  change dramatically if the parameters  $q$  and  $\omega_D$  are changed. One example of a different sequence is given in Figure 3.15, where the damping factor is

Fig. 3.14 *cont.*

reduced by a factor of 2 so that  $q = 4$ . The regions of chaotic behavior are much broader, and there is a prominent window of periodic behavior around  $g = 1.25$ .

The bifurcation diagram is an important tool for discovering interesting parameter regimes for a dynamical system. While our discussion focused upon variation of the forcing  $g$ , bifurcation diagrams utilizing  $q$  and  $\omega_D$

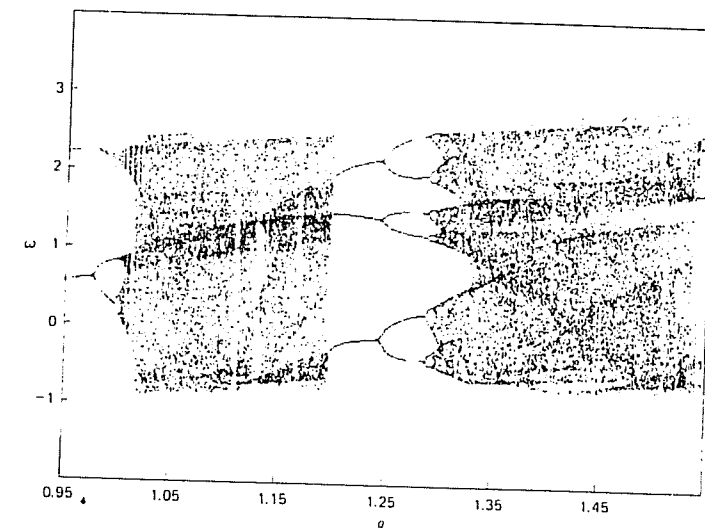


Fig. 3.15 A bifurcation diagram for  $q = 4$ ; this corresponds to lighter damping than in Figure 3.13.

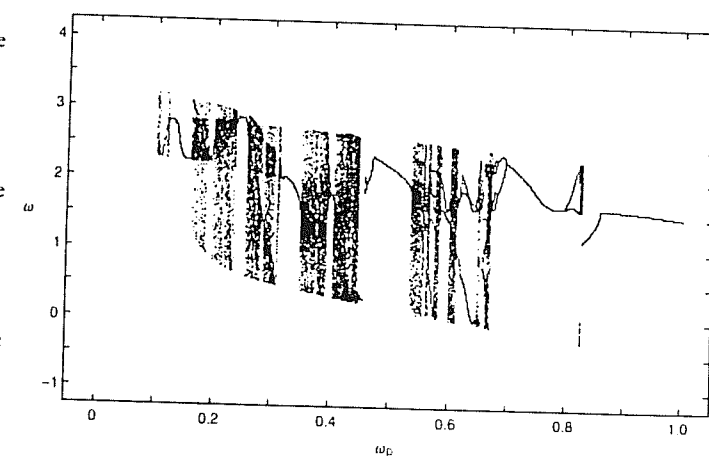


Fig. 3.16 A bifurcation diagram where the drive frequency  $\omega_D$  is varied. When the forcing is approximately a low order fraction of the natural frequency (chosen to be 1) then the pendulum motion tends to lock to the periodic forcing. Regions of chaotic behavior are interspersed between the many regions of periodic mode-locking.  $q = 2$  and  $g = 1.5$ . (See the discussion of the circle map in Chapter 4.)

as the independent variable also yield similar displays of varied dynamical behavior. Figure 3.16 illustrates the case for variation of  $\omega_D$ .

The numerical computations discussed in this chapter illustrate the complexity and variety of motions of the pendulum. Experiments illustrating some of these phenomena have been performed (Blackburn *et al.*, 1989). Analytic solution of the pendulum equations is apparently

not feasible except for special cases. Therefore, in order to understand the development of chaos we consider in Chapter 4 several nonlinear mappings, which are more tractable than differential equations. Despite their simplicity, these maps exhibit many of the phenomena illustrated by the pendulum.

### Problems and Simulations

- 3.1 Figure 3.2(b) shows the shrinkage of an initial area  $A_0$  in phase space as the points evolve in time. Using the ideas developed in Chapter 2 for dissipative systems show, for the damped, driven pendulum, that the area shrinks according to

$$dA/dt = -A/q,$$

where  $q$  is the damping factor for the pendulum. Solve this differential equation. For a value of  $q=4$ , calculate the fraction by which the area is reduced after (a) half a forcing period as in Figure 3.2 and (b) after two forcing periods. What would you conclude about the area as the system approaches a state for which the orbits generated from the initial points in  $A_0$  settle onto the attractor?

- 3.2 Use the program MOTION listed in Appendix B or the MOTION option in the menu of the program CHAOS to study the motion of the driven pendulum. Try different values of the parameter set  $(\omega_D, g, q)$ . Let the motion run for many cycles in order to observe the long term behavior.
- 3.3 Use the program PENDULUM listed in Appendix B or the 2D-PHASE DIAGRAM option in the menu of CHAOS to study the two-dimensional projection of the phase space for the pendulum. Try different values of  $(\omega_D, g, q)$  and different sets of initial conditions  $(\theta_0, \omega_0)$ . Discard the first ten cycles to allow the pendulum to reach a steady state.
- 3.4 Use the INIT. BLOCK FLO option in the menu of CHAOS (or modify PENDULUM) to study the motion of a block of initial conditions in  $(\theta, \omega)$  space. Note the change in shape and area of the block.
- 3.5 Use the program POINCARÉ listed in Appendix B or the POINCARÉ SECTION option in the menu of CHAOS to study the Poincaré section of the pendulum. Try different values of  $(\omega_D, g, q)$  and phase angle. Discard the first ten cycles to allow the

pendulum to reach a steady state.

- 3.6 An electrical circuit with resistance, inductance, and nonlinear capacitance may be driven sinusoidally into chaotic states. The differential equation for the circuit is

$$d^2x/dt^2 + Adx/dt + x^3 = B\cos t$$

where  $A$  and  $B$  are adjustable parameters. It has been suggested that the transition to chaos may be observed for parameter values  $A=0.1$  and  $9.8 < B < 13.4$  (Moon, 1987, p. 272). Modify the programs PENDULUM and POINCARÉ (listed in Appendix B) or the source code on the diskette for the libraries LPHASE2D and LPOINCAR in order to develop programs to study the behavior of this dynamical system. Note that the drive angular frequency is 1. Eliminate the periodic boundary conditions on the position coordinate and put larger boundaries on the axes.

- 3.7 Use the listing BIFURCATION in Appendix B or the BIFURCATION DIAG option in the menu of CHAOS to generate a bifurcation diagram for the pendulum. Since the process is equivalent to the computation of many Poincaré sections, the program takes a lot of processing time and you may wish to save the computed data on a separate diskette.
- 3.8 Modify the bifurcation program to develop a bifurcation diagram for the equation of Problem 3.6. Use the range of  $B$  values suggested in that problem.
- 3.9 Use the FFT listing in Appendix B or the FFT option from the CHAOS menu to generate a power spectrum for the pendulum for  $g=1.5$  and  $q=4$ .
- 3.10 Modify the Runge-Kutta procedure in the FFT program for the equation of Problem 3.6 and run the program for a value of  $B$  which gives a chaotic behavior. (Use your bifurcation diagram from Problem 3.8 to find an appropriate value of  $B$ .)
- 3.11 Use the BASINS listing in Appendix B or the BASINS OF ATTRACTION option from the CHAOS menu to generate a diagram of the basins of attraction. Try  $g=1.3$  and  $q=2$ .

# Toward an understanding of chaos

The driven pendulum, our primary example in this work, may seem to be one of the simplest physical systems to exhibit chaotic behavior. Mathematically and computationally, however, nonlinear differential equations are difficult to solve. Even more elementary model systems can give insight into the mechanisms leading to chaotic behavior. These are stated in the form of *difference equations*, rather than *differential equations*. A typical difference equation is of the form

$$x_{n+1} = f(\mu, x_n), \quad (4.1)$$

where  $x_n$  refers to the  $n$ th value of  $x$ , a real number on the unit interval  $(0,1)$ , and  $\mu$  is a parameter. One may think of  $nT$  as a time, where  $T$  is a basic time interval. The parameter  $\mu$  may vary with the particular model and, in the examples we will discuss, varying  $\mu$  leads to the onset of chaotic behavior. The function,  $f$ , is said to be a *map* of the interval  $(0,1)$  onto itself, since it generates  $x_{n+1}$  from  $x_n$ . The function  $f(\mu, x_n)$  may be nonlinear in the argument  $x_n$ , just as the differential equations for the pendulum are nonlinear in  $\theta$ . Difference equations may be solved quite readily by iteration, and their numerical solution is much less time consuming than is the case for differential equations.

Is there a relationship between a *flow* – differential equations – and a *map* – difference equations? A flow is a dynamical system that is continuous in time whereas a map is a system that is discrete in time. In principle, a two-dimensional map can represent a three-dimensional

flow. For example, the Poincaré section for the pendulum is a two-dimensional map of the coordinates  $(\theta, \omega)$  from one forcing period to the next:

$$\left. \begin{aligned} \theta_{n+1} &= G_1(\theta_n, \omega_n), \\ \omega_{n+1} &= G_2(\theta_n, \omega_n). \end{aligned} \right\} \quad (4.2)$$

A definite relation exists between the coordinates  $(\theta_n, \omega_n)$  at the end of the  $n$ th forcing period and the coordinates  $(\theta_{n+1}, \omega_{n+1})$  at the end of the  $(n+1)$ th forcing period.

The explicit form of the Poincaré map corresponding to a specific flow is usually unknown. Yet certain properties may be deduced. For example, since the flow equations are the result of deterministic laws, they obey the noncrossing rule (Chapter 2) and consequently may be integrated forward or backward in time. Poincaré sections have the corresponding property that while  $(\theta_{n+1}, \omega_{n+1})$  may be determined uniquely from  $(\theta_n, \omega_n)$ , unique determination in the reverse direction is also possible. Such maps are said to be *invertible*. From this property we deduce another connection. For a flow, chaos is possible if there are three degrees of freedom. The corresponding Poincaré section has two dimensions and therefore we see that a two-dimensional, invertible map may also exhibit chaos.

A flow may also be represented by a *time-delay map* which we discuss more fully in Chapter 6. This map is formed from values of a given dynamical variable – such as the angular velocity of the pendulum – taken at intervals separated by a fixed delay time,  $\tau$ . For example, the map might be three-dimensional and have coordinates represented by vectors:

$$\left. \begin{aligned} y_i &= (\omega(t_i), \omega(t_i + \tau), \omega(t_i + 2\tau)), \\ y_{i+1} &= (\omega(t_{i+1}), \omega(t_{i+1} + \tau), \omega(t_{i+1} + 2\tau)), \end{aligned} \right\} \quad (4.3)$$

and so on. Then the map has the form

$$y_{i+1} = \mathcal{M}(y_i), \quad (4.4)$$

where  $\mathcal{M}$  is a nonlinear transformation – usually of unknown form – that propagates the coordinates in time. This type of map is particularly suited to the analysis of experimental data. We will demonstrate its usefulness in Chapter 6.

Finally, we note that flows of dissipative systems can sometimes be represented by one-dimensional, noninvertible maps (Lichtenberg and Lieberman, 1992, p. 478). Because of their relative simplicity, one-dimensional maps provide several advantages over the differential equations. They allow for simple, clear statements of many characteristics

of chaotic behavior, such as sensitivity to initial conditions and the evolution of information. Maps also illustrate clearly the mechanisms of bifurcation of solutions, and the folding and stretching required for chaos in a finite phase space. In this chapter several maps and their properties are explored to aid in further understanding chaotic behavior.

#### 4.1 The logistic map

This simple map, given by the difference equation

$$x_{n+1} = \mu x_n(1 - x_n), \quad x_n \in [0,1], \quad (4.5)$$

takes its name from the corresponding differential equation

$$dx/dt = \mu x(1 - x) \quad (4.6)$$

originally used by P.F. Verhulst in 1845 to model population development in a limited environment (May, 1976). The logistic map is one-dimensional and nonlinear, and may be visualized as indicated in Figure 4.1. The diagram has three parts: the parabolic curve  $y = \mu x(1 - x)$ , the diagonal line  $x_{n+1} = x_n$ , and a set of lines connecting the successive iterations of the map. The time sequence produced by the mapping is obtained by choosing a value of  $\mu$  (in this case  $\mu = 2$ ), plotting the corresponding quadratic curve, and repetitively generating subsequent points starting with some initial value (in this case,  $x_0 = 0.2$ ). The first point,  $x_1$ , is found where the line  $x_0 = 0.2$  meets the quadratic curve. The next step is easily determined by moving laterally to the  $x_{n+1} = x_n$  diagonal. From the diagonal,  $x_2$  can be found by again going vertically to the quadratic curve. The process is repeated until  $x$  settles (in this case) to a steady state where  $x_{n+1} = x_n$ . Such a 'fixed' point is obtained whenever the magnitude of the slope of the map where it intersects the diagonal is less than unity.

In Figure 4.1 the sequence  $\{x_n\}$  reaches a fixed point. A little experimentation shows that this is apparently the case for all initial conditions  $x_0$  when  $\mu = 2$ . If  $\mu$  is increased to approximately 3.3 as in Figure 4.2 the situation changes. As shown in Figure 4.2(a) the quadratic curve is steep and the magnitude of its slope  $|f'(x)|$  is greater than 1 at the intersection. Therefore, the fixed point is unstable and, after an initial transient,  $x_n$  oscillates between two values so that  $x_{n+2} = x_n$ . The motion is now periodic as shown in Figure 4.2(b). This effect is reminiscent of the Poincaré map of the pendulum for values of the driving force around  $g = 1.07$ . Higher values of  $\mu$  lead to further bifurcations and even to

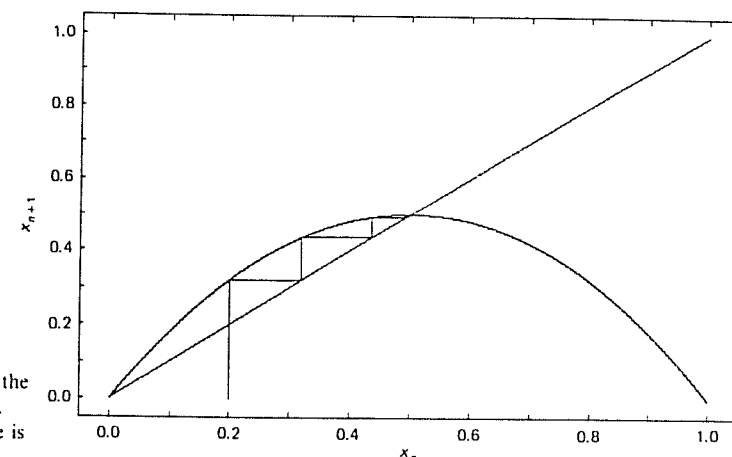


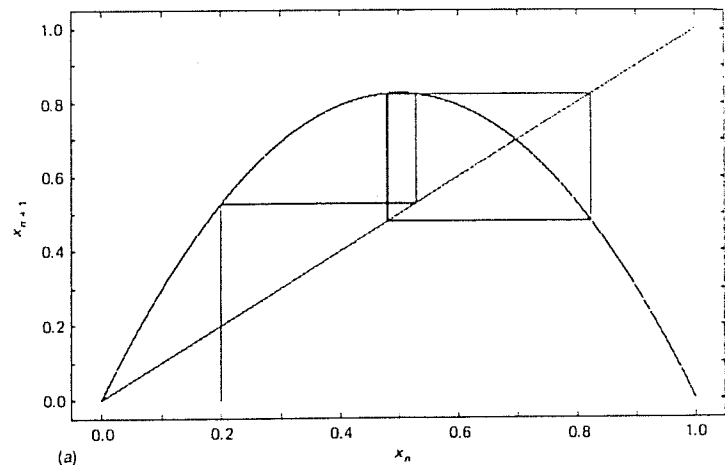
Fig. 4.1 Evolution of the logistic map for  $\mu = 2$ . The equilibrium value is  $x = 0.5$ .

chaotic behavior. Figure 4.3 shows the situation for  $\mu = 3.9$ . The long-term behavior is such that the  $x_n$  are not limited to a few points but rather fill much of the original quadratic curve, and the behavior is chaotic. This behavior is reminiscent of the Poincaré sections for the pendulum in the chaotic region.

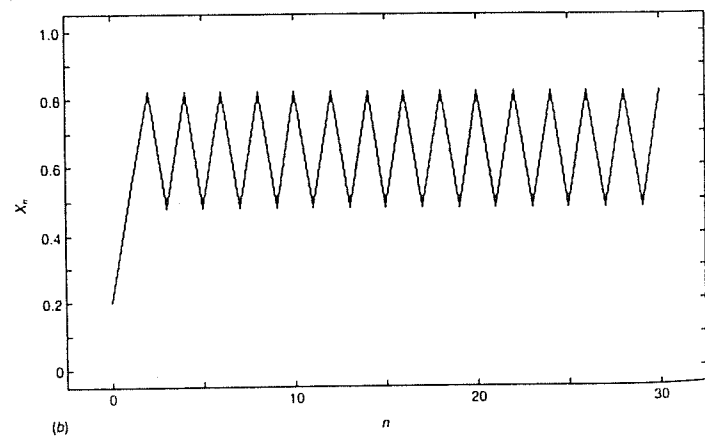
Rather than continuing to describe the behavior of the logistic map for individual values of  $\mu$ , we present a more global view of the model through a bifurcation diagram, as shown in Figure 4.4, where  $\mu$  varies smoothly from 2.9 to 4.0. In this diagram the map is iterated several hundred times at each of many intervening values of  $\mu$ , with the first 100 values discarded to ensure that only the long-term behavior is plotted. The appearance of this diagram is similar to that of the pendulum bifurcation diagram (Figure 3.13), including regions where the behavior is chaotic and regions or windows of periodicity. We now focus on some general features of chaotic maps that are illustrated by the logistic map.

##### 4.1.1 Period doubling

One important feature of the logistic map is the passage to chaos through a sequence of period doublings; the bifurcation where this doubling occurs is called a *pitchfork* bifurcation, because the local shape of the bifurcation diagram resembles a pitchfork. This *period doubling* effect is illustrated in Figure 4.5, which shows the long-term behavior of the map at  $\mu = 3.53$ . Two such bifurcations have occurred and  $x_{n+4} = x_n$ .

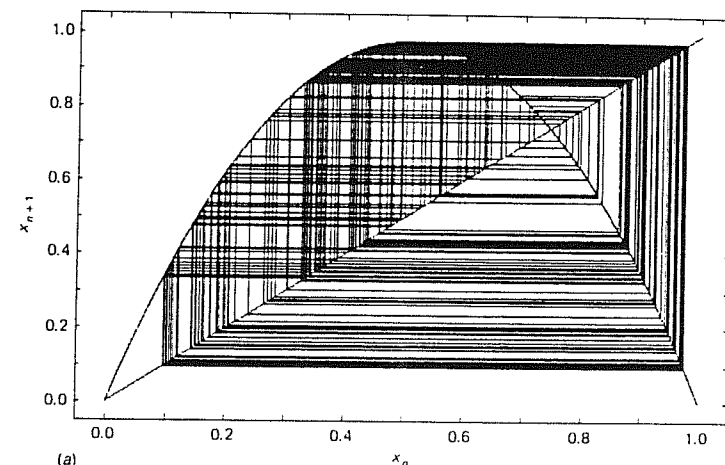


(a)

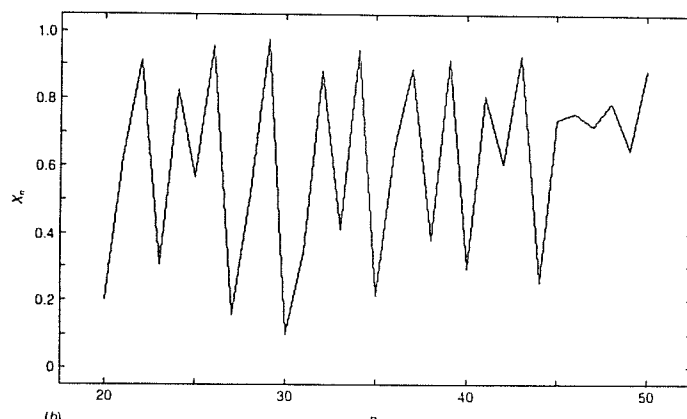


(b)

**Fig. 4.2** (a) The logistic map for  $\mu=3.3$  showing an oscillation between  $x=0.48$  and  $x=0.83$ . (b) The periodic motion shown as a function of iteration number.



(a)



(b)

**Fig. 4.3** (a) Iteration of the logistic map for a chaotic state at  $\mu=3.9$ . (b) The chaotic motion shown as a function of iteration number.

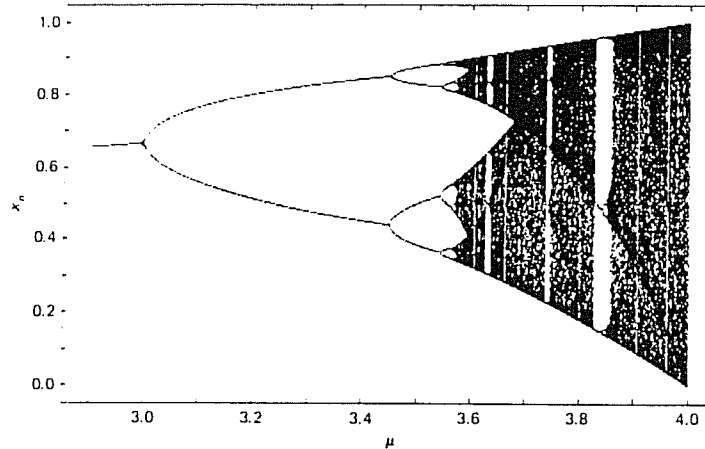


Fig. 4.4 Bifurcation diagram of the logistic map. Long-term values of  $x_n$  are plotted for  $2.9 < \mu < 4$ .

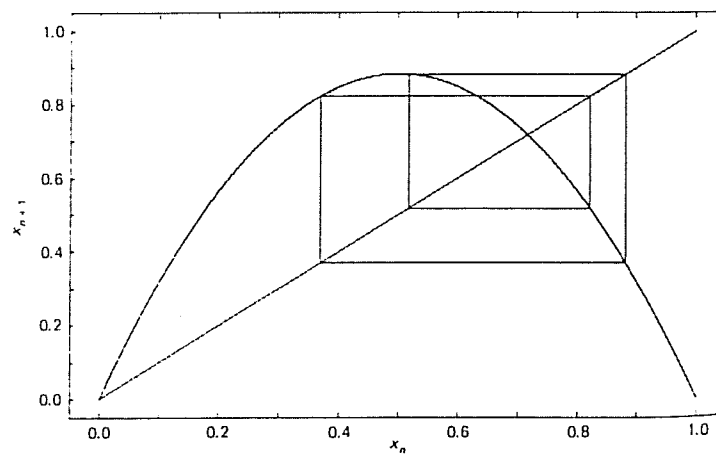


Fig. 4.5 A period-4 logistic map cycling between four values:  $x = 0.37, 0.52, 0.83$ , and  $0.88$ .

The period-doubling mechanism is one *route to chaos* that has been much studied as it is common in many dynamical systems, including the pendulum for  $g$  slightly greater than 1. The period-doubling route is particularly interesting because it may be characterized by certain universal numbers that do not depend (within certain limits) on the nature of the map (or ordinary differential equations). For example, the ratio of the spacings between consecutive values of  $\mu$  at the bifurcations approaches a universal constant, called the Feigenbaum number after its discoverer. If the first bifurcation occurs at  $\mu_1$ , the second at  $\mu_2$ , and so forth, then this universal number is defined as (Feigenbaum, 1978)

$$\lim_{k \rightarrow \infty} \frac{\mu_k - \mu_{k-1}}{\mu_{k+1} - \mu_k} = \delta = 4.669\ 201\ 609\ 102\ 990\ 9\dots \quad (4.7)$$

This number can be roughly checked by careful scrutiny of the bifurcation diagram. Furthermore, it can be used to generate the sequence  $\{\mu_k\}$ , using the bifurcation diagram to select the first few values. Finally, it can be shown that an infinite number of bifurcations occur as  $\mu = 3.569\ 944\dots$  is approached.

The Feigenbaum number is a universal property of the period-doubling route to chaos for maps that have a quadratic maximum. *Universality* expresses the notion that certain properties of nonlinear maps are independent of the specific form of the map.

#### 4.1.2 The periodic windows

The regions of chaotic behavior are interrupted by intervals of periodic behavior for  $\mu > \mu_\infty = 3.569$ . One of the largest of these *windows* occurs near  $\mu = 3.83$ , where a periodic orbit (a 3-cycle) occurs, as shown in Figure 4.6. The existence of this periodic behavior is evident from the shape of the third return map, for which

$$x_{n+3} = f(f(f(x_n))). \quad (4.8)$$

In Figure 4.7 two such maps are shown for two values of  $\mu$ : (a) at the start of the window where  $\mu = 3.8282$ , and (b) inside the window before the period-doubling cascade begins, where  $\mu \approx 3.84$ . Although these diagrams have very similar appearances there are some important differences.

At the left boundary of this window, the third order return map (Figure 4.7(a)) shows three values of  $x$  where the curve is tangent to the diagonal line,  $x_{n+3} = x_n$ . These points are the cyclic steady state values of

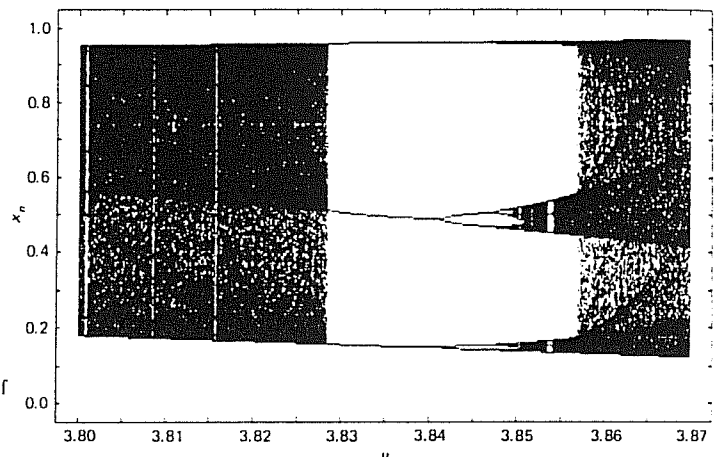


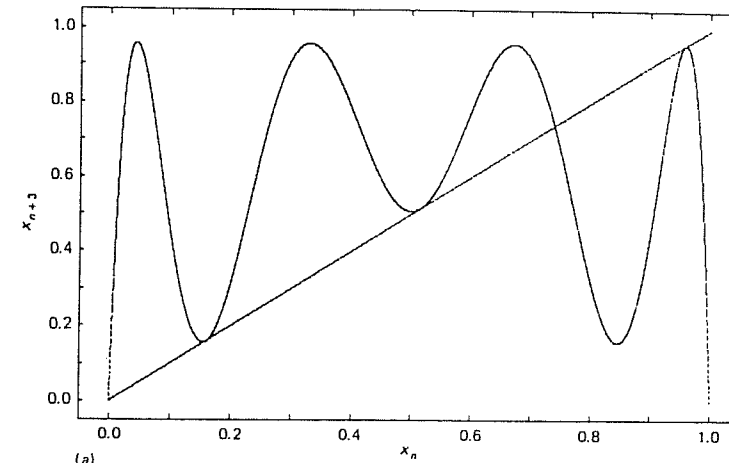
Fig. 4.6 Magnification of the bifurcation diagram in the region of the period-3 window.

$x$  which appear at the beginning of the window. Other initial values of  $x$  will be drawn to these fixed points since the shallow slopes of the curve near the fixed points lead to stability. This particular type of transition is called a *tangent bifurcation*.

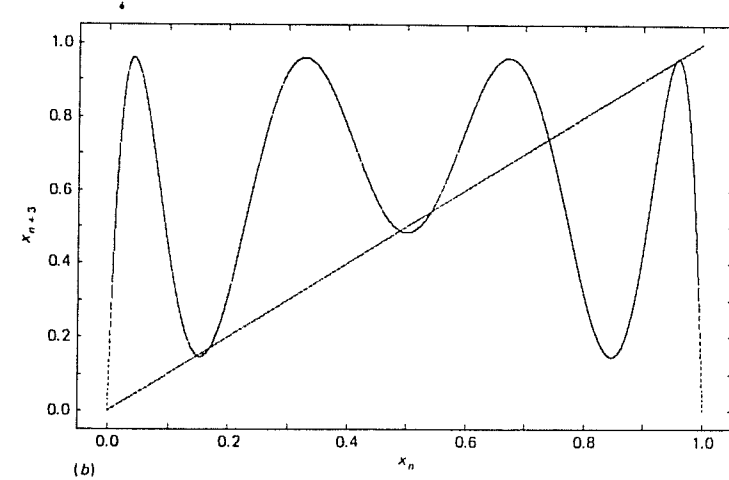
For slightly larger  $\mu$  the bifurcation diagram continues to show the period-3 behavior. Figure 4.7(b) shows the behavior of the corresponding third order return map. The curve now crosses the diagonal at three pairs of values of  $x$ . (The isolated crossing is unstable.) The slopes of the curve in the neighborhood of three of the points (one from each close pair) are sufficiently steep that the map wanders away from these fixed points. On the other hand, the magnitudes of the slopes at the other three points are less than 1 so these points are attractors. Therefore the cyclic behavior, initiated by the tangent bifurcation, continues to be stable.

At  $\mu = 3.842$  a subharmonic cascade to chaos occurs. The slopes of the third order maps near the previously stable values of  $x$  now become too steep for stability. For the first period doubling the sixth order map has six attractors; this process continues until chaotic bands form at  $\mu \approx 3.85$ . The resulting bands merge near  $\mu \approx 3.857$  to form a continuum of values of  $x$ . This expansion of the chaotic regime and similar discrete changes in a chaotic attractor are sometimes called *crises* (Grebogi, Ott, and Yorke, 1987).

For values of  $\mu$  just below the onset of the period-3 window, the third order return map is not quite tangent to the diagonal line. Therefore  $x_n$  can pass through the resulting narrow gaps and then go freely around the plane until it again becomes temporarily trapped in a narrow gap as



(a)



(b)

Fig. 4.7 (a) The map  $x_{n+3} = f^3(x_n)$  at the onset of the period-3 window ( $\mu = 3.8282$ ) showing three stable values of  $x_n$  at about 0.16, 0.51, and 0.95. An unstable point where  $x_{n+3} = x_n$  appears at about  $x_n \approx 0.76$ . The origin of the term 'tangent bifurcation' is apparent. (b) The map  $x_{n+3} = f^3(x_n)$  just inside the window at  $\mu = 3.84$ .

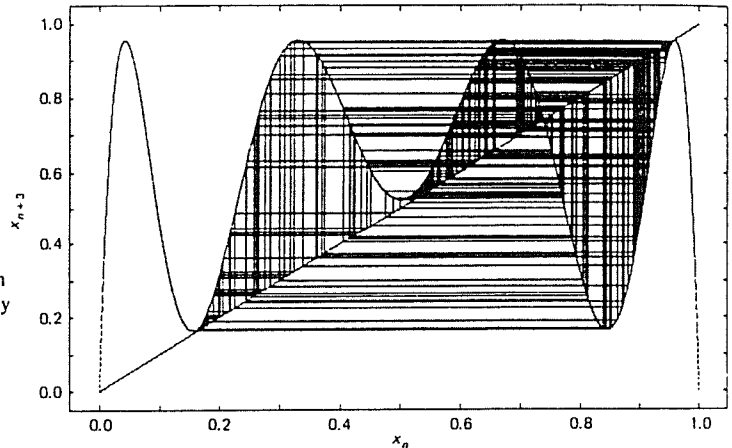


Fig. 4.8 An illustration of ‘type I’ intermittency as the trajectory squeezes through the gap between the map and the tangent line. During the passage through the gap,  $x$  changes very slowly.

shown in Figure 4.8. While it is in the gap,  $x_n$  is nearly fixed. If we think of the map as a Poincaré section for a differential equation representing a physical system such as the pendulum, the physical variable would show nearly periodic motion with occasionally irregular bursts. This common type of chaotic motion is called *type I intermittency* and occurs when a dynamical system is close to a tangent bifurcation if there is a mechanism for intermittent return to the narrow gap.

#### 4.1.3 Lyapunov exponents

The Lyapunov exponent of a map (named after A.M. Lyapunov, 1857–1918, a Russian mathematician) may be used to obtain a measure of the sensitive dependence upon initial conditions that is characteristic of chaotic behavior. This exponent (often written as  $\lambda$ ) may be readily computed for a one-dimensional map such as the logistic map. If a system is allowed to evolve from two slightly differing initial states,  $x$  and  $x+\varepsilon$ , then after  $n$  iterations their divergence may be characterized approximately as

$$\varepsilon(n) \approx \varepsilon e^{\lambda n}, \quad (4.9)$$

where the Lyapunov exponent  $\lambda$  gives the average rate of divergence. (The average must be taken over many ‘initial conditions’ spread over

the trajectory.) If  $\lambda$  is negative, slightly separated trajectories converge and the evolution is not chaotic. If  $\lambda$  is positive, nearby trajectories diverge; the evolution is sensitive to initial conditions and therefore chaotic.

Consider a specific one-dimensional map given by  $x_{n+1} = f(x_n)$ . The difference between two initially nearby states after the  $n$ th step is written as

$$f^n(x + \varepsilon) - f^n(x) \approx \varepsilon e^{\lambda n}, \quad (4.10)$$

or

$$\log_e \left[ \frac{f^n(x + \varepsilon) - f^n(x)}{\varepsilon} \right] \approx n\lambda. \quad (4.11)$$

For small  $\varepsilon$ , this expression becomes

$$\lambda \approx \frac{1}{n} \log_e \left| \frac{df^n}{dx} \right|. \quad (4.12)$$

Finally, we use the chain rule for the derivative of the  $n$ th iterate and take the limit as  $n$  tends to infinity to obtain

$$\lambda = \lim_{n \rightarrow \infty} \frac{1}{n} \sum_{i=0}^{n-1} \log_e |f'(x_i)|. \quad (4.13)$$

Therefore the Lyapunov exponent gives the stretching rate per iteration, averaged over the trajectory. In Figure 4.9, the Lyapunov exponent is plotted as a function of the parameter  $\mu$ . The sign of  $\lambda$  correlates very well

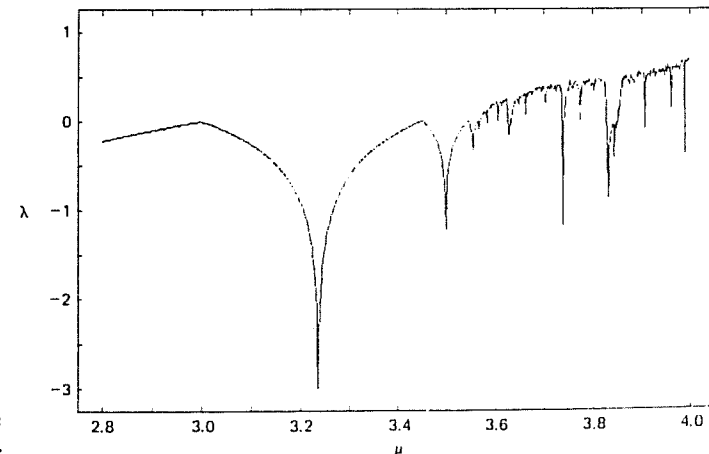


Fig. 4.9 Lyapunov exponent  $\lambda$  versus  $\mu$  for the logistic map. Sensitivity to initial conditions occurs where the exponent is positive.

with the behavior of the system as shown in the bifurcation diagram, Figure 4.4. Beyond  $\mu_\infty = 3.56$ , the regions of periodic behavior correspond to the intervals in which  $\lambda < 0$ .

For  $n$ -dimensional maps there are  $n$  Lyapunov exponents, since stretching can occur for each axis. An  $n$ -dimensional initial volume develops, on average, as

$$V = V_0 e^{(\lambda_1 + \lambda_2 + \dots + \lambda_n) n}. \quad (4.14)$$

For a dissipative system the sum of the exponents must be negative. If the system is chaotic then at least one of the exponents is positive. (See Problem 4.14 for a soluble two-dimensional map.)

Lyapunov exponents are also defined for continuous time dynamical systems such as the pendulum. An initial  $n$ -dimensional volume of phase space develops on average as

$$V = V_0 e^{(\lambda_1 + \lambda_2 + \dots + \lambda_n) t}. \quad (4.15)$$

For the driven pendulum there are three Lyapunov exponents corresponding to the three dimensions of the phase space ( $\theta, \omega, \phi$ ). Since the orbits are solutions to a set of ordinary differential equations, the calculation of Lyapunov exponents is less straightforward than for maps. On a chaotic attractor such as that of the pendulum at  $g = 1.5$ , the directions of divergence and contraction are locally defined, and the calculation must constantly adjust for this condition. Despite this difficulty, computer algorithms have been developed for calculating Lyapunov exponents both from differential equations and from experimental data; the Lyapunov exponents of the pendulum are discussed further in Chapter 5.

#### 4.1.4 Entropy

The complex appearance of the various graphical representations of chaotic behavior naturally leads to the question of the relationship between statistical mechanics and chaos. One way to connect these phenomena is to apply the concept of *entropy* to a chaotic system, comparing the result to an associated statistical system. This comparison is readily done with the logistic map.

Consider a hypothetical statistical system for which the outcome of a certain measurement must be located on the unit interval. If the line is subdivided into  $N$  subintervals, we can associate a probability  $p_i$  with the  $i$ th subinterval containing a particular range of possible outcomes. The entropy of the system is then defined as

$$S = - \sum_{i=1}^N p_i \log_e p_i. \quad (4.16)$$

This quantity may be interpreted as a measure of the amount of disorder in the system or as the information necessary to specify the state of the system. If the subintervals are equally probable so that  $p_i = 1/N$  for all  $i$ , then the entropy reduces to  $S = \log_e N$ , which can be shown to be its maximum value. (See Problem 4.5.) Conversely, if the outcome is known to be in a particular subinterval, then  $S = 0$ , the minimum value. When  $S = \log_e N$ , the amount of further information needed to specify the result of a measurement is at a maximum. On the other hand, when  $S = 0$  no further information is required. (See, for example, Baierlein (1971) for a discussion of the interpretation of entropy as ‘missing’ information.)

We now apply this formulation to the logistic map by establishing  $N$  ‘bins’ or subintervals of the unit interval into which the values of  $x_n$  may fall. In the nonchaotic state the  $x_n$  will fall in relatively few of the bins, and the entropy is low. But in the chaotic state, the entropy is higher, and if the frequencies of occurrence are equal, then it approaches  $\log_e N$ . Figure 4.10 shows the results of applying the entropy concept to the logistic map. As expected, the entropy generally increases with  $\mu$ , except for the downward spikes in the windows of periodic behavior. The entropy does not quite get to  $\log_e N$  until  $\mu = 4$ , since the distribution of  $x_n$  does not span the whole unit interval evenly for  $\mu < 4$ . This feature may be observed in the bifurcation diagram. For  $\mu = 4$ , the entropy is similar to that of a random process with a uniform probability

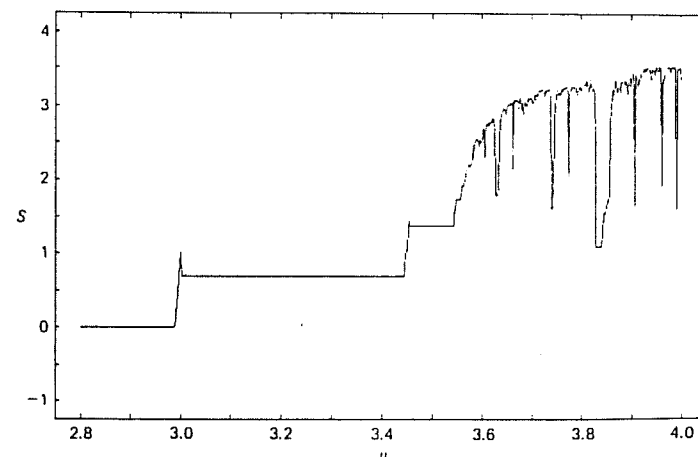


Fig. 4.10 Entropy  $S$  as a function of  $\mu$  for the logistic map. The maximum entropy corresponding to equal probability for each of the 40 cells is 3.6888.

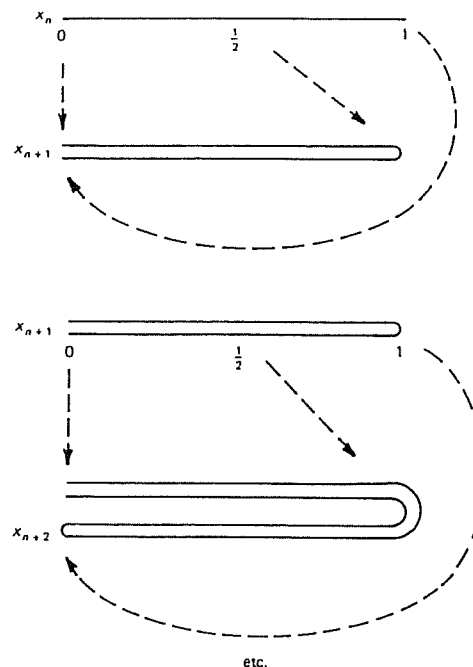


Fig. 4.11 The stretching and folding property of the logistic map for  $\mu = 4$ .

distribution. Nevertheless, short-term correlations *do* exist for chaotic motion, but not for the idealized random system.

For dynamical systems such as the pendulum, information changes in time. It turns out that the average temporal rate of information change can be related both to the Lyapunov exponents and to the fractal dimension of the attractor. These subjects and their relationships are discussed in Chapter 5.

#### 4.1.5 Stretching and folding

The logistic map also provides some insight into the stretching and folding mechanism that is necessary to keep chaotic trajectories within a finite volume of phase space, despite the exponential divergence of neighboring states. For the logistic map the stretching (divergence of neighboring trajectories) and folding (confinement to the bounded space) can be demonstrated fairly easily, by reference to Figure 4.11.

For  $\mu = 4$  the logistic map has a maximum value of 1 at  $x_n = \frac{1}{2}$  and the

values of  $x_n \in (0, \frac{1}{2})$  map to  $x_{n+1} \in (0, 1)$ . Similarly the values of  $x_n \in (\frac{1}{2}, 1)$  map to  $x_{n+1} \in (0, 1)$ , but in the reverse order. Therefore both intervals of  $x_n$  are stretched by a factor of 2, but because the order of the mappings is opposite, the second stretched interval is folded onto the first stretched interval. The figure illustrates a few cycles of the mechanism. The process resembles the one used to make taffy candy or knead dough for bread.

The stretching and folding process illustrates another important feature of chaotic systems that was implied in our discussion of entropy, namely the loss of information about the initial conditions of a system as time or iteration number increases. Mathematically this arises from the *noninvertibility* of the map  $f(\mu, x_n)$ . That is, it is always possible to predict  $x_{n+1}$  from  $x_n$  but there is ambiguity in trying to retrodict  $x_n$  from  $x_{n+1}$ . (One finds the same noninvertibility with elementary functions such as  $y = \sin x$ ,  $y = x^2$ , and so forth. The inverse functions can be defined only by limiting the original domains.) It turns out that a necessary condition for any one-dimensional map to exhibit chaotic behavior is that it be noninvertible.

#### 4.2 The circle map

The logistic model illustrates many characteristics of chaotic dynamics, such as bifurcations, period doubling, intermittency, sensitivity to initial conditions, and the stretching and folding process. However, some important features of the pendulum, especially the phenomenon of 'phase locking', require a two-parameter map for their explanation. Phase locking is said to occur when the ratio of the frequency of the pendulum to that of the forcing becomes locked at the ratio  $p/q$  of two integers, over some finite domain of parameter values (D'Humieres *et al.*, 1982). A similar phenomenon was observed by Christian Huygens in the seventeenth century: the synchronization of two clocks on the same wall. The common attachment to the same wall must have provided a coupling of the clocks to each other. (This phenomenon is mentioned in Bak (1986).)

The pendulum's Poincaré section may be modeled as a two-dimensional (but unknown) map:

$$\left. \begin{array}{l} \theta_{n+1} = G_1(\theta_n, \omega_n), \\ \omega_{n+1} = G_2(\theta_n, \omega_n). \end{array} \right\} \quad (4.17)$$

If  $\omega_n$  is a function only of  $\theta_n$  after the initial transients have died away,

then  $\omega_n = f(\theta_n)$ , and the two-dimensional Poincaré map reduces to a one-dimensional map:

$$\theta_{n+1} = G_1(\theta_n, f(\theta_n))$$

or

$$\theta_{n+1} = F(\theta_n). \quad (4.18)$$

This map may be regarded as a mapping of the circle to itself. It is one-dimensional, with an angular coordinate  $\theta_n \in [0, 1]$  and periodic boundary conditions (corresponding to the pendulum angular coordinate,  $\theta \in [0, 2\pi]$ ).

For a certain range of forcing amplitudes and frequencies, a circle map may be a reasonable approximation to the driven pendulum. The difference equation of a particularly useful circle map known as the *standard map* is

$$\theta_{n+1} = \theta_n + \Omega - (K/2\pi)\sin(2\pi\theta_n) \quad \text{mod } 1. \quad (4.19)$$

There are two parameters  $(\Omega, K)$  for the standard map, in contrast to the single parameter  $\mu$  for the logistic map. The parameter  $\Omega$  is the rotation frequency ('winding number') in the absence of nonlinearity, whereas  $K$  gives the strength of the nonlinear coupling of the oscillator to the forcing. This nonlinear coupling can modify the angular change per iteration. (A numerical justification of the connection between the standard map and the pendulum over a range of parameters is given in Jensen, Bak, and Bohr (1984).)

To obtain a sense of the behavior of the standard map, we first omit the nonlinear term by setting  $K=0$ . Then the map reduces to

$$\theta_{n+1} = \theta_n + \Omega, \quad (4.20)$$

which is illustrated in Figure 4.12 for the case  $\Omega=0.4$ . After five iterations  $\theta$  returns to its initial value  $\theta_0=0.3$ , having made two revolutions. The *winding number*,  $W$ , is  $\frac{2}{5}$ , and it is just equal to  $\Omega$ . If the winding number is a rational number,  $p/q$ , then the map is cyclic or *periodic*. If the winding number is irrational then  $\theta$  does not return exactly to its initial value and the motion is termed *quasiperiodic*. Figure 4.13 illustrates quasiperiodic motion with  $\Omega=0.404\ 004\dots$  (irrational) for 200 iterations. The angle comes arbitrarily close to any particular value if  $n$  is sufficiently large. Mode locking occurs when the nonlinear term is added; this keeps the motion periodic even when  $\Omega$  is irrational. In Figure 4.14, for example,  $K=0.95$  and  $\Omega=0.404\ 004\dots$  as before. However, the motion repeats every five iterations. The winding number

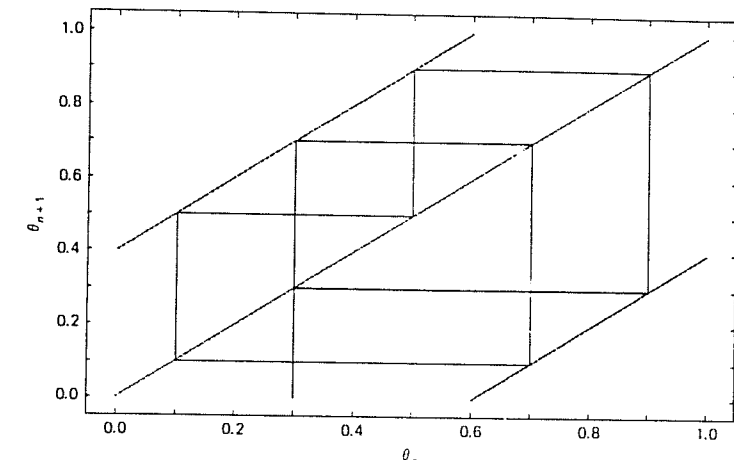


Fig. 4.12 The linearized circle map for a rational winding number of 0.4, using periodic boundary conditions on  $\theta$ . The diagonal line represents  $\theta_{n+1} = \theta_n$ .

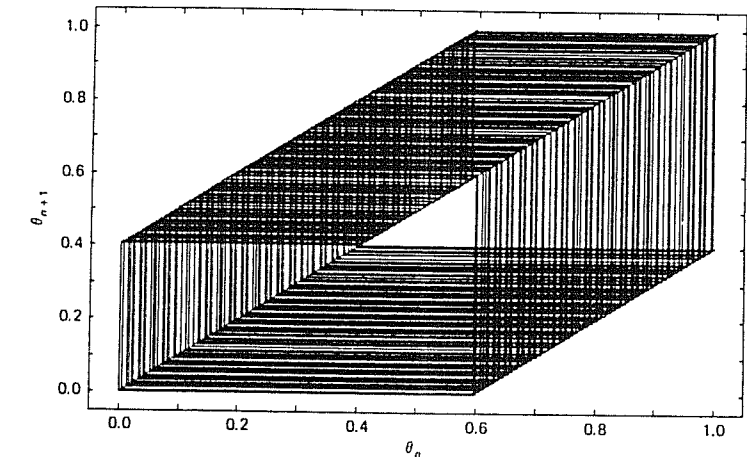


Fig. 4.13 The linearized circle map for an irrational winding number, 0.404 004 ... .

measures the average phase change per iteration. For  $K \neq 0$ , it is not equal to  $\Omega$  and is defined generally as

$$W = \lim_{n \rightarrow \infty} \left( \frac{\theta_n - \theta_0}{n} \right). \quad (4.21)$$

The nonlinear term obviously changes the shape of the function representing the map. Note that at  $K=0.95$  the map is still invertible. The widths in  $\Omega$  of the various mode-locked regions where the winding number is fixed increase with  $K$ , as shown in Figure 4.15. The resulting 'Arnold tongues' are named after the Russian mathematician who discovered this structure (Arnold, 1965).

There are an infinite number of phase-locked intervals. There are also an infinite number of irrational winding numbers. As  $\Omega$  varies at fixed  $K$ , the map displays both periodic and quasiperiodic motion. But as  $K$  approaches 1, the rational intervals increase in size. At  $K=1$  the set of rational intervals is a fractal. Figure 4.16(a) shows the rational winding numbers as plateaus in a plot of  $W$  versus  $\Omega$ . If the figure is magnified (Figure 4.16(b)), more plateaus become evident, and the curve shows repetition of the same patterns at the new magnification. Such a curve is said to be *self-similar*. This structure is called the *Devil's staircase*. (For a discussion of the Devil's staircase and some applications, see Bak (1986).)

Beyond the  $K=1$  critical value, the phase-locked motions overlap; this implies that several different periodic oscillations can occur for given  $(K, \Omega)$  depending on initial conditions. The graph of  $W$  versus  $\Omega$  ceases to be monotonic. The map develops local maxima and minima and therefore becomes noninvertible for  $K>1$ , a necessary condition for chaotic behavior, as we also noted for the logistic map. A noninvertible case of the standard map is shown in Figure 4.17. Chaos is, in fact, observed for some values of  $\Omega$ .

Several routes to chaos occur for the standard map. In Figure 4.18 we illustrate three representative paths through the Arnold tongues of the  $(\Omega, K)$  parameter space. Path (a) shows the system in a state where the winding number is irrational and the behavior is quasiperiodic. The system continues in the quasiperiodic state until it reaches the junction of two phase-locking modes at  $K=1$  and becomes chaotic. Path (b) shows the system as initially quasiperiodic but then passing into a mode-locking regime and eventually becoming chaotic. Path (c) shows the system starting in a mode-locked state, traveling toward the critical line,  $K=1$ , but then continuing to a larger value of  $K$ , beyond which a period-doubling cascade to chaos begins. The prominence of the

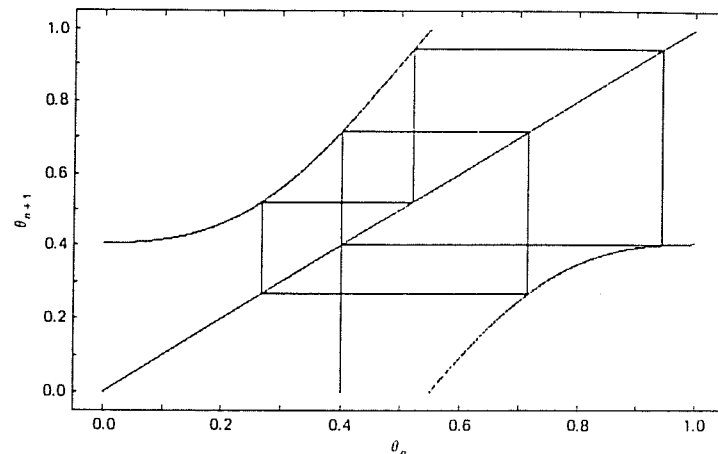


Fig. 4.14 The standard map for  $K=0.95$  and  $\Omega=0.404\,004\dots$  The nonlinear coupling produces a phase-locked state.

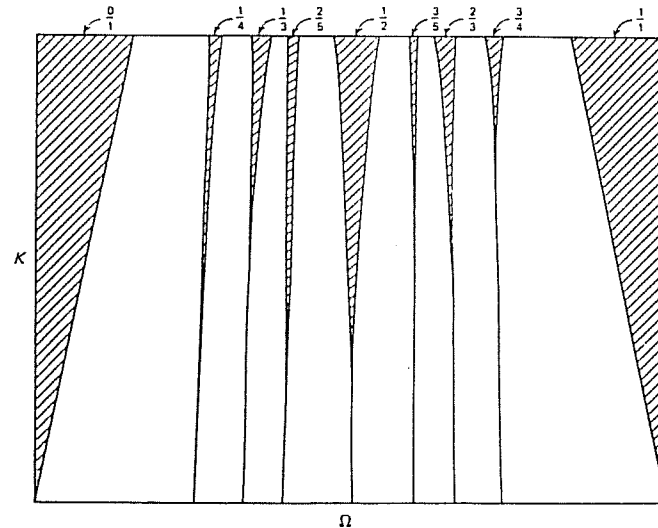


Fig. 4.15 Parameter space of the standard map as a function of  $K$  and  $\Omega$ . The motion is periodic (rational winding number) inside the 'Arnold tongues', and quasiperiodic outside them. At  $K=1$  (top of figure) only rational winding numbers are available and for  $K>1$  the tongues overlap. (Only a few of the 'tongues' are illustrated.)

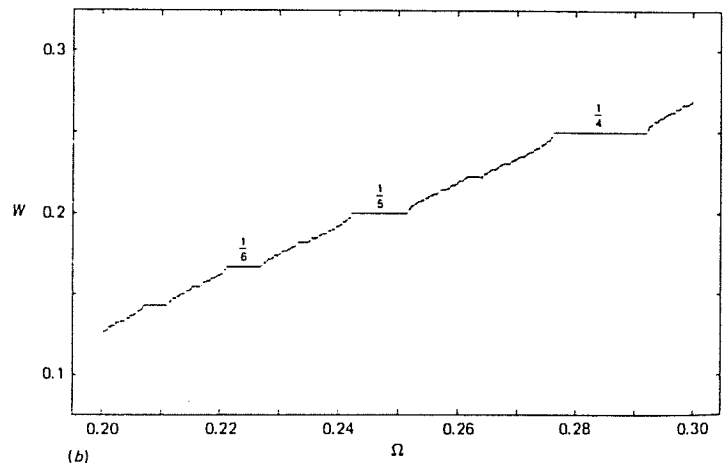
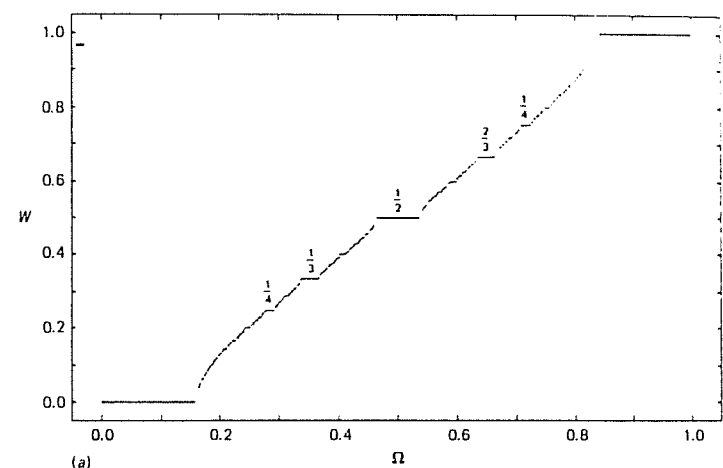


Fig. 4.16 (a) The 'Devil's staircase' generated by the rational winding numbers of the standard map.  $K = 1$ . (b) A magnification of part of the staircase. The low order phase-locked tongues are labeled by their winding numbers.

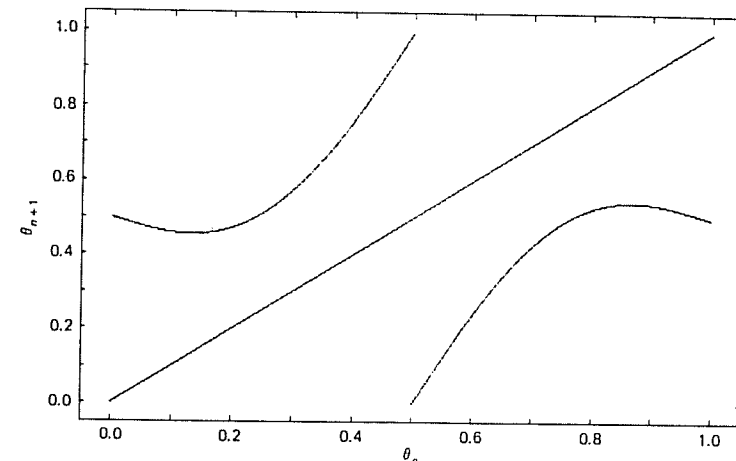


Fig. 4.17 The standard map becomes noninvertible for  $K > 1$  (here  $\Omega = 0.5$  and  $K = 1$ ).

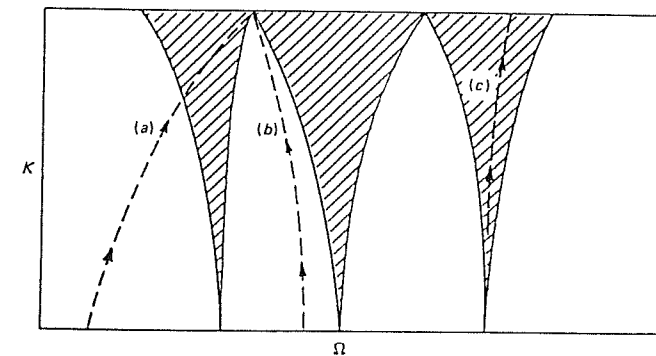


Fig. 4.18 Various possible routes to chaos: (a) quasiperiodic  $\rightarrow$  phase locking  $\rightarrow$  chaos; (b) quasiperiodic  $\rightarrow$  chaos; (c) periodic  $\rightarrow$  chaos.

period-doubling route to chaos is consistent with the existence of a quadratic maximum (Figure 4.17). This aspect of the circle map is similar to the logistic map.

The logistic and circle maps provide many valuable insights into chaotic dynamics. As we discuss in the final section of this chapter, many of the concepts developed from these one-dimensional maps apply to the driven pendulum. As a final model for chaotic behavior we consider a two-dimensional map.

### 4.3 The horseshoe map

In our discussion of the logistic map we saw that the interval  $(0,1)$  is stretched and then folded back upon itself. The stretching and folding phenomenon is a primary mechanism for allowing sensitivity to initial conditions in a finite-sized phase space. The horseshoe map introduced by Smale (1963) is a two-dimensional mapping that illustrates the stretching and folding action. It has been shown to be embedded in the dynamics of the pendulum for some parameter choices (Gwinn and Westervelt, 1986).

The horseshoe map consists of the sequence of operations shown in Figure 4.19. First consider a map  $f$  which acts upon the unit square and consists of (a) an expansion in the  $y$  direction by a factor  $\mu > 2$ , (b) a contraction in the  $x$  direction by a factor  $\lambda \in (0, \frac{1}{2})$ , and (c) a folding, as illustrated in Figure 4.19. The transformed set  $f(S)$  is then intersected with the original set  $S$  so that the map is now confined to a subset of the original unit square. If the entire sequence of operations is repeated, then four stripes appear from the original two, and so on. Repetition of the process  $n$  times leads to  $2^n$  stripes, and a cut across the stripes would, in the limit of large  $n$ , lead to a fractal (see Chapter 5).

Horseshoe configurations occur in the phase space of dynamical systems where there are regions of strong contraction and expansion. For example, we recall from the initial discussion (Chapter 2) of the pendulum phase plane that there are saddle points at  $\theta = \pm\pi$  and  $\omega = 0$ . Near these saddle points, trajectories approach most rapidly along certain ‘stable’ directions, and depart most rapidly along other ‘unstable’ directions, as shown in Figure 2.13. Along these directions, the Lyapunov exponents are negative and positive, respectively. Alternatively stated, tangent vectors along the stable directions are contracting, and tangent vectors along the unstable directions are expanding. Any region of phase

space where these two types of behavior are in close proximity may exhibit stretching and folding.

Trajectories containing both types of behavior develop in a complex way. For example, see Moon (1987), Chapter 5. This may be explained with reference to Figure 4.20, which shows the phase plane for the damped, undriven pendulum as in Figure 2.13, but with the *stable* and *unstable manifolds*  $W^s$  and  $W^u$  of the saddle points labeled, and the two basins of attractions shaded differently. The manifolds  $W^s$  and  $W^u$  are simply the trajectories that approach and depart most quickly from the unstable equilibrium. If the pendulum is now *driven periodically* but weakly, the same diagram may be regarded as a Poincaré section of the three-dimensional phase space, except that the lines should be regarded as a sequence of dots corresponding to successive passages of the trajectories through the Poincaré plane.

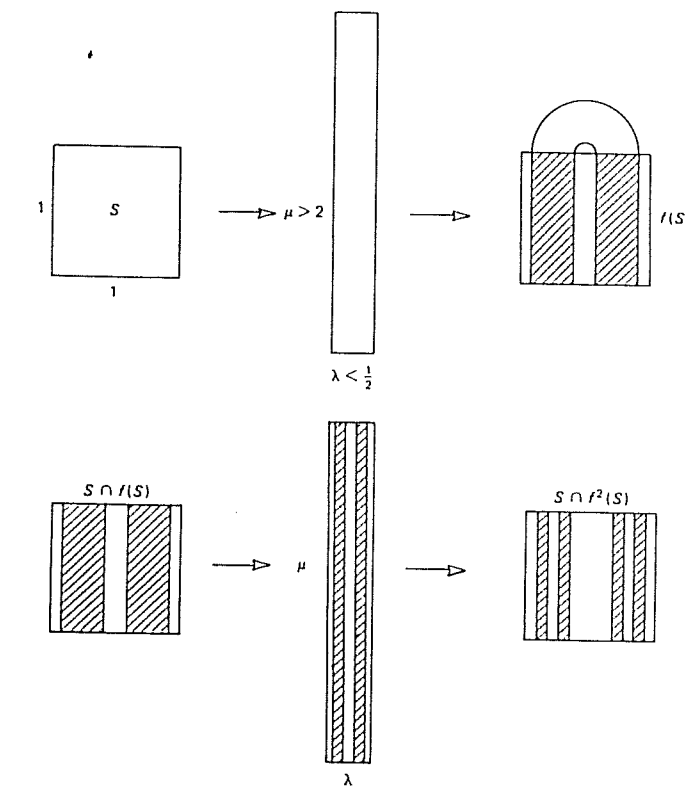


Fig. 4.19 The construction of the horseshoe map for two iterations.

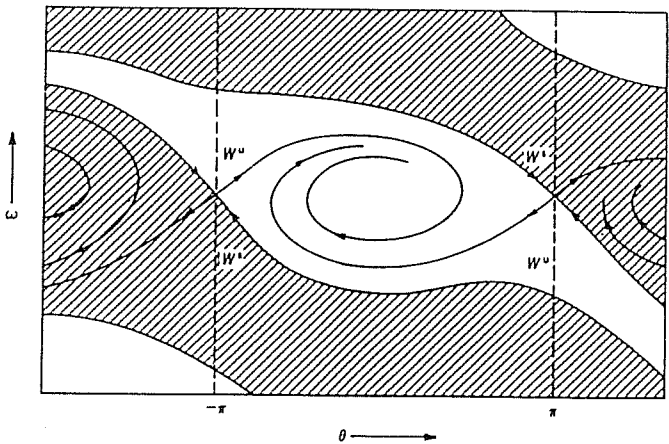
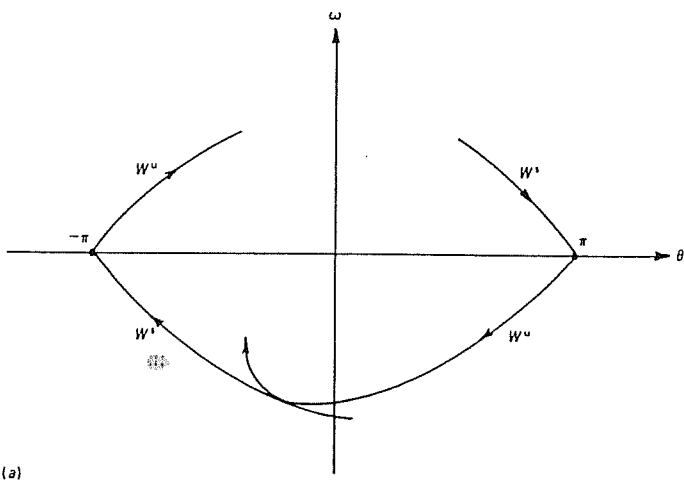
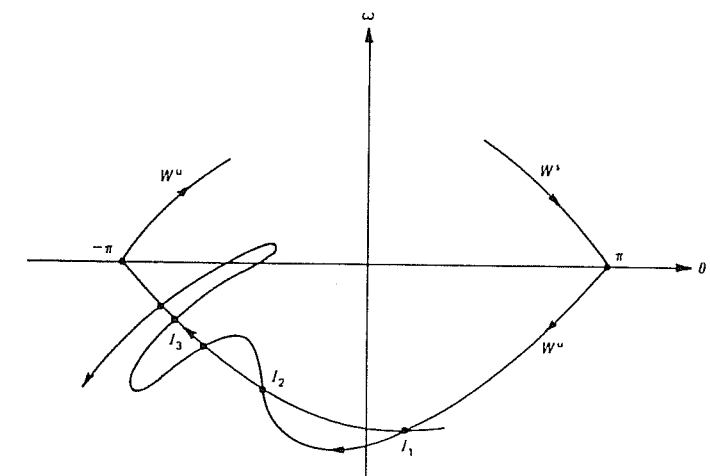


Fig. 4.20 Sketch of the phase plane of the damped, but undriven, pendulum, showing the stable and unstable manifolds of the saddle points. Shaded and unshaded regions correspond to distinct basins of attraction.



(a)

Fig. 4.21 The formation of a heteroclinic tangle in the Poincaré map of the pendulum. (a) The unstable and stable orbits barely touch, signaling the beginning of chaos. (b) The tangle forms with an infinite number of intersections  $I_1, I_2, \dots$ . Two nearby points may be mapped far apart, yielding chaos. (c) Additional detail (see text).



(b)

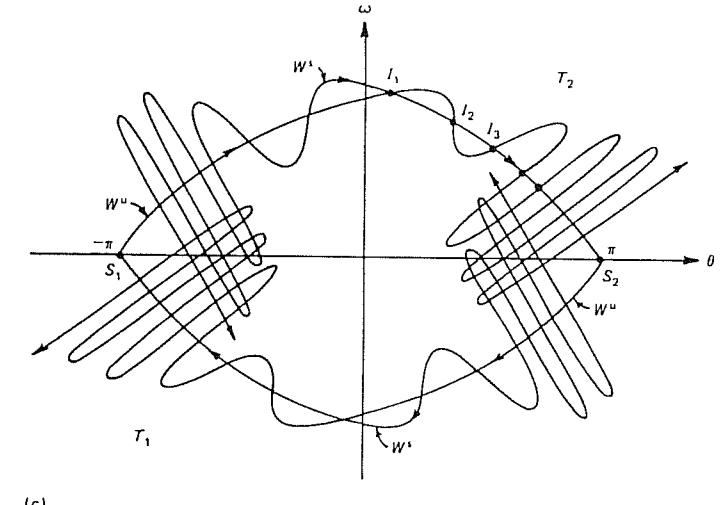


Fig. 4.21 *cont.*

If the pendulum is driven more strongly, the unstable manifold from the saddle at  $\pi$  and the stable manifold from the saddle at  $-\pi$  may approach each other and touch as shown in Figure 4.21(a), or even cross at the point  $I_1$  in Figure 4.21(b). (The actual trajectories do not cross of course, but the stable and unstable manifolds in the Poincaré section can

cross.) Now comes the surprise. Each crossing is mapped into another one closer to the saddle point, leading to an infinite number of intersections  $I_2, I_3$ , and so forth. The resulting configuration is called a *heteroclinic tangle*. (If  $W^s$  and  $W^u$  come from the same fixed point, the configuration is known as *homoclinic*.)

Because of the strong bending of the manifolds near the saddle point, a small rectangular section of the plane near  $I_1$  will suffer stretching and folding much like that of the horseshoe map. In fact, that distorted rectangle is topologically equivalent to (can be smoothly deformed into) the iterated Smale horseshoe (Abraham and Shaw, 1984). As a result, two points that are initially close together will be found far apart after a few iterations. Therefore, chaos is a natural consequence of a heteroclinic tangle.

The actual situation is even more complicated than Figure 4.21(b) suggests. Let us label the first tangle near saddle  $S_1$  as  $T_1$  (see Figure 4.21(c)). Clearly there must be a second tangle  $T_2$  near the saddle  $S_2$  at  $\pi$ , since the geometry there is the same as that near  $S_1$ . But where did the first intersection  $I_1$  in the tangle come from? It must have resulted from an earlier iteration. Going *backward* in time takes  $I_1$  back through an infinite sequence of intersections to the neighborhood of  $S_1$ . This implies that the stable and unstable manifolds from  $S_2$  must cross each other an infinite number of times near  $S_1$ . Thus, the geometry of the pendulum (as visualized in the Poincaré plane) is infinitely complex, and the essential character of that complexity is contained in the horseshoe map.

#### 4.4 Application to the pendulum

The logistic map, the standard map, and the horseshoe map illustrate the kinds of phenomena that are important aspects of the motion of the driven pendulum. Though we have alluded briefly to connections between the driven pendulum and the maps, we now discuss several of these connections in greater detail.

- (i) *Period doubling.* The logistic map illustrates the period-doubling route to chaos. Reference to the bifurcation diagram of Figure 4.22 provides evidence of similar behavior for the pendulum. A pair of period-doubling cascades begins at  $g \approx 1.07$  (preceded by symmetry breaking at  $g = 1.0$ , where the angle exceeds  $\pi$ ). An examination of the data of Figure 4.22(b) at greater magnification of  $g$  and  $\omega$  than in

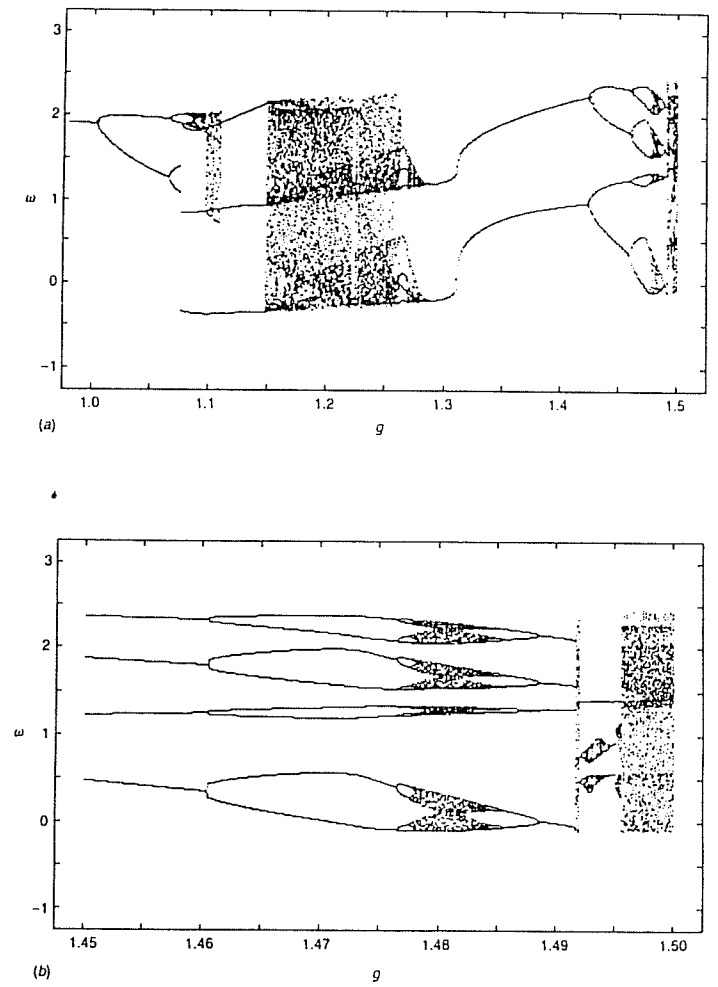


Fig. 4.22 Bifurcation diagrams for the pendulum, indicating various dynamical regimes. The diagrams are generated by following the long-term behavior of two initial points  $(\theta_0, \omega_0)$ , one each from the positive  $\langle \omega \rangle$  and negative  $\langle \omega \rangle$  basins of attraction. (b) Magnification of part (a).

Figure 4.22(a) shows period doubling at  $g = 1.067$ ,  $g = 1.079$ , and  $g \approx 1.082$ , with further bifurcations unresolved. Using these data the ratios of the changes in  $g$  can be estimated and compared with the Feigenbaum number, 4.669.... For this sequence the result is  $4 \pm 1$ . It is remarkable that the behavior of the logistic map is manifested (to within the computational accuracy) in the more complex pendulum.

- (ii) *Phase locking.* Phase locking of the pendulum is evident when the average angular velocity is some rational multiple (usually low order) of the angular forcing frequency  $\omega_D$ . This condition may be specified in the following way. If the pendulum is phase locked at a ratio  $p/q$ , then for  $q$  drive periods the angle difference is  $\theta(t+qT) - \theta(t) = 2\pi p$ , where  $T$  is the drive period,  $2\pi/\omega_D$ . Then the average value of  $\omega = d\theta/dt$  over  $q$  periods is

$$\langle \omega \rangle = (1/qT) \int_t^{t+qT} \omega dt = (p/q)\omega_D. \quad (4.22)$$

Measurement or computation of the average angular velocity is a useful tool for analysis of the pendulum motion. A graph of  $\langle \omega \rangle$  versus  $g$  as shown in Figure 4.23 should reveal phase-locked motion. This figure complements the bifurcation diagrams of Figures 4.22 and 3.1. Two sets of initial conditions were chosen, one from each basin of attraction at  $g = 1.45$ , to illustrate positive and negative rotary modes. The plateaus of  $\langle \omega \rangle$  are indicative of phase locking; they correspond to the periodic intervals of the bifurcation diagram. The regions in which  $\langle \omega \rangle$  varies erratically correspond to the chaotic state (Gwinn and Westervelt, 1986).

Another approach to the study of phase locking is direct examination of the winding number for a range of forcing amplitudes,  $g$ . In the diagrams of Figure 4.24 the winding number is shown for two ranges of  $g$ . It is defined for the pendulum as

$$W = \lim_{n \rightarrow \infty} \left( \frac{\theta_n - \theta_0}{2\pi n} \right), \quad (4.23)$$

where  $n$  is the number of drive cycles. As in the previous diagrams initial values were chosen from the two basins of attraction to show positive and negative angular velocities. For each value of  $g$  an initial motion corresponding to 50 drive cycles is discarded, and the next 30 cycles ( $n = 30$ ) of angular displacement are used to obtain  $W$ . The features of these diagrams are essentially the same as those of the

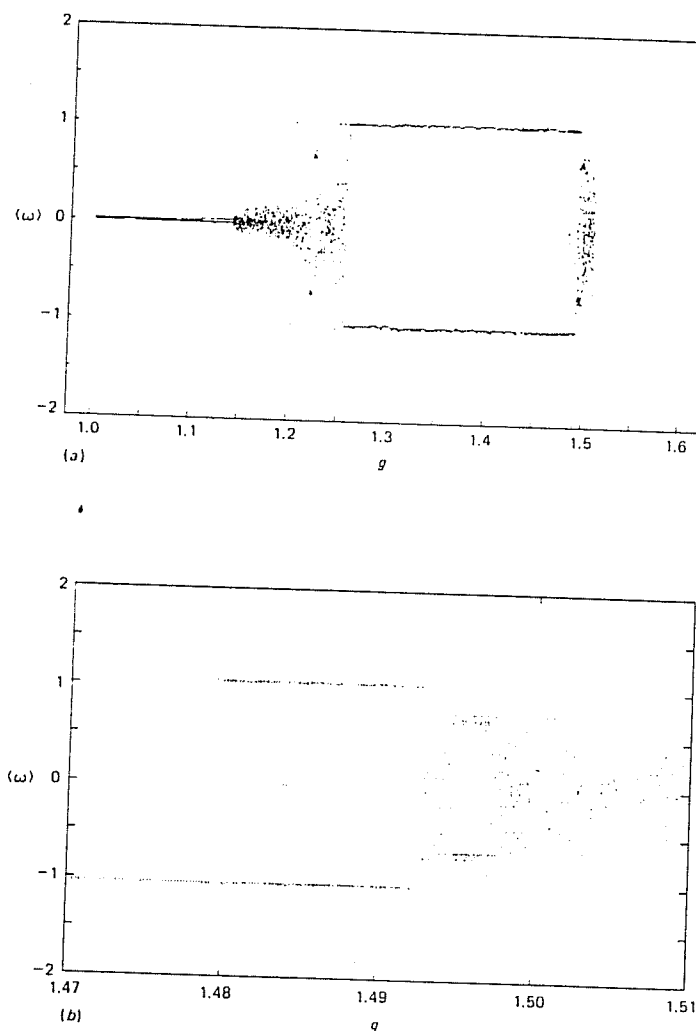


**Fig. 4.23** Phase locking of the pendulum as revealed by the average angular velocity  $\langle \omega \rangle$  (in units of  $\omega_D$ ) as a function of the driving force amplitude  $g$ . Sets of initial coordinates  $(\theta_0, \omega_0)$  were chosen from the two basins of attraction. (b) Magnification of part of (a).

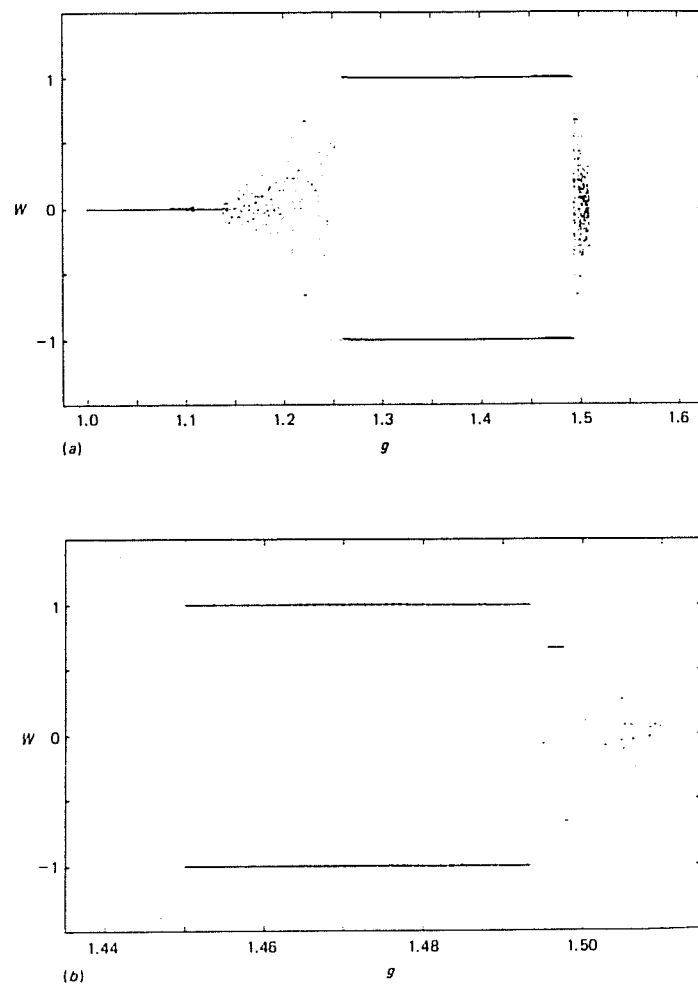


Fig. 4.24 Phase locking of the pendulum as revealed by the winding number  $W$  as a function of driving amplitude  $g$ . Sets of initial coordinates were chosen from the two basins of attraction. (b) Magnification of part of (a).

Table 4.1. Correlation of dynamical behavior with winding number. Behavior designated ‘chaotic(ma)’ indicates multiple chaotic attractor.  $q=2$  and  $\omega_D=\frac{2}{3}$

Range	Type of behavior	Winding number
$g < 1.085$	periodic	0
$1.085 < g < 1.11$	chaotic(ma)	$\sim 0$
$1.11 < g < 1.14$	periodic	0
$1.14 < g < 1.22$	chaotic	scattered
$g \sim 1.22$	periodic	$\pm \frac{2}{3}$
$1.22 < g < 1.26$	chaotic	scattered
$1.26 < g < 1.28$	chaotic(ma)	$\sim \pm 1$
$1.28 < g < 1.475$	periodic	$\pm 1$
$1.475 < g < 1.485$	chaotic(ma)	$\sim \pm 1$
$1.485 < g < 1.493$	periodic	$\pm 1$
$1.493 < g < 1.495$	chaotic	scattered
$1.495 < g < 1.497$	periodic	$\pm \frac{2}{3}$
$g > 1.497$	chaotic	scattered

graphs of  $\langle \omega \rangle$  versus  $g$ , since both measure the average rotation rate, using different computational schemes.

The graph of  $W$  versus  $g$  shows two types of behavior: (a) phase locking with constant  $W$  for periodic pendulum states, and (b) scattered values of  $W$  for chaotic states. The various types of behavior detected as  $g$  increases, and the corresponding values of  $W$ , are shown in Table 4.1.

In this chapter we have demonstrated that discrete mappings can give insight into the complex behavior of the driven pendulum. In the next chapter we examine various aspects of the fractal geometry associated with chaotic motion.

## Problems

- 4.1 Use the listing LOGISTIC MAP in Appendix B or the option LOGISTIC MAP from the CHAOS menu to study the logistic return map. Try different values of the parameter  $\mu$  and different initial values  $x_0$ .

- 4.2 Use one of the programs suggested in Problem 4.1 to study regions where period doubling occurs. First look at the appropriate first order return map and then generate higher order return maps that correspond to the degree of period doubling.
- 4.3 Using one of the programs suggested in Problem 4.1, generate a bifurcation diagram for the logistic map. Expand the scale of  $\mu$  in order to magnify certain regions of the diagram. In particular, expand the scale in a chaotic region and note that windows of periodic behavior are more evident at the higher magnifications.
- 4.4 Expand the scale of  $\mu$  for a bifurcation diagram in the region of period doubling. Try to observe many bifurcations and thereby approximately verify the Feigenbaum number.
- 4.5 For the second bifurcation of the logistic map, the entropy, as defined in the text, is constant over that region of  $\mu$ . What does this fact imply about the distribution of points over the four possible values of  $x_n$  for that range of  $\mu$ ? Now assume that the values of  $x_n$  are tossed with equal probability into each of four bins (out of a total of 40 bins). What is the entropy of this situation? Compare your answer with that of Figure 4.10, and suggest an interpretation of the diagram in that particular region. Using the method of Lagrange multipliers or otherwise, prove that the entropy function is a maximum when  $p_i = 1/N$  for all values of  $i$ .
- 4.6 Another map which shares many properties of the logistic map is the *tent map*:

$$\begin{aligned}x_{n+1} &= 2\beta x_n \quad \text{for } 0 < x < \frac{1}{2}; \quad 0 < \beta < 1, \\x_{n+1} &= 2\beta(1 - x_n) \quad \text{for } \frac{1}{2} < x < 1.\end{aligned}$$

- Use either the TENT MAP option from the CHAOS menu or your own modification of the listing LOGISTIC MAP in Appendix B to generate some mappings and bifurcation diagrams of the tent map.
- 4.7 Use one of the programs suggested in Problem 4.6 to generate a plot of the Lyapunov exponent versus  $\beta$  for the tent map. Prove analytically that the Lyapunov exponent is  $\log_e(2\beta)$ . Note that the exponent becomes positive as  $\beta$  passes through 0.5, the initial point of chaotic behavior.
- 4.8 In the chaotic region of the tent map it is possible to estimate how many iterations are necessary before knowledge of the  $x$  coordinate (with an initial uncertainty) is lost. If the uncertainty in the coordinate after the  $n$ th iteration is  $\epsilon_n$  then the uncertainty after the  $n+1$  iteration is

$$\epsilon_{n+1} = \epsilon_n e^{\log_e 2\beta}$$

(This expression uses the Lyapunov exponent from Problem 4.7.) If the initial uncertainty is  $\epsilon$  how many steps does it require to have an uncertainty equal to 1?

- 4.9 Show that the logistic map (with  $\mu = 4$ ) with the variable  $x_n$  may be transformed to the tent map with the variable  $y_n$  by the coordinate transformation:  $y_n = (2/\pi)\sin^{-1}(x_n^{1/2})$ .
- 4.10 Using either the listing CIRCLE MAP in Appendix B or the option CIRCLE MAP from the CHAOS menu generate the standard map using various values of  $K$  and  $\Omega$ . Determine the differing effects of each of these parameters on the shape of the map. For what value of  $K$  does the map become noninvertible?
- 4.11 Using one of the programs suggested in Problem 4.10, generate several versions of the Devil's staircase. By appropriate scaling of the coordinates, examine the staircase at various magnifications.
- 4.12 The phenomenon of mode locking in the driven pendulum can be examined by considering a modified version of the bifurcation diagram. Instead of keeping  $\omega_D$  constant and varying  $g$ , reverse the operation and let  $\omega_D$  be the independent variable, for constant  $g$ . (This requires the appropriate modification of the bifurcation program.) Try  $g = 1.46$ , for example, and let  $\omega_D$  vary from 0 to 1. You should observe that in the region where  $\omega_D \approx p/q$  for small integer values of  $p$  and  $q$ , the pendulum locks onto a periodic motion.
- 4.13 Horseshoes can be generated in a variety of ways. One example is the baker's transformation:

$$\begin{aligned}x_{n+1} &= 2x_n \bmod 1 \\y_{n+1} &= \begin{cases} ay_n & \text{for } 0 \leq x_n < \frac{1}{2}, \\ \frac{1}{2} + ay_n & \text{for } \frac{1}{2} \leq x_n \leq 1 \end{cases}\end{aligned}$$

for  $a \leq \frac{1}{2}$ . Consider the nondissipative case where  $a = \frac{1}{2}$ , and think about the map as involving several steps. First stretch the  $x$  direction by  $x_{n+1} = 2x_n$ . Then compress the  $y$  direction by using  $y_{n+1} = \frac{1}{2}y_n$ . Then cut the picture vertically in half by applying the mod 1 operation to the original  $x_n$  transformation. Finally, place the right block on top of the left block by adding  $\frac{1}{2}$  to all  $y_{n+1}$  for which  $x_{n+1}$  is greater than  $\frac{1}{2}$ . Write a computer program that will transform a rectangular block of initial coordinates inside the unit square according to the baker's transformation, using  $a < \frac{1}{2}$ . If the program runs many times the result should be a fractal (see Chapter 5).

- 4.14 The baker's transformation is two-dimensional and therefore has two Lyapunov exponents,  $\lambda_x$  and  $\lambda_y$ . Determine these exponents by considering the stretching process in the  $x$  direction and the contraction in the  $y$  direction. (Answer:  $\lambda_x = \log_e 2$ ,  $\lambda_y = \log_e a$ )
- 4.15 Another map that can produce horseshoes is the Hénon map:

$$\begin{aligned}x_{n+1} &= 1 - ax_n^2 + y_n, \\y_{n+1} &= bx_n.\end{aligned}$$

If  $b = 1$  then the map preserves areas, and if  $|b| < 1$  then the map is dissipative. Write a program to transform an initial block of  $(x, y)$  coordinates according to the Hénon map.

- 4.16 For  $g > 1.4$ , the pendulum exhibits period doubling. Use the BIFURCATION program through a range of  $g$  that covers the doubling region and check the ratio:

$$\frac{g_{n+1} - g_n}{g_{n+2} - g_{n+1}},$$

where  $g_n$  is the value of  $g$  at the  $n$ th bifurcation. Does this ratio appear to approach the Feigenbaum ratio?

# 5

## The characterization of chaotic attractors

Many of the geometric structures generated by chaotic maps or differential dynamical systems are extremely complex. For example, the chaotic attractor of the pendulum (Figure 3.3(d)) in its three-dimensional phase space typically consists of an infinite number of infinitely thin layers. Its Poincaré section (Figure 3.5) reveals this structure clearly. These sets are called *fractals*. In this chapter we discuss fractals, their dimensions, and the relation between the fractal character of chaotic attractors and the underlying dynamics.

An elementary example of a fractal is the *Cantor set*. This is a prototype of complex geometric structures in much the same way that the logistic map is a prototype for chaotic dynamical systems. The Cantor set is generated by iteration of a single operation on a line of unit length, as shown in Figure 5.1. The operation consists of removing the

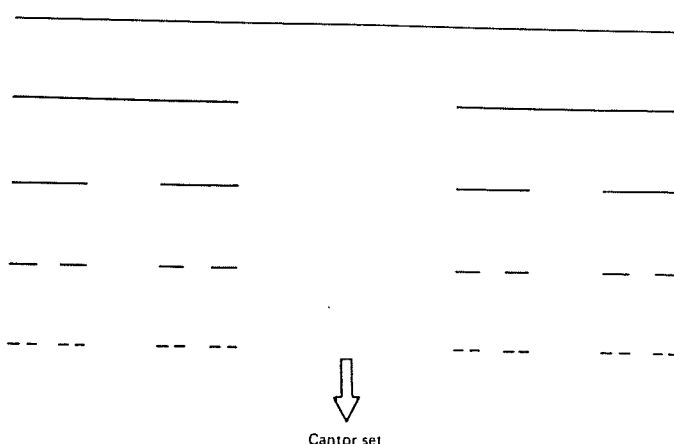


**Fig. 5.1** The Cantor set, produced by the iterated process of removing the middle third from previous segments. The Cantor set has zero length and noninteger dimension.

middle third from each line segment of the previous set. As the number of iterations increases, the number of separate pieces tends to infinity, but the length of each one approaches zero. Furthermore, if the set is examined under high magnification, its structure is essentially indistinguishable from the unmagnified version. This property of invariance under a change of scale is called *self-similarity* and is common to many, although not all, fractals. (Within the resolution of the numerical simulation, the pendulum's Poincaré section of Figure 3.6 appears to exhibit this property.)

In contrast to a line with its infinite number of points and finite length, the Cantor set has an infinite number of points but zero length. Therefore it seems plausible that the dimension of the Cantor set should be less than 1 but greater than zero, the dimension of a finite set of points. The possibility of noninteger dimension requires a more sophisticated concept of dimension than that associated with lines, surfaces, and solids.

## 5.1 Dimension

There are many ways to define the dimension,  $d(A)$ , of a set  $A$ . (The particular set will often be omitted in the notation.) One approach is the *capacity dimension*,  $d_C$ .

Consider a one-dimensional figure such as a straight line or curve of length  $L$ , as shown in Figure 5.2(a). This line can be 'covered' by  $N(\epsilon)$  one-dimensional boxes of size  $\epsilon$  on a side. If  $L$  is the length of the line then

$$N(\epsilon) = L(1/\epsilon). \quad (5.1)$$

Similarly, a two-dimensional square of side  $L$  can be covered by  $N(\epsilon) = L^2(1/\epsilon)^2$  boxes as shown in Figure 5.2(b). For a three-dimensional cube the exponents would be 3, and so on for higher dimensions. In general,

$$N(\epsilon) = L^d(1/\epsilon)^d. \quad (5.2)$$

Taking logarithms one obtains

$$d = \frac{\log N(\epsilon)}{\log L + \log(1/\epsilon)}, \quad (5.3)$$

and in the limit of small  $\epsilon$ , the term involving  $L$  becomes negligible. The *capacity dimension* is defined as

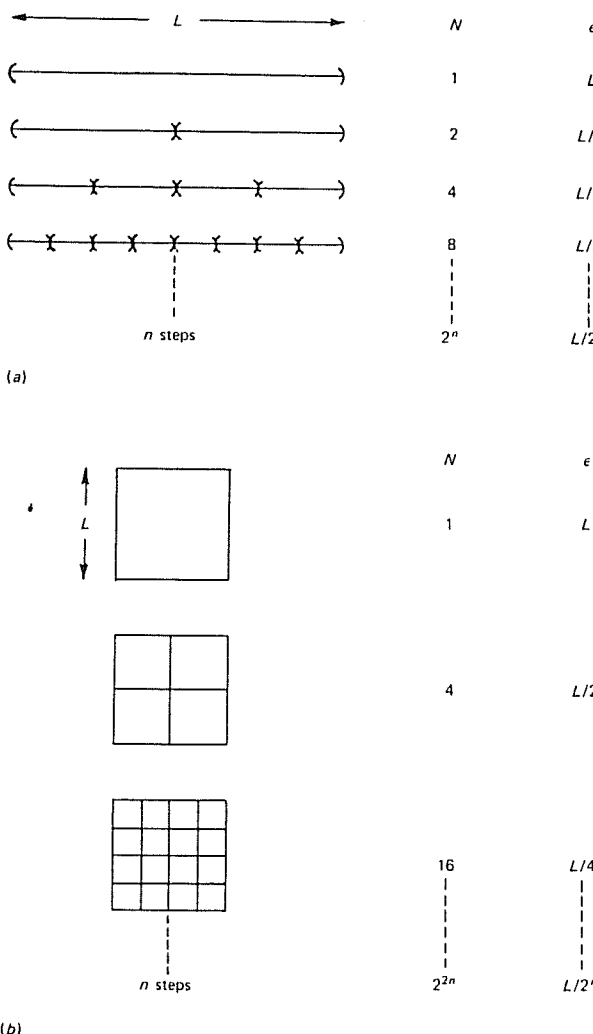


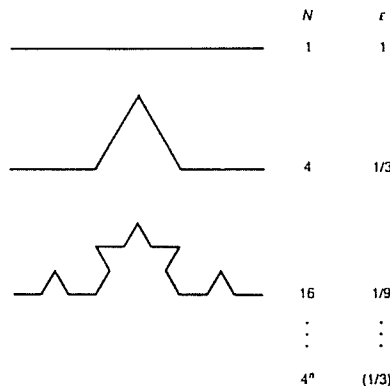
Fig. 5.2 Application of the box covering method to calculate capacity dimension. Boxes of decreasing size  $\epsilon$  are used, leading to increasing numbers of boxes. The scaling exponent gives the dimension.

$$d_C = \lim_{\epsilon \rightarrow 0} \frac{\log N(\epsilon)}{\log(1/\epsilon)}. \quad (5.4)$$

An equivalent approach is to regard  $d_C$  as the slope of the  $\log N$  versus  $\log(1/\epsilon)$  curve as  $\epsilon \rightarrow 0$ . As shown in Figure 5.3 the Cantor set has capacity dimension  $d_C = \log 2 / \log 3$ .

### Example 5.1

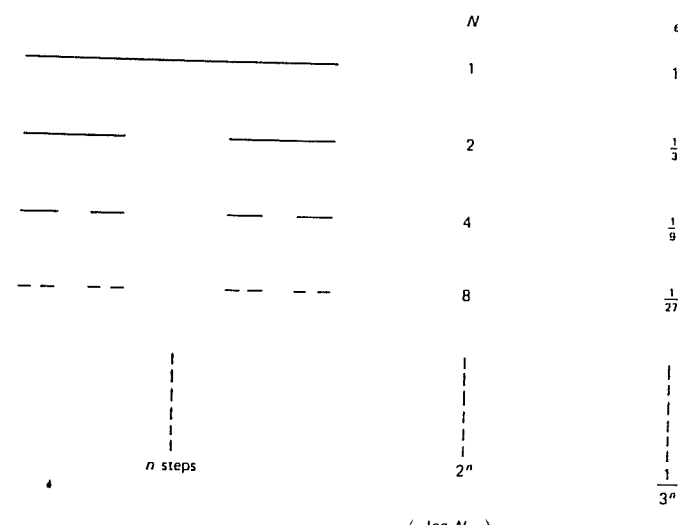
Let us calculate the dimension of the Koch curve. As with the Cantor set of Figure 5.3 we develop a general expression for  $N$  and  $\epsilon$



which leads to  $d_C = \frac{\log 4}{\log 3} = 2 \frac{\log 2}{\log 3}$ . (Note that this result is twice the dimension of the Cantor set.)

For a dissipative dynamical system such as the pendulum, the attractor resides in an  $n$ -dimensional phase space, but its dimension is less than  $n$ . For example, the periodic limit cycle of a lightly driven pendulum in  $(\theta, \omega, \phi)$  space is an elliptical spiral with  $d = 1$ , as seen in Figure 3.3(a). The chaotic attractor of Figure 3.3(d), consisting of an infinite number of closely spaced sheets, has zero volume and  $d_C$  between 2 and 3. Chaotic attractors generally have noninteger dimension, and are called *strange attractors*.

Dimension calculations for dynamical systems with periodic forcing may utilize the Poincaré section rather than the full attractor (Moon and Li, 1985). The time or  $\phi$  direction contributes 1 to the full attractor



$$\begin{aligned} d &= \lim_{\epsilon \rightarrow 0} \left( \frac{\log N}{\log(1/\epsilon)} \right) \\ &= \lim_{n \rightarrow \infty} \left( \frac{\log 2^n}{\log 3^n} \right) \\ &= \frac{\log 2}{\log 3} < 1 \end{aligned}$$

Fig. 5.3 Calculation of the capacity dimension for the Cantor set.

dimension, and therefore the dimension of the Poincaré section is  $D_C = d_C - 1$ . Hence, the Poincaré section of the lightly driven, periodic pendulum has  $D_C = 0$  (it's just a point), whereas the dimension of the Poincaré section for chaotic states is between 1 and 2. Furthermore, a transverse cut across the closely spaced lines of the Poincaré section reveals a Cantor-like structure. One can think of this transverse direction as contributing the fractional part to the overall fractional dimension of the Poincaré section.

The capacity dimension is only one of several types of dimension (Farmer, Ott, and Yorke, 1983). However, any reasonable definition is expected to have the following properties:

- (a) If  $A \subset B$  then  $d(A) \leq d(B)$ . In the case of the pendulum, the Poincaré section is a subset of the full attractor, and, in agreement with this property, the dimension of the section is less (by 1) than that of the attractor.
- (b) The null set has zero dimension.
- (c)  $d(A \times B) = d(A) + d(B)$ . (The symbol  $\times$  indicates the Cartesian prod-

uct. If  $A = \{x_i | i = 1, \dots, n\}$  and  $B = \{y_j | j = 1, \dots, m\}$ , then  $A \times B = \{(x_i, y_j) | i = 1, \dots, n; j = 1, \dots, m\}$ . For the Cantor set in two-space, the dimension is just the sum of the dimensions of two Cantor sets in one-space:

$$\frac{\log 2}{\log 3} + \frac{\log 2}{\log 3} = \frac{\log 4}{\log 3} \quad (\text{Problem 5.3})$$

- (d) If  $f$  is a differentiable and invertible function on the set  $A$ , then  $d(f(A)) = d(A)$ . For the pendulum the Poincaré section represents the state at a specific phase in the drive cycle. At a slightly later phase, the section is modified according to some unknown function,  $f$ , acting upon the previous state. Numerical simulation shows that the dimension remains constant, in conformity with this property.

The capacity dimension may be estimated from experimental or numerically generated data. (Implicit in such estimates is the assumption that the finite set of data points is only a sampling of an infinite set. If the data were actually limited to a finite set, then its dimension would be zero.) The technique of *box counting*, previously applied to the Cantor set, can be used for experimental or numerical data. In Figure 5.4, a portion of the pendulum's Poincaré section is shown covered with square boxes of length  $\varepsilon$ . The required number of boxes of size  $\varepsilon$  is  $N(\varepsilon)$ , and  $\varepsilon$  is varied to obtain  $N(\varepsilon)$ . From the definition given above,  $d_C$  is the slope of the graph of  $\log[N(\varepsilon)]$  versus  $\log[1/\varepsilon]$  as  $\varepsilon \rightarrow 0$ . For this choice of parameters of the pendulum  $d_C = 1.3 \pm 0.1$ .

For experimental data or higher-dimensional dynamical systems another type of dimension is more efficient to compute than the capacity dimension. This is the *correlation dimension*,  $d_G$  (Grassberger and Procaccia, 1983a). Suppose that many points are scattered over a set. The typical number of *neighbors* of a given point will vary more rapidly with distance from that point if the set has high dimension than otherwise. The correlation dimension may be computed from the correlation integral  $C(R)$  defined by

$$C(R) = \lim_{N \rightarrow \infty} \left[ \frac{1}{N^2} \sum_{i,j=1}^N H(R - |x_i - x_j|) \right], \quad (5.5)$$

where  $x_i$  and  $x_j$  are points on the attractor,  $H(y)$  is the Heaviside function (1 if  $y \geq 0$  and 0 if  $y < 0$ ), and  $N$  is the number of points randomly chosen from the entire data set. The Heaviside function simply counts the number of points within a radius  $R$  of the point denoted by  $x_i$ , and  $C(R)$  gives the *average* fraction of points within  $R$ . Figure 5.5 illustrates the

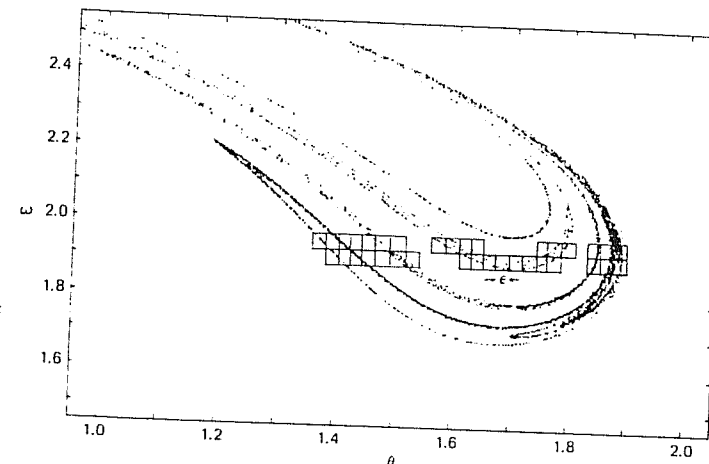


Fig. 5.4 A portion of the pendulum's Poincaré section with some representative boxes covering the points of the section.  $g = 1.4954$ ,  $q = 4$ .

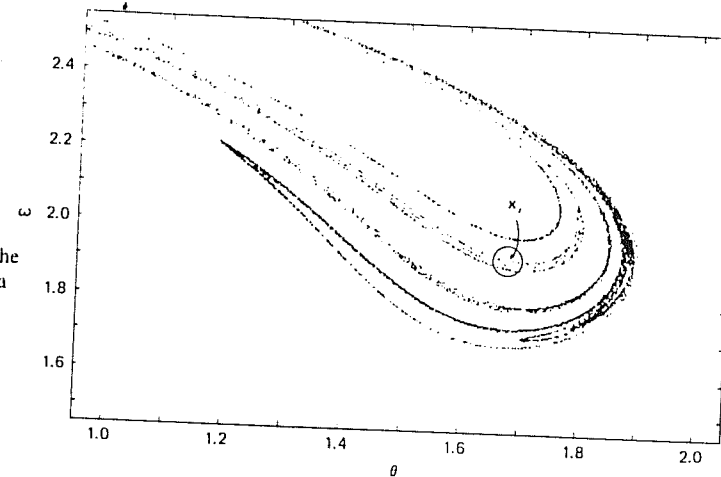
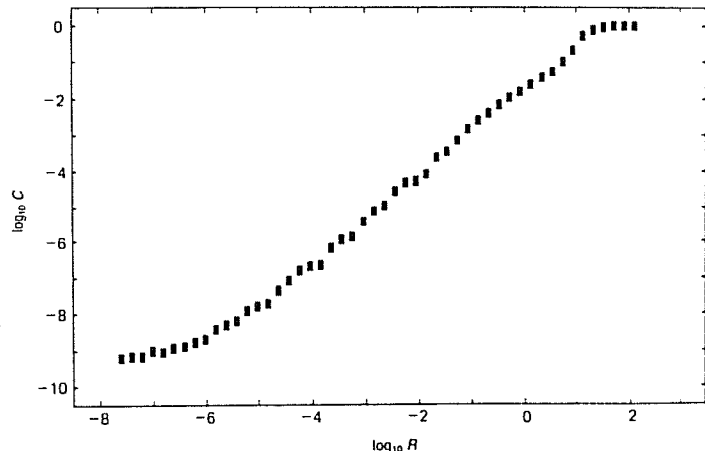


Fig. 5.5 A portion of the Poincaré section with a representative circle centered on the  $i$ th point. All the other points within the circle are counted by the Heaviside function.  $g = 1.4954$ ,  $q = 4$ .

method; each point has a circle of radius  $R$  drawn around it, and then all points within all circles of size  $R$  contribute to  $C(R)$ . This method of estimating the dimension of a set has the advantage of using less computer memory and computational time. The correlation dimension is defined by the variation of  $C(R)$  with  $R$ :

$$C(R) \sim R^{d_G} \text{ as } R \rightarrow 0. \quad (5.6)$$

Therefore the correlation dimension is the slope of a graph of  $\log C(R)$  versus  $\log R$ . Figure 5.6 shows such a graph for the driven pendulum, and



**Fig. 5.6** Graph of  $\log_{10} C$  versus  $\log_{10} R$  for a Poincaré section of the driven pendulum. The correlation dimension is the slope of the straight line portion.

its straight line portion has a slope  $d_G = 1.3 \pm 0.1$ . The line differs from a straight line for high and low values of  $R$ , for the following reasons. When  $R$  approaches the size of the phase space,  $C(R)$  saturates at unity since all points are then included in the circle. On the other hand, when  $R$  is smaller than the spacing between the data points, only one point lies in each circle, and  $C(R)$  levels off at  $1/N^2$ .

The quantities  $d_C$  and  $d_G$  are not equivalent. The capacity dimension depends only on whether small elements of phase space contain *any* points and does not take into account the differing numbers of points in the various elements. That is, small scale variations of the *density* of points are ignored. On the other hand, the correlation dimension does include this effect. Because of these differences,  $d_C$  is called a *metric dimension* and  $d_G$  is called a *frequency dimension*. (See, for example, Farmer *et al.* (1983).)

A third quantity, the *information dimension*  $d_I$ , is related to the entropy defined in Chapter 4. Like  $d_G$ , the information dimension depends on the distribution of points on the attractor. Suppose the attractor is covered by a set of  $n$  boxes of size  $\varepsilon$ , and let the probability that a point is in the  $i$ th box be  $p_i$ . Then the metric entropy or missing information (see Chapter 4) is

$$I(\varepsilon) = - \sum_{i=1}^n p_i \log p_i. \quad (5.7)$$

If the points are equally distributed on the fractal,  $I(\varepsilon)$  takes its

maximum value of  $I_0 = \log n$ . The information dimension  $d_I$  is defined by the equation:

$$d_I = \lim_{\varepsilon \rightarrow 0} \left[ -\frac{I(\varepsilon)}{\log \varepsilon} \right] = \lim_{\varepsilon \rightarrow 0} \left( \frac{\sum_{i=1}^n p_i \log p_i}{\log \varepsilon} \right). \quad (5.8)$$

The information dimension is the ‘scaling exponent’ in the variation of the entropy, or missing information, with  $\varepsilon$ . The remarkable feature of these different definitions of dimension is that they have been shown to be related:

$$d_C \leq d_I \leq d_G. \quad (5.9)$$

If the points are uniformly distributed on the fractal, the equality holds. In practice the numerical values are usually close together (Grassberger and Procaccia, 1983a).

The above definitions of dimension have been consolidated into a general definition of dimensions of *order q*:

$$d^{(q)} = \frac{1}{q-1} \lim_{\varepsilon \rightarrow 0} \left( \frac{\log \sum_{i=1}^n p_i^q}{\log \varepsilon} \right), \quad (5.10)$$

where  $n$  is the number of phase space elements and  $p_i$  is the probability that an attractor point falls in the  $i$ th element. (A concise review is given in Atmanspacher, Scheingraber, and Voges 1988). It can be shown that  $d_C$ ,  $d_I$ , and  $d_G$  are equivalent to  $d^{(0)}$ ,  $d^{(1)}$ , and  $d^{(2)}$ , respectively (see Problem 5.9 and below). The higher order dimensions are sensitive to nonuniformities in the distributions of points on the attractor.

However, for a uniform distribution of points on the attractor it can be shown that all orders of generalized dimension are the same; namely,  $d^{(q)} = d^{(0)}$ . The derivation of this result follows directly from the fact that  $p_i = 1/n$  for a uniform distribution over all  $n$  elements of the phase space for which  $p_i$  is nonzero. Then

$$\begin{aligned} d^{(q)} &= \frac{1}{q-1} \lim_{\varepsilon \rightarrow 0} \frac{\log \sum_{i=1}^n p_i^q}{\log \varepsilon} \\ &= \frac{1}{q-1} \lim_{\varepsilon \rightarrow 0} \frac{\log [n(1/n)^q]}{\log \varepsilon} \\ &= \frac{1}{q-1} \lim_{\varepsilon \rightarrow 0} \frac{\log [(1/n)^{q-1}]}{\log \varepsilon} \end{aligned}$$

$$\begin{aligned}
 &= \frac{1}{q-1} \lim_{\varepsilon \rightarrow 0} \frac{(q-1) \log(1/\varepsilon)}{\log \varepsilon} \\
 &= \lim_{\varepsilon \rightarrow 0} \frac{\log(n)}{\log(1/\varepsilon)} = d^{(0)}. \tag{5.11}
 \end{aligned}$$

But in general,  $d^{(q)} \geq d^{(q')}$  where  $q \leq q'$ .

Let us now show the equivalence of the correlation dimension and the generalized dimension of order  $q = 2$ . That is, we wish to show equality of

$$d^{(2)} = \frac{1}{2-1} \lim_{\varepsilon \rightarrow 0} \frac{\log \sum_{i=1}^N p_i^2}{\log \varepsilon} \text{ and } d_G = \lim_{R \rightarrow 0} \frac{\log [C(R)]}{\log R}.$$

The box size  $\varepsilon$  and the radius  $R$  have roughly equivalent roles, and therefore we take  $R = \varepsilon$ . With this assumption the proof of equivalence amounts to showing that

$$C(\varepsilon) = \frac{1}{N^2} \sum_{i,j=1}^N H(\varepsilon - |\mathbf{x}_i - \mathbf{x}_j|) \text{ is equal to } \sum_{i=1}^N p_i^2. \tag{5.12}$$

Let us start with the correlation integral  $C(\varepsilon)$ . In the summations for  $C(\varepsilon)$ ,  $N$  is both the number of circles (labeled  $i$ ) and the number of points (labeled  $j$ ) tested for each circle. Furthermore, the total number of circles,  $N$ , should be large enough to cover the entire attractor. In essence the circles form a covering set for the attractor. In the other summation,  $p_i$  is nonzero only for those elements of phase space which contain attractor points and therefore the upper limit of the right hand summation is also  $N$ . For these conditions

$$\sum_{i=1}^N p_i^2 = \sum_{i=1}^N p_i^2 \text{ for large enough } N. \text{ Furthermore,}$$

$$\sum_{i=1}^N p_i^2 = \sum_{i=1}^N p_i p_i = \langle p_i \rangle, \text{ the average value of } p_i, \text{ and}$$

$$\langle p_i \rangle = \frac{1}{N} \sum_{i=1}^N p_i \text{ also.} \tag{5.13}$$

We now connect this result to the circles of the correlation integral.

$$\begin{aligned}
 \frac{1}{N} \sum_{i=1}^N p_i &= \frac{1}{N} \sum_{i=1}^N (\text{probability of points in } i\text{th circle}) \\
 &\approx \frac{1}{N} \sum_{i=1}^N \frac{(\text{average number of points in any circle})}{N}
 \end{aligned}$$

$$= \frac{1}{N^2} \sum_{i>j}^N H(\varepsilon - |\mathbf{x}_i - \mathbf{x}_j|), \tag{5.14}$$

which is the desired result. (We emphasize that this result is rigorously true only as both  $N$  and  $1/\varepsilon$  approach infinity. See Ding *et al.* (1993b) for a fuller discussion of this derivation.)

Are so many dimensions really needed to describe an attractor? The answer is yes; strange attractors, like many other fractals, contain more geometrical information than can be described by a single number, in much the same way that the mass distribution of an extended object requires an infinite number of parameters (the 'moments' of a mass distribution) for a complete characterization.

In recent studies of strange attractors, an alternative to the use of these generalized dimensions has emerged. It is based on the idea that complex sets may often be described as 'multifractals', that is, sets consisting of many interwoven fractals, each with a different fractal dimension. The multifractal concept, which is now well substantiated experimentally, leads to characterization of the set by a function called the multifractal spectrum. This function contains the same information as the generalized dimensions  $d^{(q)}$ , so we will not discuss it in this book. However, an accessible account is provided in Glazier and Libchaber (1988). (See also Halsey *et al.* (1986).)

While the calculation of dimension is a common feature of the research literature on strange attractors, misleading results are often obtained, as shown by Arneodo, Grasseau, and Kostelich (1987), and microcomputers are not well suited to these calculations. Therefore we approach the dimension calculation through a remarkable connection between the dimension of the attractor and the time variation of the motion, as characterized by the Lyapunov exponents. In the next two sections we develop this aspect of the subject.

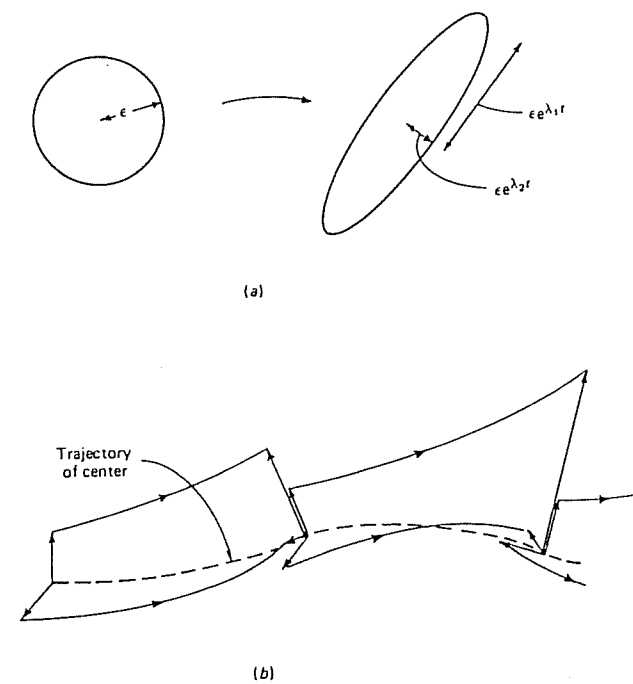
## 5.2 Lyapunov exponents

In Chapter 4 we introduced the idea of the Lyapunov exponent and gave an example for the one-dimensional map. Constraints on the exponents were also given for chaotic, dissipative systems in higher-dimensional spaces. For these systems, of which the pendulum is an example, the conditions are that the sum of all the exponents must be negative, but at least one must be positive to allow sensitive dependence on initial conditions.

For higher-dimensional systems, the calculation of Lyapunov exponents is more challenging than in the one-dimensional case. However, the idea is the same: measurement of the average rate of divergence of neighboring trajectories on the attractor. (See Wolf (1986) for a review article which gives an overview of the subject.)

The direction of maximum divergence or convergence is a changing local property on the attractor. The motion must be monitored at each point along the trajectory. Therefore, a small sphere is defined whose center is a given point on the attractor and whose surface consists of phase points from nearby trajectories. As the center of the sphere and its surface points evolve in time, the sphere becomes an ellipsoid, with principal axes in the directions of contraction and expansion. The evolution of the ellipsoid is illustrated in Figure 5.7(a). The average rates of expansion or contraction along the principal axes are the Lyapunov exponents. For the  $i$ th principal axis, the corresponding exponent is defined as

**Fig. 5.7** A two-dimensional example of the calculation of Lyapunov exponents. (a) The evolution of a sphere of initial point to an ellipsoid. (b)



$$\lambda_i = \lim_{t \rightarrow \infty} \{(1/t) \log_e [L_i(t)/L_i(0)]\}, \quad (5.15)$$

where  $L_i(t)$  is the radius of the ellipsoid along the  $i$ th principal axis at time  $t$  (Wolf *et al.*, 1985). In this expression, the growth rate is always measured along the  $i$ th principal axis, but the absolute orientation in phase space of that axis is not fixed. It is impractical to perform the actual computation in the way suggested by the definition, because the initially close phase points would soon diverge from each other by distances approaching the size of the attractor, and the computation would then fail to capture the local rates of divergence and contraction. Therefore, vectors connecting the surface of the ellipsoid to the center must be shrunk periodically or *renormalized* to ensure that the size of the ellipsoid remains small and that its surface points correspond to trajectories near that of the center point. The renormalization is illustrated in Figure 5.7(b). The Lyapunov exponents are taken to be the averages of those obtained over many segments of the central trajectory.

The algorithm for the Lyapunov exponent calculation in more than one dimension is somewhat beyond the scope of this text, although a computer program that calculates the exponents for the pendulum is included in Appendix B. The method is described in some detail in Wolf *et al.* (1985), and FORTRAN code given in that article is the basis for the program listing.

Nevertheless, it is useful to discuss some of the results for the pendulum. Figure 5.8 shows a typical graph of the three computed Lyapunov exponents for the pendulum, plotted as a function of the number of drive cycles utilized for the computation. The initial transients gradually decay as the calculation is extended over many cycles, so that the structure of the attractor is fully explored.

There are three Lyapunov exponents because the pendulum equations have three variables, and their sum should be negative since the system is dissipative. One exponent corresponds to the direction parallel to the trajectory. It contributes nothing to the expansion or contraction of phase volumes, and therefore the corresponding Lyapunov exponent ( $\lambda_2$ ) is zero.

The remaining exponents are negative or zero in the periodic states, whereas in the chaotic state one exponent is positive, indicating divergence of trajectories. For the parameters used to generate Figure 5.8 the system is chaotic, and (from the figure) the exponents are estimated to be:  $\lambda_1 = 0.16$ ,  $\lambda_2 = 0$ , and  $\lambda_3 = -0.42$ , with an uncertainty of about 0.02.

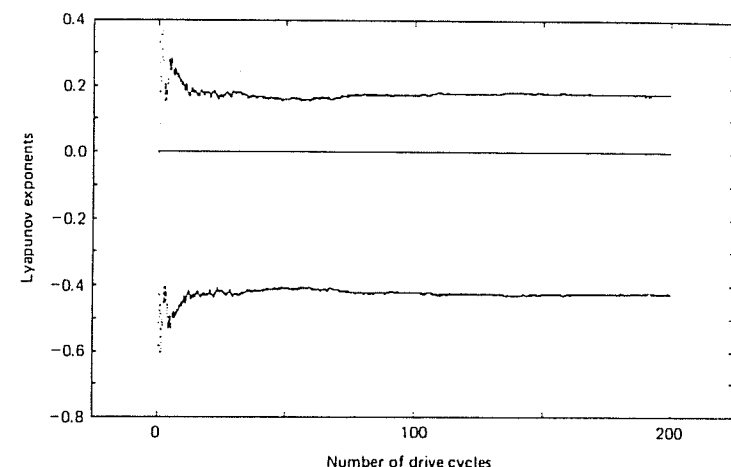


Fig. 5.8 Graph of the three Lyapunov exponents for the chaotic pendulum versus the number of orbits (or drive cycles) used in the computation. Here  $g = 1.4954$  and  $q = 4$ . After a few cycles, the steady state values are reached.

An interesting relationship can be developed between the Lyapunov exponents and the autonomous set of differential equations describing the pendulum. This relation depends on the fact that both the Lyapunov exponents and the differential equations contain information on the change of volumes in phase space, and the relation provides a check on the numerical values developed from the Lyapunov algorithm. First we note that, according to the definition of Lyapunov exponents, a small volume in phase space will change in time as

$$V(t) = V_0 e^{(\lambda_1 + \lambda_2 + \lambda_3)t}, \quad (5.16)$$

and therefore the rate of change of  $V(t)$  is simply

$$\frac{dV}{dt} = \sum_{i=1}^3 \lambda_i V(t). \quad (5.17)$$

Furthermore, the discussion of Chapter 2 concerning the change of phase volume in a time  $\delta t$  showed that the time rate of change of the phase volume can also be written as

$$\frac{dV}{dt} = \nabla \cdot F dV, \quad (5.18)$$

where  $F$  is the vector function forming the right side of the autonomous set of first order differential equations for the dynamical system. In the case of the pendulum,  $\nabla \cdot F$  equals  $-1/q$ , independently of position and time. The two expressions for rate of change of volume are combined and lead to the simple result:

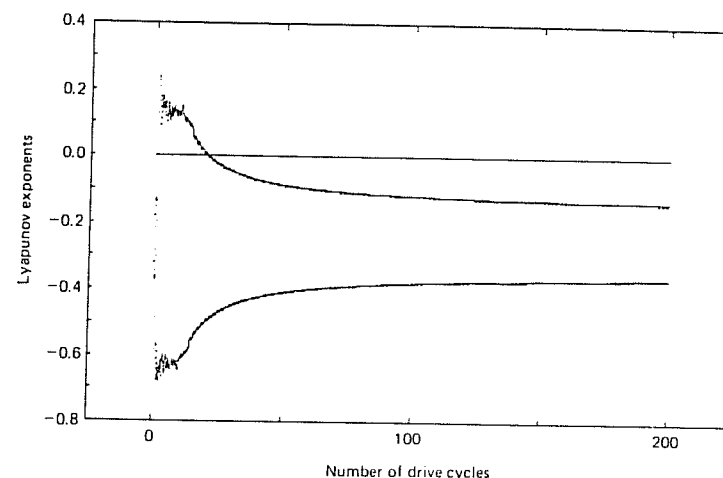


Fig. 5.9 Graphs of Lyapunov exponents computed for a periodic pendulum, with  $g = 1.125$  and  $q = 2$ . The steady state values can be used to check the relation,

$$1/q = - \sum_{i=1}^3 \lambda_i.$$

$$1/q = - \sum_{i=1}^3 \lambda_i. \quad (5.19)$$

The exponents obtained from Figure 5.8 with  $q = 4$  satisfy this relation. The Lyapunov exponents for a periodic state (Figure 5.9) also satisfy the relation to within numerical precision.

### 5.3 Lyapunov exponents and dimension

An interesting and important relationship between Lyapunov exponents and dimension was proposed by Kaplan and Yorke (1979). This conjecture can be developed heuristically by reference to Figure 5.10 where a region in  $(\theta, \omega)$  phase space evolves in time under the influence of a dissipative, chaotic system. In this simple example, one direction stretches by a factor of  $e^{\lambda_1 t}$  with  $\lambda_1 > 0$ , and the other direction shrinks according to the factor  $e^{\lambda_2 t}$  with  $\lambda_2 < 0$ . Therefore the area evolves as  $A(t) = A_0 e^{(\lambda_1 + \lambda_2)t}$ . Now we define a Lyapunov dimension  $d_L$  by analogy with the capacity dimension as

$$d_L = \lim_{\varepsilon \rightarrow 0} \left[ \frac{d(\log(N(\varepsilon)))}{d(\log(1/\varepsilon))} \right], \quad (5.20)$$

where  $N(\varepsilon)$  is the number of squares with sides of length  $\varepsilon$  required to cover  $A(t)$ . Both  $N(\varepsilon)$  and the length  $\varepsilon$  depend on time as follows:

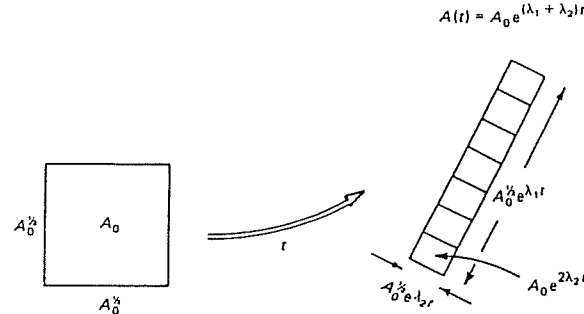


Fig. 5.10 Schematic diagram of the role of Lyapunov exponents in the stretching and contraction of an area in phase space.

$$N(t) = \frac{A(t)}{\text{square area } (t)} = \frac{A_0 e^{(\lambda_1 + \lambda_2)t}}{A_0 e^{2\lambda_2 t}} = e^{(\lambda_1 - \lambda_2)t} \quad (5.21)$$

and

$$\varepsilon(t) = A_0^{-1} e^{\lambda_2 t}.$$

Combining these expressions with the definition of  $d_L$  and using the chain rule, it follows that

$$d_L = 1 - \frac{\lambda_1}{\lambda_2}. \quad (5.22)$$

This is the Kaplan-Yorke relation. Kaplan and Yorke proposed that  $d_L \geq d_G$  and that if the points on the fractal are approximately uniformly distributed, then the equality should hold. (The above derivation depended on a simple example of contraction and expansion in fixed, mutually perpendicular directions. A discussion of the conditions under which the conjecture should be true has been given by Grassberger and Procaccia (1983a).)

The Kaplan-Yorke relation may be generalized to higher-dimensional spaces. The formula becomes

$$d_L = j + \frac{\lambda_1 + \lambda_2 + \lambda_3 + \dots + \lambda_j}{|\lambda_{j+1}|}, \quad (5.23)$$

where the  $\lambda_i$  are ordered ( $\lambda_1$  being the largest) and  $j$  is the index of the smallest nonnegative Lyapunov exponent. For example, in the phase space  $(\theta, \omega, \phi)$  the Lyapunov exponents for the pendulum were found to

Table 5.1. Dimensions of the Poincaré section for various damping factors. All states shown are chaotic. Decreasing the damping allows the Poincaré section to spread and the dimension to increase. ( $g = 1.5$ )

$q$	$\lambda_1$	$\lambda_2$	$\sum_i \lambda_i$	$\frac{1}{q}$	$d = 1 + \frac{\lambda_1}{ \lambda_2 }$
4.0	0.16	-0.42	-0.26	0.25	1.38
3.7	0.16	-0.43	-0.27	0.27	1.37
3.0	0.11	-0.44	-0.33	0.33	1.25
2.8	0.09	-0.45	-0.36	0.36	1.2
2.0	0.12	-0.58	-0.46	0.5	1.2

be  $\lambda_1 = 0.16$ ,  $\lambda_2 = 0$ , and  $\lambda_3 = -0.42$  (when  $g = 1.4954$  and  $q = 4$ ). Therefore  $j = 2$  and the predicted dimension is

$$d_L = 2 + \frac{0.16 + 0}{0.42} \approx 2.4.$$

In the two-dimensional subspace  $(\theta, \omega)$  the exponents are  $\lambda_1 = 0.16$  and  $\lambda_2 = -0.42$  and the calculated dimension is  $d_L = 1 + \frac{0.16}{0.42} \approx 1.4$ , with an uncertainty of 0.05. (Remember that the  $\phi$  dimension corresponds to time and does not contribute to the expansion or contraction of phase volume.) The result  $d_L = 1.4$  correlates well with values of both the capacity and correlation dimension calculated directly for this particular state of the pendulum.

The Lyapunov exponents, in conjunction with the Kaplan-Yorke relation, can be used to study chaotic pendulum states with different amounts of damping. For example, when  $q = 2$  the pendulum is highly damped, points in the Poincaré section are tightly packed, and the dimension is small. Table 5.1 shows Lyapunov exponents for chaotic states with various damping factors. The corresponding calculated dimensions are also given. While the changes indicated are not large, there is a general increase in dimension with decreasing damping. However, the pendulum is not chaotic for every value of  $q$  in the range shown.

From this discussion it is evident that Lyapunov exponents provide an important link between the fractal geometry of the attractor and the property of sensitive dependence on initial conditions.

#### 5.4 Information change and Lyapunov exponents

The condition of sensitivity to initial conditions that is characteristic of chaotic systems implies divergence of initially adjacent dynamical states. While an initial state of the system may be known with a high but finite degree of precision, the ability to predict later states diminishes because of trajectory divergence. Information is lost, or conversely, more information is required to specify the system with the original precision; the entropy has increased.

For many systems the information function has a simple linear time dependence (Atmanspacher and Scheingraber, 1987)

$$I(t) = I_0 + Kt. \quad (5.24)$$

In this expression,  $I(t)$  depends on the probabilities  $p_i$ , which change with time as the system evolves. Note that  $I$  also depends on the length,  $\epsilon$ , of the elemental unit that is used to partition the space. The rate of information change or *Kolmogorov entropy*  $K$  is an average rate taken over long times  $T$ , although in a numerical calculation  $T$  would have to be less than the time taken to cover the entire attractor. Subject to these conditions,  $K$  is defined as

$$K = \lim_{\epsilon \rightarrow 0} \lim_{T \rightarrow \infty} [I(\epsilon, T)/T]. \quad (5.25)$$

(See, for example, Grassberger and Procaccia (1984).)

As an illustration of Kolmogorov entropy, consider an imaginary dynamical model which is capable of (a) deterministic, nonchaotic motion, (b) deterministic, chaotic motion, and (c) random motion, for which future states are completely unknown. The value of  $K$  will depend on the type of motion. We assume that the phase space of the system may be divided into  $N$  small regions, each with probability  $p_i$ . Suppose that the system is known to be in a particular initial phase region, and that all initial probabilities are zero except the corresponding probability for that region, which is one. Therefore the initial information (entropy) is zero. The three kinds of motion will cause different types of evolution and therefore different changes in the information function.

For nonchaotic time evolution the system's phase trajectories remain close together. After a time  $T$ , nearby phase points are closely grouped in some other small region of phase space and there is no change in information. Therefore the Kolmogorov entropy is zero. For chaotic

evolution phase trajectories diverge, and the number of phase space regions available to the system after a time  $T$  is

$$e^{\lambda_+ T}$$

where  $\lambda_+$  is a positive Lyapunov exponent. Assuming that all of these regions are equally likely, the information function now becomes

$$I(T) = - \sum_{i=1}^N p_i(T) \log_e p_i(T) = \log_e e^{\lambda_+ T} = \lambda_+ T. \quad (5.26)$$

Therefore the Kolmogorov entropy in the chaotic case is  $\lambda_+$ . Finally, for random evolution all phase space regions become possible after a very short time, and assuming equal probabilities, the information entropy is

$$I = \log N \quad (5.27)$$

where  $N$  is the number of phase space cells. Although  $N$  is finite, the fact that each cell has a finite probability of being instantly accessible implies an infinite rate of information expansion. Therefore, in the case of random evolution the Kolmogorov entropy is infinite.

From this discussion it is evident that the Kolmogorov entropy for chaotic systems depends on the positive Lyapunov exponent. In systems with several positive exponents,

$$K \leq \sum_{i=1}^j \lambda_i \quad (5.28)$$

where  $j$  is the index of the smallest positive  $\lambda_i$ . Grassberger and Procaccia (1983a) suggest that equality usually holds. Hence knowledge of the Lyapunov exponents provides a good estimate of Kolmogorov entropy, and positive but finite  $K$  implies chaotic behavior. Furthermore, the Kolmogorov entropy provides a means of categorizing the motion of dynamical systems (Atmanspacher and Scheingraber, 1987). If  $K = 0$ , then the motion is regular (periodic, quasiperiodic, or stationary). If  $K > 0$ , then the motion is chaotic, and if  $K = \infty$ , then the motion is random.

Another feature of the Kolmogorov entropy is that it may be used to estimate the time for which future predictions of the state of a chaotic system are valid. After this prediction time, the system's uncertainty has diverged to the size of the phase space (at least in some direction), and the folding action has to occur. Then the system can be described only by a probability density that depends on location in phase space. For purposes of prediction the system becomes probabilistic.

Suppose the system is characterized by a positive Lyapunov exponent,  $\lambda_+$ , and its initial state is defined to within a size  $\epsilon$ . Then, in a time,  $T$ , the uncertainty in the coordinates will have expanded to the size  $L$  of the attractor:

$$L \sim \epsilon e^{\lambda_+ T} \text{ or } L \sim \epsilon e^{KT}. \quad (5.29)$$

Either of these relations may be solved for the prediction time:

$$T \sim (1/\lambda_+) \log_e(L/\epsilon) \text{ or } T \sim (1/K) \log_e(L/\epsilon). \quad (5.30)$$

Therefore, the prediction time increases only logarithmically with the precision of the initial measurement. For this reason, chaotic states allow only short-term prediction.

In chapter 3 we raised a question about the efficacy of very long computer simulations of chaotic systems when such simulations introduced errors that would apparently be rapidly multiplied in chaotic systems. Our derivation of a formula for prediction time allows us to calculate the effect. For example, if the phase space coordinates are in error by only 1 part in  $10^8$  of the attractor size and  $\lambda_+ = 0.16$  then the prediction time is about 115 time units. A computer simulation that introduces errors of this magnitude will then be accurate for only this relatively short prediction time. We can illustrate the effect by providing an artificial 'error' in the form of a small change of initial conditions. In Figure 5.11 we show time series of two pendula with slightly different initial conditions. The starting values of the angular velocity differ by

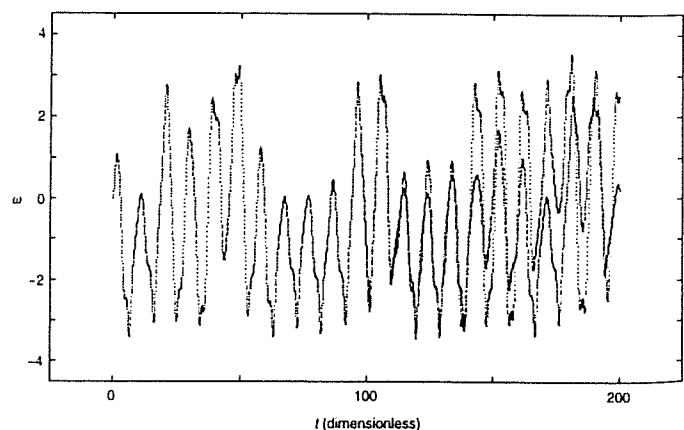


Fig. 5.11 Time series for two pendula whose initial angular velocities differ by  $\Delta\omega/\omega = 10^{-8}$ . The time for divergence of these systems is estimated to be 115 time units.

$4 \times 10^{-8}$  or one part in  $10^8$  relative to the attractor size. As expected, the two time series begin to diverge very close to the prediction time.

Does the divergence inherent in chaotic systems mean that strange attractors produced by long simulations are meaningless? The answer appears to be no (Grebogi *et al.*, 1990, Fryska and Zohdy, 1992). For many chaotic systems the 'true' orbits (error-free) are very dense on the attractor in the phase space. Therefore a 'false' trajectory – one from a simulation with inherent error – is often very close to a true orbit that will shadow the false orbit. Occasionally false and true orbits will break apart and then another nearby true orbit will shadow the false orbit. The result is that, in many circumstances, an attractor developed from a computer simulation will have the same structure as an attractor for true orbits. While an individual time series from a computer simulation may not match a true orbit, the resultant attractor still has the appropriate geometry as well as the correct dimension, Lyapunov exponents, and other more sophisticated invariant measures.

## Problems

- 5.1 The length of the Cantor set may be determined by subtracting the length of each segment taken out of the set during each step in its formation. For example, a length  $\frac{1}{3}$  is taken out in the first step,  $2(\frac{1}{3})$  in the second step,  $4(\frac{1}{3})$  in the third step, and so on. Form the infinite geometric series which this process describes and show that the sum approaches 1. Therefore the Cantor set has no length.
- 5.2 Construct a fractal that is similar to the Cantor set, but instead remove the middle  $\frac{1}{2}$  from each previous section. Show that its dimension is  $\frac{1}{2}$ .
- 5.3 Construct a 'two-dimensional' Cantor set in the following way. Draw two Cantor sets at right angles to each other so they just touch at one corner. Then fill in those two-dimensional regions where each 'one-dimensional' set intersects the other. In other words form the set which is the Cartesian product of the two original sets, as in Figure (a) below. Show that the capacity dimension is  $2(\log 2 / \log 3)$ . (This set resembles the invariant set of the horseshoe transformation; that is, the points which remain from the original set after many iterations.)
- 5.4 Following a procedure analogous to that used in Problem 5.1, calculate the area of the two-dimensional Cantor set defined in

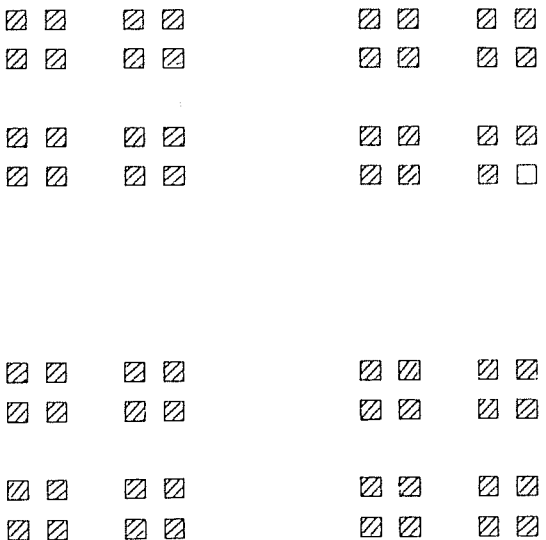


Fig. (a)

## Problem 5.3.

- 5.5 Construct a Cantor-like set by taking squares of relative area  $\frac{1}{9}$  out of the center of larger squares. The process is illustrated in Figure (b). Show that the dimension of the structure is  $3(\log 2 / \log 3)$ .
- 5.6 The Cantor set may be used to study some properties of information dimension. Recall that  $I = -\sum_{i=1}^N p_i \log p_i$ . Calculate  $I$  for each state in the development of the set (as shown in Figure 5.1), assuming that each line segment is equally probable at each iteration. Then use the defining expression for information dimension to show that  $d_I = d_C = \log 2 / \log 3$ , in this case.
- 5.7 Repeat the calculation of Problem 5.6 but do not assume equal probabilities. At every iteration of the set let the right segment have twice the probability of the left segment. For example, when there are four segments the probabilities are, from left to right,  $\frac{1}{9}, \frac{2}{9}, \frac{2}{9}$ , and  $\frac{4}{9}$ . Develop the expression for entropy when there are  $2^n$  segments. Show that, in the limit as  $n$  tends to infinity,  $d_I = 1 - (\frac{2}{3}) (\log 2 / \log 3)$ . (Hint: Be careful with the factorial terms.)
- 5.8 By finding the maximum of the function  $I = -\sum_{i=1}^N p_i \log p_i$ , show that  $d_I$  is maximized when  $d_I = d_C$  (See Problem 4.5.)
- 5.9 Show that the generalized dimensions are equivalent to  $d_C$  and  $d_I$  for  $q=0$  and  $q=1$ , respectively. (Hint: For  $q=1$ , use L'Hôpital's rule.)

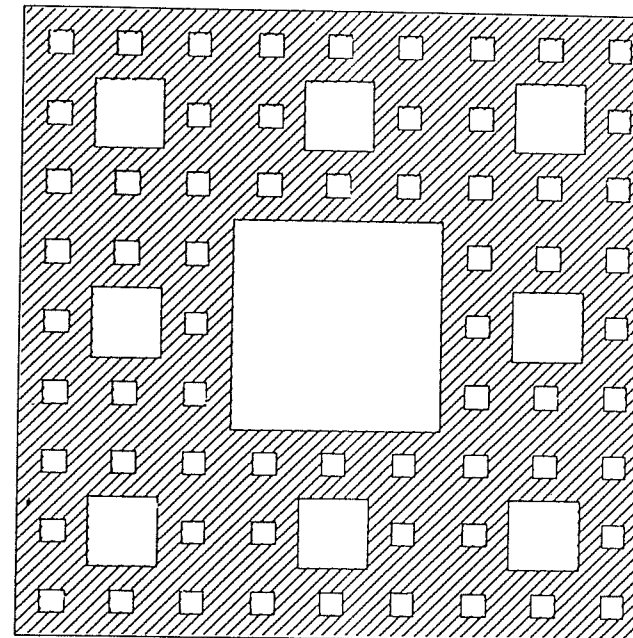


Fig. (b)

- 5.10 For a pendulum with  $q=5$  and  $g=1.5$  the Lyapunov exponents are  $\lambda_1=0.06, \lambda_2=0, \lambda_3=-0.26$ . Verify the relation between Lyapunov exponents and the damping factor. Calculate the Lyapunov dimension for the attractor in  $(\theta, \omega, \phi)$  space.
- 5.11 Estimate the time for predictability of the pendulum of Problem 5.10, assuming its state is initially known to within 1% of the range of the phase variables. How would you expect this time to change if the damping were increased?
- 5.12 Moon and Li (1985) suggested a way to estimate Lyapunov exponents. The method is based on the fact that at a saddle point the stable and unstable trajectories meet and define directions of convergence and divergence of trajectories, respectively. The rates of these behaviors approximate the respective Lyapunov exponents. To study the behavior of the trajectories in the saddle point region the equation of motion is linearized at the saddle point and then solved. Furthermore it is only necessary to solve the homogeneous part of the differential equation because the saddle point is a fixed point in any Poincaré section taken at frequency  $\omega_D$ . An examin-

ation of Poincaré sections taken at various phases shows that  $\theta = \pm \pi$  appears to be the  $\theta$  saddle point coordinate and therefore the required homogeneous, linearized equation is

$$\frac{d^2\theta}{dt^2} + (d\theta/dt)/q - \theta = 0.$$

Substitute the solution  $\theta = e^{mt}$  into the differential equation to obtain the relation

$$m = -\frac{1}{2q} \pm \left( \frac{1}{4q^2} + 1 \right)^{\frac{1}{2}},$$

which has both positive and negative values. These values are the estimates of  $\lambda_+$  and  $\lambda_-$ . Check that they sum to  $V \cdot F$ . Substitute these values into the Kaplan-Yorke relation for  $d_L$ , thereby obtaining a relation for  $d_L$  in terms of  $q$ . Find  $d_L$  in the limiting cases where  $q=0$  (infinite damping) and  $q=\infty$  (no damping). Calculate  $d_L$  in the cases where  $q=2$  and  $q=5$ . Do your results match those given in the text and developed in a previous problem? If not suggest a reason. (Moon and Li change the value of the damping parameter to an *effective* value giving numerical results that better match the dimension. If you were to follow a similar procedure, what value of  $q$  would you choose for essential agreement with the numerically derived  $d_L$ ?)

- 5.13 Use the program PENDLYAP in Appendix B to calculate Lyapunov exponents in various cases. Examine both chaotic and nonchaotic states. Use the bifurcation diagrams to choose the appropriate values of  $g$ .

# 6

## Experimental characterization, prediction, and modification of chaotic states

‘

Chaotic states occur widely in natural phenomena, but closed form mathematical models are rarely available. This situation leads to a number of related problems that bear on the use of experimental data. First, how is it possible to tell whether a set of apparently noisy data in fact arises from chaotic dynamics? Second, how can chaotic data be used to make short-term predictions or forecasts? Finally, how can experimental data be used to influence and control nonlinear systems? We address these questions in the present chapter.

### 6.1 Characterization of chaotic states

In this section, we consider the use of experimental data to *test* for the existence of chaos, to *reconstruct* the chaotic attractor if it exists, and to *characterize* its structure quantitatively.

One rarely has complete information about all of the degrees of freedom in a complex dynamical system. For example, in a chaotic fluid system, this information would include the velocity of the fluid at many different positions as a function of time. Even for the pendulum, a complete specification would seem to require measurement of three distinct time-dependent quantities (the angle, the angular velocity, and the phase of the forcing function).

Although this information can easily be obtained for a pendulum, it is more informative to use the pendulum to learn how to handle situations where a fuller description is unavailable. It is frequently possible to learn a considerable amount from a single *time series*, a list of successive values of one dynamical quantity. This is the case even if the measured variable is not one that appears in the dynamical equations describing the system. Consequently, we focus attention on methods for analyzing time series.

There are quite a few conventional approaches to analyzing time series. One approach, developed for linear systems, is based on spectral analysis, and has been discussed in Chapters 1 and 3. The power spectra of oscillatory *linear* systems can often be interpreted directly in terms of normal modes of oscillation. Furthermore, some of the measurement noise typically occurs outside the frequency range of interest; if so, it can be removed by filtering.

On the other hand, the power spectra of nonlinear systems are more problematic to interpret. It is sometimes difficult to distinguish conclusively between (a) a deterministic periodic oscillation that appears noisy due to a *fluctuating parameter*, and (b) a chaotic oscillation. Filtering generally does not help; it may destroy information about the dynamics. (Kostelich and Schreiber, 1993, Abarbanel *et al.*, 1993)

If a dynamical model is available, one can imagine simply computing the variable that is measured and comparing the computed and measured time series. But how should such a comparison be carried out? They cannot be expected to agree, both because of sensitive dependence on initial conditions, and also because the parameters of the model may not be known sufficiently well. One could compare the statistical properties (such as moments and probability distributions) of computed and measured time series, but even this approach is difficult to carry out successfully.

Consequently, it is useful to consider methods of analyzing experimental data that do not rely on a particular model, but which can be used to detect chaotic dynamics and characterize it quantitatively. Methods for dynamical analysis of experimental time series are still developing, but a common method is a two-step process: (1) reconstruction of the strange attractor of the unknown dynamical system from the time series, and (2) determination of certain invariant quantities of the system from the reconstructed attractor. These invariants might include one or more Lyapunov exponents and the dimension of the attractor. In principle, one can then compare these invariants to their corresponding values as derived from some model system. A close match would lead to

further insight into the dynamics of the experimental system.<sup>†</sup> However, the success of this approach has generally been limited.

In the next few sections of this chapter we describe some of these techniques of dynamical data analysis using a time series for  $\omega(t)$ , the angular velocity of the driven pendulum. A typical example is shown in Figure 6.1 where the angular velocity values are taken at intervals of 7 ms. We use experimental data provided by James A. Blackburn, coinventor (with H.J.T. Smith) of the mechanical pendulum whose motion is simulated by equations that are essentially the same as those used in this book (Blackburn *et al.*, 1989).<sup>‡</sup> Throughout this chapter reference to experimental data implies use of this data set. Reference to simulated data, both periodic and chaotic, implies use of data obtained from numerical solution of the differential equation for the pendulum.

The experimental time series becomes the basis for reconstruction of the attractor and calculation of the dimension and positive Lyapunov exponent. The reconstructed attractor and the invariant quantities are then compared to those same quantities computed directly from the pendulum equations using the methods of Chapter 5.

### 6.1.1 Experiment and simulation

The Blackburn pendulum is constructed so as to be modeled by the equation

$$I \frac{d^2\theta}{dt^2} + b \frac{d\theta}{dt} + \omega_0^2 I \sin\theta = T \sin\omega_f t, \quad (6.1)$$

where  $I$  is the moment of inertia of the physical pendulum,  $b$  is a damping factor,  $\omega_0$  is the natural frequency,  $T$  is the amplitude of the forcing torque, and  $\omega_f$  is the forcing frequency.

The main parts of the pendulum are shown in Figure 6.2 (Blackburn *et al.*, 1989.) A small pendulum bob is attached to a shaft with damping and forcing mechanisms. Damping occurs through the induction of eddy currents in a copper plate whose position may be adjusted relative to a magnet attached to the moving shaft. The forcing frequency and amplitude are adjusted electronically. Optical encoding of the pendulum's motion allows data to be transmitted to a computer for storage on

<sup>†</sup>For example, Ciliberto and Gollub (1985) compared a model of chaotic surface waves with experimental results.

<sup>‡</sup>This pendulum is produced commercially by the Daedelon Corporation and the data for this chapter were gathered from a production model.

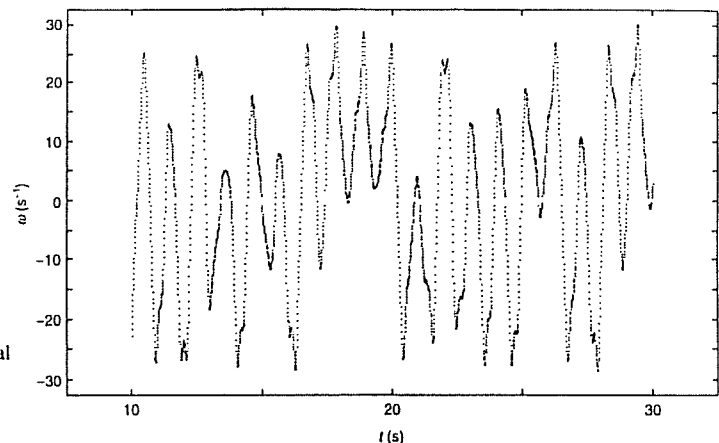


Fig. 6.1 An experimental time series of the angular velocity of the driven pendulum. The sampling interval is 7 ms.

diskette and eventual analysis. Procedures described in the manual that accompanies the commercial version are used to calibrate the pendulum and thereby to obtain conditions that correspond to the chosen parameter values.

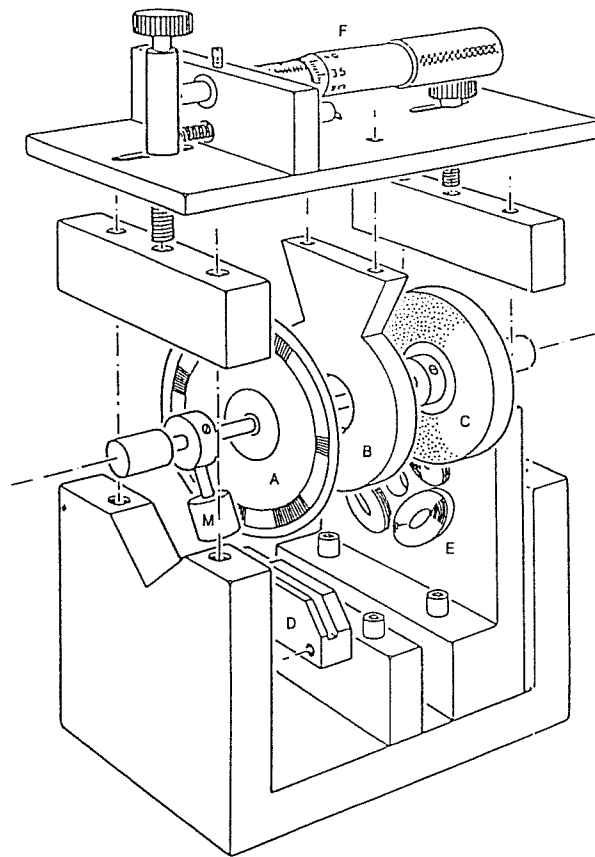
With the exception of a phase difference of  $\pi/2$  in the forcing term, equation (6.1) may be transformed to our previous dimensionless form,

$$\frac{d^2\theta}{dt'^2} + \frac{1}{q} \frac{d\theta}{dt'} + \sin\theta = g \cos\omega_D t', \quad (6.2)$$

by a time transformation  $t' = \omega_0 t$ . (See Problem 6.1.) As a result, the dimensionless parameters  $q$ ,  $\omega_D$ , and  $g$  are expressed in terms of the physical parameters  $b$ ,  $I$ ,  $T$ ,  $\omega_0$ , and  $\omega_f$ . (See Problem 6.2.) All simulations and experimental data from the pendulum were obtained so that the parameters of equation (6.1) corresponded to the values  $g = 1.5$ ,  $\omega_D = 2/3$ , and  $q = 4$ , in equation (6.2). In this way experimental data may be directly compared with some of the figures presented in Chapters 3 and 5. The corresponding parameters for the physical pendulum are  $b/I = 2.24 \pm 0.1 \text{ s}^{-1}$ ,  $T/I = 121 \pm 6 \text{ s}^{-2}$ ,  $\omega_0 = 8.98 \pm 0.05 \text{ s}^{-1}$ , and  $\omega_f = 5.98 \pm 0.02 \text{ s}^{-1}$ .

An initial comparison of the experimental pendulum and its simulation using equation (6.1) may be made by comparing their Poincaré sections shown in Figure 6.3. While there are some similarities, the experimental Poincaré section is somewhat noisy and contains features that are not in the simulated section. Despite these differences, we will see that the

Fig. 6.2 Exploded view of the experimental pendulum. Approximate dimensions are 5 cm  $\times$  9 cm  $\times$  9 cm. Labeled components are: M, pendulum mass; A, code wheel; B, copper damping plate; C, ring magnet; D, encoder module; E, motor coils; and F, micrometer. (From Blackburn *et al.*, 1989, reprinted with permission.)

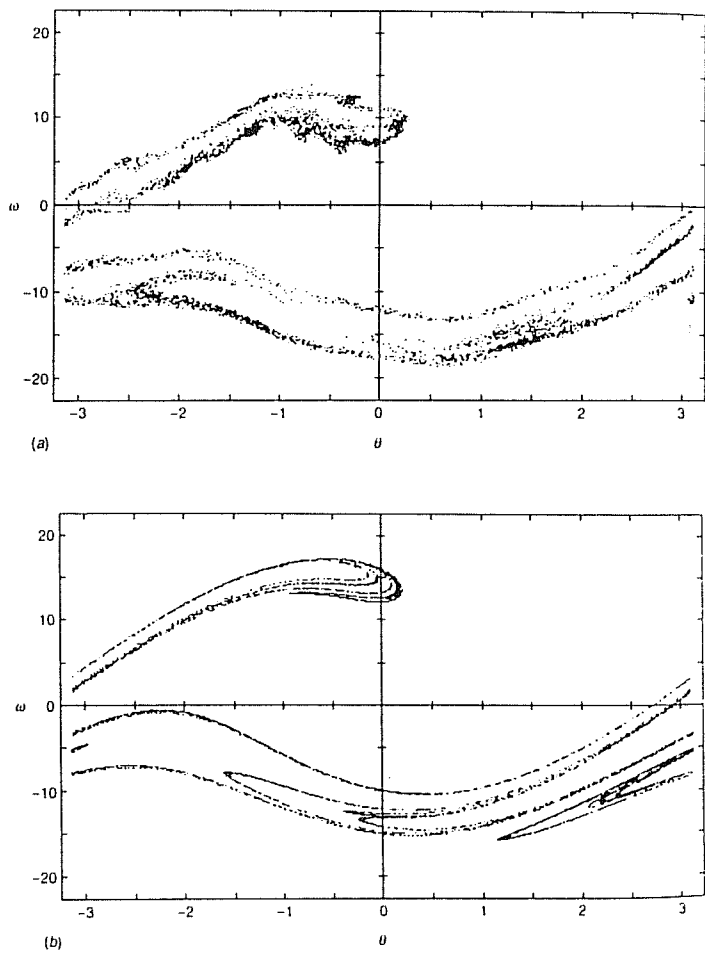


discrepancies between the corresponding invariant quantities are remarkably small.

### 6.1.2 Reconstruction of the attractor

In this experiment we *could* have access to all of the variables. Nevertheless we do not utilize this complete set of information in order to illustrate situations where only a single time series is obtainable. A single experimental time series is affected by all of the relevant dynamical variables, and therefore it contains a relatively complete historical record of the dynamics. It is possible to glean the dynamics from a single

Fig. 6.3 (a)  
Experimental Poincaré section and (b)  
simulation using  
equation (6.1). The  
parameters for the  
simulation are  
 $b/I = 2.245 \text{ s}^{-1}$ ,  
 $T/I = 120.691 \text{ s}^{-2}$ ,  
 $\omega_0 = 8.98 \text{ s}^{-1}$ , and  
 $\omega_t = 5.987 \text{ s}^{-1}$ .



time series without reference to other physical variables. This concept was first illustrated by Packard *et al.* (1980) and given a rigorous mathematical basis by Takens (1981) and Mané (1981).

Reconstruction of the attractor from a single time series requires the generation of additional variables. For some experimental systems the effective number of degrees of freedom is relatively small. Consequently, it is possible to define a low-dimensional ‘phase’ space that captures the dynamics in a geometric structure embedded in that space. The embedded geometric set is called the *reconstructed attractor* and it is

usually topologically equivalent to that attractor which would be produced by numerical solution of the dynamical system equations if they were known. In particular, the dimension and Lyapunov exponents are usually approximately the same for both the original and reconstructed attractors.

The dimensionality of the required phase space is frequently not known in advance; here it is 3. It must be relatively small for reconstruction to be practical. In choosing the coordinate axes of this space we look for relatively independent pieces of information. For example, we might choose the time series variable  $\omega(t)$  and its  $(n-1)$  derivatives to span an  $n$ -dimensional space. If data points are separated by an interval  $\Delta t$  then the derivatives may be approximated by finite differences:

$$\left. \begin{aligned} \frac{d\omega}{dt} &\approx \frac{\omega(t + \Delta t) - \omega(t)}{\Delta t}, \\ \frac{d^2\omega}{dt^2} &\approx \frac{\omega(t + 2\Delta t) - 2\omega(t + \Delta t) - \omega(t)}{\Delta t^2}, \end{aligned} \right\} \quad (6.3)$$

and so on. In practice, high order derivatives are quite noisy. It is simpler and better to use the set of coordinates introduced in Chapter 4; namely, *time delay coordinates*, where each point in the space is an ordered  $n$ -tuple of consecutive values of the time series:  $(\omega(t), \omega(t + \tau), \omega(t + 2\tau), \dots, \omega(t + [n-1]\tau))$ . The time  $\tau$  is typically some multiple of the spacing  $\Delta t$  between the time series points.

In the next sections we discuss the mechanics of attractor reconstruction in the phase space of time-delay coordinates, and calculation of the attractor dimension and the largest Lyapunov exponent.

### 6.1.3 Time-delay coordinates

Consider the time series  $\{\omega(t_1), \omega(t_2), \dots\}$ . Successive points in the phase space formed from time-delay coordinates can be written as vectors,  $\mathbf{y}_j$ :

$$\left. \begin{aligned} \mathbf{y}_1 &= (\omega(t_1), \omega(t_1 + \tau), \omega(t_1 + 2\tau), \dots, \omega(t_1 + (n-1)\tau)), \\ \mathbf{y}_2 &= (\omega(t_2), \omega(t_2 + \tau), \omega(t_2 + 2\tau), \dots, \omega(t_2 + (n-1)\tau)), \\ &\vdots \\ \mathbf{y}_j &= (\omega(t_j), \omega(t_j + \tau), \omega(t_j + 2\tau), \dots, \omega(t_j + (n-1)\tau)), \end{aligned} \right\} \quad (6.4)$$

(Note that  $(t_{j+1} - t_j) = \Delta t$  whereas  $\tau = \text{integer} \cdot \Delta t$ .) Because the time series is presumed (by hypothesis) to be the result of a deterministic process, each  $y_{j+1}$  is the result of a mapping,  $\mathcal{M}$  – generally unknown – from the vector,  $y_j$ . That is,

$$y_{j+1} = \mathcal{M}(y_j). \quad (6.5)$$

Note the similarity of this relation to that defining a Poincaré section and to the other mappings we have discussed.

Often the appearance of reconstructed and numerically simulated attractors are similar. Yet sometimes the attractors may, for various reasons, look very different. We use the Lorenz model as an example of the first case and the pendulum as an example of the second case.

### The Lorenz model

Let us consider the dynamical system introduced by Edward Lorenz (1963) as a simple model of convection. These equations were the first to illustrate chaotic behavior in a model inspired by fluid dynamics. They have the form

$$\left. \begin{aligned} dx/dt &= -\sigma(x + y), \\ dy/dt &= -xz + rx - y, \\ dz/dt &= xy - bz, \end{aligned} \right\} \quad (6.6)$$

where  $\sigma$ ,  $r$ , and  $b$  are parameters that characterize the properties of the fluid and of the thermal and geometric configuration of the experiment. The variable  $x$  is related to the fluid's *streamfunction* (a function which characterizes the fluid flow),  $y$  is proportional to the temperature difference between the upward and downward moving parts of a convection roll, and  $z$  describes the nonlinearity in temperature difference along the roll. Numerical solution of these equations with parameter values  $\sigma = 10$ ,  $r = 28$ , and  $b = 8/3$  leads to an attractor embedded in a three-dimensional space with coordinates  $(x, y, z)$ , as shown in Figure 6.4(a). The trajectory rotates about one of two unstable fixed points (where the derivatives are zero) and eventually escapes to orbit the other fixed point. This process is repeated indefinitely.

An attractor of similar appearance can be reconstructed from the time series of  $x(t)$  alone. Figure 6.4(b) shows the reconstructed Lorenz attractor in a space with coordinates,  $x(t)$ ,  $x(t + \tau)$ , and  $x(t + 2\tau)$ . (The choice of delay  $\tau$  is a nontrivial one and some guidance is provided in the next section.) Note that both figures have the same ‘butterfly’ appearance.

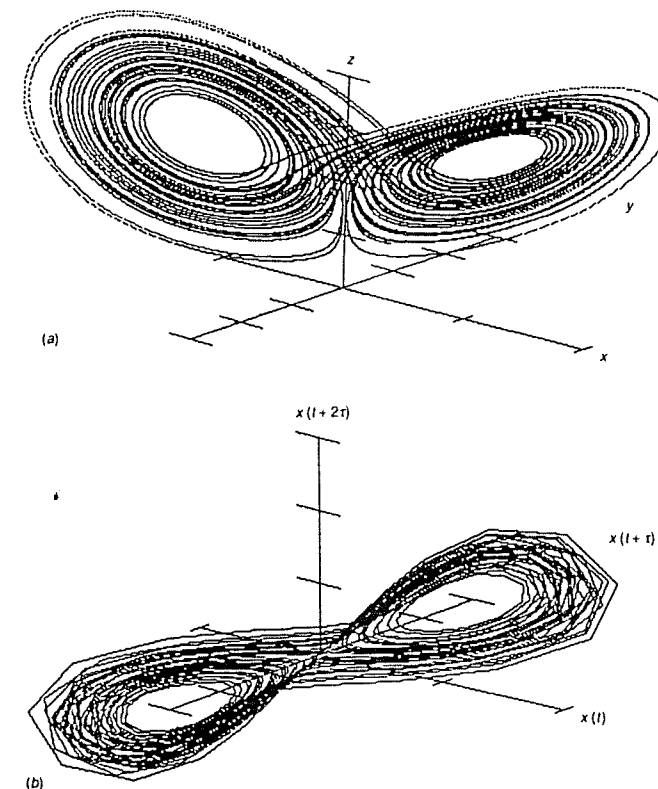
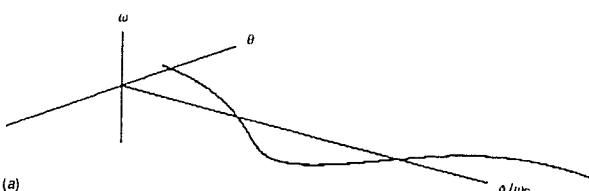


**Fig. 6.4** Chaotic attractors for the Lorenz system. (a) Attractor generated from numerical solution of the differential equations. (b) Attractor reconstructed with time-delay coordinates from the time series for  $x(t)$ .

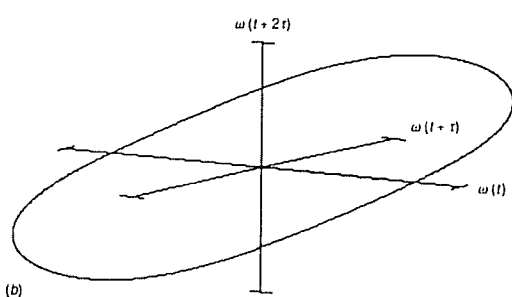
This qualitative geometrical similarity is also found for many other dynamical systems.

### The pendulum

We recall that the pendulum attractor is portrayed in the three-dimensional space with coordinates  $(\omega, \theta, \phi)$  and that both  $\theta$  and  $\phi$  have periodic boundary conditions. These periodic boundary conditions cause the original and reconstructed attractors to differ qualitatively even for the nonchaotic pendulum as shown in Figure 6.5. Figure 6.5(a) shows the numerically simulated spiral attractor for a periodic state of the pendulum. If the periodic motion becomes more complex through period doubling, additional open-ended spirals appear along with the original one, as shown in Figure 3.3.



(a)



(b)

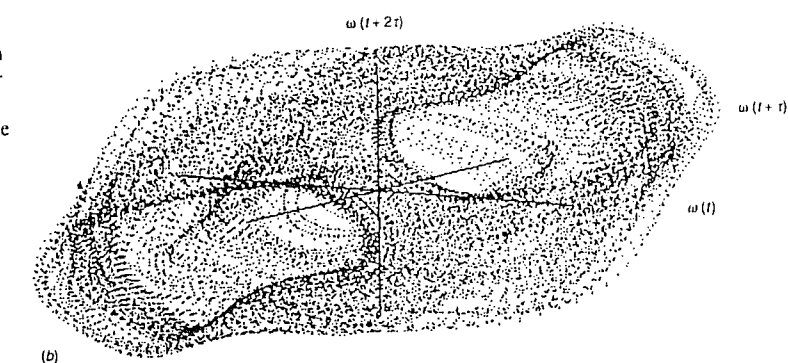
**Fig. 6.5** Periodic attractors for the driven pendulum. (a) The attractor is generated from numerical solution of the differential equations. Because of the periodic boundary conditions on the time variable  $\phi = \omega_D t$ , the orbit is actually closed. (b) Attractor generated by the periodic time series  $\omega(t)$ .

A single time series of the angular velocity from the numerical simulation of Figure 6.5(a) can be used to reconstruct the attractor. (An experimentally determined time series of the angular velocity for a periodic pendulum would give the same reconstructed attractor.) Unlike  $\theta$  and  $\phi$ , this coordinate does not have periodic boundary conditions, and therefore has no discontinuities in its time series. In the regime of small forcing amplitude,  $\omega(t)$  is periodic and its reconstructed attractor, shown in Figure 6.5(b), is a *closed* loop. Period doubling is easily recognized in the reconstructed attractor as a closed loop of two turns (one twist), whereas in  $(\theta, \omega, \phi)$  space the attractor consists of two spirals. Therefore, even in the periodic regime, the original attractor and the reconstructed attractor have a different appearance.

In the chaotic regime the contrast between the numerically simulated attractor with coordinate axes  $(\theta, \omega, \phi)$  and the attractor reconstructed from an experimental time series  $\omega(t)$  is quite marked. The attractor generated from a numerical simulation of equation (6.1) is shown in Figure 6.6(a), and it is very similar to the attractor of Figure 3.3(d) which is a simulation of equation (6.2). On the other hand, the attractor reconstructed from experimental data, shown in Figure 6.6.(b), is quite different in topology from either of the previous figures. As in the periodic case the differences in appearance are primarily due to the



(a)



(b)

**Fig. 6.6** Chaotic attractors for the driven pendulum. (a) Attractor generated from numerical solution of the differential equations with periodic boundary conditions on  $t$  and the angle  $\theta$ . (b) Attractor reconstructed from the time series  $\omega(t)$ . It consists of an infinite number of orbits that never completely close.

existence of periodic boundary conditions in the original attractor, but not in the reconstructed attractor.

#### 6.1.4 Choosing the time delay

The reconstruction of the attractor with time-delay coordinates is not an automatic process. The choice of an appropriate delay  $\tau$  is important to the success of the reconstruction. If  $\tau$  is too short then the coordinates  $\omega(t_j), \omega(t_j + \tau), \omega(t_j + 2\tau), \dots$  of a given vector  $y_j$  are almost equal to each other. The tip of each vector in the space of delay coordinates will lie near the diagonal, and the reconstruction will be useless. In essence, the sampled points from the time series for  $\omega(t)$  are too closely spaced to provide information about the dynamics of the system. (The use of very closely spaced points is somewhat equivalent to the use of derivatives as phase coordinates – a process described earlier. Coordinates of derivatives tend to produce high levels of noise (Eckmann and Ruelle, 1985).)

On the other hand, we know from Chapter 5 that correlations between dynamical states in chaotic systems last for a relatively short time that depends on the positive Lyapunov exponents. If  $\tau$  is too large then the coordinates are so far apart as to be uncorrelated. Significant folding and stretching will have occurred and there is no causal relation between the data used to form the coordinates of a point in phase space.

Several methods for choosing  $\tau$  have been suggested (Fraser and Swinney, 1986, Fraser, 1989, Albano *et al.*, 1988). If the system has some rough periodicity, as occurs with the forced motion of the pendulum, then a value comparable to but somewhat less than that period is typically chosen. When there is no dominant period more sophisticated methods are used. One straightforward approach is to examine the correlation between pairs of data points as a function of their time separation. Define a correlation function

$$f(\mathcal{T}) = \frac{\langle \omega(t)\omega(t+\mathcal{T}) \rangle_t}{\langle \omega(t)^2 \rangle_t}, \quad (6.7)$$

where  $\langle \cdot \rangle_t$  denotes an average over all data points in a time series. Then determine the time  $\mathcal{T}_0$  of the first zero crossing of  $f(\mathcal{T})$  as a measure of the correlation time. Since we seek a value of  $\tau$  that yields high correlation and yet also allows some time development of the system, a modest fraction of  $\mathcal{T}_0$  would be a reasonable choice. Figure 6.7 shows the correlation function for the angular velocity from the experimental chaotic pendulum. The first zero crossing occurs at about  $\mathcal{T}_0 = \frac{1}{3}$  s which, since the data sampling time is 7 ms, corresponds to a delay of 47 points.

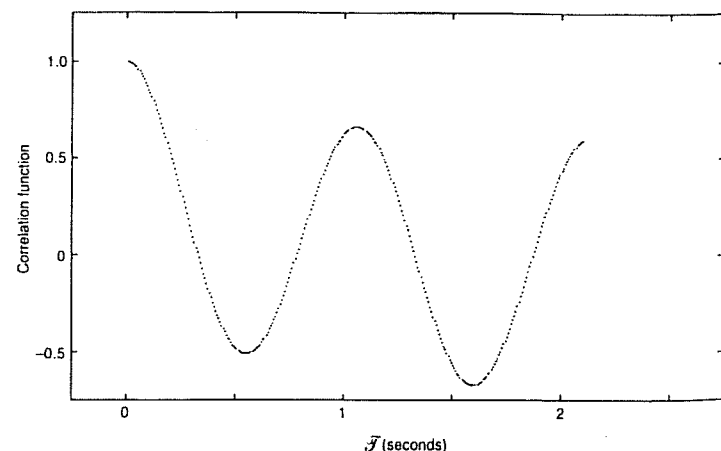


Fig. 6.7 Correlation function for the time series  $\omega(t)$  for the pendulum.

While a typical correlation function might be expected to decay monotonically, the correlation function in Figure 6.7 has a slowly decaying oscillation at the forcing period of 0.95 s. It eventually decays to zero for sufficiently large  $\mathcal{T}$ . In general, the correlation function and the Fourier spectrum provide the same information (see, for example, Press *et al.* (1986)). This oscillation of the correlation function is related to the strong spectral peak at the forcing frequency, shown in Figure 3.9.

Fraser and Swinney (1986) use a more sophisticated approach for selecting  $\tau$  that involves the concept of mutual information. Mutual information provides a measure of the probability that neighboring data points,  $\omega(t)$  and  $\omega(t+\mathcal{T})$ , are not statistically independent. If  $P(\omega(t))$  and  $P(\omega(t+\mathcal{T}))$  are separate probability distributions of the neighboring data points, and if  $P(\omega(t), \omega(t+\mathcal{T}))$  is the joint probability distribution then the mutual information may be defined as

$$I(\mathcal{T}) = \sum_t P(\omega(t), \omega(t+\mathcal{T})) \log \frac{P(\omega(t), \omega(t+\mathcal{T}))}{P(\omega(t)) \cdot P(\omega(t+\mathcal{T}))}. \quad (6.8)$$

If  $\mathcal{T}$  is large then the joint probability is equal to the product of the separate distributions and the mutual information is zero. Therefore the delay  $\tau$  is sometimes chosen to be equal to  $\mathcal{T}_{\min}$  where the mutual information achieves its first minimum. However, in some cases where there is no minimum (such as with the Hénon map) other criteria are used (Abarbanel *et al.*, 1993.)

Because there is no simple rule for choosing  $\tau$  in all cases (Albano *et al.*, 1988, Abarbanel *et al.*, 1993), investigators sometimes adjust  $\tau$  until the results seem satisfactory. This procedure could introduce bias, but the invariant quantities computed from reconstructed attractors are often not too sensitive to  $\tau$  (within a reasonable range) if the number of degrees of freedom is small. For the reconstructions in this chapter a value of  $\tau$  corresponding to about  $\frac{1}{3}\mathcal{T}_0$  seems to work well. The experimental configuration recorded data every 7 ms and therefore the delay  $\tau$  is about 140 ms, or 20 data points. Since the forcing frequency was 0.953 Hz this delay is 15% of the forcing period,  $2\pi/\omega_F$ .

### 6.1.5 Embedding dimension and attractor dimension

The Lorenz attractors in Figure 6.4 are well represented in a three-dimensional space. Similarly we represent the pendulum attractor in the three-dimensional space  $(\omega, \theta, \phi)$  and therefore suspect that its delay

coordinate reconstruction can also be fully represented in a three-dimensional space. However, in reconstructing an attractor from an arbitrary experimental time series of unknown dynamics, the dimensionality of the attractor is unknown. It is important that the reconstruction be *embedded* in a space of sufficiently large dimension to represent the dynamics completely.

One criterion for determining this dimension utilizes the *noncrossing* property (Chapter 2) that ensures the deterministic nature of trajectories. The map for the reconstruction in time-delay coordinates,

$$y_{j+1} = \pi/\pi y_j, \quad (6.9)$$

must be invertible since it is the result of some underlying dynamical system. Takens (1981) suggested that it is sufficient for the embedding dimension  $D$  to be greater than the attractor dimension  $d$  according to the relation

$$D \geq 2d + 1. \quad (6.10)$$

Figure 6.8 illustrates the situation for a hypothetical one-dimensional attractor. The embeddings in one- and two-dimensional spaces lead to spurious crossings that suggest noninvertibility of the map. Furthermore, spurious crossings lead to spurious near neighbors – an effect that produces errors in calculation of the Lyapunov exponent. Only the three-dimensional phase space displays this attractor fully.

(Calculation of the correlation dimension does not require that  $D$  be large enough to satisfy equation (6.10). Ding *et al.* (1993a) have shown that, for long time series with little noise, it is often sufficient that the phase space dimension be greater than the attractor dimension. Therefore the stringent Takens condition may not be required for dimension calculations.)

Nevertheless, the attractor dimension is usually unknown for experimental data and therefore the required embedding dimension is unknown. Fortunately there is a procedure that yields both quantities simultaneously. If the attractor is embedded in spaces of increasingly higher dimension it exhibits an increasingly complex structure as it unfolds, and its measured dimension increases. This progression continues until the attractor is fully revealed, at which point the dimension saturates (in principle). When this condition is reached the embedding dimension is sufficiently high.

The process (first proposed by Grassberger and Procaccia (1983b)) is as follows. We reconstruct the attractor in a low-dimensional space and calculate its apparent dimension. The correlation dimension, described

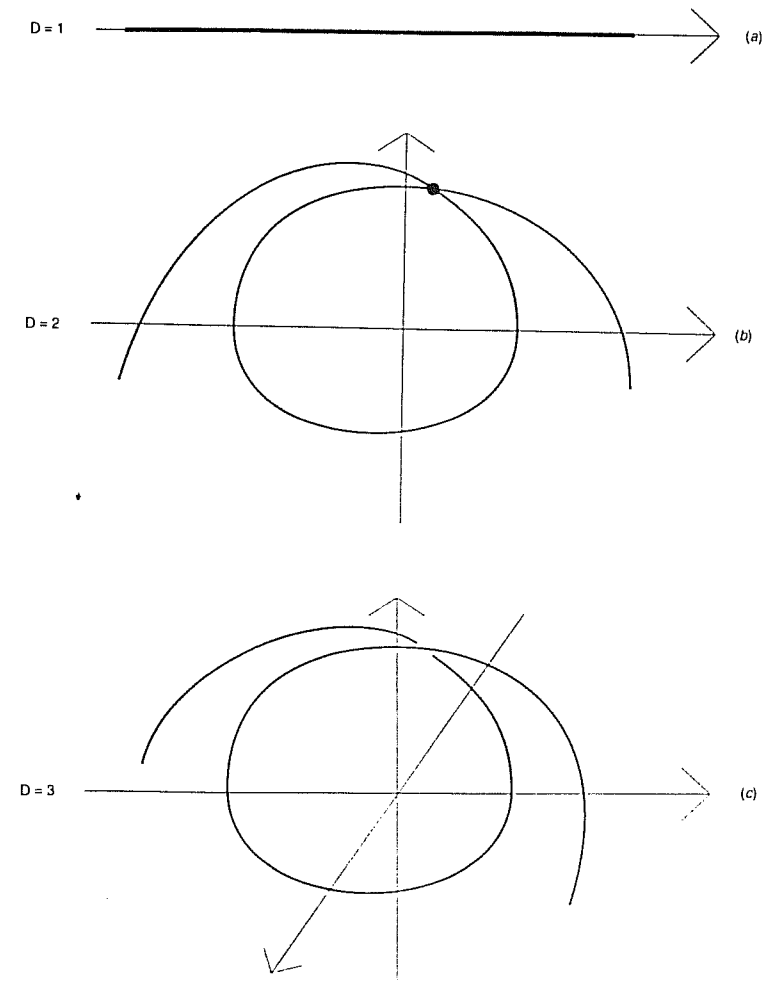


Fig. 6.8 Effect of embedding a hypothetical one-dimensional attractor in spaces of different dimensionality. In (a) and (b) spurious crossings occur, whereas the attractor is fully represented in the three-dimensional space (c).

in Chapter 5, is the typical algorithm used for reconstructed attractors. The dimension of the embedding space is now increased by 1; the attractor is then reconstructed in this new space and its dimension is recalculated. The process is continued until a limiting value of the correlation dimension  $d_G$  is reached.

Such an analysis, using data from the experimental pendulum, is shown in Figures 6.9 and 6.10. The graphs of  $\log C$  versus  $\log R$  appear to

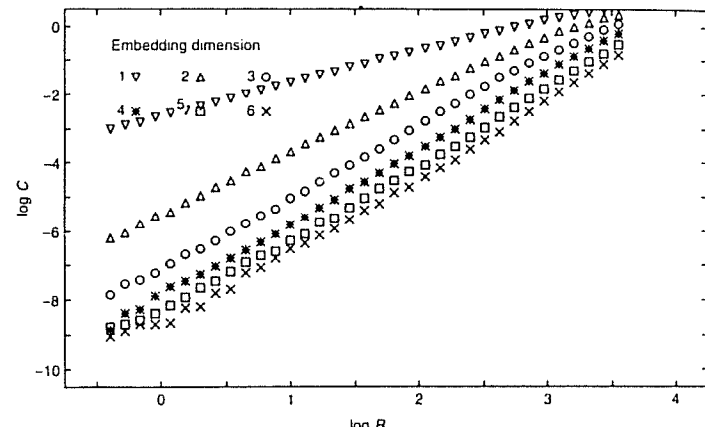


Fig. 6.9 Correlation integral for embedding spaces of increasing dimension, from the experimental data.

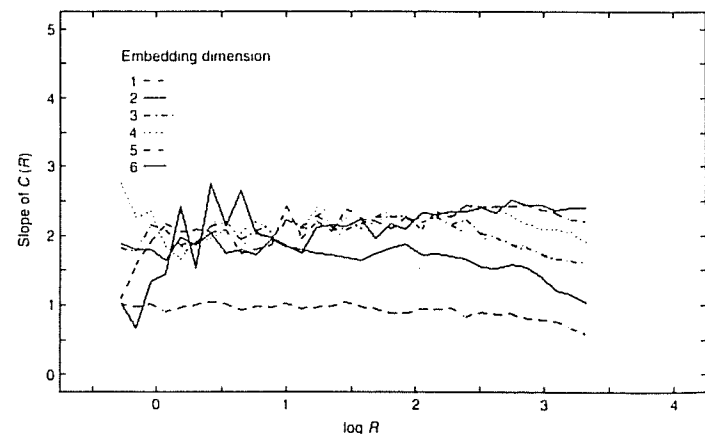


Fig. 6.10 Slopes of correlation integral graphs for  $1 \leq D \leq 6$ . The middle sections of these graphs are approximately horizontal, showing that  $d \approx 2.3$  over a modest range. The slope saturates when  $D \geq 3$ .

have linear scaling regions whose slopes increase with the embedding dimension until a limiting value is reached. However, to make a quantitative test, it is best to plot the slope,  $d(\log C(R))/d(\log R)$ ; this quantity is shown in Figure 6.10 for embedding dimensions 1–6. The slope fluctuates wildly for small  $R$  due to the limited number of points in the time series from which  $C(R)$  was computed. However, the slope does become flat and essentially independent of  $D$  for  $-0.5 < \log R < 2.0$ , provided  $D$  is at least 3. Over this range, the fitted slope (and its estimated statistical uncertainty) is given in Table 6.1 for each choice of

Table 6.1. Saturation of apparent attractor dimension.

Dimension of embedding space $D$	Apparent attractor dimension $d$
1	$0.9 \pm 0.1$
2	$1.8 \pm 0.2$
3	$2.2 \pm 0.2$
4	$2.3 \pm 0.2$
5	$2.3 \pm 0.2$
6	$2.2 \pm 0.2$

embedding dimension. It is apparent that the attractor dimension is approximately 2.3 under these conditions. However, choosing a different scaling range might change these values appreciably, so the quoted uncertainty, which is based on statistical fluctuations only, is probably an underestimate. Furthermore, the use of even moderately noisy experimental data can reduce the scaling range and therefore make the dimension estimate much less precise. (See Ding *et al.* (1993b).)

Nevertheless, the value obtained for the dimension of the attractor reconstructed from the experimental time series compares favorably with the value of  $d = 2.35$  calculated from the pendulum simulation as given in Chapter 5 for the corresponding parameters. (Recall that the experimental pendulum configuration corresponds to a simulation configuration of  $g = 1.5$ ,  $q = 4$ , and  $\omega_D = \frac{2}{3}$ .)

It is best not to use an embedding space of higher dimensionality than is required to produce a limiting value of  $d$  because the undesirable effects of experimental noise become more pronounced for embeddings of higher dimension. Another method that also reveals the minimum embedding dimension is the method of *false nearest neighbors*. (See Brown (1992) and Abarbanel *et al.* (1993).) This procedure is based on the fact that if the embedding space has too low a dimension  $D$  then a given vector may have a neighboring vector that is a false neighbor. That is, if these vectors were embedded in a phase space of dimension  $D + 1$  they would no longer be close neighbors. Therefore one computes the change in distance between these vectors as the phase space dimensionality is increased from  $D$  to  $D + 1$ . If the change is greater than some appropriate constant then the neighbor is presumed false. When the dimension of the phase space is sufficiently large, the number of false neighbors drops abruptly. The dimension for which the transition occurs is the minimal embedding dimension.

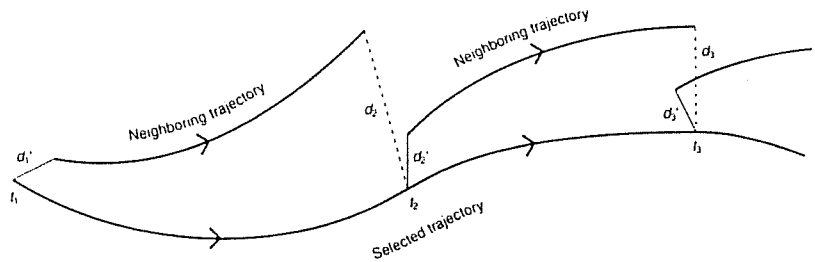
Attractor reconstruction provides, in principle, a way to distinguish between stochastic noise and deterministic dynamics. Data dominated by stochastic noise will populate an embedding space of arbitrarily high dimension, so that the apparent attractor dimension will not reach a limiting value as  $D$  is increased. Of course, any experimental data contain measurement noise, which primarily affects the correlation function at small scales. Therefore, it is necessary to disregard those scales in examining  $C(R)$  for scaling and in determining the attractor dimension.

### 6.1.6 Lyapunov exponents

The spectrum of Lyapunov exponents may also be calculated from the reconstructed attractor. Most of the methods for doing so are complex and beyond the scope of this book, especially when the deterministic data are contaminated with noise. (See, for example, Brown, Bryant, and Abarbanel (1991).) However, there is a straightforward algorithm for calculating the largest positive Lyapunov exponent. This exponent measures how quickly linear distances grow (Abarbanel *et al.*, 1993) and it places an upper limit on the prediction time for the system. Smaller positive exponents have less effect but shorten the prediction time, while negative exponents especially affect the approach of trajectories to the attractor during the initial transient stages of the motion. For the pendulum, there is only one positive Lyapunov exponent.

Wolf *et al.* (1985) give an algorithm for obtaining the largest Lyapunov exponent from a time series. (In principle, this method would also yield the smaller positive exponents, but limitations of the data size often preclude accurate calculation of these smaller exponents.) The approach is based upon following the divergence of a neighboring trajectory from a selected trajectory as shown in Figure 6.11. Over a time

Fig. 6.11 Illustration of the process by which time series data can be used to calculate the largest Lyapunov exponent.



### 6.1 Characterization of chaotic states

interval  $t_2 - t_1$ , the rate of divergence of two points that evolve from a spacing  $\mathcal{D}_1'$  to a spacing  $\mathcal{D}_2$  may be characterized by the quantity

$$\frac{\log_e(\mathcal{D}_2/\mathcal{D}_1')}{t_2 - t_1}. \quad (6.11)$$

Because the separation must be kept small compared with the size of the attractor, a new neighbor must be chosen periodically for subsequent estimates of the divergence rates. After  $n$  repetitions of stretching and renormalizing the spacing, the rates are weighted by the fraction of time between each renormalization and then added to yield an experimental value for the largest positive Lyapunov exponent:

$$\lambda_1 = \sum_{i=1}^{n-1} \left\{ \left[ \frac{(t_{i+1} - t_i)}{\sum_{i=1}^{n-1} (t_{i+1} - t_i)} \right] \left[ \frac{\log_e(\mathcal{D}_{i+1}/\mathcal{D}_i')}{(t_{i+1} - t_i)} \right] \right\}. \quad (6.12)$$

Since  $\sum_{i=1}^{n-1} (t_{i+1} - t_i) = t_n - t_1$  we have

$$\lambda_1 = \frac{\sum_{i=1}^{n-1} \log_e(\mathcal{D}_{i+1}/\mathcal{D}_i')}{t_n - t_1} \quad (\text{Wolf } et \text{ al., 1985}). \quad (6.13)$$

Figure 6.12 shows the result obtained from the experimental pendulum data for  $\omega(t)$ . (We used code from Wolf *et al.* (1985).) We find  $\lambda_1 \approx 1.5 \text{ s}^{-1}$ , but small fluctuations remain at  $t = 200 \text{ s}$ . In order to

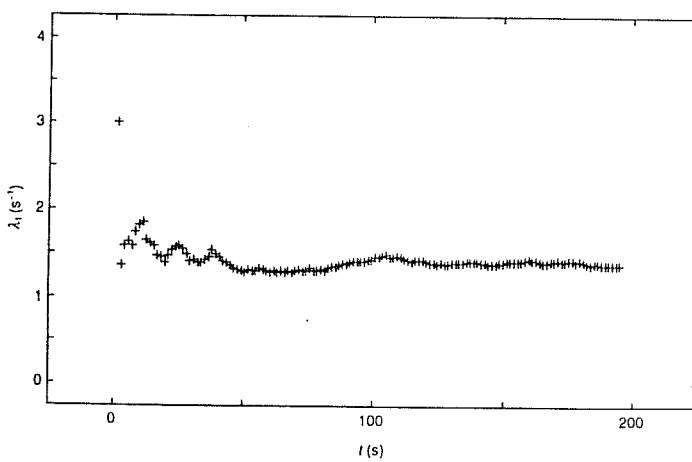


Fig. 6.12 Convergence of the largest Lyapunov exponent calculated from the experimental time series  $\omega(t)$  with the algorithm of Wolf *et al.* (1985).

compare this result with that obtained numerically in Chapter 5 from equation (1.4), which is equivalent to the dimensionless model equation (6.2), we need to convert  $\lambda_1$  to dimensionless form by dividing by  $\omega_0 = 9 \text{ s}^{-1}$ :

$$\lambda_1/\omega_0 = 0.17.$$

This value is in good agreement with the result (0.16) shown in Table 5.1. Finally, using certain assumptions, it is possible to check the consistency of the measured  $\lambda_1$  with the experimental value of the attractor dimension. (See Problem 6.5.)

### 6.1.7 Summary

In this section, we have described some methods for determining properties of chaotic attractors directly from measured time series. The values obtained for the attractor dimension and the positive Lyapunov exponent are in substantial agreement with those found from direct numerical simulation of the model equations. This agreement gives one confidence that the methods can also be applied in circumstances where suitable model equations (or appropriate parameters) are unknown, provided that the dynamics is low-dimensional.

These methods have a number of limitations. First, attractors cannot be completely described by only two or three measured invariant quantities. Therefore, measuring them does not fully characterize the dynamics or uniquely determine an appropriate model. Second, when applied to a chaos in a spatially extended system with many degrees of freedom, the embedding method can produce a severe underestimate of the dimension of the attractor (Lorenz, 1991). For example, local sampling of atmospheric data has been suggested to provide evidence for low-dimensional dynamics. However, a local variable in a strongly turbulent fluid is only slightly influenced by the dynamics even a short distance away, and hence cannot be used to reconstruct an attractor. In general, dynamical systems methods are ineffective when more than a few degrees of freedom are excited.

## 6.2 Prediction of chaotic states

A fundamental goal of scientific inquiry is the prediction of future states of a system. There are also many practical circumstances in which one

might wish to forecast the future of a chaotic system that has been observed up to a given time. Whereas periodic systems are predictable indefinitely, the variables of a chaotic system are partially predictable only for a short time that is related to the positive Lyapunov exponents. (Stochastic systems also generally have a short correlation time during which partial prediction is possible.)

A variety of forecasting techniques have been developed for chaotic systems (Abarbanel *et al.*, 1993, Weigend and Gershenfeld, 1994). In this section we describe several methods and apply them to experimental data from the pendulum.

### 6.2.1 Method of analogues

Probably the simplest prediction technique for time series is the method of ‘analogues’ (Lorenz, 1963). The presumption is that short sequences of points in a chaotic time series are *approximately* repeated throughout the time series. In particular, the final short section of a given time series has a close relative earlier in the series. The continuation of this earlier section then provides a reasonable set of prediction points. For example, we could formulate a crude weather forecast by first looking at all previous local meteorological behavior, and then predicting tomorrow’s weather as the continuation of a previous behavior that mimicked the weather of the past few days. While this method seems crude, it can (with some refinements) be used effectively if the dimension of the attractor is small and the time series contains a large number of points (Kostelich and Lathrop, 1994).

In general, prediction techniques take advantage of the geometry of the orbits on the reconstructed chaotic attractor. One approach combines the method of analogues with the attractor geometry. Recall that any trajectory on a chaotic attractor will generally exhibit near recurrences. We find the nearest earlier neighbor to the latest point on the attractor, and then use the sequence of points following this earlier neighbor as a basis for prediction. Figure 6.13 illustrates the method.

We apply this method to the pendulum using part of the experimental time series to form the attractor from which short-term predictions are made, and the remainder to test the quality of the predictions. The results are shown in Figure 6.14(a) and (b). In the first diagram prediction begins after 22 000 points in the time series and continues for another 700 points. Comparison with the experimental data shows that the forecast is remarkably good given the simplicity of the model. The

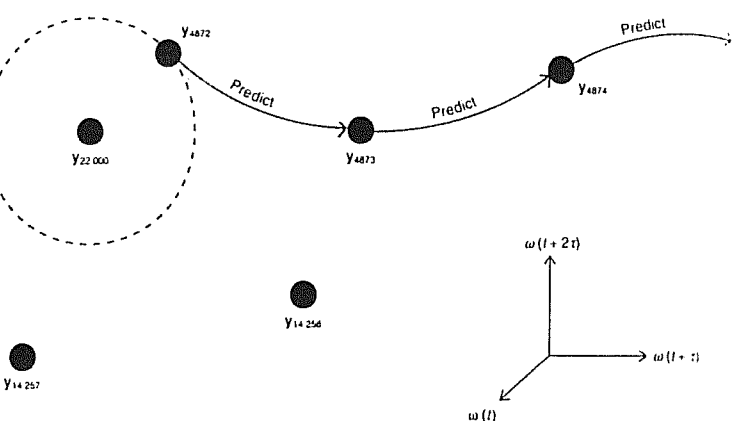


Fig. 6.13 Schematic diagram of the 'nearest neighbor' prediction algorithm.

next figure provides a quantitative measure of deviation of prediction from the experimental values. Following Farmer and Sidorowich (1987) we define an error function

$$E = \frac{\sigma_{\text{pred}}}{\sigma} \quad (6.14)$$

where  $\sigma_{\text{pred}} = \langle [\omega_{\text{pred}}(t) - \omega_{\text{obs}}(t)]^2 \rangle_t^{1/2}$  is the cumulative root mean square deviation of predicted time series from the actual data. This error function is normalized by  $\sigma = \langle [\omega(t) - \langle \omega(t) \rangle]^2 \rangle_t^{1/2}$ , the cumulative standard deviation of the time series data. Therefore, as the prediction becomes meaningless,  $E$  approaches unity and  $\log E$  approaches zero.

Figure 6.14(a) and (b) suggest that the prediction has meaning for 200 or 300 steps (several periods) in the times series. We can make a rough estimate of the maximum time over which any prediction can be expected to be valid. In Chapter 5 the approximate prediction time for a chaotic system was given as

$$T = (1/\lambda_+) \log_e(L/\varepsilon), \quad (6.15)$$

where  $L$  is the attractor size,  $\varepsilon$  is the uncertainty in initial coordinates and  $\lambda_+$  is the positive Lyapunov exponent. The attractor size can be taken to be the length of a diagonal in the phase space, and the Lyapunov exponent is  $1.5 \text{ s}^{-1}$ . The estimation of  $\varepsilon$  is more problematic. One might interpret  $\varepsilon$  as the typical distance between a predicted point and the nearest neighbor used for the next prediction. On average this distance will roughly equal the mean separation between points on the attractor.

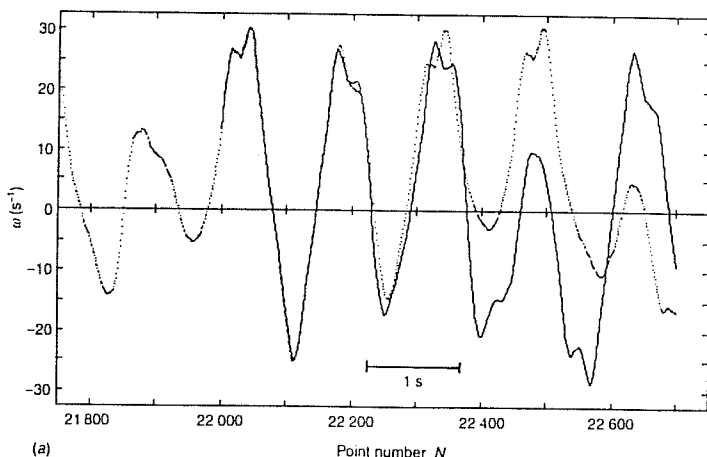
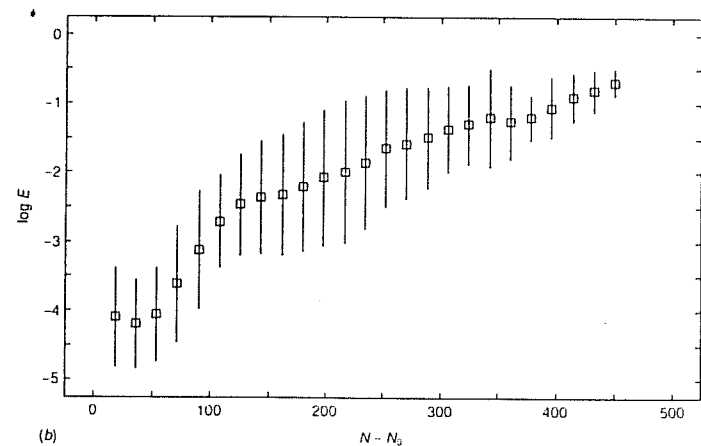


Fig. 6.14 Comparison of predicted and actual data values for the angular velocity of the experimental pendulum using the 'method of analogues' algorithm. In (a) the prediction is compared directly with the experimental points. The predicted values start at point number  $N_0 = 22000$  and are indicated by the solid line. Experimental data are represented by the dotted line. In (b) the natural log of the error function is shown as a function of time or point number. The vertical lines show the variation due to different starting points in the region of  $N_0$ .



If  $N$  is the number of points, then for an attractor of dimension  $d$  each point occupies a 'volume' of size  $\varepsilon^d$  out of a total volume of  $L^d = N\varepsilon^d$ . Using these relationships we rewrite the prediction time as

$$T = (1/\lambda_+) (1/d) \log_e(N). \quad (6.16)$$

For  $d = 2.3$  and  $N = 22000$  points, the maximum prediction time is about 2.8 s, which corresponds to about 400 data points. The estimate is in reasonable agreement with the results shown in Figure 6.14.

### 6.2.2 Linear approximation method

A more satisfying approach to prediction is to develop an approximation for the map

$$\mathbf{y}_{j+1} = M(\mathbf{y}_j). \quad (6.17)$$

Many different mathematical forms may be used. Since the chaotic system is nonlinear one might attempt to fit the data with some combination of nonlinear functions. Undoubtedly, this set would be complex; instead we adopt a simpler approach. The behavior near each point of the attractor may be approximated by a unique *local* map. Then the evolution of points on the attractor is governed by the collection of all such local maps. Furthermore, since the points are close together the map is assumed to be a *linear* map at each point. That is,

$$\mathbf{y}_{j+1} = \mathbf{a} \mathbf{y}_j + \mathbf{b}, \quad (6.18)$$

where the matrix  $\mathbf{a}$  and vector  $\mathbf{b}$  are specific to each point. The aggregate of all these *local* linear maps forms a *global* nonlinear map (Abarbanel *et al.*, 1993). In the three-dimensional embedding space of the pendulum, the explicit form of this transformation is

$$\begin{pmatrix} \omega(t_{j+1}) \\ \omega(t_{j+1} + \tau) \\ \omega(t_{j+1} + 2\tau) \end{pmatrix} = \begin{pmatrix} a_{11} & a_{12} & a_{13} \\ a_{21} & a_{22} & a_{23} \\ a_{31} & a_{32} & a_{33} \end{pmatrix} \begin{pmatrix} \omega(t_j) \\ \omega(t_j + \tau) \\ \omega(t_j + 2\tau) \end{pmatrix} + \begin{pmatrix} b_1 \\ b_2 \\ b_3 \end{pmatrix}. \quad (6.19)$$

The components of  $\mathbf{a}$  and  $\mathbf{b}$  are determined at each point by a *least squares fit*. That is, the function

$$f(\mathbf{a}, \mathbf{b}) = \sum \| \mathbf{y}_{j+1} - (\mathbf{a} \cdot \mathbf{y}_j + \mathbf{b}) \| \quad (6.20)$$

is minimized, where the sum is taken over  $n$  nearest neighbors of the particular point from which the single step prediction is to be made. (See Problem 6.5.) Each  $\mathbf{y}_j$  is a near neighbor of the particular phase point and the corresponding  $\mathbf{y}_{j+1}$  is the successor of that same neighbor. Since a given set of  $\mathbf{a}$  and  $\mathbf{b}$  coefficients applies to a small region, these points must be close neighbors to the point from which the prediction is to be made. The least squares process yields three sets of four linear equations. (See Problem 6.5.) The unknowns,  $a_{11}$ ,  $a_{12}$ ,  $a_{13}$ , and  $b_i$  are determined from equations of the form

$$\left. \begin{array}{l} a_{11} \sum \omega_1 \omega_1 + a_{12} \sum \omega_1 \omega_2 + a_{13} \sum \omega_1 \omega_3 + b_i \sum \omega_1 = \sum \omega'_i \omega_1 \\ a_{11} \sum \omega_2 \omega_1 + a_{12} \sum \omega_2 \omega_2 + a_{13} \sum \omega_2 \omega_3 + b_i \sum \omega_2 = \sum \omega'_i \omega_2 \\ a_{11} \sum \omega_3 \omega_1 + a_{12} \sum \omega_3 \omega_2 + a_{13} \sum \omega_3 \omega_3 + b_i \sum \omega_3 = \sum \omega'_i \omega_3 \\ a_{11} \sum \omega_1 + a_{12} \sum \omega_2 + a_{13} \sum \omega_3 + b_i n = \sum \omega'_i \end{array} \right\} \quad (6.21)$$

where  $i = \{1, 2, 3\}$ ,  $\sum = \sum_{k=1}^n$  is a sum over  $n$  nearest neighbors,  $\omega_m = \omega(t_j + (m-1)\tau)$ , and  $\omega'_m = \omega(t_{j+1} + (m-1)\tau)$ . In a refinement of this process, the terms in the sums that are associated with specific points are weighted by a Gaussian factor that depends on the distance from the point in question to a particular neighbor (Casdagli *et al.*, 1992). If that distance is  $d_k$ , the weighting factor is  $e^{-d_k^2/\sigma^2}$  where  $\sigma^2$  is an adjustable cutoff length beyond which neighbors do not contribute appreciably to the summations. Gaussian weighting does improve the prediction.

Let us summarize the procedure.

- (1) Start with the last known point in phase space.
- (2) Search for its  $n$  nearest neighbors in phase space.
- (3) Calculate the sums of coordinates of these points and their corresponding next points as described in the last paragraph.
- (4) Form the linear equations (6.21).
- (5) Solve the equations for the local  $a$  and  $b$  coefficients. (A Gauss-Seidal iterative method works well. See Press *et al.* (1986).)
- (6) With the coefficients as components of the linear transformation, apply the linear map to the last point to obtain a predicted point.
- (7) Repeat the process with the predicted point at the new starting point.

Figure 6.15 shows the resulting prediction for  $\omega(t)$  with a weighting of  $\sigma=2$  and  $n=12$  neighbors.

It is interesting to compare the quality of this prediction with that given by the method of analogues. Although work on some other systems by Farmer and Sidorowich (1987) shows that analogues are less effective for short-term prediction, that approach seems surprisingly to

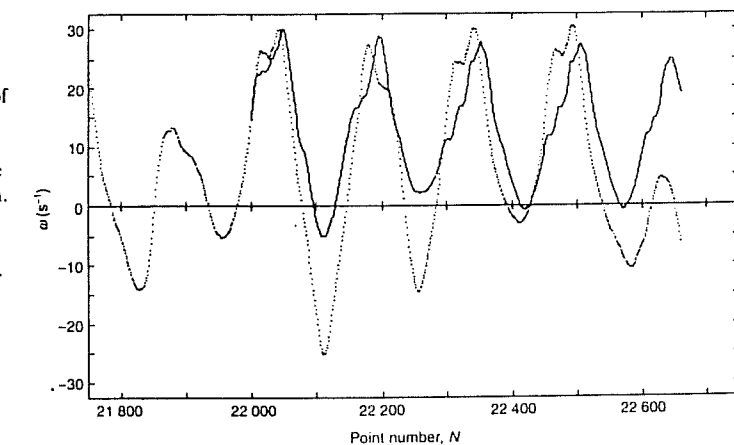


**Fig. 6.15** Comparison of predicted and actual data values for  $\omega(t)$  (experimental) using the 'least squares' algorithm. The prediction is compared directly with the experimental points. The predicted values start at  $N_0 = 22\,000$  and are indicated by the solid line. The experimental data are shown by the dotted line.

be better here. How can we understand this result? First, the result shown in Figure 6.14(a) is one of the better predictions from an ensemble of predictions done in the neighborhood of  $N_0 = 22\,000$ . The error bars in Figure 6.14(b) indicate that the quality of these predictions depends heavily on where the prediction begins. Second, the method of analogues naturally incorporates the nonlinearity of the system, whereas the least squares method approximates the local nonlinear dynamics by a linear map. If the actual dynamics contains strong second derivative terms in the region of prediction, then the linear mapping may be less accurate. Finally, averaging caused by use of the large numbers of neighbors required by the least squares method may result in some further insensitivity to complex dynamics.

On the other hand, the least squares method provides a basis for more sophisticated approaches. For example, least squares models can incorporate nonlinear terms in the map, an extension that is consistent with the spirit of nonlinear dynamics. Furthermore, since least squares methods are optimization techniques, one can add constraints involving invariant quantities. These quantities may include the Lyapunov exponents and the spatial density of points on the attractor. That is, the time series predictions can be constrained to be consistent with Lyapunov exponents and densities that were calculated from the experimental data (Abarbanel, Brown, and Kadtke, 1990). Of course, increasing sophistication brings increasing complexity and greatly increased computation time. Nevertheless, even the crude predictions shown here are an example of what can be achieved for short-term forecasting.

Beyond these refinements there exists a variety of other forecasting methods. For example, efforts have been made to train neural networks – nonlinear devices that simulate neural input/output mechanisms – to predict chaotic states (Lapedes and Farber, 1987). In an attempt to bring together and evaluate these methods, Weigend and Gershenfeld (1994) proposed and organized a contest to predict chaotic states of data taken from such diverse sources as financial markets, fluctuations of a far-infrared laser, time variations of a white dwarf star, and even a Bach fugue. One conclusion that may be derived from the many responses to this contest is that superior short-term prediction is not automatic – computer algorithms must be used with great care and with attention to the nature of the data. The researcher's insight into the nature of the system remains an essential ingredient of the forecasting process. While these developments are quite exciting, accurate prediction is fundamentally limited in time by a chaotic system's sensitivity to initial data as manifested by the positive Lyapunov exponents.

### 6.3 Modification of chaotic states

Chaotic states are inherently unstable and unpredictable; therefore it is sometimes desirable to avoid them. Situations of this type occur, for example, in the design of elastic mechanical structures and electronic circuits. The simplest way to avoid chaos is to adjust the parameters of a system to a regime of periodic rather than chaotic oscillation. However, suitable values of the control parameters may not be known, or the power to change them sufficiently may be absent. One example of a practical attempt at control of chaotic states is the use of pacemakers to control cardiac arrhythmias, some of which are believed to be chaotic oscillations.

An alternative approach is to modify the dynamics in such a way that an unstable periodic orbit becomes stable, so that the motion (if it is in the basin of attraction of this periodic orbit) becomes periodic. Such stabilization is often given the apparently contradictory name 'control of chaos'. For the pendulum, the resulting periodic motion might occur at the forcing frequency or one of its subharmonics.

Are there ways to stabilize a chaotic system without drastically changing its dynamics? One simple method is based on a small periodic perturbation at the frequency of an unstable periodic orbit. (See Braiman and Goldhirsch (1991).) An example of this method, applied to the simulated chaotic pendulum, is given in Figure 6.16. Here a chaotic state is converted to a periodic oscillation by adding a secondary forcing at frequency  $\omega_b/2$  to the basic forcing at  $\omega_b$ . However, the required

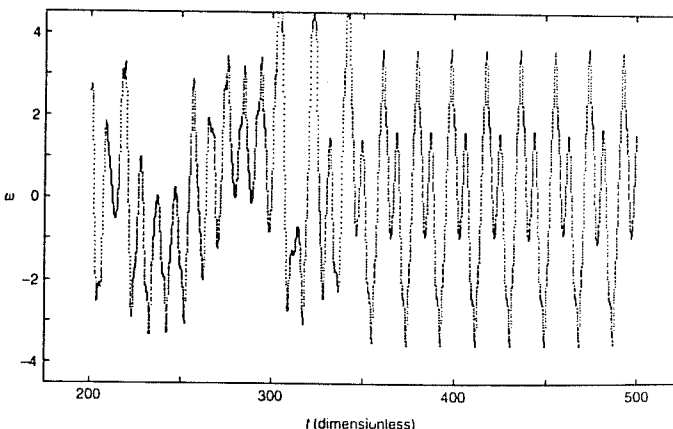


**Fig. 6.16** Time series of a simulated pendulum that is perturbed by a period-2 sinusoidal forcing term. The period-2 motion becomes stable when the perturbation is about 67% of the original forcing amplitude. The control forcing was initiated at  $t = 300$ .

amplitude of the secondary forcing is fairly substantial; in this case the ratio of the secondary amplitude to the primary forcing is about  $\frac{2}{3}$ . Partial control – a reduction in the amount of chaos – may be achieved with smaller secondary forcing and may, in some contexts, be useful. For example, partial control may result in a narrowing of the Fourier spectrum of an experimental time series.

Ott, Grebogi, and Yorke (OGY 1990) proposed an elegant scheme to stabilize an unstable periodic orbit. Their idea was based on the use of feedback to induce small modifications of the control parameter. They applied the idea to simulations of the Hénon map, and stabilized both period-1 and period-2 orbits. The OGY method was subsequently demonstrated in a variety of experiments. Ditto, Rauseo, and Spano (1990) studied the buckling in a magnetic field of a thin ribbon of magnetoelastic material that is attached at its base and free to vibrate elsewhere. Since its elastic constants are affected by magnetic fields, the ribbon can be driven by application of a time-varying field. Changes in the amplitude of the field oscillation cause typical transitions from periodic to chaotic motion. A small dc magnetic field, whose size is about 5% of the amplitude of the ac field, is also present. Control of chaos – stabilization of an unstable periodic orbit – is achieved with very small changes (less than 8%) in the static magnetic field, made once during each ac cycle. This small feedback allows the chaotic motion to be stabilized indefinitely. More recently, Starrett and Tagg (1995) have stabilized an experimental parametric pendulum – a pendulum driven by periodic vertical motion of its pivot. Control is achieved through adjustment of the eddy current damping of the pendulum with proportional feedback, once each forcing cycle. The OGY method has also been modified to apply when the attractor is reconstructed from a time series (Nitsche and Dressler, 1992) and was used successfully to control a simulated Duffing oscillator. However, this last technique is beyond the scope of the present discussion.

Our primary example, the simulated pendulum, may also be controlled with the OGY method (Baker, 1995). (We summarize the main steps here and refer the reader to the previous reference for details.) Following OGY we consider a map, in this case the two-dimensional map represented by a Poincaré section of the pendulum:

$$\begin{pmatrix} \theta_{n+1} \\ \omega_{n+1} \end{pmatrix} = M(\theta, \omega) \begin{pmatrix} \theta_n \\ \omega_n \end{pmatrix}, \quad (6.22)$$

where  $M$  is unknown and dependent on position in the phase plane.

Fixed points of this map may be found by determining the distance between consecutive iterates. If this distance is small then the given point may be a fixed point of an unstable periodic orbit. For period-2 fixed points, second iterates are compared, and so forth for higher order periodic orbits. An important property of unstable fixed points is that they are saddle points: there are both attracting and repelling directions. These directions lie along the stable and unstable manifolds, respectively. (See Chapter 4.)

Once the fixed point is chosen,  $M$  is determined near the fixed point. Although the Poincaré section is a nonlinear map, a linear approximation is found by observing the evolution of a few points in the vicinity of the fixed point with coordinates  $\theta_F = 1.523$  and  $\omega_F = -0.415$ . (See Figure 6.17.) Vectors may be formed from pairs of these points, and the evolution of these vectors determines the elements of  $M$ . Finally, the eigenvalue problem associated with  $M$  may be solved. The eigenvectors  $e_s$  and  $e_u$  give the directions of contraction and expansion – the stable and unstable manifolds – near the fixed point. Similarly the eigenvalues  $L_s$  and  $L_u$  give the rates of contraction and expansion near the fixed point. We also determine vectors  $f_s$  and  $f_u$  that are perpendicular to  $e_u$  and  $e_s$ , respectively. All these quantities characterize the geometry near the fixed point.

Once the local geometry is determined, one of the pendulum's parameters, for example the damping constant  $q$ , is chosen as the control parameter. The effect on the fixed point coordinates of varying  $q$  is determined by simulation with  $q$  slightly displaced from its value  $q_0$  at

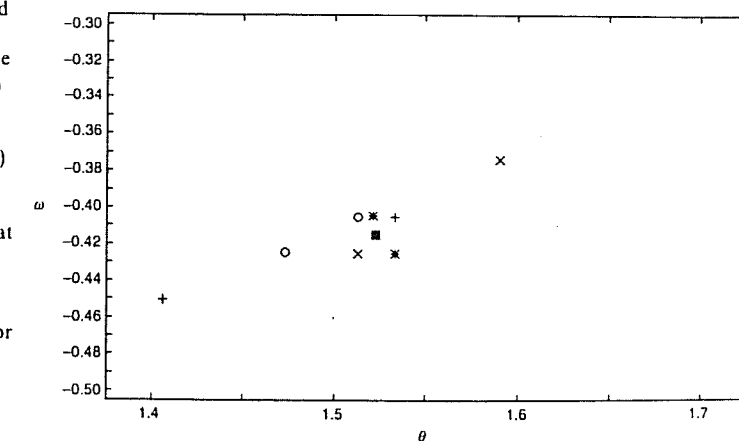


**Fig. 6.17** Evolution of a small patch near a fixed point of the forced pendulum. Points at the corner of a rectangle in the phase plane evolve to new locations (with corresponding symbols) after one cycle. Vectors may be formed by joining pairs of points at the vertices of the original rectangle; for example, a vector from + to O and a vector from + to \*. (See text.) The solid square is located at the unstable fixed point.

the fixed point. This variation is linearized near  $q_0$  and described by the vector  $(\partial\theta_F/\partial q, \partial\omega_F/\partial q)$ .

The control algorithm uses slight changes  $\delta q$  in the control parameter to force the orbit toward the direction of contraction (the stable manifold) near the fixed point. The natural contraction then drives the orbit toward the fixed point. However, a small error will cause the orbit to miss the fixed point, so the adjustment process must be carried out repetitively to achieve stabilization (constant values of the phase plane coordinates). The required parameter change is given by the formula

$$\delta q = \frac{L_u}{L_u - 1} \frac{(f_{u1}, f_{u2}) \begin{pmatrix} \Delta\theta_n \\ \Delta\omega_n \end{pmatrix}}{(f_{u1}, f_{u2}) \begin{pmatrix} \partial\theta/\partial q \\ \partial\omega/\partial q \end{pmatrix}}, \quad (6.23)$$

where  $(f_{u1}, f_{u2})$  is a vector that is perpendicular to the stable manifold and  $(\Delta\theta_n, \Delta\omega_n)$  is the vector from the fixed point to the  $n$ th iterate. The change  $\delta q$  is reevaluated at each cycle using the current value of the latter vector.

A series of successive iterates showing control of a simulated pendulum is given in Figure 6.18. The control algorithm is turned on at  $t = 1000$  and turned off at  $t = 3000$ . In fact, control is not immediately achieved at its activation. The control mechanism is only operable when the iterate happens to approach the fixed point. Several cycles may be required for a sufficiently close approach to occur. Moreover, the necessary closeness is determined by the maximum possible variation  $\delta q_{\max}$  in the control

**Fig. 6.18** Stabilization of a chaotic pendulum as indicated by the angular velocity at the start of each forcing cycle. The control mechanism is initiated at  $t = 1000$  and terminated at  $t = 3000$ . During this interval the constant (cyclic) value of the angular velocity indicates the stabilization of period-1 motion. The maximum relative change in  $q$  was 4%.

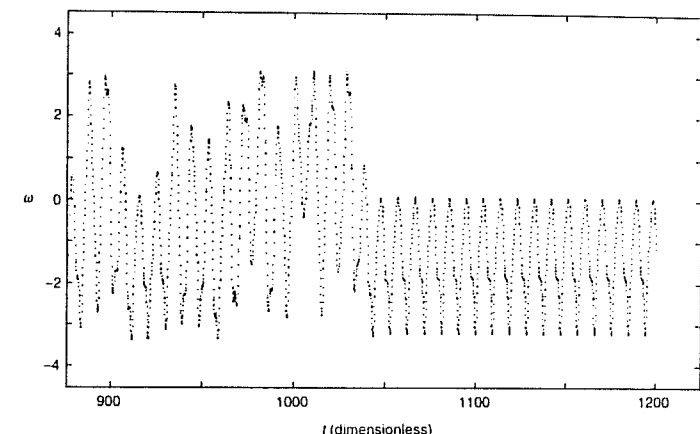
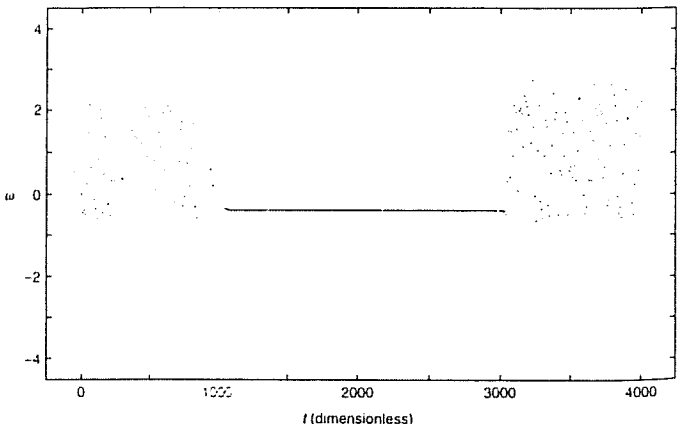


**Fig. 6.19** Time series of the angular velocity during the initiation of control at  $t = 1000$ . Note that several cycles are required to stabilize the period-1 orbit.

parameter. Ott *et al.* (1990) have developed a relationship between  $\delta q_{\max}$  and the average time to establish control. The delay is demonstrated in Figure 6.19, where the entire velocity time series is displayed during the initiation of control. Control lags initiation by about four forcing cycles. The techniques we have used to control the motion of the simulated pendulum are similar to those used by various investigators to control experimental systems.

We have chosen to demonstrate the basic OGY method. There are, however, other control schemes that are especially suited to nonlinear dynamics. In this connection we mention the work of Bradley (1992) on the simulated pendulum and that of Hubinger, Doerner, and Martienssen (1993) on the experimental pendulum. For an entry into the literature of this fascinating subject see, for example, Abarbanel *et al.*, 1993.

## 6.4 Conclusion

This chapter has introduced techniques that are commonly used for analyzing chaotic experimental data, predicting the future behavior for a limited period of time, and modifying chaotic states. These methods are often applicable even when a suitable model is unknown. In many areas of science, it has been presumed that understanding leads to prediction and control. The early development of nonlinear dynamics, on the other hand, suggested that nonlinear dynamics might be different. However,

progress in prediction and control for chaotic systems shows that such a pessimistic view is at least partially incorrect.

## Problems

- 6.1 Use the transformation  $t' = t\omega_0$  to show the equivalence of

$$\begin{aligned} I \frac{d^2\theta}{dt^2} + b \frac{d\theta}{dt} + \omega_0^2 I \sin\theta &= T \sin\omega_t t \\ \text{and } \frac{d^2\theta}{dt'^2} + \frac{1}{q} \frac{d\theta}{dt'} + \sin\theta &= g \sin\omega_{D't'}. \end{aligned}$$

(Hint: Remember to transform the derivatives.) Using intermediate results from the above exercise give values for  $g, q$ , and  $\omega_D$  in terms of  $I, b, \omega_0, T$ , and  $\omega_t$ .

- 6.2 Consider a time series of experimental data  $\{\omega_1, \omega_2, \dots, \omega_n\}$ , each point being separated by 7 ms. Let  $\tau = 21$  ms and suppose you wish to reconstruct points in a three-dimensional phase space. Write out the coordinates of the first four points in the phase space. Using the transformation  $t' = t\omega_0$  with  $\omega_0 = 9 \text{ s}^{-1}$ , determine the value of  $\tau'$  for a pendulum represented by the second, dimensionless differential equation in Problem 6.1.
- 6.3 Using the least squares method, derive equations (6.21) for prediction as outlined in Section 6.2.2.
- 6.4 For the experimental data used in this chapter the positive Lyapunov exponent is  $\lambda_+ = 1.5 \text{ s}^{-1}$ . Assume that the second Lyapunov exponent is zero and calculate the third (negative) exponent from the relationship

$$\nabla \cdot F = -b/I = \sum_{i=1}^3 \lambda_i,$$

where  $b/I = 2.25 \text{ s}^{-1}$ . With these values for the Lyapunov exponents use the Kaplan-Yorke relation to estimate the fractal dimension of the attractor. Compare your value with that given in the text.

- 6.5 Derive the expression  $T = (1/\lambda_+ d) \log_e(N)$  that is used as an estimate of the prediction time.

Problems 6.6, 6.7, and 6.8 require use of the data and programs found on the optional CHAOS II Diskette.

- 6.6 Use the program RECDIM and the data file VEL\_FILE.TRU to

reconstruct the attractor and calculate dimension in an embedding space of three dimensions. Use a delay ( $\tau$ ) of 30 data points. Comment on any differences from the results in the text, where the delay is 20 data points.

- 6.7 Use the program RECLYAP and the data file VEL\_FILE.TRU to calculate the positive experimental Lyapunov exponent with a delay of 30 data points. Using your answer to Problem 6.6 and the Kaplan-Yorke relation, check the consistency of the Lyapunov exponent and the dimension results.
- 6.8 Use the program PREDICT1 with various segments of the data on the file VEL\_FILE.TRU to do prediction at different epochs in the time series. Is the prediction time approximately constant for these segments. Does the number of data points 'known' prior to the beginning of prediction have an effect upon the prediction time?
- 6.9 Modify the program POINCARE so that you can determine the fixed points of a pendulum simulation. Use the bifurcation diagrams in the text to find a parameter set in a chaotic region and then determine some of the fixed points. Then vary one of the parameters and determine the effect on the fixed point. Next, by observing the evolution of Poincaré points near the fixed point through one forcing cycle, determine a linear map for the Poincaré section. Calculate the eigenvectors and eigenvalues of  $M$ , together with the corresponding vectors  $f_s$  and  $f_u$ . (Note that the normalization of these vectors is arbitrary.) Finally, use the program CONTROL, or a modification of it, to attempt control of your simulation.

# Chaos broadly applied

The primary physical example discussed up to this point is the driven pendulum, which provides an elementary pedagogical example of a chaotic system. Its behavior is extraordinarily complex. Varying the parameters leads to an intricate pattern of periodic and chaotic states with several types of transitions between them. In the chaotic regions, nearby orbits diverge exponentially from each other, with consequent long-term unpredictability. We have also discussed how a single experimental time series can be used to characterize chaotic states, to control them, or to achieve short-term predictability.

Chaos occurs widely in nature. In this chapter we briefly describe examples of chaotic behavior in lasers, chemical reactions, fluid dynamics, interfacial growth, and earthquake models. We emphasize the fact that natural systems are often *spatially extended* and therefore have intrinsically many degrees of freedom. Thus, their chaotic behavior may be more complicated than that of the pendulum and other systems with only a few degrees of freedom. Still, the main concepts of nonlinear dynamics continue to play a significant role in organizing our knowledge of spatially extended nonlinear systems. At the end of this final chapter, we consider the impact of our understanding of chaos on two major fields of theoretical physics: quantum mechanics and statistical mechanics.

## 7.1 Chaos in lasers

Since the early days of laser technology, instabilities in laser action have been apparent. That is, the light output need not be time-independent

(Harrison and Biswas, 1986). More recently, efforts have been made to study the chaotic aspects of lasers systematically.

A laser consists of a dielectric material confined between two reflecting mirrors. The energy spectrum of the dielectric must contain two atomic or molecular energy levels whose populations are inverted by an external electrical, optical or chemical energy source so that the upper state is more populous. Photons corresponding to the differences in energy between the two states stimulate atoms in the higher level to decay to the lower level and emit additional photons. The radiation is reflected between the mirrors many times, thus generating the high intensity characteristic of the laser.

One semiclassical model of the laser is a set of differential equations known as the Maxwell–Bloch equations. These describe the time dependence of the electric field  $E$ , the mean polarization  $P$  of the atoms, and the amount of population inversion,  $D$ . They are:

$$\left. \begin{aligned} \frac{dE}{dt} &= -\kappa E + \kappa P, \\ \frac{dP}{dt} &= \gamma_1 ED - \gamma_1 P, \\ \frac{dD}{dt} &= \gamma_2(\lambda + 1) - \gamma_2 D - \gamma_2 \lambda EP. \end{aligned} \right\} \quad (7.1)$$

where  $\kappa$  is the decay rate in the laser cavity due to beam transmission,  $\gamma_1$  is the decay rate of the atomic polarization,  $\gamma_2$  is the decay rate of the population inversion, and  $\lambda$  is a pumping energy parameter. (To relate this semiclassical model to a quantum description, note that  $E$  is proportional to the expectation value of the photon number density.) The three variables and nonlinear coupling of these equations suggest the possibility of chaotic behavior. Furthermore, the form of these equations is quite similar to the Lorenz model for chaotic convection.

While numerical solutions to the Maxwell–Bloch equations can exhibit chaos, many practical lasers do not operate within a parameter range where chaos occurs. (In many conventional laser configurations, the polarization and population inversion quickly relax to steady values, effectively causing  $P$  and  $D$  to drop out of the Maxwell–Bloch equations. The equations then do not contain enough variables for chaotic behavior.) However, chaotic behavior may be realized when the laser configuration is modified by tuning the cavity length, varying the laser gain, tilting one of the mirrors, or adding feedback from an external cavity (Fischer *et al.*, 1994). Time series and Fourier spectra of these laser outputs have shown various routes to chaos, including period doubling, intermittency, and quasiperiodicity. (See Gioggia and Abraham (1983) and the review by Abraham, Arimondo, and Boyd (1988).)

Special kinds of lasers, such as those where the frequency is broadened

by the characteristics of the laser medium (inhomogeneous broadening), readily exhibit both periodic and chaotic behavior (Firth, 1986).

More recently, lasers with complex behavior have been stabilized over a fairly large parameter regime by sophisticated versions of the feedback control mechanism described in Chapter 6. (See Gills *et al.* (1992).) The importance of lasers in modern technology provides a special incentive for the study of their stability. (See the proceedings volume edited by Abraham, Garmire, and Mandel (1991).)

## 7.2 Chaotic chemical reactions

Chemical reactions can be modeled by nonlinear kinetic equations. For example, consider the elementary reaction



Suppose that the reactants A and B are injected into a closed container at rate  $r$ , and that an exit port prevents the buildup of excess material, as shown in Figure 7.1. The rate equations describing this simple reaction exhibit nonlinear coupling between the chemical concentrations:

$$\begin{aligned} dA/dt &= -k_f AB + k_r C - r(A - A_0), \\ dB/dt &= -k_f AB + k_r C - r(B - B_0), \\ dC/dt &= k_f AB - k_r C - rC. \end{aligned} \quad \left. \right\} \quad (7.3)$$

Here  $A_0$  and  $B_0$  are the reactant concentrations at the input port, and  $C_0 = 0$ . Although this simple reaction *cannot be chaotic*, several others that involve reactive intermediates do show complex periodic and chaotic behavior.

The most famous of these is the Belousov-Zhabotinskii (BZ) reaction, which is a catalytic oxidation of malonic acid in a bromate solution. Originally discovered in a somewhat different form by Belousov in 1951, it was not published until 1959 and then only in an obscure journal, because chemical oscillations were thought to be unlikely in a homogeneous system. Belousov observed periodic changes in color and found that the oscillation frequency increased with temperature. In 1961 Zhabotinskii, a biophysicist at the Moscow State University, modified the reactants and began a sustained effort to improve the experiments and to understand the chemical mechanisms (Zhabotinskii, 1991). In 1972, a comprehensive scheme for the chemical kinetics was proposed,

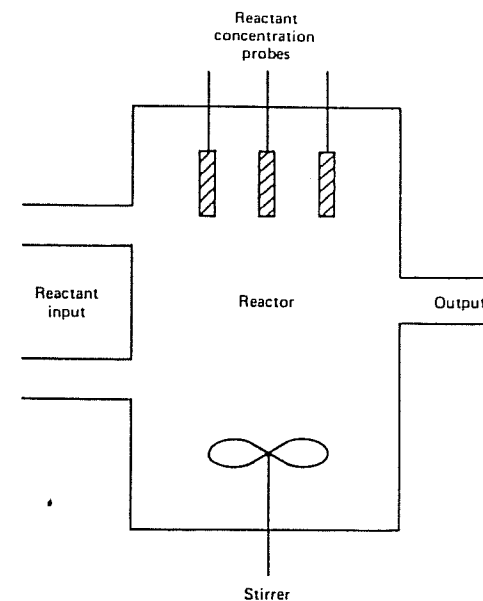


**Fig. 7.1** Experimental arrangement of a chemical reaction with mixing. The probes monitor the reactant concentrations. (Adapted from Swinney (1983).)

thereby initiating efforts to explain the experimental results by mathematical models. The BZ reaction is the most widely studied chemical reaction associated with complex dynamics.

Several experimental research groups have studied periodic and chaotic dynamics in the BZ reaction as a function of the input flow rates (Argoul *et al.*, 1987). For example, a strange attractor can be reconstructed from the chaotic time series of one of the variables, such as the voltage from an electrode that is sensitive to a particular reactant. An example is shown in Figure 7.2. Realistic simulation for the BZ reaction requires many coupled nonlinear differential equations, since over 80 different chemical steps have been discovered! Nevertheless, numerical simulation using simplified model equations do reflect, at least qualitatively, the experimental results (for example, see Lindberg, Turner, and Barkley (1990).)

The existence of chaos in the BZ reaction suggests that similar behavior might occur for other chemical oscillators, such as those found in biological systems. Chaotic behavior in these systems may indicate pathological conditions, and therefore an analysis of chaotic reactions may prove useful in the study and treatment of disease. For example, a comparison of high risk cardiac patients, involving a subset of patients

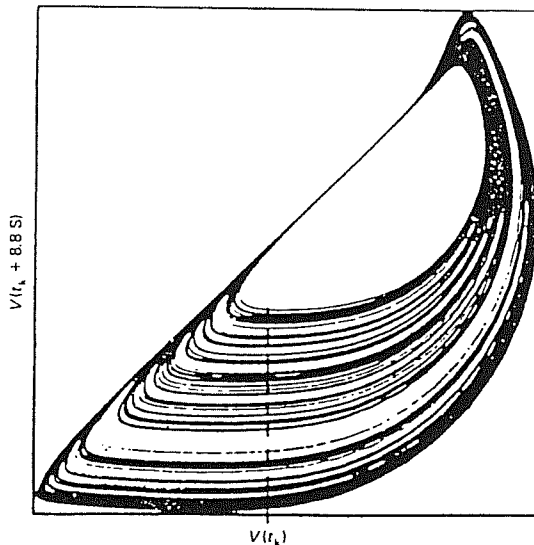


Fig. 7.2 A two-dimensional projection of a three-dimensional phase space construction for the BZ reaction, showing a strange attractor. (From Swinney, (1983).) Reprinted by permission of H.L. Swinney.

who developed lethal cardiac arrhythmias, showed that the reconstructed attractor of those in the subset was of lower dimension than that of high risk patients who survived (Skinner, 1994). It appears that nonlinear techniques can possibly provide a significant degree of specificity in the diagnosis of the lethal condition and thereby alert the caregiver to the need for intervention. More generally, it has been found that the process of aging in physiological and anatomical systems may be documented by techniques from nonlinear dynamics. In some cases there is a loss of complexity that is manifest by lower fractal dimension and Kolmogorov entropy (Lipsitz and Goldberger, 1992). Finally, we note that nucleotide sequencing in DNA has been claimed to show fractal patterning. Perhaps a nonlinear mechanism is active in this most fundamental biological system (Skinner, 1994.)

### 7.3 Chaos in fluid dynamics

Chaotic motion has been observed prominently in fluids subject to temperature gradients, differential rotation, vibration, and other forms of energy input. Extensive references may be found in several reviews (for example, Swinney and Gollub (1986)). A much studied example is

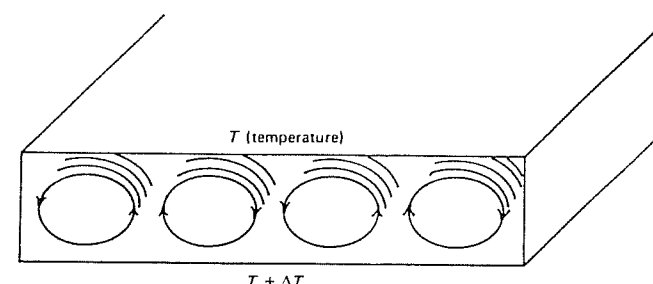
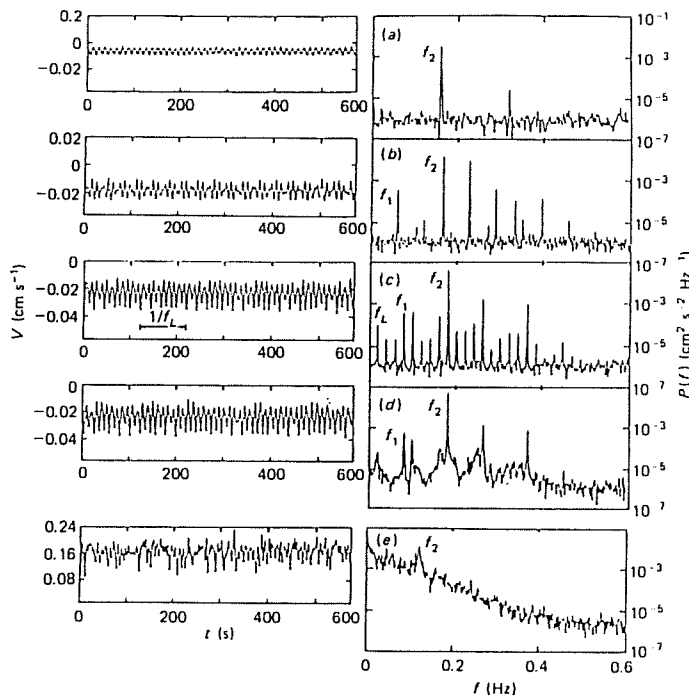


Fig. 7.3 Schematic diagram of Rayleigh-Bénard convection. Arrows indicate the direction of fluid circulation when the temperature difference  $\Delta T$  is large enough to produce convection.

Rayleigh-Bénard convection, in which a fluid is placed between two horizontal thermally conducting plates, with the lower one warmer than the upper one, as shown in Figure 7.3. When the temperature difference  $\Delta T$  exceeds a critical value  $\Delta T_c$ , convection occurs as a series of 'rolls' resembling rotating parallel cylinders. Hot fluid rises, cools, and falls in a spatially periodic pattern. The rolls begin to oscillate transversely in complex ways as  $\Delta T$  is increased beyond a second threshold  $\Delta T_{c2} > \Delta T_c$ , and chaotic behavior occurs for even higher values of  $\Delta T$ . The famous 'Lorenz model' of convection (Lorenz, 1963), though not realistic, was a turning point in the history of nonlinear dynamics. It consists of three coupled ordinary differential equations, and was the first strange attractor to be studied numerically.

Fluid systems are often characterized by experimentally measured time series of the local velocity at a point in the fluid. This can be done remotely using the method known as laser Doppler velocimetry. (For example, see Gollub and Benson (1980).) A laser beam is scattered from the moving fluid; light collected from a chosen point in the cell is slightly Doppler shifted by the moving fluid. Measurement of that small frequency shift (about 1 part in  $10^{12}$ !) gives the instantaneous local fluid velocity. Repetitive measurement yields a time series of the local velocity. Fourier spectra of these time series show the varieties of behavior typically associated with nonlinear systems such as the pendulum, including period-doubling cascades, phase locking between distinct oscillatory modes, and sensitive dependence on initial conditions. One typical route to chaos is shown in Figure 7.4. Two independent oscillations at frequencies  $f_1$  and  $f_2$  develop and interact to produce various sum and difference frequencies. The oscillations phase lock (Figure 7.4(c)) yielding a 'comb' of equally spaced spectral peaks. Chaos appears in Figure 7.4(d), and finally a broad, nearly featureless spectrum is attained at very large values of  $\Delta T$ .



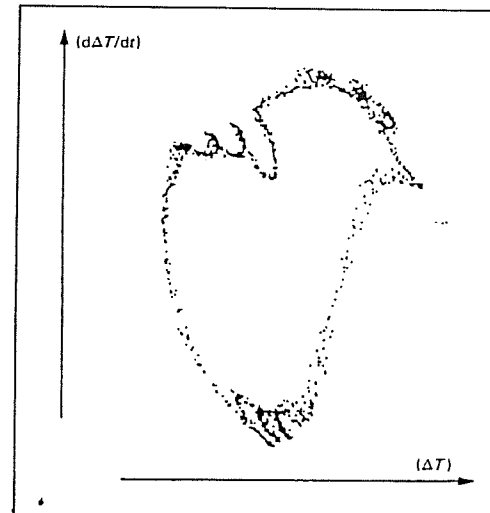
**Fig. 7.4** Time series and power spectra of the local fluid velocity showing a sequence (a)–(e) of dynamical states as  $\Delta T$  is increased. Two distinct oscillations at frequencies  $f_1$  and  $f_2$  develop, then phase lock, and finally lead to chaos in (d). For large  $\Delta T$ , the spectrum is quite broad. This behavior is analogous to that of a nonlinear circle map (Chapter 4). (From Gollub and Benson (1980).)

Well-defined chaotic states are especially prominent if the horizontal dimensions of the fluid cell are only two or three times its depth. Under these conditions, the fluid behaves as if it has only a few degrees of freedom. It is possible to measure phase space trajectories for this system, and then to determine the dimension of the resulting strange attractor (e.g. Malraison *et al.*, 1983). An example of a Poincaré section near the onset of chaos, showing the folding process typical of strange attractors, is given in Figure 7.5. Dimensions less than 5 are typically found near the onset of chaos. Since a fluid continuum in principle has an infinite number of dynamical variables, the ‘condensation’ of the dynamics onto only a few of them is quite remarkable.

#### 7.4 Spatio-temporal chaos in fluids

In the example of hydrodynamic chaos just discussed (and many others) the time dependence is nonperiodic, while the spatial structure of the

**Fig. 7.5** Poincaré section for chaotic thermal convection showing the folding that is characteristic of a strange attractor. The coordinates are the temperature difference  $\Delta T$  across the fluid layer and its time derivative, both sampled at the frequency of natural oscillation. (From Berge, Pomeau, and Vidal (1984).)

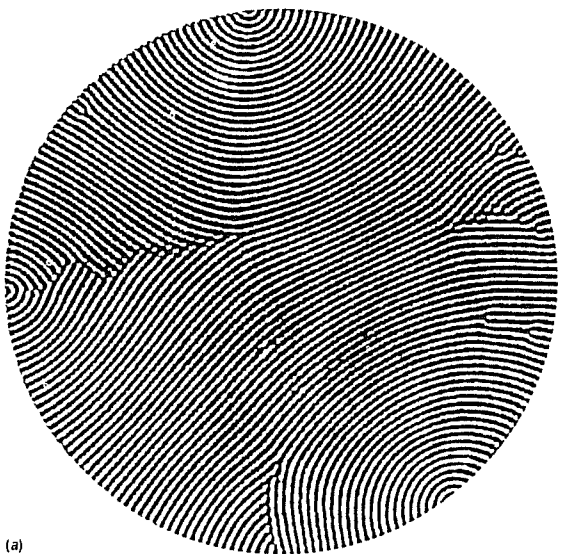


flow is coherent across the system. This means that the chaotic motion is highly correlated from one point in the fluid to any other. The maintenance of such a condition over an appreciable range of temperature differences is generally the consequence of geometrical constraints that limit the system size to at most a few times the size of the largest flow structure. On the other hand, if the dimensions of the system (or the energy injection rate) are larger, then the dynamical behavior can be much more complex.

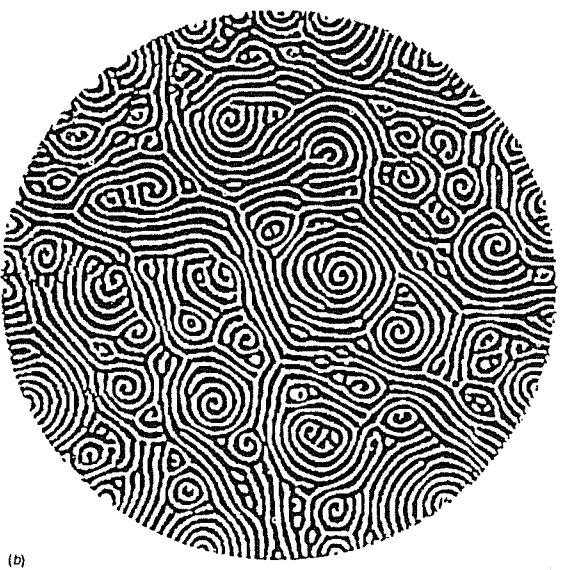
##### 7.4.1 Spatio-temporal chaos in thermal convection

Let us consider as an example the case of a convection cell whose diameter is much larger than its depth. Somewhat above the onset of convection, highly ordered roll patterns are produced, as shown in Figure 7.6(a) (Morris *et al.*, 1993). The rolls are curved because friction at the outer boundary of the convection cell causes them to be aligned locally perpendicular to the boundary, unless special efforts are made to eliminate these effects. Rolls (or deformed rolls) are not the only possible convection patterns. For example, if the temperature difference is sufficiently large that the viscosity varies significantly across the layer, then hexagonal cells can form near the onset of convection.

As the mean temperature difference  $\Delta T$  across the fluid layer is



(a)



(b)

Fig. 7.6 (a) Pattern of convection rolls in  $\text{CO}_2$  gas for a temperature difference  $\Delta T$  approximately 11% above onset, in a large convection cell. (b) Spiral chaos for a larger value of  $\Delta T$ . (From Morris *et al.*, 1993) Reprinted by permission of G. Ahlers.

increased, a state of 'spiral chaos' appears (Figure 7.6(b)). At any given point, the local fluid temperature (or velocity) has a broadband spectrum. The spiral features rotate, appear, and disappear, while defects in the rolls come and go at unpredictable locations. However, in contrast to the dynamics of a small convection cell, the temperature fluctuations at different points are uncorrelated with each other if separated by more than a few roll spacings. The distance  $\xi$  over which the motion is correlated decreases with increasing  $\Delta T$ . The fact that  $\xi$  is smaller than the diameter of the system implies that each correlation area of size roughly  $\xi^2$  is dynamically independent, so that the number of degrees of freedom required to describe the motion must be at least a few times  $A/\xi^2$ , where  $A$  is the area of the cell.

This type of state is often called 'spatio-temporal chaos' to denote the fact that the spatial degrees of freedom are quite important. It is a form of deterministic chaos and is believed to be contained within the partial differential equations of hydrodynamics that are appropriate for thermal convection, without any need to introduce sources of noise or random fluctuations. In fact, spiral chaos has been successfully simulated numerically from these equations, with only modest simplification to make the computation tractable in a reasonable time (Decker, Pesch, and Weber, 1994.)

However, the state of spiral chaos was a surprise when it was discovered because a stability analysis of the hydrodynamic equations leads one to believe that convection rolls would be stable for the parameters where spiral chaos occurs. That may well be the case if such parallel rolls are created as initial conditions; however, the chaotic state can apparently occur for the same region of parameters but with different initial conditions. In the language of dynamical systems, we would say that multiple attractors of quite different character occur simultaneously and have different basins of attraction.

Can the methods described in Chapter 6 be used to characterize this state of spatio-temporal chaos experimentally? It is certainly not possible to use a single time series (say the temperature at a single spatial location) to represent the entire dynamics, because widely separated points are uncorrelated. In principle, it might be possible to use an array of many time series to represent the dynamics, and methods for doing so have been suggested (Abarbanel *et al.*, 1993). However, the amount of data required to populate an attractor in a phase space of high dimensionality would be staggering. It would be impossible to use the graphical techniques described in Chapter 6 to display the results. Because of these difficulties, the notion of a chaotic attractor for

spatio-temporal chaos has been mainly conceptual up to the time of this writing.

One interesting and important point is that the dimensionality of the attractor for spatio-temporal chaos must be proportional to the size of the system (that is, its area for a thin layer), so that one can speak of a 'dimension density.' This property has been used in numerical work, but is hard to measure experimentally.

When the temperature difference  $\Delta T$  is sufficiently large, the motion becomes fully turbulent. The entire transition process from the quiescent fluid through the chaotic regime to the final state of thermal turbulence has been thoroughly investigated. (For a review, see Siggia (1994).)

#### 7.4.2 Spatio-temporal chaos on a rotating fluid film

There are many other examples of spatio-temporal chaos, and it may be useful to cite another to illustrate the idea that the transitions leading to spatio-temporal chaos can be quite well defined and that symmetry considerations limit their variety. An interesting case occurs when a cylinder containing a small amount of fluid is rotated about its horizontal axis (Melo and Douady, 1993; Vallette, Edwards, and Gollub, 1994). The fluid coats the cylinder to form a film, but the film sags to produce a linear ridge or 'front' as shown in Figure 7.7(a). This front is sustained against gravity by shear forces provided by the rotating inner wall of the cylinder. The phenomenon is sometimes termed 'rimming flow.'

The front can be stable for a certain range of rotation rates (for a given fluid volume and viscosity). However, when the rotation rate is increased, a cellular structure (Figure 7.7(b)) bifurcates smoothly from the featureless 'ground state'. This instability has not been studied using the Navier-Stokes equations because free surfaces are difficult to treat analytically. On the other hand, similar cellular fronts are known in a variety of nonlinear systems. The wavelength of the pattern is a function of the rotation rate, fluid volume, and viscosity.

Let us consider how the ordered pattern is transformed into a state of spatio-temporal chaos as the rotation rate is increased. There are only a limited number of ways in which a spatially periodic pattern can be modified by a subsequent bifurcation (Coullet and Iooss, 1990). The bifurcations reduce the symmetry of the system, and they can be classified by the symmetries that they break. For example, the cells can become tilted, thus breaking reflection symmetry, and begin to translate.

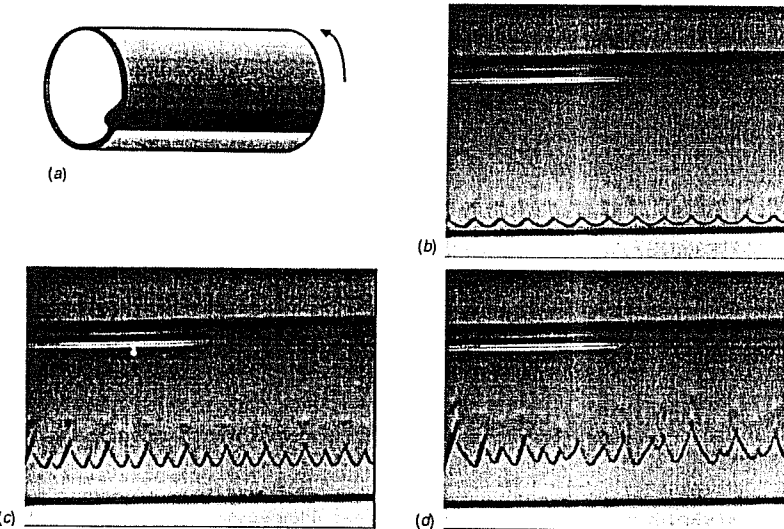
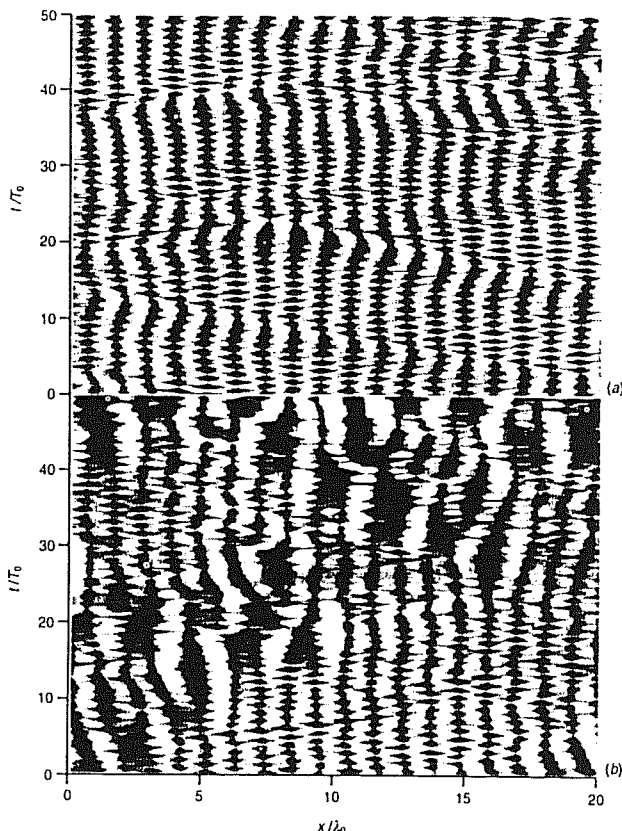


Fig. 7.7 (a) A linear film front formed in a rotating cylinder. (b) Cellular structure on the front for higher rotation rate. (c) Oscillating state, with alternate cells oscillating out of phase. (d) Spatio-temporal chaos. (From Vallette *et al.* (1994).)

Alternatively, the pattern can begin to oscillate, uniformly, breaking time translation invariance.

In the case of the rimming flow, the bifurcation that actually occurs is a bit more complex. An oscillation appears with *twice* the period of the cells. This is shown in Figure 7.7(c), where each cell rises and falls periodically, but alternate cells are a half cycle out of phase. The oscillation is uniform in space near its onset. However, as the rotation rate is increased slightly farther, the oscillation becomes nonuniform (Figure 7.7(d)), and in fact *waves* of nonuniformity in the oscillation amplitude travel across the system unpredictably, creating a state of spatio-temporal chaos. This state can be represented on a 'space-time diagram' (Figure 7.8) with the spatial coordinate plotted horizontally, the time coordinate vertically, and a gray scale to encode the local film height. The fluctuations are a form of deterministic chaos, but it is clearly not low-dimensional.

However, the behavior shown in Figure 7.8 is only one of several distinct types of spatio-temporal chaos found in rimming flow. Another that is substantially different is found if the quantity of fluid is reduced somewhat. In this case, the motion is dominated by traveling localized waves rather than oscillating cells. It is not known at the time of this writing why a small change in a parameter (the fluid volume) leads to a dramatic change in the nature of the spatio-temporal chaos.



**Fig. 7.8** Space-time diagram showing spatio-temporal chaos in rimming flow. The spatial coordinate is given in units of the basic wavelength of the pattern; the time coordinate is given in units of the oscillation period. The shape of the front is encoded with darker regions corresponding to higher front positions (Valllette *et al.*, 1994). In (a) the chaos is relatively weak, while in (b), the rotation rate is slightly higher and new cells are constantly being created and annihilated.

## 7.5 Spatio-temporal intermittency in model equations

Numerical simulations of simplified model equations have made important contributions to our (still limited) knowledge of spatio-temporal chaos, as they did earlier for ordinary temporal chaos. The full hydrodynamic equations are generally too complicated to serve this purpose well, since they describe a three-dimensional vector velocity field, have subtle boundary conditions, and are time-consuming to integrate, even on a supercomputer. However, several one-dimensional nonlinear model equations have been extensively studied (Cross and

Hohenberg, 1994). We will mention as an example the Kuramoto-Sivashinsky equation, which was originally devised as a continuum model of coupled oscillators, and (in a more general form) has provided an excellent testing ground for ideas about spatio-temporal chaos. The equation describes the space-time evolution of a field  $u(x,t)$  on the unit interval  $(0,1)$ :

$$\frac{\partial u(x,t)}{\partial t} = -\eta u - \frac{\partial^2 u}{\partial x^2} - \frac{\partial^4 u}{\partial x^4} - u \frac{\partial u}{\partial x}. \quad (7.4)$$

Note that the nonlinearity is confined to the last term. When the control parameter  $\eta$  is smaller than 0.078, a fluctuating disordered cellular pattern is found. It has the interesting property of being composed of separate regions where the field  $u$  is relatively small or relatively large. These are sometimes termed ‘laminar’ and ‘chaotic’ or ‘turbulent’ domains, respectively, though the motion should certainly not be regarded as approximating hydrodynamic turbulence. The dynamics has been characterized by the statistical distribution of sizes of the laminar (or chaotic) domains, which is a strong function of  $\eta$ .

Simulations of another nonlinear partial differential equation, known as the complex Ginzburg–Landau equation, gave rise to the concept of *defect mediated turbulence* (or *chaos*), in which the irregularities of a fluctuating two-dimensional pattern are concentrated in localized *defects* that are nucleated and annihilated at irregular intervals and locations. Examples of this phenomenon have in fact been found in many experiments. Some authors have speculated that a theory of this type of spatio-temporal chaos might be formulated in terms of the interactions of the defects themselves.

## 7.6 Strong turbulence

Strong turbulence in fluids may be regarded as an extreme form of spatio-temporal chaos in which there is no dominant cellular structure, and a wide range of spatial scales are important. In a turbulent flow, kinetic energy is added at large scales, is transferred to smaller scales by various nonlinear processes, and is eventually dissipated by viscosity at the smallest scales. In between the injection and dissipation scales, a remarkable nearly isotropic behavior arises in which the power spectrum of velocity component fluctuations along an arbitrary axis (say  $x$ ) varies

in proportion to the  $-5/3$  power of the wavenumber  $k_x$ . This so-called inertial range scaling is terminated by a roughly exponential cutoff in the spectrum beyond a scale  $\eta$  that is determined by viscosity. First predicted by Kolmogorov in 1941, this basic spectral behavior has been amply confirmed experimentally. (For a recent review, see Nelkin (1995).)

However, the actual energy dissipation process is rather complicated: it is known to be highly intermittent, with most of the energy dissipation being concentrated in small regions of space. Some experiments (Sreenivasan, 1991) support the notion that the dissipation field  $\epsilon(\mathbf{r})$  (energy dissipation per unit volume as a function of position  $\mathbf{r}$ ) forms a *multifractal set* that is characterized by many scaling indices or dimensions. (See Chapter 5.)

Can the methods of low-dimensional chaos play a useful role in understanding turbulent flows? In most turbulent flows there is substantial kinetic energy in large features sometimes known as 'coherent structures.' Some researchers have proposed that a dynamical systems approach might be feasible for describing just these large scale features, and several examples have been published (for example, see Berkooz, Holmes, and Lumley (1992, 1993)).

## 7.7 Chaotic mixing in fluids

Mixing by fluid flows is of considerable practical importance in technology and nature. It is common knowledge that turbulent flows exhibit strong mixing. For example, a spot of dye rapidly disperses in a turbulent flow. It is less commonly appreciated that mixing can also occur rapidly without turbulence, due to *chaotic mixing*, in which nearby fluid trajectories in real space (not in phase space) diverge from each other exponentially. This phenomenon was first described in detail by Aref (1984) and has been explored experimentally (for a review, see Ottino (1990)). A very nice example is shown in Figure 7.9. A viscous fluid fills the gap between two cylinders which are seen from above. The inner one (mounted asymmetrically) rotates, reversing direction periodically. A spot of dye placed in the fluid is stretched and folded by the motion to form a pattern of fine striations. Two fluid elements that are initially close together separate exponentially (on the average) in time. This behavior is basically chaotic in real space. The mean spacing between striations rapidly declines, until the increasing concentration gradients allow molecular diffusion to complete the mixing process.

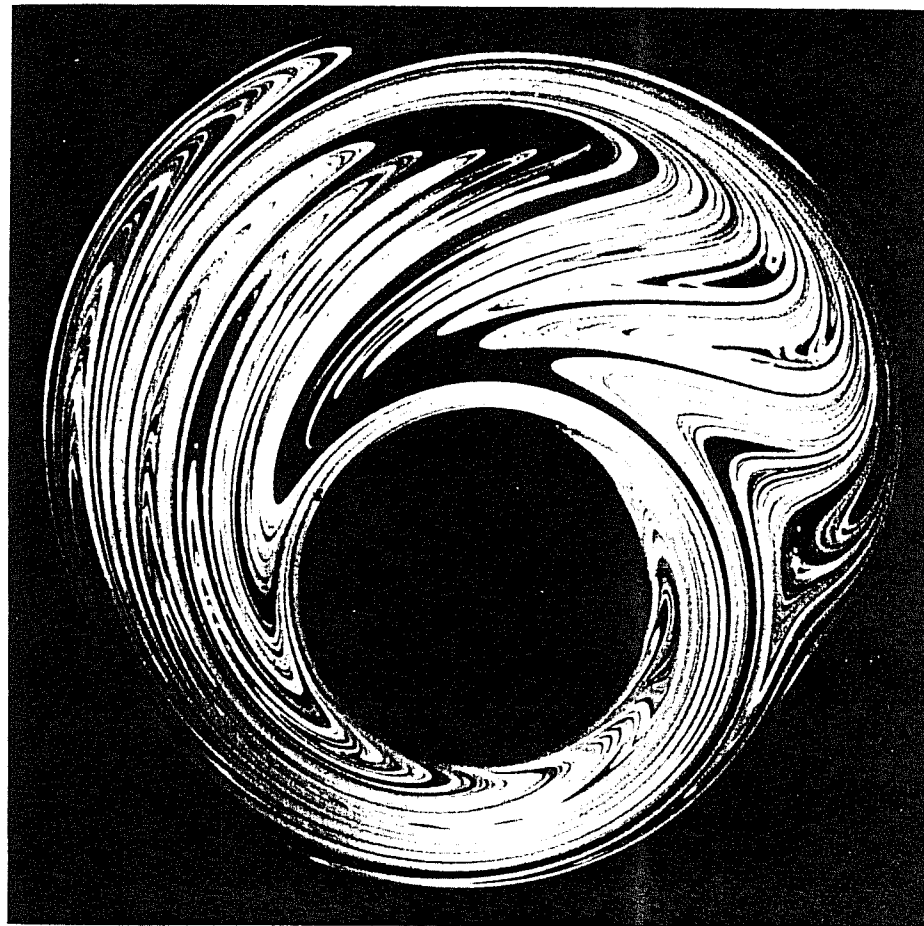
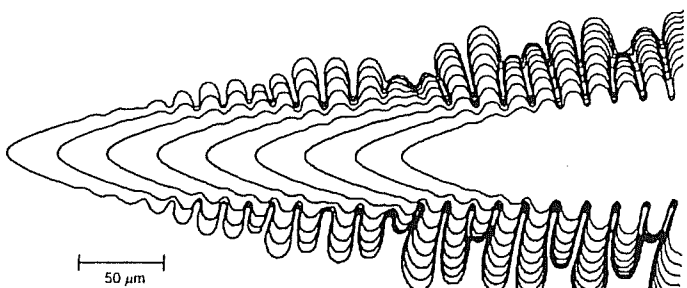


Fig. 7.9 Chaotic mixing in the gap between two cylinders; the inner one oscillates slowly (Ottino, 1989). Reprinted by permission of J.M. Ottino.

## 7.8 Complex dynamics of interfacial growth: artificial snowflakes

Another fascinating problem of nonlinear dynamics is the phenomenon of pattern formation at the interface between two phases of matter when one phase grows into the other. An interfacial instability can give rise to

Fig. 7.10 Contours of an ammonium bromide dendritic crystal growing from supersaturated solution. The contours are obtained by digital processing of microscopic images taken at 20 s intervals. (Dougherty *et al.*, 1987.)



complex and beautiful patterns during interfacial growth. This is precisely what happens during the solidification of a solid from either the liquid or the vapor phase. The convoluted crystals we call snowflakes (or more generally dendrites) are one result of this process.

To understand why growing interfaces are unstable, imagine a crystal that is growing into a supercooled liquid phase or a supersaturated solution. As material diffuses toward and becomes attached to the solid interface, small irregularities are easily amplified, provided that the energetic preference for growth along a particular crystalline axis is not too strong, or that the supersaturation is sufficiently high. The reason is simple: new material takes longer to diffuse toward local valleys than toward local peaks. Eventually, these protrusions begin to compete with each other for material, and the larger ones grow at the expense of the smaller ones.

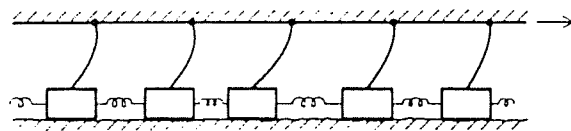
This process can lead to formation of complex interfaces in a very wide variety of materials. An example of a laboratory dendrite is presented in Figure 7.10. It shows the outline of the boundary of a small growing crystal of ammonium bromide at 20 s intervals (Dougherty, Kaplan, and Gollub, 1987). The tip of the crystal advances at constant velocity into the supercooled solution, and irregular sidebranches develop behind the tip. The tip of the dendrite is a paraboloid whose radius of curvature, here a few micrometers, is very stable, a kind of nonequilibrium steady state. On the other hand, the sidebranches are quite irregular and evolve chaotically. This structure, a mixture of order and disorder, is essentially the same as one of the tips of a snowflake. It also occurs in metal castings, which often consist of an intricate mixture of dendrites that have grown in various directions. The process of dendritic growth significantly affects the structure and physical properties of castings.

Considerable research has gone into the question of how to explain the structure of growing dendrites (Kessler, Koplik, and Levine, 1988). It is not hard to explain why the tip should be a paraboloid, though the issue of how its radius is determined has been controversial. The subtle influence of the anisotropy of the crystal lattice is an especially problematic issue. It clearly affects the overall morphology of a dendritic crystal, which generally grows along one of the microscopic crystalline axes. For example, if the crystal has a cubic lattice, as does the ammonium bromide crystal shown in Figure 7.10, and if the tip points along the  $z$  axis, then sidebranches point along the  $x$  and  $y$  axes in a pattern with fourfold rotational symmetry. (This means that there are also sidebranches growing out of the plane of the diagram, which are not shown.)

However, the sidebranching process can still be quite irregular. The sidebranches are nucleated near the tip as a result of very small fluctuations which could involve both thermal noise and possibly microscopic crystal defects. As the branches grow, the intrinsic nonlinear dynamics of the growth process (and its sensitivity to current conditions) overwhelms the effects of the *initial* noise; this probably leads to *deterministic chaotic* dynamics away from the tip. Even though the diffusion of material is a linear process, the fact that boundary conditions must be applied on a moving interface causes the overall mathematical description to be highly nonlinear. Since the process is spread out in space (and not fully correlated over the entire crystal), many degrees of freedom must be involved, so a low-dimensional dynamical description is presumed not to be feasible.

Quite a few other examples of complex structures produced during interfacial growth have been studied experimentally and theoretically. In some cases, structures that are fractal over a fairly wide range of length scales can develop. One well-studied example is the process known as *diffusion-limited aggregation* (DLA), in which individual particles undergo a random walk and stick when they encounter an aggregate that has been previously nucleated. (For example, see Vicsek (1989).) The structure of the resulting aggregate has been shown to be fractal, with irregularities on a wide range of scales. However, this process should definitely *not* be regarded as an example of deterministic chaos, because in this case, external noise (that is, a random walk) is important *at each stage* in the process, and not merely at the beginning. We mention DLA here mainly to distinguish clearly between chaotic and stochastic processes. Not every process that shows complex spatial structure should be regarded as chaotic!

**Fig. 7.11** The idealized Burridge–Knopoff model of earthquake faults, consisting of a chain of blocks coupled to each other by springs, sliding on a surface, and pulled from above by weaker springs. This model produces chaotic space-time dynamics. (After Carlson *et al.*, 1994.)



### 7.9 Chaos in earthquake dynamics

Earthquakes are the result of frictional instabilities that allow sudden slipping to occur between fairly rigid segments of the earth's crust, thus releasing stored elastic energy. Earthquake faults form a complex network that, in some regions, approximates a fractal over a reasonable range of scales. What is the origin of the unpredictability of the timing and strength of earthquakes? This question forms the basis of major research efforts in geophysics. Although earthquakes are so far largely unpredictable, there is a striking regularity in their size distribution. If one plots the frequency of occurrence of earthquakes of different sizes or energy release as a function of size, one finds that the frequency distribution is typically quite close to a power law, with a negative exponent since strong earthquakes are much less frequent. This frequency distribution is known as the Gutenberg–Richter law.

It is likely that the geometrical complexity of fault networks is important in understanding the unpredictability of earthquakes. However, it turns out that simple deterministic models of even a single straight fault are known to exhibit chaotic spatio-temporal dynamics (Carlson, Langer, and Shaw, 1994). Therefore, it seems quite possible that chaos is also an important part of the problem of understanding real earthquakes. In the basic 'Burridge–Knopoff model' of an earthquake fault, the elasticity of the fault structure is represented by a chain of blocks which are coupled to each other by springs, as shown in Figure 7.11. The blocks are imagined to slide on a surface (whose boundary represents the fault), and are pulled slowly to the right from above. This displacement allows the gradual buildup of internal stored elastic energy, which is then released when a group of blocks slips. The possibility of a slipping instability arises because the frictional force is assumed to become weaker as the velocity increases. (This assumption is similar to the notion that the coefficient of sliding friction is generally less than that of static friction.)

This model has been simulated numerically in great detail. It does

produce chaotic spatio-temporal dynamics, in the sense that an unpredictable sequence of slipping events occurs, some involving many blocks, and some only a few. The frequency distribution of the smaller events is approximately a power law, although very large events are much more frequent than the power law would predict, and the results also depend somewhat on the choices of parameters. Although this is not viewed as a realistic model of a fault, it can be used both to learn about the slipping process and to test proposed schemes for making short-term predictions.

### 7.10 Chaos and quantum physics

The quantum physics of nonrelativistic systems is based on the Schrödinger equation, a linear differential equation whose solutions give rise to probability distributions for observable quantities. One important feature of quantum physics is the existence of uncertainty relations between certain dynamical variables, such as the position  $x$  and the momentum  $p$  of particles in a collection or ensemble. It is not possible to prepare an initial state in which both of these are well defined. Instead, the collection of particles has distributions of positions and momenta with widths  $\Delta x$  and  $\Delta p$  constrained by Heisenberg's uncertainty relation  $\Delta p \Delta x \geq h/4\pi$ , where  $h$  is Planck's constant. The lack of predictability inherent in quantum mechanics is (at least largely) contained in this mandatory uncertainty in initial conditions.

Quantum systems are not chaotic in the sense used in this book. The Schrödinger equation is linear and yields periodic and quasiperiodic solutions only. Furthermore, the Heisenberg uncertainty relation implies that well-defined trajectories in phase space do not exist over long times. While classical chaos produces the infinite number of infinitely thin layers characteristic of a strange attractor, quantum physics limits the precision of phase trajectories (Gutzwiller, 1985).

On the other hand, quantum systems can sometimes be modeled classically over short time intervals. Bohr's correspondence principle implies that highly excited and closely spaced atomic states near the ionization threshold may be described classically, at least for a limited time during which the probability distributions of the dynamical variables remain localized in phase space. For longer times, the distributions spread and a quantum calculation is required. Even then, the wavefunctions of highly excited states reveal structure that is

characteristic of the classical counterpart system. For example, the probability density of a particle in a two-dimensional box shaped like a stadium is enhanced in the neighborhood of unstable periodic orbits of the corresponding classical particle (Heller, 1984). Heller called these enhancements 'scars' since they suggest some residue of classical motion in the quantum mechanical calculation.

Semiclassical atomic phenomena may be studied by means of the ionization of electrons from outlying energy states of hydrogen-like atoms (Jensen, 1985). In such states – where the principle quantum number,  $n$ , is typically about 60 – the addition of a forcing microwave field causes ionization at a rate that depends strongly on the field amplitude and only weakly on the frequency. This unusual behavior has been successfully simulated by a *classical* model of the outer electron in a one-dimensional Coulomb potential, subject to a time-dependent electric field. In the action-angle space of the model, chaotic orbits are observed as the field amplitude is increased through a certain critical value. Trajectories wander over large regions of phase space and provide a diffusion mechanism by which the electrons achieve states of higher energy and eventually ionize. It is quite remarkable that, in fact, the experimental values of the microwave field amplitude required for ionization agree, in one regime, with the threshold value for the onset of chaos in the classical model (Jensen, 1987a). However, in another regime there appear to be quantum effects that partially suppress the ionization predicted by the classical calculation.

Another quantum system that exhibits chaotic behavior in the classical limit is a highly excited atom in a strong dc magnetic field. In the classical limit an outer electron of the atom is modeled as a charged particle in a Coulomb field and a magnetic field. This classical 'atom' makes a transition from regular to chaotic behavior as the field strength is increased. Quantum mechanically, a weak magnetic field is treated as a perturbation and leads to the well-known Zeeman splitting of the atomic energy levels. However, for strong fields, perturbation calculations are not valid and the energy spectrum becomes complex as the magnetic splitting overwhelms the atomic energy spacings. One method of analysis is to study the statistical distribution of energy levels, as was done by Wigner in 1951 for the energy level structure of the atomic nucleus. The surprising result is that the Wigner distribution for nuclear states seems to apply to the high field atomic case. This distribution leads to at least one interesting distinction between the periodic and chaotic classical cases. When the classical motion is regular, the corresponding quantum system can have energy levels that are close together; on the

other hand, at fields large enough to cause the classical system to be chaotic, small level spacings are suppressed in the quantum version. This phenomenon is called 'level repulsion' (Gutzwiller, 1992.)

The study of quantum mechanical systems with classically chaotic counterparts is challenging and subtle. Recent applications include the problem of understanding electrical conduction in small samples (comparable to 1  $\mu\text{m}$ ). (See, for example, Chang *et al.* (1994).)

## 7.11 Foundations of statistical mechanics

The phenomenon of irreversibility as exemplified by the second law of thermodynamics ( $\Delta S \geq 0$  for isolated systems) leads to a difficult problem within classical physics. On the one hand, irreversibility implies a preferred direction of time for macroscopic systems. On the other hand, the laws of classical dynamics do not change when the direction of time is reversed. (They are invariant under time reversal.) Therefore the origin of irreversibility in classical dynamics was problematic until Boltzmann proposed a statistical model which accurately predicts macroscopic values of thermodynamic quantities. (A brief history and an elementary version of Boltzmann's original conception is given in Baker (1986). Boltzmann's model is worth examining here because chaotic dynamics may reduce the need for a statistical assumption.

Boltzmann proposed an explanation of irreversibility for the case of a dilute gas consisting of a large number of hard spheres interacting with each other according to the usual laws of conservation of momentum and energy. The 'gas' is assumed sufficiently dilute that only binary collisions occur. These mechanical aspects of the model seem quite straight-forward. The second assumption, perhaps less appealing, is the statistical hypothesis of 'molecular chaos.' After collisions, particles are assumed to lose all memory of their previous velocities. Velocities and position become uncorrelated with each other, and knowledge only of the *distribution* of velocities remains. Since it contains an implicit assumption as to the time direction of events, this statistical hypothesis leads to irreversibility. (A readily accessible demonstration of irreversibility using these assumptions is provided in Baker (1986).)

The discovery of chaotic behavior may render Boltzmann's statistical assumption unnecessary in some cases. Almost 100 years after Boltzmann presented his model, Sinai published the results of an examination of the hard sphere gas as a chaotic system (Sinai, 1970). One can see why this

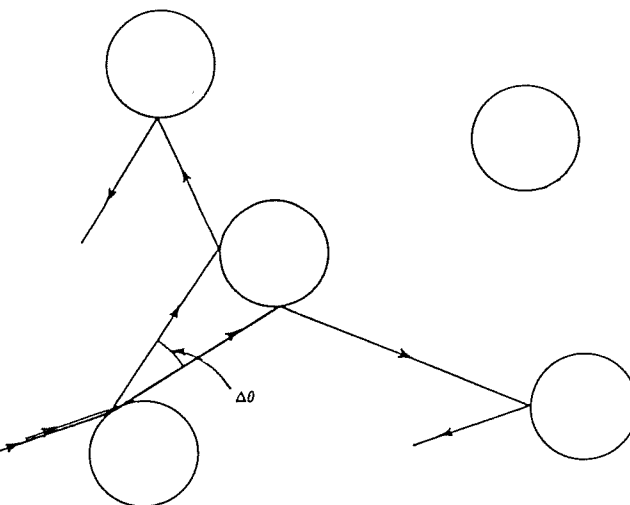


Fig. 7.12 The origin of sensitivity to initial conditions in a hard sphere gas.

system might be chaotic, as follows. Consider two nearby parallel trajectories for a sphere impinging on one of an array of fixed spheres (see Figure 7.12). The two outgoing trajectories are not parallel, but instead have a small angular divergence  $\Delta\theta$ . After a second collision the angular divergence is much larger. This leads to exponential growth (on average) of the angle between the two trajectories, and sensitive dependence on initial conditions. (However, there is no dissipation and hence no strange attractor.) The proof that the hard sphere gas may be found to occupy all microscopic states  $(r_i, p_i)$  with roughly equal probabilities is lengthy and difficult. There is still no proof that many-body systems *in general* will have this property. Still, it is reasonable to think of chaotic dynamics as providing a mechanism for justifying the statistical assumption required for irreversibility. (For a technical book that shows the relationships between the main concepts of statistical mechanics and chaotic dynamics, see Mackey (1992).)

These brief discussions of the connections of chaos to statistical and quantum physics may be sufficient to show that the foundations of physics are being significantly affected by recent insights into nonlinear dynamics. The impact of chaos on physics may be summarized by the statement that unpredictability enters physics in three major ways: (a) through nonlinearity; (b) through the uncertainty principle; (c) through the statistical behavior of large numbers of particles. However, (c) may

be in part a consequence of (a). The interested reader may pursue the subject further through the references (for example, see Jensen (1987b)).

## 7.12 Conclusion

The examples given in this chapter illustrate the ubiquity of chaotic dynamics. We have included a number of examples of spatially extended systems for which the methods of analysis described in Chapter 6 are inappropriate. In fact, serious errors have been made by researchers attempting to determine the attractor dimension of spatially extended systems such as the weather from a single local time series. This problem has been discussed lucidly by Lorenz (1991).

Many basic issues and applications could not be considered in this brief introductory text. Among them are the following interesting topics: fractal basin boundaries (Grebogi *et al.*, 1987); the chaotic scattering of a particle by a complex potential (Ott, 1993); chaos in the solar system (Sussman and Wisdom, 1992); the Josephson junction, an important superconducting device that is an analog of the pendulum (Davidson, Dueholm, and Beasley, 1986; Iansiti *et al.*, 1985); and a host of biological applications of chaos including the dynamics of cardiac tissue (Karma, 1993) and neural networks (Hjelmfelt and Ross, 1994; Sompolinsky and Crisanti, 1988; Aihara, Takabe, and Toyoda, 1990). Still we hope that this pedagogical introduction to the basic concepts, along with the examples and references in this final chapter, can provide the interested reader with many opportunities to look more deeply into the world of nonlinear dynamics.

# Further reading

The following list of books and papers provides alternative or expanded treatments of many of the subjects in this book. These readings are more accessible to the student and nonspecialist reader than some of the text references to the research literature.

- Bak, P., 'The Devil's staircase', *Physics Today*, December 1986, 38–45.
- Baker, G.L., *Religion and science: from Swedenborg to chaotic dynamics*. Solomon Press, New York, 1990. A popular treatment that explores connections between science and religion. One chapter discusses these connections for chaotic systems.
- Barcellos, A., 'The fractal geometry of Mandelbrot', *College Mathematics Journal*, 15, 1984, 98–114. A good introduction that should be read before attempting Mandelbrot's books on fractals.
- Barnsley, M., *Fractals everywhere*, Academic Press, San Diego, 1988. A mathematical treatment of fractals at the undergraduate level. The work contains many simulations of naturally occurring phenomena.
- Bergé, P., Pomeau, Y., and Vidal, C., *Order within chaos*, John Wiley and Sons Inc., NY, 1984. A comprehensive treatment of chaos, containing a readable account of many aspects of the subject.
- Chernikov, A.C., Sagdeev, R.Z., and Zaslavsky, G.M. 'Chaos: how regular can it be?', *Physics Today*, November 1988, 27–35.
- Cross, M.C. and Hohenberg, P.C., 'Pattern formation outside of equilibrium'. *Rev. Mod. Phys.*, 65, 1994, 851–1112. A massive and scholarly review of the pattern formation that includes an extensive discussion of spatiotemporal chaos.
- Crutchfield, P.J., Farmer, J.D., Packard, N.H., and Shaw, R.S., 'Chaos'. *Scientific American*, 255, December 1986, 46–57.
- De Souza-Machado, S., Rollins, R.W., Jacobs, D.T., and Hartman, J.L..

- 'Studying chaotic systems using microcomputer simulations and Lyapunov exponents', *Am. J. Phys.*, 1990.
- Ford, J., 'How random is a coin toss?', *Physics Today*, April, 1983, 40–7.
- Grebogi, C., Ott, E., and Yorke, J.A., 'Chaos, strange attractors, and fractal basin boundaries in nonlinear dynamics', *Science*, 238, 1987, 632–8.
- Hilborn, R.C., *Chaos and nonlinear dynamics: an introduction for scientists and engineers*, Oxford University Press, Oxford, 1994. A large, upper-level undergraduate text that discusses a wide variety of topics from chaotic dynamics.
- Hofstader, D.R., 'Metamagical themas', *Scientific American*, 245, November, 1981, 33–43. A detailed, qualitative discussion of the logistic map and some description of related phenomena.
- Holden, V.A. (ed.) *Chaos*, Princeton Univ. Press, Princeton 1986. A collection of review papers on subjects as diverse as Lyapunov exponents and the possibilities of chaos in epidemiology.
- Jensen, R.V., 'Classical chaos', *American Scientist*, 75, 1987, 168–81.
- Kadahoff, L.P., 'Roads to chaos', *Physics Today*, December 1983, 46–53.
- Lorenz, E.N., *The essence of chaos*. University of Washington Press, Seattle. 1993. A very readable and interesting book by one of the pioneers of chaotic dynamics with emphasis on the role of nonlinear dynamics in weather forecasting.
- Mandelbrot, B., *The fractal geometry of nature*, W.H. Freeman and Co., NY, 1983.
- May, R.M., 'Simple mathematical models with very complicated dynamics', *Nature*, 261, 1976, 459–67. The logistic map is treated in great detail, at a somewhat deeper level than that found in Hofstader's paper.
- Moon, Francis C., *Chaotic vibrations*, John Wiley and Sons, Inc., NY, 1987. A comprehensive but quite readable treatment of chaos aimed at the applied scientist or engineer. Emphasis is placed on vibrating systems. One of the appendices has some brief, but useful, prescriptions for numerical simulations.
- Ott, E., *Chaos in dynamical systems*, Cambridge University Press, Cambridge. An authoritative and well-written graduate text for scientists and engineers.
- Ottino, J.M., 'The Mixing of fluids', *Scientific American*, 260, January 1989, 56–67.
- Peterson, I., *Newton's clock: chaos in the solar system*, Freeman, New York, 1993. A popular and readable account of the history of celestial mechanics with emphasis on the distinctions between periodic and chaotic motion.
- Pool, R., 'Quantum chaos: enigma wrapped in a mystery', *Science*, 243, February, 1989, 893–5.
- Strogatz, S.H., *Nonlinear dynamics and chaos*, Addison Wesley, Reading MA, 1994. An elegant introductory textbook with applications, from the viewpoint of an applied mathematician.

- Tagg, R., 'Fluid dynamics, nonequilibrium', *Encyclopedia of applied physics*, 6, 1993, VCH Publishers, Inc. A readable technical introduction to nonequilibrium fluid dynamics with a useful glossary of terms.
- Thompson, J.M.T., and Stewart, H.B. *Nonlinear dynamics and chaos*, John Wiley and Sons., Inc., NY, 1986. A comprehensive work aimed at scientists and engineers. The choice of topics is somewhat different from that found in Moon's work, including more emphasis upon stability and bifurcation theory.
- Tufillaro, N.B., and Albano, A.M., 'Chaotic dynamics of a bouncing ball', *Am. J. Phys.*, 54, 1986, 939–44.

## Numerical integration – Runge–Kutta method

The mathematical model of the driven pendulum is a nonlinear, second order differential equation, whose solution is obtained numerically. This appendix explains a standard method of numerical integration, the Runge–Kutta method.

As a starting point, consider the simple but not very accurate technique called *Euler's method*, and its application to the first order differential equation:

$$\frac{dy}{dt} = f(t, y),$$

with initial conditions for  $(t, y)$  of  $(t_0, y_0)$ . With Euler's method, one converts the  $dt$  and  $dy$  differentials to finite quantities  $\Delta t$  and  $\Delta y$  so that the differential equation becomes

$$\Delta y = \Delta t f(t, y),$$

and this, in turn, may be written as the difference equation:

$$y_{n+1} = y_n + (t_{n+1} - t_n) f(t_n, y_n).$$

Using a fixed interval  $\Delta t = (t_{n+1} - t_n)$ , the initial values are iterated leading to new  $(t, y)$  pairs which eventually form the required solution.

The technique may be extended to higher order differential equations by converting to first order equations. For example, suppose the differential equation has the form:

$$\frac{d^2y}{dt^2} = f(t, y, \frac{dy}{dt}).$$

By the substitution  $x = \frac{dy}{dt}$  the following conversion results:

$$\begin{aligned}\frac{dy}{dt} &= x, \\ \frac{dx}{dt} &= f(t, y, x),\end{aligned}$$

yielding two first order equations. These can now be replaced by difference equations for the Euler method:

$$x_{n+1} = x_n + (t_{n+1} - t_n) f(t_n, x_n, y_n),$$

$$y_{n+1} = y_n + (t_{n+1} - t_n)k_n.$$

Using the fixed interval,  $\Delta t = t_{n+1} - t_n$ , the initial values ( $t_0, x_0, y_0$ ) can be iterated to obtain successive values of ( $t, x, y$ ).

While conceptually simple, the errors generated by the Euler method grow rapidly with the number of iterations compared to more sophisticated methods. Therefore it should be avoided for extended calculations.

A primary source of error in the Euler technique is that the change in  $y$  value is made to depend only on the derivative calculated at the beginning of the  $\Delta t$  step. A better approximation can be found by evaluating the derivative more often during  $\Delta t$ . In the case of a single, first order equation  $y' = f(t, y)$  the interval can be split in half and then successive calculations

$$k_1 = \Delta t f(t_n, y_n)$$

and

$$k_2 = \Delta t f(t_n + \Delta t/2, y_n + k_1/2)$$

lead to

$$y_{n+1} = y_n + k_2.$$

This algorithm is the second order Runge-Kutta method, and the process can include more steps for better accuracy. The fourth order Runge-Kutta algorithm is commonly used and seems to represent a reasonable compromise between computer speed and accuracy of solution. The steps in the calculation are as follows:

$$\begin{aligned} k_1 &= \Delta t f(t_n, y_n), \\ k_2 &= \Delta t f(t_n + \Delta t/2, y_n + k_1/2), \\ k_3 &= \Delta t f(t_n + \Delta t/2, y_n + k_2/2), \\ k_4 &= \Delta t f(t_n + \Delta t, y_n + k_3). \end{aligned}$$

Then  $y_{n+1}$  is evaluated as a weighted average over the  $k$  values as:

$$y_{n+1} = y_n + k_1/6 + k_2/3 + k_3/3 + k_4/6.$$

If more than one first order differential equation is to be solved, then the algorithm is applied to each one during each  $\Delta t$  interval. In many of the programs that are listed in Appendix B the subroutine RK4(X,V,TSTEP,XNEW,VNEW,T,W,G,Q), together with the defined function ACCEL(X,V,T,W,G,Q), does this procedure.

It is important to keep the step interval  $\Delta t$  small enough to maintain accuracy in the solution. Yet if  $\Delta t$  is smaller than necessary the computation will involve excessive time. Furthermore, the requisite size of  $\Delta t$  may vary with the rate at which the solution itself varies. These requirements suggest that  $\Delta t$  should be made adjustable during the calculation. One way to do this is to tie the step size to the computed difference  $\Delta y$ . If the  $\Delta y$  is greater than a certain predetermined

value  $\epsilon$ , then the program can back up and use a smaller  $\Delta t$  to evaluate  $y_{n+1}$ . In the programs used in this work  $\Delta t$  was increased with the formula:

$$\Delta t = \Delta t(0.95)(\epsilon/\Delta y)^{1/2}$$

when

$\Delta y < \epsilon$ , and decreased according to the formula:

$$\Delta t = \Delta t(0.95)(\epsilon/\Delta y)^{1/2}$$

when  $\Delta y > \epsilon$ .

Most of the pendulum programs listed in Appendix B use the Runge-Kutta method with the adaptive stepsize. Other more sophisticated algorithms are available in books on numerical methods, such as Press *et al.* (1986).

# Computer program listings

This appendix provides listings which may be used in their present or modified versions for exercises in the text. The listings are in the language True BASIC™ and their implementation requires the use of the True BASIC™ Language System together with the True BASIC™ toolkits for scientific and 3D graphics. These are available from True BASIC Inc., 12 Commerce Ave., West Lebanon, NH 03784, USA. The language system may be used to run or modify the programs. Hardware requirements include an IBM compatible machine with 512K of memory, and a Hercules, CGA, EGA, or VGA graphics adaptor. A math coprocessor is highly desirable. These programs and some others are also available bound in an executable, menu-driven, self-contained software package from one of the authors (GLB) as indicated under 'diskette order information'.

The programs are of three types: those which solve the differential equations of the pendulum, those which iterate discrete maps, and those which analyse experimental data. (The last group requires the data file found on the above mentioned software package.) Because the Runge-Kutta algorithm is complex, the computer processing time for differential equations solutions is much longer than for the iteration of maps. The reader is warned that a few of the text diagrams took many hours to produce even with a 486 IBM compatible machine.

The computer exercises of Chapter 2 are based upon the programs, PENDULUM, POINCARE, and EXPFFT. PENDULUM, Listing 1, provides a two-dimensional phase plane representation of the pendulum. The differential equation is that of the nonlinear, damped, driven pendulum. Modification of the external function ACCEL(X,V,T,W,G,Q) is required to linearize the pendulum. The term  $-X$  would then be substituted for the term  $-\text{SIN}(X)$ . The subroutine RK4(X,V,TSTEP,XNEW,VNEW,T,W,G,Q) is the Runge-Kutta integrator that is common to all the pendulum programs. Aside from input and graphics statements, the program consists of repeated callings of RK4 and the subsequent plotting of phase points at times which are consistent with the variable stepsize procedure outlined in Appendix A. The angular coordinate is kept periodic at each plotting by adjusting, if necessary, its absolute value to a number less than  $\pi$ . Modification of the program to show the evolution of a block of initial  $\theta$  and  $\omega$

coordinates requires a loop through the main part of the program. The initial coordinates, denoted XINT and VINT, then take successive values for each initial coordinate pair in the block.

The Poincaré section program, POINCARE (Listing 2), is quite similar to PENDULUM. However, since phase points are not generally calculated at the precise point of section, an additional procedure is required. For each pair of two consecutive phase points a check is made as to whether they straddle (in time) the moment of section. If they do satisfy this condition, the time variable is backed up to the precise moment of section by interpolation. The phase point computation is made at that moment, and the phase point is then plotted as part of the Poincaré section.

The program EXPFFT (Listing 3) computes the power spectrum of a linear combination of periodic components. It will provide both a time series and the power spectrum. A cursor will appear on the screen following the time series display. Any key may be pressed to continue the processing. For the most reliable spectrum, 4096 points of the time series should be used. To obtain the spectrum of some function other than the periodic function, one must change the dozen lines of code following the comment line, '!DEVELOP PERIODIC TIME SERIES DATA'.

The problems of Chapter 3 utilize the programs MOTION (Listing 4), BIFURCATION (Listing 5), FFT (Listing 6), and BASINS (Listing 7), as well as PENDULUM and POINCARE. MOTION is an animation of the pendulum motion in 'real' space and time. The program uses RK4 to solve the pendulum equations at equal time intervals. Animation is achieved by rotating the 'pendulum' image through the appropriate angle at each time step. The angular velocity is therefore determined by the computer processing speed.

BIFURCATION generates a 'bifurcation diagram' or scatter plot of angular velocity at closely spaced forcing amplitudes,  $g$ . The angular velocity values are taken at fixed phase  $\phi = 0$ , so the resulting diagram is equivalent to a sequence of Poincaré sections at increasing  $g$  values. The processing time is quite long.

FFT calculates the power spectrum of a time series of either  $\theta(t)$  or  $\omega(t)$ . The program first displays a phase diagram of  $\theta$  versus  $\omega$ , then a time series of the chosen quantity, and finally, the appropriate power spectrum. The time series algorithm is similar to that used for the Poincaré section in that the dynamical variable must be calculated at precise times, as regulated by the maximum frequency for the power spectrum. At various stages the program requires inputs, either to proceed to the next step, or to specify a variable and type of display. The user may choose the 'Hanning' option which has the ability to diminish spurious sidebands caused by the finite length of the data record. As with EXPFFT, the largest number of points, 4096, is recommended for the most accurate spectrum.

BASINS generates a display of the basins of attraction of the pendulum for a given driving force amplitude. In addition to incorporating the phase plane algorithm of PENDULUM, this program computes the average pendulum velocity  $\langle \omega \rangle$ , over the time interval  $(t_{\min}, t_{\max})$ , for each pair of initial

coordinates of the phase plane. The sign of  $\langle \omega \rangle$  determines the basin toward which the phase trajectory tends from an initial point. If  $\langle \omega \rangle$  is positive, a circle is placed at the corresponding initial point. Otherwise the point is unmarked. This program also provides the option to superpose the Poincaré sections on the basins. As with BIFURCATION the processing time of BASINS is quite long.

These programs may be modified to display graphs of other dynamical systems. Specific changes would be required in the ACCEL function, in the parameters of the graphs, and in the input statements.

The program listings for the problems of Chapter 4 are entitled LOGISTIC MAP (Listing 8), CIRCLE MAP (Listing 9), and HENON MAP (Listing 10). LOGISTIC MAP is a multipurpose program that gives the user four display options: a return map, a bifurcation diagram, an entropy diagram, and a Lyapunov exponent diagram. With the possible exception of the entropy algorithm, none of the routines is especially complex. The entropy calculation keeps track of the number of  $x(n)$  values that end up in each equally-sized cell of the  $x$  interval,  $[0,1]$ . The entropy is then obtained from the relative frequencies for each cell. LOGISTIC MAP may be readily modified to display the tent map (Problem 4.6) – primarily by changing the external function which specifies the particular map.

CIRCLE MAP is a multipurpose program that gives the user three options: a return map, a bifurcation map, and a Devil's staircase. As with LOGISTIC MAP, the three calculation subroutines are relatively straightforward. HENON MAP provides an illustration of a two-dimensional map.

PENDLYAP (Listing 11), calculates the Lyapunov exponents of the driven pendulum, as discussed in Chapter 5. The code is an adaptation of a FORTRAN program for the exponents of the Lorenz system of equations. (See the appendix of Wolf *et al.* (1985)). The resultant graph illustrates the gradual convergence of the exponents to their respective values.

The final set of listings illustrates the techniques described in Chapter 6. RECDIM (Listing 12) uses experimental values of the time series for the angular velocity. These data are first reconstructed in a three-dimensional phase space of delay coordinates. Then the data are embedded in phase spaces of varying dimension and the corresponding correlation integral is plotted for each case. Finally, the slopes of the various curves leads to an estimation of the attractor dimension. RECLYAP (Listing 13) also uses the file of experimental data. It calculates the largest Lyapunov exponent for the data, using an algorithm that, like PENDLYAP, is found in the paper by Wolf *et al.* (1985). PREDICTION (Listing 14) uses the method of analogs and the experimental data file to make a short term prediction of future behavior of the experimental pendulum's angular velocity. And finally, CONTROL (Listing 15) illustrates the stabilization of a simulated chaotic pendulum.

All of the above programs and the experimental data file are available with the above mentioned software package for IBM compatible PCs. This package obviates the need for any True BASIC™ software or typing of the listings. See the section on 'Diskette order information'.

## Listing 1

```

!PROGRAM TITLE *****PENDULUM*****
!XPHASE2D.TRU
!THIS PROGRAM DISPLAYS THE 2-DIMENSIONAL PHASE DIAGRAM
!FOR THE DRIVEN AND UNDRIVEN PENDULUM. DIAGRAM CAN BE
!PRINTED IF SUITABLE DRIVER INSTALLED.
!
LIBRARY "SGLIB.TRC"
LIBRARY "SCRNDUMP.TRC"
DECLARE DEF ACCEL
DIM A(1), B(1)
!INPUT STATEMENTS
INPUT PROMPT"INPUT FORCING STRENGTH(.5 FOR PERIODIC, 1.5 FOR CHAOTIC):":g
INPUT PROMPT"INPUT DAMPING (IF NO DAMPING THEN INPUT 9999999):":q
INPUT PROMPT"INPUT ANGULAR FORCING FREQUENCY ( TRY .66666666):":w
INPUT PROMPT"INPUT: INITIAL ANGLE , ANGULAR VELOCITY:"":XINT,VINT
INPUT PROMPT"INPUT: MINIMUM TIME , MAXIMUM TIME:"":THIN,THAX
INPUT PROMPT"AVVERAGE VELOCITY CALCULATION; YES(1) , NO(2):":AVC
INPUT PROMPT"DUMPSCREEN TO PRINTER (Y=1 /N=0) :"":P
IF P=1 THEN
  INPUT PROMPT"PRINTER TYPE (0)EPSON (1)HP LASERJET :"":PRNTR
  CALL SCRNDUMPDEVICE(PRNTR)
END IF
CALL PARAMS(EPS,TSTEP,XMIN,XMAX,YMIN,YMAX) !SETS MISC AND GRAPH PARAMETERS
CALL SETXSCALE(XMIN,XMAX) !FROM SGLIB
CALL SETYSCALE(YMIN,YMAX) !FROM SGLIB
CALL SETTEXT("PENDULUM - 2-D PHASE DIAGRAM","ANGLE","ANGULAR VELOCITY")
CALL RESERVELEGEND !FROM SGLIB , SAVES SPACE FOR LEGENDS

DATA 0,0
CALL DATAGRAPH(A,B,1,0,"WHITE") !FROM SGLIB - PLOTS INITIAL POINT
LET T=0
LET X=XINT
LET V=VINT
CALL GOTOCANVAS !SETS SCREEN FOR GRAPH
!
!CALCULATION AND GRAPHING BLOCK
FOR I=1 TO 10000000
  CALL RK4(X,V,TSTEP,XNEW,VNEW,T,W,G,Q) !CALL RUNGE-KUTTA, STEP = TSTEP
  LET TSHALF=TSTEP/2 ! SPLIT INTERVAL
  CALL RK4(X,V,TSHALF,XNH,VNH,T,W,G,Q) !DO TWO HALF STEPS
  CALL RK4(XNH,VNH,TSHALF,XN,VN,T+TSHALF,W,G,Q)
  LET D1=ABS(XN-XNEW)
  LET D2=ABS(VN-VNEW)
  LET DELTA=MAX(D1,D2)
  IF DELTA<EPS THEN
    IF T>THIN THEN
      IF ABS(X)>PI THEN LET X=X-2*PI*ABS(X)/X
      CALL GRAPHPOINT(X,V,1)
      LET SUMVEL=SUMVEL+V*TSTEP !UPDATE AVERAGE
    END IF
  END IF
END

```

```

LET X=XNEW
LET V=VNEW
LET T=T+TSTEP
LET TSTEP=TSTEP*.95*(EPS/DELTA)^.25
IF ABS(X)>PI THEN LET X=X-2*PI*ABS(X)/X
ELSE
  LET TSTEP=TSTEP*.95*(EPS/DELTA)^.2  IREDUCE STEP SIZE
END IF
IF T>THMAX THEN LET I=100000001
NEXT I
LET MEANVEL=SUMVEL/(THMAX-THMIN)
CALL ADDLEGEND("G="&STR5(G)) Q=&STR5(Q),0,1,"WHITE")
IF AVC=1 THEN CALL ADDLEGEND("AV. VEL. = "&STR5(MEANVEL),0,1,"WHITE")
CALL DRAWLEGEND  IADDS G AND Q VALUES TO LEGEND
IF P=1 THEN CALL SCREENDUMP
get key variable
clear
print"press <esc> key to finish"
END
!
SUB RK4(X,V,TSTEP,XNEW,VNEW,T,W,G,Q)  IRUNGE-KUTTA INTEGRATOR
DECLARE DEF ACCEL
LET XK1=TSTEP*V
LET VK1=TSTEP*ACCEL(X,V,T,W,G,Q)
LET XK2=TSTEP*(V+VK1/2)
LET VK2=TSTEP*ACCEL(X+XK1/2,V+VK1/2,T+TSTEP/2,W,G,Q)
LET XK3=TSTEP*(V+VK2/2)
LET VK3=TSTEP*ACCEL(X+XK2/2,V+VK2/2,T+TSTEP/2,W,G,Q)
LET XK4=TSTEP*(V+VK3)
LET VK4=TSTEP*ACCEL(X+XK3,V+VK3,T+TSTEP,W,G,Q)
LET VNEW=V+(VK1+2*VK2+2*VK3+VK4)/6
LET XNEW=X+(XK1+2*XK2+2*XK3+XK4)/6
END SUB
!
DEF ACCEL(X,V,T,W,G,Q)
  LET DAHP=1/Q
    LET ACCEL=-SIN(X)-DAHP*V+G*COS(W*T)
END DEF
!
SUB PARMS(EPS,TSTEP,XMIN,XMAX,YMIN,YMAX)
  LET EPS=1.0E-8
  LET TSTEP=0.5
  LET XMIN=-3
  LET XMAX=3
  LET YMIN=-4
  LET YMAX=4
END SUB

```

## Listing 2

```

!PROGRAM TITLE *****POINCARE*****
!XPOINCAR.TRU
CLEAR
PRINT" ***PENDULUM - POINCARE SECTION***"
PRINT
PRINT"THIS PROGRAM DISPLAYS THE POINCARE SECTION OF THE PENDULUM"
PRINT"AND CAN SAVE THE DATA TO A FILE. DISPLAY CAN BE PRINTED IF"
PRINT"APPROPRIATE DRIVER INSTALLED."
LIBRARY "SGLIB.TRC"
LIBRARY "SCRNDUMP.TRC"
!
DECLARE DEF accel
DIM A(1),B(1)
INPUT prompt"Input driving force strength(0.5 periodic, 1.5 chaotic): ":g
INPUT prompt"Input damping (If no damping then input 9999999):":q
INPUT prompt"input forcing angular frequency (try .66666666) ::w
INPUT prompt"Input initial angle, angular velocity: ::xint,vint
INPUT Prompt"Input min. and max. time::tmin,tmax
INPUT prompt"Input phase angle/(2*pi): "phi
INPUT prompt"Dumpscreen to printer ? (y=1 / n=0) ::p
IF p=1 then
  Input prompt"Printer type (0)Epson (1)HP laserjet ::prntr
  Call SCREENDUMPDEVICE(PRNTR)
End if
INPUT PROMPT" SAVE DATA TO A FILE? YES(1), NO(2)::SAVEFILE
IF SAVEFILE=1 THEN
  INPUT PROMPT"FILE NAME FORMAT EX. 14954020 ::FILENAME
  INPUT PROMPT"DRIVE FOR FILE DISK A,B,C,ETC. ::DISK$
  LET NAMES=DISK$&"&STR$(FILENAME)
  END IF
!
CALL PARAMS(EPS,TSTEP,XMIN,XMAX,YMIN,YMAX)
CALL SETSCALE(XMIN,XMAX)
CALL SETSCALE(YMIN,YMAX)
CALL SETTEXT("PENDULUM POINCARE SECTION","THETA","OMEGA")
CALL RESERVELEGEND
!
DATA O,O
CALL DATAGRAPH(A,B,1,O,"white")
LET t=0
LET x=xint
LET v=vint
CALL GOTOCANVAS
!
!CALCULATION AND GRAPHING BLOCK
LET phi=phi*2*pi
IF SAVEFILE=1 THEN
  OPEN #1:NAME NAMES, ORGANIZATION RECORD, CREATE NEWOLD
  ASK #1:FILESIZE LENGTH
  IF LENGTH=0 THEN SET#1:RECSIZE 10
  SET #1: POINTER END
  END IF

```

```

FOR i=1 to 1000000000
  CALL rk4(x,v,tstep,xnew,vnew,t,w,g,q)    ! Take a step of size tstep
  LET tshalf=tstep/2
  CALL rk4(x,v,tshalf,xnh,vnh,t,w,g,q)      !Take two half steps
  CALL rk4(xnh,vnh,tshalf,xn,vn,t+tshalf,w,g,q)
  LET d1=abs(xn-xnew)
  LET d2=abs(vn-vnew)
  LET delta=max(d1,d2)
  IF delta<eps then
    IF t>tmin then
      LET tnew=t+tstep
      LET w1=mod(phi-w*t,2*pi)    !Check for Poincare section
      LET w2=mod(v*tnew-phi,2*pi)
      IF w1<w*tstep then
        IF w2<w*tstep then
          LET ts=w1/w
          CALL rk4(x,v,ts,xp,vp,t,w,g,q)  !CALCULATES POINT AT SECTION
          IF abs(xp)>pi then LET xp*xp-2*pi*abs(xp)/xp
          CALL GRAPHPOINT(XP,VP,1)
        IF SAVEFILE=1 THEN WRITE #1:XP,VP
      END IF
    END IF
    LET x=xnew
    LET v=vnew
    LET t+=tstep      !Expand step size
    LET tstep=tstep*.95*(eps/delta)^.25
    IF abs(x)>pi then      !bring theta back into range
      LET x=x-2*pi*abs(x)/x
    END IF
  ELSE
    !else reduce step size
    LET tstep=tstep*.95*(eps/delta)^.2
  END IF
  IF t>tmax then LET i=100000001
NEXT i
LET GS=STR$(G)
LET QS=STR$(Q)
CALL ADDLEGEND("G="&STR$(G)&" Q="&STR$(Q)&" PHI="&STR$(PHI),0,1,"WHITE")
CALL DRAWLEGEND
IF P=1 THEN CALL SCREENDUMP
END
!
SUB rk4(x,v,tstep,xnew,vnew,t,w,g,q)
  DECLARE DEF accel
  LET xk1=tstep*v
  LET vk1=tstep*accel(x,v,t,w,g,q)
  LET xk2=tstep*(v+vk1/2)
  LET vk2=tstep*accel(x+xk1/2,v+vk1/2,t+tstep/2,w,g,q)
  LET xk3=tstep*(v+vk2/2)
  LET vk3=tstep*accel(x+xk2/2,v+vk2/2,t+tstep/2,w,g,q)
  LET xk4=tstep*(v+vk3)
  LET vk4=tstep*accel(x+xk3,v+vk3,t+tstep,w,g,q)
  LET vnew=v+(vk1+2*vk2+2*vk3+vk4)/6
  LET xnew=x+(xk1+2*xk2+2*xk3+xk4)/6
END SUB

```

```

DEF accel(x,v,t,w,g,q)
  LET accel=-sin(x)-(1/q)*v+g*cos(w*t)
END def
!
SUB PARMS(EPS,TSTEP,XMIN,XMAX,YMIN,YMAX)
  LET EPS=1.0E-6
  LET TSTEP=0.5
  LET XMIN=-3
  LET XMAX=3
  LET YMIN=-4
  LET YMAX=4
END SUB

```

### Listing 3

```

1000 !PROGRAM *****EXPFFT*****
1010 !EXPFFT.TRU
1020 LIBRARY "SCRNDUMP.TRC"
1030 LIBRARY "SGLIB.TRC"
1040 CLEAR
1050 PRINT* ***FFT OF SUPERPOSED SINE WAVES***
1060 PRINT
1070 PRINT* THIS PROGRAM TAKES THE FOURIER TRANSFORM OF A GROUP OF SINE*
1080 PRINT* WAVES WHOSE AMPLITUDES AND FREQUENCIES ARE INPUTS. BOTH THE*
1090 PRINT* TIME SERIES AND THE TRANSFORM ARE GRAPHED. IF A BLINKING CURSOR*
1100 PRINT* APPEARS PRESS ANY KEY TO CONTINUE. THE HANNING OPTION SMOOTHES*
1110 PRINT* THE ABRUPT EFFECT OF THE WINDOW*
1120 PRINT* AND SUPPRESSES SPURIOUS COMPONENTS.*
1130 PRINT* DISPLAYS CAN BE PRINTED IF APPROPRIATE DRIVER IS PRESENT.*
1140 DIM thetadata(5000),thetadotdata(5000),xreal(0 to 5000),ximag(0 to 10000)
1150 DIM tpoint(0 to 5000),power(2048),frequency(2048),FREQ(10),AMPL(10)
1160 DECLARE DEF bitr
1170 INPUT prompt"Max frequency : ":maxfreq
1180 INPUT Prompt"Input min.time":tmin
1190 INPUT prompt"No. of FFT points(..256,512,1024,2048,4096) : ":number
1200 LET ps=1
1210 LET del=.5/maxfreq
1220 LET tmax=number*del+tmin
1230 LET n=number
1240
1250 LET count=0
1260 LET p=1
1270 !DEVELOP PERIODIC TIME SERIES DATA
1280 INPUT PROMPT "HOW MANY FREQUENCY COMPONENTS?":NUMBFREQ
1290 FOR NF = 1 TO NUMBFREQ
1300   INPUT PROMPT" STATE FREQUENCY ::FREQ(NF)
1310   INPUT PROMPT" COMPONENT AMPLITUDE::AMPL(NF)
1320 NEXT NF
1330 INPUT PROMPT" DUMPSCREEN TO PRINTER (Y=1/ N=0) ::DUMPER
1340 IF DUMPER=1 THEN
1350   INPUT PROMPT"PRINTER TYPE (0)EPSON (1)HP LASERJET ::PRNTR
1360   CALL SCREENDUMPDEVICE(PRNTR)

```

```

1370 END IF
1380 FOR P = 1 TO N
1390   LET TOTAL = 0
1400   FOR NF = 1 TO NUMBFREQ
1410     LET TOTAL = TOTAL + AMPL(NF)*SIN(2*PI*FREQ(NF)*(THIN+P*DEL))
1420   NEXT NF
1430   LET THETADOTDATA(P)=TOTAL
1440 NEXT P
1450 I
1460 I
1470 !PREPARATION OF THE FFT DATA
1480 CLEAR
1490 INPUT prompt" HANNING OPTION Y/N? ": hanning$
1500 LET tgamma=log2(n)
1510 IF abs(int(tgamma)-tgamma)=0 then
1520   LET gamma=tgamma
1530   GOTO 1560
1540 END IF
1550 LET gamma=int(tgamma)+1
1560 PRINT "gamma= ";gamma
1570 LET newn=2^gamma
1580 LET nu=gamma
1590 FOR i=n+1 to newn
1600   LET xreal(i)=0
1610 NEXT i
1620 LET n=newn
1630 PRINT "n= ";n
1640 CLEAR
1650 IF ps=1 then LET title$="WAVE DISPLACEMENT"
1660 CALL settext("TIME SERIES","TIME",title$)
1670 CALL setxscale(tmin,tmax)
1680 FOR k=0 to n-1
1690
1700   IF ps = 1 then
1710     LET xreal(k)=thetadotdata(k+1)
1720   ELSE IF ps = 2 then
1730     LET xreal(k)=thetadata(k+1)
1740   END IF
1750 IF hanning$="y" then LET xreal(k) = xreal(k)*(.5-.5*cos(2*pi*k/(n-1)))
1760 LET ximag(k)=0
1770 LET tpoint(k)=tmin+k*del
1780 NEXT k
1790 CALL SETAXES(0)
1800 CALL setgraphtype("")
1810 CALL datagraph(tpoint,xreal,1,0,"white")
1820 GET KEY keyvariable
1830 FOR i= 1 to 100
1840 NEXT i
1850
1860 !FFT ALGORITHM
1870 CLEAR
1880 PRINT "Calculating FFT"
1890 LET n2=n/2
1900 LET nul=nu-1
1910 LET k=0
1920 FOR i=1 to nu
1930   DO while k<(n-1)

```

```

1940   FOR i=1 to n2
1950     LET argument=k/2^nul
1960     LET garbage=int(argument)
1970     LET pbitr(garbage,nu)
1980     LET arg = 2*pi*p/n
1990     LET c=cos(arg)
2000     LET s=sin(arg)
2010     LET k1=k+1
2020     LET kln2=k1+n2
2030     LET treal=xreal(kln2)*c+ximag(kln2)*s
2040     LET timag=ximag(kln2)*c-xreal(kln2)*s
2050     LET xreal(kln2)=xreal(k1)-treal
2060     LET ximag(kln2)=ximag(k1)-timag
2070     LET xreal(k1)=xreal(k1)+treal
2080     LET ximag(k1)=ximag(k1)+timag
2090     LET k=k+1
2100   NEXT i
2110   LET k=k+n2
2120   LOOP
2130   LET k=0
2140   LET nul=nul-1
2150   LET n2=int(n2/2)
2160 NEXT i
2170
2180 FOR k=1 to n
2190   LET i=bitr(k-1,nu)+1
2200   IF i<=k then GOTO 2270
2210   LET treal=xreal(k)
2220   LET timag=ximag(k)
2230   LET xreal(k)=xreal(i)
2240   LET ximag(k)=ximag(i)
2250   LET xreal(i)=treal
2260   LET ximag(i)=timag
2270 NEXT k
2280
2290 !GRAPHING THE FFT
2300 CLEAR
2310 INPUT prompt"Plot 1)power spectrum, or 2)log power spectrum: ":pps
2320 INPUT prompt"Frequency variable - 1)linear, or 2)log: ":freqvar
2330 LET maxfreq=.5/del
2340 LET minfreq=1/(number*del)
2350
2360 CLEAR
2370 IY-AXIS
2380 IF pps = 1 then
2390   LET TITLE$="POWER SPECTRUM"
2400   LET YAXISS$="POWER"
2410 ELSE
2420   LET TITLE$="LOG POWER SPECTRUM"
2430   LET YAXISS$="LOG POWER"
2440 END IF
2450 IX-AXIS
2460 IF freqvar=2 then
2470   LET XAXISS$="LOG FREQUENCY"
2480 ELSE
2490   LET XAXISS$="FREQUENCY"

```

```

2500 END IF
2510
2520 !DRAW AXES
2530 CLEAR
2540 CALL setxscale(minfreq,maxfreq)
2550 CALL setyscale(1e-6,.99)
2560 CALL SETTEXT(TITLE$,XAXIS$,YAXIS$)
2570 CALL RESERVELEGEND
2580
2590 !PLOT POINTS
2600 FOR i=1 to n/2
2610   LET frequency(i)=i/(n*del)
2620   LET power(i)=(((xreal(i))^2+(ximag(i))^2))^.5)/n
2630
2640 NEXT i
2650 !PLOT TEXT
2660 CALL setaxes(0)
2670 IF ppa=1 then
2680   IF freqvar=1 then CALL setgraphtype("xy")
2690   IF freqvar=2 then CALL setgraphtype("logx")
2700 END IF
2710 IF ppa=2 then
2720   IF freqvar=1 then CALL setgraphtype("logy")
2730   IF freqvar=2 then CALL setgraphtype("logxy")
2740 END IF
2750 IF NUMBER =4096 THEN
2760   LET SYMBOL=1
2770 ELSE
2780   LET SYMBOL=0
2790 END IF
2800 CALL datagraph(frequency,power,1,SYMBOL,"white")
2810 CALL ADDLEGEND("N="&STR$(N)&" MAX FREQ="&STR$(MAXFREQ)&" DEL F="&STR$(MINFREQ),0,1,"WHITE")
2820 CALL drawlegend
2830 IF hanning="-" then
2840   CALL ADDLEGEND("- HANNING",0,1,"WHITE")
2850 END IF
2860 IF DUMPER=1 THEN CALL SCREENDUMP
2870 GET KEY keyvariable
2880 INPUT PROMPT "Another with Hanning? y/n: ":hann$
2890 IF hann$= "y" THEN GOTO 1480
2900 INPUT PROMPT "Different presentation of same FFT? (y/n): ":diffplot$
2910 IF diffplot$ = "y" THEN GOTO 2300
2920 END
2930 !
2940 !BIT REVERSER FUNCTION
2950 DEF bitr(j,nu)
2960   LET j1=j
2970   LET ibitr=0
2980   FOR i=1 to nu
2990     LET j2 = int(j1/2)
3000     LET ibitr=ibitr*2+(j1-2*j2)
3010     LET j1=j2
3020   NEXT i
3030   LET bitr=ibitr
3040 END DEF

```

## Listing 4

```

!PROGRAM TITLE *****MOTION*****
!XMOTION.TRU
LIBRARY "SGLIB.TRC"
DIM A(1),B(1)
!
CLEAR
PRINT"      ***PENDULUM - ANIMATION OF ITS MOTION***"
PRINT"This program draws the motion of the pendulum at equal time intervals."
PRINT
INPUT prompt"Input driving force strength (0.5 to 1.5)::g
INPUT prompt"input damping ,q (2 to 4)::q
INPUT prompt"Input initial position::xint
INPUT Prompt"Input initial velocity::vint
INPUT prompt"Input min. and max. time::tmin,tmax
INPUT prompt"Input drive angular frequency (try .66666666)::w
INPUT prompt"Animation speed on 486(try 1000 for fast, 50000 for slow)::spd
LET tstep=.5

!SET WINDOW -1,1,-1,1
!BOX LINES -.95,.95,-.95,.95
CALL SETXSCALE(-1,1)
CALL SETYSCALE(-1,1)
CALL SETAXES(0,0)
CALL SETTICKSIZES(0,0)
CALL SETTITLE("PENDULUM ANIMATION")
DATA 0,0
CALL DATAGRAPH(A,B,0,0,"WHITE")
CALL GOTOCANVAS
PICTURE Pendulum
  SET COLOR "white"
  FOR k=1 to 2
    IF k=1 then
      SET COLOR "WHITE"
      LET dummy=0
    END IF
    IF k=2 then
      DO while dummy<spd
        LET dummy=dummy +1
      LOOP
      SET COLOR "BLACK"
    END IF
    I           SET COLOR "black"
    PLOT LINES:0,0;0,-.5;.05,-.5;-.05,-.55;-.05,-.05,-.5;0,-.5
  NEXT k

END PICTURE

FOR i=1 to 1000000
  CALL rk4(x,v,tstep,xnew,vnew,t,w,g,q)
  LET t=t+tstep
  LET x=xnew
  LET v=vnew

```

```

IF t>tmin then
  LET angle=x
  DRAW pendulum with rotate(angle)
  PLOT
END IF
IF t>tmax then LET i=1000001
NEXT i
GET KEY variable
CLEAR
END

DEF accel(x,v,t,w,g,q)
  LET accel= -sin(x)-(1/q)*v+g*cos(w*t)
END DEF

SUB rk4(x,v,tstep,xnew,vnew,t,w,g,q)
  DECLARE DEF accel
  LET xk1=tstep*v
  LET vki=tstep*accel(x,v,t,w,g,q)
  LET xk2=tstep*(v+vki/2)
  LET vk2=tstep*accel(x+xk1/2,v+vk1/2,t+tstep/2,w,g,q)
  LET xk3=tstep*(v+vk2/2)
  LET vk3=tstep*accel(x+xk2/2,v+vk2/2,t+tstep/2,w,g,q)
  LET xk4=tstep*(v+vk3)
  LET vk4=tstep*accel(x+xk3,v+vk3,t+tstep,w,g,q)
  LET vnew=v+(vk1+2*vk2+2*vk3+vk4)/6
  LET xnew=x+(xk1+2*xk2+2*xk3+xk4)/6
END SUB

```

## Listing 5

```

!PROGRAM TITLE *****BIFURCATION*****
!XBIFURCA.TRU
CLEAR
PRINT" ***PENDULUM - BIFURCATION DIAGRAM***"
PRINT"THIS PROGRAM DISPLAYS THE BIFURCATION DIAGRAM FOR THE PENDULUM."
PRINT"FOR EACH VALUE OF FORCING AMPLITUDE, G, THE SYSTEM COMES TO A "
PRINT"STEADY STATE (AFTER MIN.TIME) AND THEN THE ANGULAR VELOCITY AT"
PRINT"AT THE BEGINNING OF EACH FORCING CYCLE IS DISPLAYED FOR A NUMBER OF"
PRINT"FURTHER CYCLES (GOVERNED BY MAX. TIME). THE DATA CAN BE SAVED TO A FILE"
PRINT"THE DIAGRAM CAN BE PRINTED IF APPROPRIATE DRIVE IS INSTALLED."
!
DIM XINT(10), VINT(10)
LIBRARY "SGLIB.TRC"
LIBRARY "SCRNDUMP.TRC"
!
DECLARE DEF accel
DIM A(1),B(1)
INPUT prompt"Input LOWEST DRIVING FORCE STRENGTH: ":GMIN
INPUT prompt"INPUT HIGHEST DRIVING FORCE STRENGTH:":GMAX
INPUT prompt"INPUT G STEPSIZE:":DELTAG
INPUT prompt"INPUT NUMBER OF SETS OF INITIAL CONDITIONS:":NUMSETS
FOR I=1 TO NUMSETS
  INPUT PROMPT"INPUT INITIAL ANGLE:":XINT(I)
  INPUT PROMPT"INPUT INITIAL ANGULAR VELOCITY:":VINT(I)
NEXT I
INPUT prompt"Input damping (try 2 - 4) :::q
INPUT prompt"Input forcing frequency (try .666666666666) :::w
INPUT Prompt"Input min. and max. time:::tmin,tmax
INPUT prompt"Input phase angle/(2*pi) - USE ZERO IF WANT BEGINNING OF CYCLE:::PHI
PRINT
PRINT" SINCE THE RUNTIME IS VERY LONG THE NEXT SET OF INPUTS GIVE AN OPTION"
PRINT" TO SAVE THE DATA TO A FILE"
INPUT PROMPT"SAVE TO A FILE? YES(1), NO(2):::SV
IF SV=1 THEN
  PRINT "A REASONABLE 8 CHARACTER FILE NAME (USE A NUMBER) MIGHT INCLUDE"
  PRINT"1)FIRST 2 DIGITS FOR Q VALUE"
  PRINT"2)NEXT 3 DIGITS FOR LOWEST G VALUE"
  PRINT"3)LAST 3 DIGITS FOR HIGHEST G VALUE"
  PRINT" EXAMPLE 20145150"
  INPUT PROMPT"FILE NAME ::::FILENAME
  INPUT PROMPT"DATA FILE DRIVE (A/B/C/D):::BS
  LET NAME$=STR$(FILENAME)
END IF
INPUT PROMPT"DUMP SCREEN TO PRINTER (Y=1 / N=0):::DUMP
IF DUMP=1 THEN
  INPUT PROMPT"PRINTER TYPE (0)EPSON, (1)HP LASERJET :::PRNTR
  CALL SCREENDUMPDEVICE(PRNTR)
END IF
CLEAR
CALL PARAMSL(EPS,TSTEP)
CALL SETAXES(0)
CALL SETSCALE(GMIN,GMAX)
CALL SETSCALE(-1,3)
CALL SETTEXT("PENDULUM BIFURCATION DIAGRAM","FORCING-G","ANGULAR VELOCITY")
CALL RESERVELEGEND
!
DATA 0,0
CALL DATAGRAPH(A,B,1,0,"WHITE")
!
IF SV=1 THEN
  OPEN #1:NAME BS$:::ENAMES,ORGANIZATION RECORD, CREATE NEWOLD
  ASK #1:FILESIZE LENGTH
  IF LENGTH=0 THEN SET#1: RECSIZE 10
  SET #1: POINTER END
END IF
!
FOR II=1 TO NUMSETS
  !LOOPS FOR ALL INITIAL CONDITIONS
  LET T=0
  LET XP=XINT(II)
  LET VP=VINT(II)
  FOR G=GMIN TO GMAX STEP DELTAG !LOOPS FOR ALL G VALUES
    LET t=0
    LET x=xp
    LET v=vp
    CALL GOTOCANVAS
    !
    !CALCULATION AND GRAPHING BLOCK
    LET phi=phi*2*pi

```

```

FOR i=1 to 1000000
  CALL rk4(x,v,tstep,xnew,vnew,t,w,g,q)      ! Take a step of size tstep
  LET tshalf=tstep/2
  CALL rk4(x,v,tshalf,xnh,vnh,t,w,g,q)      !Take two half steps
  CALL rk4(xnh,vnh,tshalf,xn,vn,t+tshalf,w,g,q)
  LET d1=abs(xn-xnew)
  LET d2=abs(vn-vnew)
  LET delta=max(d1,d2)
  IF delta<eps then
    IF t>tmin then
      LET tnew=t+tstep
      LET w1=mod(phi-w*t,2*pi) !Check for Poincare section
      LET w2=mod(w*tnew-phi,2*pi)
      IF w1<w*tstep then
        IF w2<w*tstep then
          LET tsw=w1/w
          CALL rk4(x,v,ts,wp,vp,t,w,g,q)      !CALCULATES POINT AT SECTION
          IF abs(wp)>pi then LET wp=wp-2*pi*abs(wp)/wp
          CALL GRAPHPOINT(G,VP,1)
          IF SV=1 THEN WRITE #1:G,VP
        END IF
      END IF
    END IF
  END IF
  LET x=xnew
  LET v=vnew
  LET t=t+tstep      !Expand step size
  LET tstep=tstep*.95*(eps/delta)^.25
  IF abs(x)>pi then !bring theta back into range
    LET x=x-2*pi*abs(x)/x
  END IF
  ELSE                !else reduce step size
    LET tstep=tstep*.95*(eps/delta)^.2
  END IF
  IF t>tmax then LET i=1000001
NEXT i
NEXT G
LET GS=STR$(G)
LET QS=STR$(Q)
CALL ADDLEGEND(" Q="&STR$(Q)&" PHI="&STR$(PHI),0,1,"WHITE")
CALL DRAWLEGEND
IF DUMP=1 THEN CALL SCREENDUMP
get key variable
clear
END
!
SUB rk4(x,v,tstep,xnew,vnew,t,w,g,q)
  DECLARE DEF accel
  LET xk1=tstep*v
  LET vk1=tstep*accel(x,v,t,w,g,q)
  LET xk2=tstep*(v+vk1/2)
  LET vk2=tstep*accel(x+xk1/2,v+vk1/2,t+tstep/2,w,g,q)
  LET xk3=tstep*(v+vk2/2)
  LET vk3=tstep*accel(x+xk2/2,v+vk2/2,t+tstep/2,w,g,q)
  LET xk4=tstep*(v+vk3)

```

```

  LET vk4=tstep*accel(x+xk3,v+vk3,t+tstep,w,g,q)
  LET vnew=v+(vk1+2*vk2+2*vk3+vk4)/6
  LET xnew=x+(xk1+2*xk2+2*xk3+xk4)/6
END SUB
DEF accel(x,v,t,w,g,q)
  LET accel=-sin(x)-(1/q)*v+g*cos(w*t)
END DEF
!
SUB PARAMS1(EPS,TSTEP)
  LET EPS=1.0E-6
  LET TSTEP=0.5
END SUB

```

## Listing 6

```

1000 !PROGRAM TITLE ****FFT*****
1010 !XFFT.TRU
1020 CLEAR
1030 PRINT" ***PENDULUM - FAST FOURIER TRANSFORM OF VARIABLES***"
1040 PRINT"
1050 PRINT"THIS PROGRAM PROVIDES A PHASE DIAGRAM, TIME SERIES, AND FFT OF THE"
1060 PRINT"ANGLE OR ANG. VELOCITY OF THE PENDULUM. A BLINKING CURSOR INDICATES"
1070 PRINT"THAT THE PROGRAM IS READY FOR THE NEXT STEP. PRESS ANY KEY TO CONTINUE."
1080 PRINT"THE HANNING OPTION IS USED TO SMOOTH THE EFFECT OF THE ABRUPT WINDOW"
1090 PRINT"AND IS RECOMMENDED IN MOST CASES."
1100 PRINT"
1110 LIBRARY "SGLIB.TRC"
1120 LIBRARY "SCRNDUMP.TRC"
1130 !
1140 DIM thetadata(5000),thetadotdata(5000),xreal(0 to 5000),ximag(0 to 10000)
1150 DIM tpoint(0 to 5000).power(2048),frequency(2048)
1160 DECLARE DEF accel
1170 DECLARE DEF bitr
1180 INPUT prompt"Max frequency (try 0.5): ::maxfreq
1190 INPUT prompt"Input driving force strength (try .5 to 1.5): ::g
1200 INPUT prompt"Input damping term (try 2 to 4): ::q
1210 INPUT prompt"Input forcing frequency (try .6666666) :::w
1220 INPUT prompt"Input initial position: :: xint
1230 INPUT prompt"Input initial velocity: :: vint
1240 INPUT prompt"Input min.time::tmin
1250 INPUT prompt"No. of FFT points(..256,512,1024,2048,4096) :::number
1260 PRINT"Desired power spectrum quantity"
1270 PRINT" 1)Power spectrum of angular velocity"
1280 PRINT" 2)Power spectrum of angle"
1290 INPUT prompt"Choose 1 or 2 :::ps
1300 INPUT prompt"Dump screen to printer (y=1 / n=0) :::dump
1310 IF dump=1 then
1320   INPUT prompt"Printer type (0)Epson, (1)HP Laserjet :::prntr
1330   CALL SCREENDUMPDEVICE(prntr)
1340   INPUT prompt"Hardcopy of time series (y=1 / n=0) :::dumptime
1350   INPUT prompt"Hardcopy of fft (y=1 / n=0) :::dumpfft
1360 END IF

```

```

1370
1380 LET del=.5/maxfreq
1390 LET tmax=number*del+tmin
1400 LET eps=1.0e-6
1410 LET tstep=0.5
1420
1430 LET t=0
1440 LET x=xint
1450 LET v=vint
1460 LET sumvel=0
1470 LET count=0
1480 LET p=1
1490 CALL SETTEXT("PENDULUM PHASE DIAGRAM","ANGLE","ANGULAR VELOCITY")
1500 CALL RESERVELEGEND
1510 PRINT"computing data"
1520 I
1530 FOR i=1 to 10000000
1540     CALL rk4(x,v,tstep,xnew,vnew,t,w,g,q)    ! Take a step of size tstep
1550     LET tshalf=tstep/2
1560     CALL rk4(x,v,tshalf,xnh,vnh,t,w,g,q)    !Take two half steps
1570     CALL rk4(xnh,vnh,tshalf,xn,vn,t+tshalf,w,g,q)
1580     LET d1=abs(xn-xnew)
1590     LET d2=abs(vn-vnew)
1600     LET delta=max(d1,d2)
1610     IF delta<eps then
1620         IF t>tmin then
1630             LET tnew=t + tstep
1640             LET w1=mod(-t,del)
1650             LET w2=mod(tnew,del)
1660             IF w1<tstep then
1670                 IF w2<tstep then
1680                     LET ts=w1
1690                     CALL rk4(x,v,ts,xp,vp,t,w,g,q)
1700                     IF abs(xp)>pi then LET xp=xp-2*pi*abs(x)/x
1710                     LET thetadata(p)=xp
1720                     LET thetadotdata(p)=vp
1730                     LET p=p+1
1740                     LET sumvel= sumvel + v
1750                     LET count = count + 1
1760                 END IF
1770             END IF
1780         END IF
1790         LET x=xnew
1800         LET v=vnew
1810         LET t=t+tstep
1820         LET tstep=tstep*.95*(eps/delta)^.25
1830         IF abs(x)>pi then
1840             LET x=x-2*pi*abs(x)/x
1850         END IF
1860     ELSE
1870         LET tstep=tstep*.95*(eps/delta)^.2
1880     END IF
1890     IF t>tmax then LET i=10000001
1900 NEXT i
1910 LET n=p-1
1920 LET meanvel=sumvel/count
1930 CLEAR

```

```

1940 CALL setmargins(60,60,0,0)
1950 CALL setgraphtype("xy")
1960 CALL datagraph(thetaidata,thetadotdata,1,0,"white")
1970 CALL ADDLEGEND("G=""&STR$(G)E"   Q=""&STR$(Q),0,1,"WHITE")
1980 CALL DRAWLEGEND
1990 IF dumptime=1 then CALL screendump
2000 GET KEY keyvariable
2010 I
2020 I
2030 !PREPARATION OF THE FFT DATA
2040 CLEAR
2050 INPUT prompt" HANNING OPTION Y/N? ": hanning5
2060 LET tgamma=log2(n)
2070 IF abs(int(tgamma)-tgamma)=0 then
2080     LET gamma=tgamma
2090     GOTO 2120
2100 END IF
2110 LET gamma=int(tgamma)+1
2120 PRINT "gamma=";gamma
2130 LET newn=2^gamma
2140 LET nu=gamma
2150 FOR i=n+1 to newn
2160     LET xreal(i)=0
2170 NEXT i
2180 LET n=newn
2190 PRINT"n=";n
2200 CLEAR
2210 IF ps=1 then LET title$="ANGULAR VELOCITY"
2220 IF ps=2 then LET title$="ANGLE"
2230 CALL settext("TIME SERIES","TIME",title$)
2240 CALL setxscale(tmin,tmax)
2250 FOR k=0 to n-1
2260
2270     IF ps = 1 then
2280         LET xreal(k)=thetadata(k+1)
2290     ELSE IF ps = 2 then
2300         LET xreal(k)=thetadotdata(k+1)
2310     END IF
2320     IF hanning$="y" then LET xreal(k) = xreal(k)*(.5-.5*cos(2*pi*k/(n-1)))
2330     LET ximag(k)=0
2340     LET tpoint(k)=tmin+k*del
2350 NEXT k
2360 CALL setgraphtype("")
2370 CALL datagraph(tpoint,xreal,1,0,"white")
2380 GET KEY keyvariable
2390 FOR i= 1 to 100
2400 NEXT i
2410
2420 !FFT ALGORITHM
2430 CLEAR
2440 PRINT "Calculating FFT"
2450 LET n2=n/2
2460 LET nul=nu-1
2470 LET k=0
2480 FOR l=1 to nu
2490     DO while k<(n-1)

```

```

2500   FOR i=1 to n2
2510     LET argument=k/2^nul
2520     LET garbage=int(argument)
2530     LET p=bitr(garbage,nu)
2540     LET arg =2*pi*p/n
2550     LET c=cos(arg)
2560     LET s=sin(arg)
2570     LET k1=k+1
2580     LET kln2=k1+n2
2590     LET treal=xreal(kln2)*c+ximag(kln2)*s
2600     LET timag=ximag(kln2)*c-xreal(kln2)*s
2610     LET xreal(kln2)=xreal(k1)-treal
2620     LET ximag(kln2)=ximag(k1)-timag
2630     LET xreal(k1)=xreal(k1)+treal
2640     LET ximag(k1)=ximag(k1)+timag
2650     LET k=k+1
2660   NEXT i
2670   LET k=k+n2
2680 LOOP
2690 LET k=0
2700 LET nul=nul-1
2710 LET n2=int(n2/2)
2720 NEXT 1
2730
2740 FOR k=1 to n
2750   LET i=bitr(k-1,nu)+1
2760   IF i<k then GOTO 2830
2770   LET treal=xreal(k)
2780   LET timag=ximag(k)
2790   LET xreal(k)=xreal(i)
2800   LET ximag(k)=ximag(i)
2810   LET xreal(i)=treal
2820   LET ximag(i)=timag
2830 NEXT k
2840
2850 !GRAPHING THE FFT
2860 CLEAR
2870 INPUT prompt"Plot 1)power spectrum, or 2)log power spectrum: ":pps
2880 INPUT prompt"Frequency variable - 1)linear, or 2)log: ":freqvar
2890 LET maxfreq=.5/del
2900 LET minfreq=1/(number*del)
2910
2920 CLEAR
2930 !Y-AXIS
2940 IF pps = 1 then
2950   LET TITLE$="POWER SPECTRUM"
2960   LET YAXISS$="POWER"
2970 ELSE
2980   LET TITLE$="LOG POWER SPECTRUM"
2990   LET YAXISS$="LOG POWER"
3000 END IF
3010 !X-AXIS
3020 IF freqvar=2 then
3030   LET XAXISS$="LOG FREQUENCY"
3040 ELSE
3050   LET XAXISS$="FREQUENCY"
3060 END IF

3070
3080 !DRAW AXES
3090 CLEAR
3100 CALL setmargins(60,60,0,0)
3110 CALL setxscale(minfreq,maxfreq)
3120 CALL setyscale(1e-6,.99)
3130 CALL SETTEXT(TITLE$,XAXISS$,YAXISS$)
3140 CALL RESERVELEGEND
3150
3160 IPLOT POINTS
3170 FOR i=1 to n/2
3180   LET frequency(i)=i/(n*del)
3190   LET power(i)=((xreal(i))^2+(ximag(i))^2)/(n^2)
3200
3210 NEXT i
3220 IPLOT TEXT
3230 CALL setmargins(60,60,0,0)
3240 CALL setaxes(0)
3250 IF pps=1 then
3260   IF freqvar=1 then CALL setgraphtype("xy")
3270   IF freqvar=2 then CALL setgraphtype("logx")
3280 END IF
3290 IF pps=2 then
3300   IF freqvar=1 then CALL setgraphtype("logy")
3310   IF freqvar=2 then CALL setgraphtype("logxy")
3320 END IF
3330 IF NUMBER=4096 THEN
3340   CALL datagraph(frequency,power,1,1,"white")
3350 ELSE
3360   CALL DATAGRAPH(FREQUENCY,POWER,1,0,"WHITE")
3370 END IF
3380 CALL ADDLEGEND("N="&STR$(N)&" MAX FREQ ="&STR$(MAXFREQ)&" DEL F="&STR$(MINFREQ),
0,1,"WHITE")
3390 CALL ADDLEGEND(" G="&STR$(G)&" Q="&STR$(Q),0,1,"WHITE")
3400 CALL drawlegend
3410 IF dumpfft=1 then CALL screendump
3420 IF hanning$="y" then
3430   i   CALL ADDLEGEND(" HANNING",0,1,"WHITE")
3440 END IF
3450 GET KEY keyvariable
3460 INPUT PROMPT "Another with Hanning? y/n: ":hann$
3470 IF hann$="y" THEN GOTO 2040
3480 INPUT PROMPT "FFT of different quantity (y/n)? ":" diffquant$
3490 IF diffquant$ = "y" THEN
3500   IF ps = 2 THEN LET ps = 1
3510   IF ps = 1 THEN LET ps = 2
3520   GOTO 2200
3530 END IF
3540 INPUT PROMPT "Different presentation of same FFT? (y/n): ":"diffplot$"
3550 IF diffplot$ = "y" THEN GOTO 2860
3552 GET KEY VARIABLE
3555 CLEAR
3560 END
3570 i
3580 SUB rk4(x,v,tstep,xnew,vnew,t,w,g,q)
3590   DECLARE DEF accel
3600   LET xk1=tstep*v

```

```

3610 LET vk1=tstep*accel(x,v,t,w,g,q)
3620 LET xk2=tstep*(v+vk1/2)
3630 LET vk2=tstep*accel(x+xk1/2,v+vk1/2,t+tstep/2,w,g,q)
3640 LET xk3=tstep*(v+vk2/2)
3650 LET vk3=tstep*accel(x+xk2/2,v+vk2/2,t+tstep/2,w,g,q)
3660 LET xk4=tstep*(v+vk3)
3670 LET vk4=tstep*accel(x+xk3,v+vk3,t+tstep,w,g,q)
3680 LET vnew=v+(vk1+2*vk2+2*vk3+vk4)/6
3690 LET xnew=x+(xk1+2*xk2+2*xk3+xk4)/6
3700 END SUB
3710 !
3720 !
3730 DEF accel(x,v,t,w,g,q)
3740   LET accel=-sin(x)-(1/q)*v+g*cos(w*t)
3750 END DEF
3760
3770 !BIT REVERSER FUNCTION
3780 DEF bitr(j,nu)
3790   LET j1=j
3800   LET ibitr=0
3810   FOR i=1 to nu
3820     LET j2 = int(j1/2)
3830     LET ibitr=ibitr+2^(j1-2*j2)
3840     LET j1=j2
3850   NEXT i
3860   LET bitr=ibitr
3870 END DEF

```

## Listing 7

```

!PROGRAM TITLE *****BASINS*****
!XBASINPO.TRU
CLEAR
PRINT" ***PENDULUM - BASINS OF ATTRACTION***"
PRINT"This program calculates the average angular velocity for"
PRINT"an array of initial conditions."
PRINT"velocity (-3,3) and angle (-pi ,pi). If the average angular velocity"
PRINT"from a given initial point is positive then circle is placed at the"
PRINT"point, otherwise the average is negative. This program can also "
PRINT"superpose the appropriate Poincare section on the graph."
PRINT"The program can also save the data sets to two different files."
PRINT"The display can be printed if appropriate driver is installed."
LIBRARY "aglib.trc"
LIBRARY "scrndump.trc"
DIM a(1),b(1)

DECLARE DEF accel

INPUT prompt"Input driving force strength (try 0.5 to 1.5): ":g
INPUT prompt"input damping (try 2 to 4)"::q
INPUT prompt"Input forcing frequency (try 0.6666666666)"::w
INPUT Prompt"Input min. and max. time of averaging":tmin,tmax
INPUT Prompt"Poincare attractor yes (1), no(2) ":Poincare

INPUT prompt"Dump screen to printer (y=1 / n=0) :::dump
IF dump=1 then
  INPUT prompt"Printer type (0)Epson, (1)HP Laserjet :::prntr
  Call SCREENDUMPDEVICE(prntr)
END IF
INPUT prompt"Save data to a file, yes(1), no(2):::sv
IF sv=1 then
  PRINT"Basin of attraction File name includes:"
  PRINT" 1)First 2 digits for q value"
  PRINT" 2)Next needed digits for g value"
  PRINT" 3)last digits as 0's"
  INPUT prompt"file name - format ex. 20150000::filename
  INPUT prompt"data file drive a,b,c,etc.:::b$"
  IF poincare=1 then
    PRINT"Superposed Poincare section file name is similar to above except"
    PRINT"that the numeral '0' is added, for example, 20015000."
    INPUT prompt"Input corresponding Poincare file name:::poinfile
  END IF
  LET FILENAME$=STR$(FILENAME)
  LET POINFILE$=STR$(POINFILE)
END IF
!
CALL PARAMS2(EPS,TSTEP)
CALL SETMARGINS(60,60,0,0)
CALL SETXSCALE(-3,3)
CALL SETYSCALE(-3,3)
CALL SETTEXT("PENDULUM - BASINS OF ATTRACTION","INIT. ANGLE","INIT. ANG. VEL.")
CALL RESERVELEGEND
IF sv=1 then
  OPEN #1: name b$&":&filename$,organization record,create newold
  ASK #1: FILESIZE length
  IF length=0 then SET#1:rECSIZE 10
  SET #1: POINTER end
  IF poincare=1 then
    OPEN #2: name b$&":&poinfile$,organization record,create newold
    ASK #2: FILESIZE length
    IF length=0 then SET#2:rECSIZE 10
    SET #2:p POINTER end
  END IF
END IF

DATA 0,0
CALL DATAGRAPH(A,B,1,0,"WHITE")
CALL gotocanvas
LET phi=0
FOR xint=-pi to pi step .1
  FOR vint=-3 to 3 step .15
    LET x = xint
    LET v=vint
    LET t=0
    LET s=0
    FOR i=1 to 1000000
      CALL rk4(x,v,tstep,xnew,vnew,t,w,g,q)    ! Take a step of size tstep
      LET tshalf=tstep/2
      CALL rk4(x,v,tshalf,xnh,vnh,t,w,g,q)    !Take two half steps
      CALL rk4(xnh,vnh,tshalf,xn,vn,t+tshalf,w,g,q)
      LET d1=abs(xn-xnew)

```

```

LET d2=abs(vn-vnew)
LET delta=max(d1,d2)
IF delta<eps then
  IF t>tmin then
    LET tnew=t+tstep
    LET s+=vnew*tstep
    IF Poincare=1 then
      LET w1=mod(phi-w*t,2*pi)
      LET w2=mod(w*tnew-phi,2*pi)
      IF w1<w*tstep then
        IF w2<=tstep then
          LET ts=w1/w
          CALL rk4(x,v,ts,xp,vp,t,w,g,q)
          IF abs(xp)>pi then LET xp=xp-2*pi-abs(xp)/xp
          CALL GRAPHPOINT(xp, vp, 1)
          IF sv=1 then WRITE #2:xp, vp
        END IF
      END IF
    END IF
  END IF
  LET x=xnew
  LET v=vnew
  LET t=t+tstep !Expand step size
  LET tstep=tstep*.95*(eps/delta)^.25
  IF abs(x)>pi then !bring theta back in range
    LET x=x-2*pi*abs(x)/x
  END IF
  ELSE !else reduce step size
    LET tstep=tstep*.95*(eps/delta)^.2
  END IF
  IF t>tmax then
    LET average=s/(tmax-tmin)
    IF average>0 then
      CALL GRAPHPOINT(XINT,VINT,4)
      IF sv=1 then WRITE #1:xint,vint
    END IF
    LET i=1000001
  END IF
  NEXT i
  NEXT vint
  NEXT xint
  CALL addlegend("g="&str$(g)&" q="&str$(q)&" circle=positive",0,1,"white")
  CALL drawlegend
  If dump=1 then Call SCREENDUMP
  GET KEY VARIABLE
  CLEAR
END
!
SUB rk4(x,v,tstep,xnew,vnew,t,w,g,q)
  DECLARE DEF accel
  LET xk1=tstep*v
  LET vk1=tstep*accel(x,v,t,w,g,q)
  LET xk2=tstep*(v+vk1/2)
  LET vk2=tstep*accel(x+xk1/2,v+vk1/2,t+tstep/2,w,g,q)
  LET xk3=tstep*(v+vk2/2)
  LET vk3=tstep*accel(x+xk2/2,v+vk2/2,t+tstep/2,w,g,q)

```

```

  LET xk4=tstep*(v+vk3)
  LET vk4=tstep*accel(x+xk3,v+vk3,t+tstep,w,g,q)
  LET vnew=v+(vk1+2*vk2+2*vk3+vk4)/6
  LET xnew=x+(xk1+2*xk2+2*xk3+xk4)/6
END SUB
!
DEF accel(x,v,t,w,g,q)
  LET accel=-sin(x)-(1/q)*v+g*cos(w*t)
END DEF
!
SUB PARAMS2(EPS,TSTEP)
  LET EPS=1E-6
  LET TSTEP=.5
END SUB

```

### Listing 8

```

!PROGRAM TITLE *****LOGISTIC MAP*****
!XLOGISTI.TRU
LIBRARY "SGLIB.TRC"
LIBRARY "SCRNDUMP.TRC"
DECLARE DEF LOGISTIC
DIM CELL(1000),PROB(1000),G(1),H(1)
CLEAR
PRINT" COMPREHENSIVE LOGISTIC MAP PROGRAM"
PRINT
PRINT"DIAGRAMS CAN BE PRINTED IF APPROPRIATE DRIVER IS PRESENT."
PRINT
PRINT"CHOOSE ONE OF THE FOLLOWING OPTIONS FOR THE LOGISTIC MAP:"
PRINT" 1)RETURN MAP"
PRINT" 2)BIFURCATION DIAGRAM"
PRINT" 3)ENTROPY DIAGRAM"
PRINT" 4)LYAPUNOV EXPONENT DIAGRAM"
PRINT" 5)TIME SERIES"
INPUT PROMPT" CHOOSE 1,2,3,4 OR 5: ::CHOICE
INPUT PROMPT"DUMP SCREEN TO PRINTER? (Y=1 / N=0) :::DUMP
IF DUMP=1 THEN
  INPUT PROMPT"PRINTER TYPE (0)EPSON, (1)HP LASERJET :::PRNTR
  CALL SCRNDUMPDEVICE(PRNTR)
END IF
CLEAR
!
CALL LINPUTS(CHOICE,XINT,LAMBDA,INITLAMBDA,FINLAMBDA,STEPLAMBDA,INITNUM,FINNUM,ORDER,NUMCELLS,
             XMIN,XMAX,YMIN,YMAX,TITLE1$,TITLE2$,VLABEL$,HLABEL$)
!
!GRAPHING SET-UP PROCEDURE
CALL SETMARGINS(60,60,0,0)
CALL SETXSCALE(XMIN,XMAX)
CALL SETYSCALE(YMIN,YMAX)
CALL SETAXES(0)
CALL SETTEXT(TITLE1$,HLABEL$,VLABEL$)

```

```

CALL RESERVELEGEND
DATA 0,0
CALL DATAGRAPH(G,H,0,0,"WHITE")
CALL GOTOCANVAS
!
IF CHOICE=1 THEN CALL CALCULATION1(LAMBDA,XINT,INITNUM,FINNUM,ORDER)
IF CHOICE=2 THEN CALL CALCULATION2(XINT,INITLAMBDA,FINLAMBDA,STEPLAMBDA,INITNUM,FINNUM)
IF CHOICE=3 THEN CALL CALCULATION3(XINT,INITLAMBDA,FINLAMBDA,STEPLAMBDA,INITNUM,FINNUM,NUMCELLS)
IF CHOICE=4 THEN CALL CALCULATION4(XINT,INITLAMBDA,FINLAMBDA,STEPLAMBDA,INITNUM,FINNUM)
IF CHOICE=5 THEN CALL CALCULATIONS(XINT,LAMBDA,XMIN,XMAX)
!
SUB LINPUTS(CHOICE,XINT,LAHBDA,INITLAMBDA,FINLAMBDA,STEPLAMBDA,INITNUM,FINNUM,ORDER,NUMCELLS,
    XMIN,XMAX,YMIN,YMAX,TITLE1$,TITLE2$,VLABELS,HLABELS)
    INPUT PROMPT"INPUT INITIAL X VALUE:";XINT
    IF (CHOICE=1) OR (CHOICE=5) THEN INPUT PROMPT"INPUT MU:";LAMBDA
    IF CHOICE=5 THEN
        INPUT PROMPT"INPUT NUMBER OF INITIAL THROWAWAY ITERATIONS:";INITNUM
        INPUT PROMPT"INPUT TOTAL NUMBER OF ITERATIONS:";FINNUM
    END IF
    IF (CHOICE>1) AND (CHOICE<5) THEN
        INPUT PROMPT"INPUT LOWEST MU VALUE:";INITLAMBDA
        INPUT PROMPT"INPUT HIGHEST MU VALUE:";FINLAMBDA
    END IF
    IF CHOICE=1 THEN INPUT PROMPT"INPUT ORDER OF MAP:";ORDER
    IF CHOICE=3 THEN INPUT PROMPT"INPUT # OF CELLS:";NUMCELLS
    IF CHOICE=1 THEN LET ORDERS=$STR$(ORDER)
    IF CHOICE=2 THEN
        LET XMIN=0
        LET XMAX=1
        LET YMIN=0
        LET YMAX=1
        LET TITLE1$="LOGISTIC MAP"
        LET TITLE2$="X(N+ORDER$)" VERSUS X(N)"
        LET VLABELS="N+"$ORDERS$" VALUE"
        LET HLABELS="N VALUE"
    END IF
    IF (CHOICE>1) AND (CHOICE<5) THEN
        LET XMIN=INITLAMBDA
        LET XMAX=FINLAMBDA
        LET STEPLAMBDA=(XMAX-XMIN)/740
    END IF
    IF CHOICE=2 THEN
        LET YMIN=0
        LET YMAX=1
        LET TITLE1$="LOGISTIC MAP BIFURCATION DIAGRAM"
        LET TITLE2$="MU="+$STR$(XMIN)+" TO MU="+$STR$(XMAX)
        LET VLABELS="X"
        LET HLABELS="MU"
    END IF
    IF CHOICE=3 THEN
        LET YMIN=-1           !INT(LOG(1/NUMCELLS))
        LET YMAX=INT(LOG(NUMCELLS))+1   !
        LET TITLE1$="LOGISTIC MAP ENTROPY"
        LET TITLE2$="MU="+$STR$(INITLAMBDA)+" TO MU="+$STR$(FINLAMBDA)+";" #CELLS="+$STR$(NUMCELLS)
            $STR$(LOG(NUMCELLS))
        LET VLABELS="S"
        LET HLABELS="MU"
    END IF
END SUB

SUB CALCULATION1(LAMBDA,XINT,INITITERATION,ITERATIONNUM,ORDER)
    PLOT LINES: 0,0;1,1          !PLOTS X(N+1)=X(N) LINE
    FOR I=0 TO 1 STEP .001      !PLOTS CURVE OF Y=LAMBDA*X*(1-X)
        LET J=I
        FOR ORD=1 TO ORDER
            LET Z=LAMBDA*J*(1-J)
            LET J=Z
        NEXT ORD
        PLOT I,Z
    NEXT I
    LET X=XINT                  !PLOTS RETURN MAP
    IF INITITERATION= 0 THEN
        PLOT X,0;
    END IF
    FOR I=1 TO ITERATIONNUM
        LET J=X
        FOR ORD= 1 TO ORDER
            LET Y=LOGISTIC(J,LAMBDA)
            LET J=Y
        NEXT ORD
        IF I>INITITERATION THEN
            PLOT X,Y;
            PLOT Y,X;
        END IF
        LET X=Y
    NEXT I
    END SUB
!
SUB CALCULATION2(XINT,INITLAMBDA,FINLAMBDA,STEPLAMBDA,INITNUM,FINNUM)
    FOR LAMBDA=INITLAMBDA TO FINLAMBDA STEP STEPLAMBDA
        LET X=XINT
        FOR I=1 TO FINNUM
            LET Y=LOGISTIC(X,LAMBDA)
            IF I>INITNUM THEN
                PLOT LAMBDA,Y
            END IF
        NEXT I
    END SUB
!
```

```

        END IF
        LET X=Y
        NEXT I
    NEXT LAMBDA
END SUB
!
SUB CALCULATION3(XINT,INITLAMBDA,FINLAMBDA,STEPLAMBDA,INITNUM,FINNUM,NUMCELLS)
FOR LAMBDA=INITLAMBDA TO FINLAMBDA STEP STEPLAMBDA
    LET ENTROPY=0
    FOR L=1 TO NUMCELLS
        LET CELL(L)=0
    NEXT L
    LET X=XINT
    FOR I=1 TO FINNUM
        LET Y=LOGISTIC(X,LAMBDA)
        IF I>INITNUM THEN
            LET L=INT(NUMCELLS*Y)+1
            LET CELL(L)=CELL(L)+1
        END IF
        LET X=Y
    NEXT I
    FOR L=1 TO NUMCELLS
        LET PROB(L)=CELL(L)/(FINNUM-INITNUM)
        IF PROB(L)>0 THEN
            LET ENTROPY=ENTROPY+PROB(L)*LOG(PROM(L))
        END IF
    NEXT L
    PLOT LAMBDA,ENTROPY;
NEXT LAMBDA
END SUB
!
SUB CALCULATION4(XINT,INITLAMBDA,FINLAMBDA,STEPLAMBDA,INITNUM,FINNUM)
FOR LAMBDA=INITLAMBDA TO FINLAMBDA STEP STEPLAMBDA
    LET LYAP=0
    LET X=XINT
    FOR I = 1 TO FINNUM
        LET Y=LOGISTIC(X,LAMBDA)
        IF I>INITNUM THEN
            LET LYAP=LYAP+LOG(ABS(LAMBDA*(1-2*Y)))      ISUM LOG DERIVATIVES
        END IF
        LET X=Y
    NEXT I
    LET LYAP=LYAP/(FINNUM-INITNUM)
    IF LYAP<-3 THEN LET LYAP=-3
    PLOT LAMBDA,LYAP;
NEXT LAMBDA
END SUB
!
SUB CALCULATION5(XINT,LAMBDA,XMIN,XMAX)
LET X=XINT
FOR I=XMIN TO XMAX
    LET Y=LAMBDA*X*(1-X)
    PLOT I,Y;
    LET X=Y
NEXT I
END SUB

```

```

DEF LOGISTIC(X,LAMBDA)
    LET LOGISTIC =LAMBDA*X*(1-X)
END DEF
CALL ADDLEGEND(TITLE2$,0,1,"WHITE")
CALL DRAWLEGEND
IF DUMP=1 THEN CALL SCREENDUMP
GET KEY VARIABLE
CLEAR
END

!PROGRAM TITLE ****CIRCLE MAP*****
!XCIRCLE.TRU
LIBRARY "SLIB.TRC"
LIBRARY "SCRNDUMP.TRC"
DECLARE DEF CIRCLE
DIM XINT(10),G(1),H(1)
CLEAR
PRINT"                                     *COMPREHENSIVE CIRCLE MAP PROGRAM*"
PRINT
PRINT"DISPLAYS CAN BE PRINTED IF APPROPRIATE DRIVER IS PRESENT."
PRINT
PRINT"CHOOSE ONE OF THE FOLLOWING OPTIONS FOR THE CIRCLE MAP:"
PRINT" 1)RETURN MAP"
PRINT" 2)BIFURCATION MAP"
PRINT" 3)DEVIL'S STAIRCASE"
INPUT PROMPT" CHOOSE 1,2,OR 3:"CHOICE
INPUT PROMPT"DUMP SCREEN TO PRINTER (Y=1 / N=0) :"DUMP
IF DUMP=1 THEN
    INPUT PROMPT"TYPE OF PRINTER (0)EPSON, (1)HP LASERJET :"PRNTR
    CALL SCREENDUMPDEVICE(PRNTR)
END IF
CLEAR
!
CALL LINPUTS(CHOICE,XIN,XINT(),NUMXINT,KVALUE,INITK,FINK,STEPK,OMEGA,INITNUM,
             FINNUM,ORDER,XMIN,XMAX,YMIN,YMAX,TITLE1$,TITLE2$,VLABELS,HLABELS)
!
IGRAPHING SET-UP PROCEDURE
CALL SETMARGINS(60,60,0,0)
CALL SETXSCALE(XMIN,XMAX)
CALL SETYSCALE(YMIN,YMAX)
CALL SETAXES(0)
CALL SETTEXT(TITLE1$,HLABELS,VLABELS)
CALL RESERVELEGEND
DATA 0,0
CALL DATAGRAPH(G,H,0,0,"WHITE")
CALL GOTOCANVAS
!
IF CHOICE= 1 THEN CALL CALCULATION1(XIN,KVALUE,OMEGA,INITNUM,FINNUM,ORDER)
IF CHOICE= 2 THEN CALL CALCULATION2(NUMXINT,XINT,INITK,FINK,STEPK,OMEGA,INITNUM,FINNUM)
IF CHOICE= 3 THEN CALL CALCULATION3(XIN,INITNUM,FINNUM,INITK,FINK,STEPK,KVALUE)
!
```

### Listing 9

```

SUB LINPUTS(CHOICE,XIN,XINT(),NUMXINT,KVALUE,INITK,FINK,STEPK,OMEGA,INITNUM,FINNUM,ORDER,XMIN,XH
IF CHOICE=2 THEN
  INPUT PROMPT"INPUT NUMBER OF INITIAL CONDITIONS:"::NUMXINT
  FOR J = 1 TO NUMXINT
    INPUT PROMPT"INPUT AN INITIAL CONDITION:"::XINT(J)
  NEXT J
ELSE
  INPUT PROMPT"INPUT INITIAL ANGLE, [0,1] ::XIN
END IF
IF CHOICE = 3 THEN
  INPUT PROMPT"INPUT INITIAL VALUE OF OMEGA (TRY 0):"::INITK
  INPUT PROMPT"INPUT FINAL VALUE OF OMEGA (TRY 1):"::FINK
  LET STEPK=(FINK-INITK)/740
  INPUT PROMPT"INPUT K VALUE (TRY 0.95):"::KVALUE
ELSE IF CHOICE=2 THEN
  INPUT PROMPT"INPUT INITIAL VALUE OF K:"::INITK
  INPUT PROMPT"INPUT FINAL VALUE OF K:"::FINK
  LET STEPK=(FINK-INITK)/740
  INPUT PROMPT"INPUT OMEGA VALUE:"::OMEGA
END IF
INPUT PROMPT"INPUT NUMBER OF THROWAWAY ITERATIONS:"::INITNUM
INPUT PROMPT"INPUT TOTAL NUMBER OF ITERATIONS:"::FINNUM
IF CHOICE = 1 THEN
  INPUT PROMPT"INPUT ORDER OF MAP:"::ORDER
  INPUT PROMPT"INPUT OMEGA VALUE:"::OMEGA
  INPUT PROMPT"INPUT K-VALUE:"::KVALUE
  LET XMIN=0
  LET XMAX=1
  LET YMIN=0
  LET YMAX=1
  LET TITLE1$="CIRCLE MAP"
  LET TITLE2$="K="&STR$(KVALUE)&" OMEGA="&STR$(OMEGA)
  LET VLABELS="N+"&STR$(ORDER)&" ANGLE VALUE"
  LET HLABELS="N ANGLE VALUE"
END IF
IF CHOICE = 2 THEN
  LET XMIN=INITK
  LET XMAX=FINK
  LET YMIN=0
  LET YMAX=1
  LET TITLE1$="CIRCLE MAP BIFURCATION DIAGRAM"
  LET TITLE2$=""
  LET VLABELS="THETA"
  LET HLABELS="K-VALUE"
END IF
IF CHOICE=3 THEN
  LET XMIN=INITK
  LET XMAX=FINK
  INPUT PROMPT"INPUT YMIN (USUALLY 0), AND YMAX (USUALLY 1):"::YMIN,YMAX
  LET TITLE1$="DEVIL'S STAIRCASE (CIRCLE MAP)"
  LET TITLE2$="DRIVE K="&STR$(KVALUE)
  LET VLABELS="WINDING #"
  LET HLABELS="OMEGA"
END IF
END SUB
!
```

```

SUB CALCULATION1(XIN,KVALUE,OMEGA,INITNUM,FINNUM,ORDER)
PLOT LINES: 0,0;1,1          !PLOTS DIAGONAL
FOR I=0 TO 1 STEP .001        !PLOTS CURVE
  LET J=I
  FOR ORD=1 TO ORDER
    LET Z=CIRCLE(J,KVALUE,OMEGA)
    LET J=Z
  NEXT ORD
  PLOT I,Z
NEXT I
LET X=XIN
LET Y=0
IF INITNUM=0 THEN PLOT X,0;
FOR I=1 TO FINNUM
  LET J=X
  FOR ORD=1 TO ORDER
    LET Y=CIRCLE(J,KVALUE,OMEGA)
    LET J=Y
  NEXT ORD
  IF I>INITNUM THEN
    PLOT X,Y;
    PLOT Y,Y;
  END IF
  LET X=Y
NEXT I
END SUB
!
SUB CALCULATION2(NUMXINT,XINT(),INITK,FINK,STEPK,OMEGA,INITNUM,FINNUM)
FOR KVAL=INITK TO FINK STEP STEPK
  FOR K=1 TO NUMXINT
    LET X=XINT(K)
    FOR I=1 TO FINNUM
      LET Y=CIRCLE(X,KVAL,OMEGA)
      IF I>INITNUM THEN
        PLOT KVAL,Y
      END IF
      LET X=Y
    NEXT I
    NEXT K
  NEXT KVAL
END SUB
!
SUB CALCULATION3(XIN,INITNUM,FINNUM,INITOMEGA,FINOMEGA,STEPOMEGA,KVALUE)
FOR OMEGA=INITOMEGA TO FINOMEGA STEP STEPOMEGA
  LET SUM=0
  LET X=XIN
  FOR I=1 TO FINNUM
    LET Y=X+OMEGA-(KVALUE/(2*PI))*SIN(2*PI*X)
    IF I>INITNUM THEN LET X0=Y
    LET X=Y
  NEXT I
  LET WINDING=(Y-X0)/(FINNUM-INITNUM)
  IF WINDING <=YMIN THEN
    PLOT OMEGA,WINDING
  END IF

```

```

        )END IF
NEXT OMEGA
END SUB
!
DEF CIRCLE(X,KVALUE,OMEGA)
LET TEMPCIRCLE = X+OMEGA-(KVALUE/(2*PI))*SIN(2*PI*X)
LET CIRCLE = MOD(TEMPCIRCLE,1)
END DEF
IF DUMP=1 THEN CALL SCREENDUMP
GET KEY VARIABLE
CLEAR
PRINT "PRESS <ESC> FOR MENU"
END

```

## Listing 10

```

!PROGRAM TITLE *****HENON MAP*****
!XHENON.TRU"
LIBRARY "SGLIB.TRC"
LIBRARY "SCRNDUMP.TRC"
CLEAR
PRINT"          ***HENON MAP***"
PRINT
PRINT"THIS PROGRAM GENERATES THE (X,Y) PHASE DIAGRAM FOR THE HENON MAP."
PRINT"      X(N+1)=1-A*X(N)^2 + Y(N)*"
PRINT"      Y(N+1)=B*X(N)"
PRINT" TWO PARAMETERS ARE REQUIRED, A AND B. IF B=1 THE MAP IS "
PRINT"CONSERVATIVE. IF B < ABS(1) THEN THE MAP IS DISSIPATIVE."
PRINT"TRY A=1.4 AND B=0.3 INITIALLY."
PRINT
PRINT"DISPLAY MAY BE PRINTED IF APPROPRIATE DRIVER IS INSTALLED."
PRINT
DIM L(1),M(1)
INPUT PROMPT"INPUT INITIAL X , Y VALUES:::XINT,YINT
INPUT PROMPT"INPUT A,B VALUES:::A,B
INPUT PROMPT"INPUT NUMBER OF THROWAWAY ITERATIONS:::INITNUM
INPUT PROMPT"INPUT NUMBER OF TOTAL ITERATIONS:::PINNUM
INPUT PROMPT"DUMP SCREEN TO PRINTER (Y=1 / N=0) :::DUMP
IF DUMP=1 THEN
    INPUT PROMPT"TYPE OF PRINTER (0)EPSON, (1)HP LASERJET:::PRNTR
    CALL SCREENDUMPDEVICE(PRNTR)
END IF
!
CALL SETMARGINS(60,60,0,0)
CALL SETXSCALE(-1.5,1.5)
CALL SETYSCALE(-.5,.5)
CALL SETTEXT("HENON MAP","X","Y")
CALL RESERVELEGEND
!
DATA 0,0
CALL DATAGRAPH(L,M,1,0,"WHITE")
CALL GOTOCANVAS
LET X=XINT

```

```

LET Y=YINT
FOR I=INITNUM+1 TO PINNUM+1
    LET XNEW=1-A*(X^2)+Y
    LET YNEW=B*X
    CALL GRAPHPOINT(XNEW,YNEW,1)
    LET X=XNEW
    LET Y=YNEW
NEXT I
CALL ADDLEGEND("A=""&STR$(A)&"   B=""&STR$(B),0,1,"WHITE")
CALL DRAWLEGEND
IF DUMP=1 THEN CALL SCREENDUMP
get key variable
clear
print"press <esc> key to finish"
END

```

## Listing 11

```

!PROGRAM TITLE *****PENDLYAP*****
!XPENDLYA.TRU"
LIBRARY "SGLIB.TRC"
LIBRARY "SCRNDUMP.TRC"
DIM A(1),B(1)
CLEAR
PRINT"          ***PENDULUM - LYAPUNOV EXPONENTS***"
PRINT
PRINT"THIS PROGRAM CALCULATES THE 3 LYAPUNOV EXPONENTS FOR THE DRIVEN PENDULUM"
PRINT"USING THE ALGORITHM OF WOLF ET AL. THE EXPONENTS ARE SMOOTHED OVER "
PRINT"MANY DRIVE CYCLES (ORBITS)."
!
IN=# OF NONLINEAR EQUATNS., NN= TOTAL # OF EQUATIONS
LET N=3
LET NN=12
DECLARE DEF YPRIM
!
DIM Y(12), ZNORM(3), GSC(3), CUM(3), YNEW(12)
!
!INITIAL CONDITIONS FOR NONLINEAR SYSTEM
LET Y(1)=.5
LET Y(2)=0
LET Y(3)=0
!
!INITIAL CONDITIONS FOR LINEAR SYSTEM (ORTHONORMAL FRAME)
FOR I=N+1 TO NN
    LET Y(I)=0.0
NEXT I
FOR I=1 TO n
    LET Y((N+1)*I) = 1.0
    LET CUM(I)=0.0
NEXT I
!
INPUT PROMPT"INTEGRATION STEPSIZE (TRY 0.5):::TSTEP
INPUT PROMPT"NUMBER OF ORBITS (TRY 100):::NUMORBITS

```

```

INPUT PROMPT"DRIVING FORCE(.5 FOR PERIODIC, 1.5 FOR CHAOS):":G
INPUT PROMPT"DRIVE FREQUENCY( TRY 0.666666666)":"W
INPUT PROMPT"DAMPING FACTOR( TRY 4)":"Q
INPUT PROMPT"LOG BASE (1)NATURAL (2)INFO-2 CHOOSE 1 OR 2":":BASE
INPUT PROMPT" DUMP SCREEN TO PRINTER (YES=1, NO=0)":":P
IF P=1 THEN
  INPUT PROMPT"PRINTER TYPE (0)EPSON (1)HPLASERJET":":PRNTR
  CALL SCREENDUMPDEVICE(PRNTR)
END IF
!
!SET UP GRAPHICS
CALL SETHARGINS(60,60,0,0)
IF BASE=1 THEN CALL SETSCALE(-.7,.3)
IF BASE=2 THEN CALL SETSCALE(-1,1)
CALL SETXSCALE(0,NUMORBITS)
CALL SETTEXT("PENDULUM - LYAPUNOV EXPONENTS","# DRIVE CYCLES","LYAP. EXPNS.")
CALL SETAXES(0)
CALL RESERVELEGEND
DATA 0,0
CALL DATAGRAPH(A,B,1,0,"WHITE")
CALL GOTOCANVAS
!
DO WHILE Y(3)<2*PI*NUMORBITS
  !INITIALIZE INTEGRATOR
  CALL RKK4(Y(),NN,TSTEP,Q,W,G,YNEW())
  FOR K=1 TO 12
    LET Y(K)=YNEW(K)
  NEXT K
  !
  !CONSTRUCT A NEW ORTHONORMAL BASIS BY GRAM-SCHMIDT METHOD
  !NORMALIZE FIRST VECTOR
  LET ZNORM(1)=0.0
  FOR J = 1 TO N
    LET ZNORM(1) = ZNORM(1) + Y(N*J+1)^2
  NEXT J
  LET ZNORM(1)=(ZNORM(1))^.5
  FOR J=1 TO N
    LET Y(N*J+1)=Y(N*J+1)/ZNORM(1)
  NEXT J
  !
  !GENERATE THE NEW ORTHONORMAL SET OF VECTORS
  FOR J=2 TO N
    ! GENERATE J-1 COEFFICIENTS
    FOR K = 1 TO (J-1)
      LET GSC(K)=0.0
      FOR L = 1 TO N
        LET GSC(K) = GSC(K) + Y(N*L+J)*Y(N*L+K)
      NEXT L
    NEXT K
    !
    ! CONSTRUCT A NEW VECTOR
    FOR K = 1 TO N
      FOR L= 1 TO J-1
        LET Y(N*K+J) = Y(N*K+J) -GSC(L)*Y(N*K+L)
      NEXT L
    NEXT K
    !

```

```

    ! CALCULATE THE VECTOR'S NORM
    LET ZNORM(J) = 0.0
    FOR K= 1 TO N
      LET ZNORM(J) = ZNORM(J)+Y(N*K+J)^2
    NEXT K
    LET ZNORM(J) = (ZNORM(J))^.5
    !
    ! NORMALIZE THE NEW VECTOR
    FOR K = 1 TO N
      LET Y(N*K+J) = Y(N*K+J)/ZNORM(J)
    NEXT K
    !
    ! UPDATE RUNNING VECTOR MAGNITUDES
    FOR K = 1 TO N
      LET CUM(K) = CUM(K) + LOG(2*ZNORM(K))
    NEXT K
    !
    !NORMALIZE EXPONENT AND PLOT EXPONENTS
    IF Y(3)>0 THEN
      LET T=Y(3)/W
      FOR K = 1 TO N
        IF BASE = 1 THEN LET CUMKT=CUM(K)/T
        IF BASE = 2 THEN LET CUMKT=CUM(K)/T/LOG(2)
        CALL GRAPHPOINT(T*W/(2*PI),CUMKT,1)
      NEXT K
    END IF
    !
    LOOP
    !
    CALL ADDLEGEND("G="&STR$(G)&" Q="&STR$(Q)&" W="&STR$(W),0,1,"WHITE")
    CALL DRAWLEGEND
    IF P=1 THEN CALL SCREENDUMP
    GET KEY VARIABLE
    CLEAR
    END
    !
    SUB RKK4(Y(),NN,TSTEP,Q,W,G,YNEW())
      DIM Y1(12), Y2(12), Y3(12), Y4(12), YY1(12), YY2(12), YY3(12)
      DECLARE DEF YPRIM
      FOR K= 1 TO NN
        LET Y1(K)=TSTEP*YPRIM(Y(),K,Q,W,G)
      NEXT K
      FOR K= 1 TO NN
        LET YY1(K)=Y(K)+Y1(K)/2
      NEXT K
      FOR K= 1 TO NN
        LET Y2(K)=TSTEP*YPRIM(YY1(),K,Q,W,G)
      NEXT K
      FOR K = 1 TO NN
        LET YY2(K)=Y(K)+Y2(K)/2
      NEXT K
      FOR K= 1 TO NN
        LET Y3(K)=TSTEP*YPRIM(YY2(),K,Q,W,G)
      NEXT K
      FOR K = 1 TO NN
        LET YY3(K)=Y(K)+Y3(K)
      NEXT K
    END SUB
  END IF
END IF

```

```

        FOR K= 1 TO NN
          LET Y4(K)=TSTEP*YPRIM(YY3(),K,Q,W,G)
        NEXT K
        FOR K = 1 TO NN
          LET YNEW(K) = Y(K)+(Y1(K) +2*Y2(K)+2*Y3(K)+Y4(K))/6
        NEXT K
      END SUB

!DEFINE DERIVATIVES FUNCTIONS
DEF YPRIM(Y(),K,Q,W,G)
  IF K=1 THEN LET YPRIM=-Y(1)/Q-SIN(Y(2))+G*COS(Y(3))
  IF K=2 THEN LET YPRIM=Y(1)
  IF K=3 THEN LET YPRIM=W
  IF K>3 THEN
    IF K<7 THEN
      LET I = K-4
      LET YPRIM=-Y(4+I)/Q-Y(7+I)*COS(Y(2))-G*Y(10+I)*sin(Y(3))
    END IF
  END IF
  IF K>6 THEN
    IF K<10 THEN
      LET I = K-7
      LET YPRIM=Y(4+I)
    END IF
  END IF
  IF K>9 THEN LET YPRIM = 0
END DEF

```

## Listing 12

```

!PROGRAM TITLE *****RECDIM*****
!XRECDIM.TRU"
CLEAR
DIM V(31000)
DEF ZZ(I,J)=V(I+(J-1)*NUMPOINTS)
PRINT" ****PENDULUM - READS PHASE3D DATA AND RECONSTRUCTS ATTRACTOR****"
PRINT
PRINT" PROGRAM USES ANGULAR VELOCITY TIME SERIES TO RECONSTRUCTS ATTRACTOR"
PRINT" BY THE METHOD OF DELAYS WITH ANGULAR VELOCITY DATA FROM A FILE."
PRINT" IT THEN CALCULATES COORDS FOR A LOG(CORRELATION) VS LOG(RADIUS) GRAPH"
PRINT" USING THE GRASSBERGER CORRELATION CALCULATION."
PRINT" THEN A GRAPH OF SLOPE(DIMENSION) VS LOG(RADIUS) IS PRODUCED."
PRINT" GRAPHS ARE PRODUCED FOR CHOICE OF EMBEDDING DIMENSION 1 THROUGH 6"
PRINT" GRAPHS MAY BE PRINTED IF APPROPRIATE DRIVER IS INSTALLED.-"
!
LIBRARY "3DLIB.TRC"
LIBRARY "SGLIB.TRC"
LIBRARY "SCRNDUMP.TRC"
!
PRINT"DATA MAY BE TAKEN FROM A FILE SUCH AS VEL_FILE.TRU"
INPUT PROMPT"GIVE NUMBER OF DATA POINTS (<29000);":NUMDATA

```

```

INPUT PROMPT"GIVE NUMBER OF RADIUS VALUES NEEDED(TRY 35);":NUMSTEP
INPUT PROMPT"GIVE MINIMUM RADIUS (TRY 0.5); ":"RMIN
INPUT PROMPT"GIVE MAXIMUM RADIUS (TRY 50); ":"RMAX
DIM RADIUS(1 TO 40),A(1),B(1),X(6,40),R(6,40)
LET DELTA = (LOG(RMAX)-LOG(RMIN))/NUMSTEP
FOR I=1 TO NUMSTEP
  LET RADIUS(I)=EXP(LOG(RMIN)+I*DELTA)
NEXT I
PRINT
INPUT PROMPT"GIVE NUMBER OF CENTERS FOR EACH DIM CALCULATION(TRY 1000); ":NUMCENTERS
INPUT PROMPT"How MANY POINTS ARE INCLUDED IN TAU (TRY 20);":NUMPOINTS
INPUT PROMPT"INPUT INITIAL EMBEDDING DIMENSION (1,2,3,4,5,6); ":"INITEMBED
INPUT PROMPT"INPUT FINAL EMBEDDING DIMENSION (1,2,3,4,5,6); ":"FINALEMBED
INPUT PROMPT"INPUT # POINTS IN SLOPE CALC ,(>=2); ":"AVPTS
INPUT PROMPT"INPUT DRIVE (A,B,ETC.) OF FILE DRIVE:"":DRIVES
INPUT PROMPT"INPUT FILE NAME (E.G. VEL_FILE.TRU):":NAME$ 
LET THROW=0
LET REC=1
!INPUT PROMPT"INPUT NUMBER OF THROWAWAY DATA SETS (USE 0);":THROW
!INPUT PROMPT"SET POINT # (USE 1 FOR BEGINNING) :"":REC
INPUT PROMPT"Do you want HARDCOPY (YES=1, NO=0) :"":PRINTIT
IF PRINTIT=1 THEN
  INPUT PROMPT"      OF ATTRACTOR (YES=1, NO=0) :"":PRINT1
  INPUT PROMPT"      OF CORR INTEGRAL (YES=1, NO=0) :"":PRINT2
  INPUT PROMPT"      OF DIMENSION DIAG (YES=1, NO=0) :"":PRINT3
  INPUT PROMPT"INPUT PRINTER TYPE (HP LASER=1, EPSON=0) :"":PRNTR
  CALL SCRNDUMPDEVICE(PRNTR)
END IF
SET MODE "HIRES"
CALL SCALEPARAWINDOW(-30,30,-30,30,-30,30,$$)
CALL TICKS3(0,0,0,$$) ! CALL TICKS3(10,10,10,$$)
CALL PLOTTEXT3(-60,0,70,"EXPERIMENTAL PENDULUM PHASE SPACE RECONSTRUCTION",$$)
!
LET COUNT=1
OPEN#1: NAME DRIVE$&"&NAME$, ORGANIZATION RECORD
SET#1: RECORD REC
LET K=0
WHEN ERROR IN
  DO WHILE (MORE #1) AND (K<(NUMDATA-6*NUMPOINTS))
    READ #1: VP
    LET K=K+1
    LET V(K)=VP
  LOOP
USE
END WHEN
FOR I = 2 TO K-1
  LET VEL1 = ZZ(I,1)
  LET VEL2 = ZZ(I,2)
  LET VEL3 = ZZ(I,3)
  !
  IF I=> THROW THEN CALL PLOTOFF3(VEL1,VEL2,VEL3,$$)
NEXT I
!
CALL PLOTTEXT3(54,0,0,"W(t)",$$)
CALL PLOTTEXT3(0,60,0,"W(t+T)",$$)
CALL PLOTTEXT3(0,0,51,"W(t+2T)",$$)
IF PRINT1=1 THEN CALL SCRNDUMP

```

```

GET KEY KEYVARIABLE
!
CLEAR
CALL SETXSCALE(LOG(RADIUS(1)),LOG(RADIUS(NUMSTEP)))
LET M1 = LOG(RADIUS(1))
LET M2 = M1 + .2
CALL SETMARGINS(60,60,0,0)
CALL SETYSCALE(-10,0)
CALL SETAXES(0)
CALL SETTEXT("Correlation dimension graph","Log R","Log C")
CALL RESERVELEGEND

DATA 0,0
CALL DATAGRAPH(A,B,1,0,"WHITE")
CALL GOTOCANVAS

FOR EMBED=INITEMBED TO FINALEMBED
  FOR SIZES=1 TO NUMSTEP
    LET CORR=0.0
    FOR N=1 TO NUMCENTERS
      LET I=INT(RND*K)+2
      FOR M=1 TO NUMCENTERS
        LET J=INT(RND*K)+2
        LET DIST2=0.0
        FOR MM=1 TO EMBED
          LET DIST2=DIST2+((Z(Z,I,MM)-Z(Z,J,MM))^2)
        NEXT MM
        LET QUANTITY=(RADIUS(SIZES))^2-DIST2
        IF QUANTITY>0 THEN LET CORR=CORR+1
      NEXT M
    NEXT N
    LET NORMCORR=2*CORR/(NUMCENTERS^2)
    IF NORMCORR=0 THEN LET NORMCORR=1E-12
    LET R(EMBED,SIZES)=LOG(RADIUS(SIZES))
    LET Y(EMBED,SIZES)=LOG(NORMCORR)
    IF EMBED=1 THEN CALL GRAPHPOINT(LOG(RADIUS(SIZES)),LOG(NORMCORR),8)
    IF EMBED=2 THEN CALL GRAPHPOINT(LOG(RADIUS(SIZES)),LOG(NORMCORR),7)
    IF EMBED=3 THEN CALL GRAPHPOINT(LOG(RADIUS(SIZES)),LOG(NORMCORR),4)
    IF EMBED=4 THEN CALL GRAPHPOINT(LOG(RADIUS(SIZES)),LOG(NORMCORR),3)
    IF EMBED=5 THEN CALL GRAPHPOINT(LOG(RADIUS(SIZES)),LOG(NORMCORR),6)
    IF EMBED=6 THEN CALL GRAPHPOINT(LOG(RADIUS(SIZES)),LOG(NORMCORR),5)
  NEXT SIZES
NEXT EMBED
CALL GRAPHTEXT(2,-7,"Embedding Dimension")
CALL GRAPHTEXT(2,-7.7,"1")
CALL GRAPHTEXT(2.5,-7.7,"2")
CALL GRAPHTEXT(3,-7.7,"3")
CALL GRAPHTEXT(2,-8.5,"4")
CALL GRAPHTEXT(2.5,-8.5,"5")
CALL GRAPHTEXT(3,-8.5,"6")
CALL GRAPHPOINT(2.2,-7.7,8)
CALL GRAPHPOINT(2.7,-7.7,7)
CALL GRAPHPOINT(3.2,-7.7,4)
CALL GRAPHPOINT(2.2,-8.5,3)
CALL GRAPHPOINT(2.7,-8.5,6)
CALL GRAPHPOINT(3.2,-8.5,5)

```

```

CALL ADDLEGEND("TAU="&STR$(NUMPOINTS)&" FILE="&STR$(NAME)&" # CENTERS="&
               STR$(NUMCENTERS),0,1,"WHITE")
CALL DRAWLEGEND
IF PRINT2=1 THEN CALL SCREENDUMP
GET KEY KEYVARIABLE
DO
  CLEAR
  CALL SETXSCALE(LOG(RADIUS(1)),LOG(RADIUS(NUMSTEP)))
  CALL SETMARGINS(60,60,0,0)
  CALL SETYSCALE(0,4)
  CALL SETAXES(0)
  CALL SETTEXT("Correlation dimension calculation graph","Log R","D")
  CALL RESERVELEGEND
  DATA 0,0
  CALL DATAGRAPH(A,B,1,0,"WHITE")
  CALL GOTOCANVAS

  FOR EMBED = MAX(INITEMBED,1) TO FINALEMBED
    LET SLOPEOLD=(Y(EMBED,AVPTS)-Y(EMBED,1))/(R(EMBED,AVPTS)-R(EMBED,1))
    FOR SIZES=AVPTS+1 TO NUMSTEP
      LET SLOPE=(Y(EMBED,SIZES)-Y(EMBED,SIZES-AVPTS+1))/(R(EMBED,SIZES)
                                                 -R(EMBED,SIZES-AVPTS+1))
      LET SLOPENEW=SLOPE
      IF EMBED=6 THEN LET LINE=1
      IF EMBED=5 THEN LET LINE=2
      IF EMBED=4 THEN LET LINE=3
      IF EMBED=3 THEN LET LINE=4
      IF EMBED=2 THEN LET LINE=1
      IF EMBED=1 THEN LET LINE=2
      CALL GRAPHLINE(R(EMBED,SIZES-AVPTS+1),SLOPEOLD,
                     R(EMBED,SIZES-AVPTS+2),SLOPENEW,LINE)
      LET SLOPEOLD=SLOPENEW
    NEXT SIZES
    CALL GRAPHTEXT(R(EMBED,1),3.5-(EMBED)*.25,STR$(EMBED))
    CALL GRAPHLINE(R(EMBED,1)+.3,3.5-(EMBED)*.25,R(EMBED,5),
                   3.5-(EMBED)*.25,LINE)
  NEXT EMBED
  CALL GRAPHTEXT(R(FINALEMBED,1),3.7,"Embedding Dimension")
  CALL ADDLEGEND("FILE "&STR$(NAME)&" TAU="&STR$(NUMPOINTS)&
                 "# CENTERS="&STR$(NUMCENTERS),0,1,"WHITE")
  CALL ADDLEGEND("NUM PTS/VAL="&STR$(AVPTS),0,1,"WHITE")
  CALL DRAWLEGEND
  IF PRINT3=1 THEN CALL SCREENDUMP
  GET KEY KEYVARIABLE
  INPUT PROMPT"AGAIN ? (Y/N) :"&RESPONSE$&
  IF (RESPONSE$="Y") OR (RESPONSE$="y") THEN
    INPUT PROMPT"GIVE NEW VALUE OF NUM PTS/VAL :"&AVPTS
  END IF
  LOOP UNTIL (RESPONSE$="n") OR (RESPONSE$="N")
  GET KEY KEYVARIABLE
  CLEAR
END

```

## Listing 13

```

1000 !PROGRAM TITLE *****RECLYAP*****
1010 !"XRECLYAP.TRU"
1020 LIBRARY "SCLIB.TRC"
1030 LIBRARY "SCRNDUMP.TRC"
1040 DIM V(28000),A(1),B(1),PT1(20),PT2(20)
1050 CLEAR
1060 DEF Z(I,J)=V(I+(J-1)*TAU)
1070 PRINT" ****PENDULUM - READS PHASE3D DATA AND CALCULATES LYAPUNOV EXPONENT****"
1080 PRINT
1090 PRINT" THIS PROGRAM READS TIME DELAY COORDS OF "
1095 PRINT" VELOCITY DATA FROM THE BLACKBURN PENDULUM."
1100 PRINT" IT THEN CALCULATES THE LARGEST POSITIVE LYAPUNOV"
1110 PRINT" BY THE WOLF ET AL METHOD. VARIOUS NUMBERS OF DATA POINTS, "
1120 PRINT" DELAYS, AND EMBEDDING DIMENSIONS MAY BE USED."
1130 !
1170 PRINT"INPUT TYPE OF DATA TO BE ANALYSED "
1180 !PRINT" (1)THEORETICAL FROM PHASE3D"
1190 !INPUT PROMPT" (2)EXPERIMENTAL FROM PHYSICAL PENDULUM :::SOURCE
1191 LET SOURCE=2
1200 INPUT PROMPT"DUMP SCREEN TO PRINTER (Y=1 / N=0):::PRINTIT
1210 IF PRINTIT = 1 THEN
1220   INPUT PROMPT"PRINTER TYPE (0)EPSON (1)HP LASERJET:::PRNTR
1230   CALL SCREENDUMPDEVICE(PRNTR)
1240 END IF
1250 INPUT PROMPT"INPUT NUMBER OF DATA POINTS FROM FILE (TRY 10000): ::NUMDATA
1260 INPUT PROMPT"INPUT NUMBER OF INITIAL POINTS TO IGNORE (TRY 200): ::INITPOINTS
1270 INPUT PROMPT"INPUT NUMBER OF POINTS INCLUDED IN TAU DELAY (TRY 30): ::TAU
1280 INPUT PROMPT"INPUT NUMBER OF POINTS INCLUDED BEFORE REPLACEMENT (TRY 200): ::EVOLV
1290 INPUT PROMPT"INPUT EMBEDDING DIMENSION (TRY 3): ::EMBED
1300 INPUT PROMPT"INPUT DRIVE (A,B,ETC.) OF FILE DRIVE:::DRIVES
1310 INPUT PROMPT"INPUT FILE NAME (E.G. VEL_FILE.TRU):::NAME$ 
1320 INPUT PROMPT"INPUT NUMBER OF THROWAWAY DATA SETS (USE 0):::THROW
1330 INPUT PROMPT"SET POINT # (USE 1 FOR BEGINNING) :::REC
1340 !
1350 OPEN#1: NAME DRIVES$:::ENAMES, ORGANIZATION RECORD
1360 SET#1: RECORD REC
1370 LET IND=1
1380 LET SUM=0.0
1390 LET ITS=0
1400 LET SCALMX=.5
1410 LET SCALMN=.0001
1420 LET COUNT=0
1430 LET I=0
1440 WHEN ERROR IN
1450   DO WHILE (COUNT<NUMDATA+INITPOINTS)    ! MORE #1
1460     IF SOURCE=2 THEN
1470       READ #1: VP
1480       LET DT=0.007
1490     END IF
1500     IF SOURCE=1 THEN
1510       READ #1:TYHE,XP,VP
1520       IF COUNT=10 THEN LET LOW=TYHE
1530     IF COUNT=11 THEN

```

```

1540           LET HI=TYHE
1550           LET DT=HI-LOW
1560         END IF
1570         END IF
1580         LET COUNT=COUNT + 1
1590         IF COUNT > INITPOINTS THEN
1600           LET I=I+1
1610           LET V(I)=VP
1620         END IF
1630       LOOP
1640 USE
1650 END WHEN
1660 LET NPT=I-EMBED-TAU - EVOLV
1670 I
1680 CLEAR
1690 CALL SETMARGINS(60,60,0,0)
1700 CALL SETXSCALE(0,NUMDATA*DT)
1710 IF SOURCE=1 THEN CALL SETYSCALE(0,0.5)
1720 IF SOURCE=2 THEN CALL SETYSCALE(0,4)
1730 CALL SETTAXES(0)
1740 CALL SETTEXT("PENDULUM LYAPUNOV EXPONENT", "TIME-SECONDS", "LYAPUNOV EXPONENT")
1750 CALL RESERVELEGEND
1760 I
1770 DATA 0,0
1780 CALL DATAGRAPH(A,B,D,O,"WHITE")
1790 CALL GOTOCANVAS
1800 I
1810 LET DI = 100000000000
1820 FOR I=11 TO NPT          !GET POINT CLOSEST TO INITIAL POINT OF FIDUCIAL TRAJECTORY
1830   LET D=0.0
1840   FOR J=1 TO EMBED
1850     LET D=D+(Z(IND,J)-Z(I,J))^2    !CALCULATE SEPARATION
1860   NEXT J
1870   LET D=SQR(D)
1880   IF ((D>DI) OR (D<SCALMN)) THEN GOTO 1910
1890   LET DI=D
1900   LET IND2=I
1910 NEXT I
1920
1930 FOR J= 1 TO EMBED          !GET COORDS OF EVOLVED POINT
1940   LET PT1(J)=Z(IND+EVOLV,J)
1950   LET PT2(J)=Z(IND2+EVOLV,J)
1960 NEXT J
1970
1980 LET DF=0.0
1990 FOR J=1 TO EMBED          !COMPUTE FINAL SEPARATION
2000   LET DF=DF+(PT1(J)-PT2(J))^2
2010 NEXT J
2020
2030 LET DP=SQR(DF)
2040 LET ITS=ITS+1              !UPDATE LYAPUNOV EXPONENT
2050 LET SUM=SUM+LOG(DF/DI)/(EVOLV*DT)
2060 LET ZLYAP=SUM/ITS
2070 I
2080 I
2090 CALL GRAPHPOINT(EVOLV*ITS*DT,ZLYAP,2) !GRAPH EXPONENT
2100 I

```

```

2110 LET INDOLD=IND2
2120 LET ZMULT=1.0          !LOOK FOR REPLACEMENT POINT (RENORMALIZE)
2130 LET ANGLMX=0.3
2140 LET THMIN=3.14
2150 FOR I=1 TO NPT
2160   LET III=ABS(I-(IND+EVOLV))
2170   IF III<10 THEN GOTO 2350    !DONT TAKE POINTS TOO NEAR FIDUCIAL POINT
2180   LET DNEW=0.0
2190   FOR J=1 TO EMBED          !CALC DISTANCE TO CANDIDATE POINT
2200     LET DNEW = DNEW+(PT1(J)-Z(I,J))^2
2210   NEXT J
2220   LET DNEW = SQR(DNEW)
2230   IF (DNEW>ZMULT*SCALMX OR DNEW<SCALMN) THEN GOTO 2350
2240   LET DOT = 0.0
2250   FOR J=1 TO EMBED          !CALC ANGULAR CHANGE
2260     LET DOT=DOT+(PT1(J)-Z(I,J))*(PT1(J)-PT2(J))
2270   NEXT J
2280   LET CTH=ABS(DOT/(DNEW*DF))
2290   IF CTH>1.0 THEN LET CTH=1.0
2300   LET TH=ATN((SQR(1-CTH^2))/CTH)
2310   IF TH>THMIN THEN GOTO 2350
2320   LET THMIN=TH           !SAVE POINT WITH SMALLEST ANGLE SO FAR
2330   LET DII=DNEW
2340   LET IND2=I
2350 NEXT I
2360 !
2370 IF THMIN < ANGLMX THEN GOTO 2470
2380 LET ZMULT=ZMULT + 1.0
2390 !      LOOP UNTIL (THMIN<ANGLMX AND DNEW<(ZMULT-1)
2400 IF ZMULT<5 THEN GOTO 2140
2410 LET ZMULT=1.0
2420 LET ANGLMX= 2.*ANGLMX
2430 IF ANGLMX < 3.14 THEN GOTO 2140
2440 LET IND2=INDOLD+EVOLV
2450 LET DII=DF
2460
2470 LET IND=IND+EVOLV
2480 IF IND>NPT THEN GOTO 2510
2490 LET DI=DII
2500 GOTO 1930
2510 CALL ADDLEGEND("#DATA PTS=""&STR$ (NUMDATA)&" EVOLV=""&STR$ (EVOLV),0,1,"WHITE")
2520 CALL ADDLEGEND("EMBED DIH=""&STR$ (EMBED)&" TAU PTS=""&STR$ (TAU)&
                  " DT=""&STR$ (DT),0,1,"WHITE")
2530 CALL DRAWLEGEND
2540 IF PRINTIT=1 THEN CALL SCREENDUMP
2550 GET KEY ANYTHING
2555 CLEAR
2560 END

```

## Listing 14

```

!PROGRAM TITLE *****PREDICTION**FROM**HISTORY*****
!*"XPREDHIS.TRU"
CLEAR
DIM V(30001),AI(1),BI(1),ERROR(2050)
DEF ZZ(I,J)=V(I+(J-1)*NUMPOINTS)
PRINT" *****PREDICTION OF PENDULUM ANGULAR VELOCITY TIME SERIES*****"
PRINT
PRINT" THIS PROGRAM DOES THE FOLLOWING STEPS:"
PRINT" 1) READS EXPT ANGULAR VELOCITY TIME SERIES POINTS, V(T)"
PRINT" 2) GENERATES VECTORS (V1,V2,V3) IN RECONSTRUCTED PHASE SPACE"
PRINT" 3) FINDS NEAREST NEIGHBOR OF LAST VECTOR"
PRINT" 4) FINDS POINT ONE TIMESTEP LATER AND GIVE THIS POINT AS PREDICTION"
PRINT" 5) EACH NEW STEP FOLLOWS CONSECUTIVELY THE POINTS IN TIME SERIES V(T)"
PRINT" 6) GRAPHS PREDICTED TIME SERIES WITH EXPT TIME SERIES FOR"
PRINT"      COMPARISON"
PRINT
PRINT
PRINT "HIT ANY KEY TO PROCEED"
GET KEY KEYVARIABLE
CLEAR
!
LIBRARY "SGLIB.TRC"
LIBRARY "SCRNDUMP.TRC"
! INPUT STATEMENTS
INPUT PROMPT" NUMBER OF DATA POINTS (TRY 25000) :::NUMDATA
INPUT PROMPT" NUMBER OF POINTS INCLUDED IN TAU (TRY 20) :::NUMPOINTS
INPUT PROMPT" DRIVE OF INPUT FILE (A,B,C,D) :::INDRIVES
INPUT PROMPT" INPUT FILE NAME (TRY VEL_FILE.TRU) :::INFILES
INPUT PROMPT" INDEX OF LAST 'KNOWN' STATE (TRY 22000) :::LASTK
INPUT PROMPT" INDEX OF LAST PREDICTION STATE (TRY 22700) :::LASTP
INPUT PROMPT" INDEX OF LAST COMPARISON STATE (EX. 22700) :::LASTC
INPUT PROMPT" FRACTION OF POINTS PRIOR TO PREDICTION (TRY .2): ::F
INPUT PROMPT" HARDCOPY (Y=1, N=0) :::PRINTIT
IF PRINTIT=1 THEN INPUT PROMPT" PRINTER TYPE: HP LASER=1, EPSON=0) :::PRNTR
!
CALL SETMARGINS(60,60,0,0)
CALL SETXSCALE((1+F)*LASTK-F*LASTP,LASTP)
CALL SETYSCALE(-30,30)
CALL SETTEXT("PREDICTION OF ANG VELOCITY BASED ON 'HISTORY'", "PT. NUM.", "ANG. VEL.")
CALL RESERVELEGEND
DATA 0,0
CALL DATAGRAPH(AI,BI,1,0,"WHITE")
CALL GOTOCANVAS
!
OPEN#1:NAME INDRIVES$:::INFILES$, ORGANIZATION RECORD
SET#1: RECORD 1
LET MEANSUM=0
LET K=0
WHEN ERROR IN
DO WHILE (MORE #1) AND (K<(NUMDATA - 3*NUMPOINTS))
  READ #1: VP
  LET K=K+1

```

```

        LET V(K)=VP
        IF K<LASTK THEN
            CALL GRAPHPOINT(K,V(K),1)
            LET MEANSUM=MEANSUM + V(K)
        END IF
    LOOP
    USE
    END WHEN
    !
    LET MEAN=MEANSUM/(LASTK-1)
    LET DIFFNEXT=0.0
    LET DIFFPRED=0.0
    LET OLDDISTANCE=100
    LET YOLD=V(LASTK-1)
    FOR NEWPT=0 TO (LASTP-LASTK)
        IF NEWPT=0 THEN
            LET A=ZZ(LASTK,1)
            LET B=ZZ(LASTK,2)
            LET C=ZZ(LASTK,3)
            FOR I=1 TO LASTK-10
                LET D=(ZZ(I,1)-(A))2 + (ZZ(I,2)-(B))2 + (ZZ(I,3)-(C))2
                IF (D < OLDDISTANCE) THEN
                    LET OLDDISTANCE=D
                    LET PLACE=I
                    LET PLACE=I
                END IF
            NEXT I
        END IF
        LET XP=V(PLACE+NEWPT)
        LET XA=V(LASTK+NEWPT)
        CALL GRAPHLINE(LASTK-1+NEWPT,YOLD,LASTK+NEWPT,XP,1) !PREDICTED POINT
        CALL GRAPHPOINT(LASTK+NEWPT,XA,1) !ACTUAL POINT
        LET YOLD=XP
        LET POINT = NEWPT + 1
        LET DIFFNEXT = DIFFNEXT + (XA-MEAN)2
        LET DIFFNEXTRMS = SQR(DIFFNEXT)
        LET DIFFPRED = DIFFPRED + (XA-XP)2
        LET DIFFPREDRMS = SQR(DIFFPRED)
        LET ERROR(POINT) = DIFFPREDRMS/DIFFNEXTRMS
    NEXT NEWPT
    !CALL ADDLEGEND("FILE: "&INFILE$& pred=solid TAU: "&STR$(NUMPOINTS)&
    !      DATE : "&DATES,0,1,"WHITE")
    CALL ADDLEGEND(" ",0,1,"WHITE")
    CALL DRAWLEGEND
    CALL SCREENDUMPDEVICE(PRNR)
    IF PRINTIT = 1 THEN CALL SCREENDUMP
    GET KEY VARIABLE
    CALL SETAXES(0)
    CALL SETXSCALE(0,(LASTC-LASTK)*0.7)
    CALL SETYSCALE(-5,0)
    CALL SETTEXT("LOG OF NORMALIZED ERROR OF PREDICTION BASED ON 'HISTORY'",
               "# PREDICTION POINTS","LOG E")
    CALL RESERVELEGEND
    DATA 0,0
    CALL DATAGRAPH(AI,BI,1,0,"WHITE")
    CALL GOTOCANVAS
    FOR POINT= 1 TO INT((LASTC-LASTK)*0.7)
        IF MOD(POINT,INT((LASTC-LASTK)/75))=0 THEN CALL GRAPHPOINT(POINT,
          LOG(ERROR(POINT)),6)

```

```

    NEXT POINT
    !CALL ADDLEGEND("FILE: "&INFILE$& TAU: "&STR$(NUMPOINTS)&
    !      DATE : "&DATES,0,1,"WHITE")
    CALL ADDLEGEND(" ",0,1,"WHITE")
    CALL DRAWLEGEND
    CALL SCREENDUMPDEVICE(PRNR)
    IF PRINTIT = 1 THEN CALL SCREENDUMP
    CALL SETAXES(1)
    GET KEY VARIABLE
    CLEAR
    END

```

### Listing 15

```

!PROGRAM TITLE *****CONTROL*****
!XCONTROL.TRU
CLEAR
PRINT" ***PENDULUM - CONTROL AT POINCARÉ SECTION FIXED POINT***"
PRINT" "
PRINT"THIS PROGRAM DISPLAYS ANG. VEL. VERSUS TIME"
PRINT"AND CAN SAVE THE DATA TO A FILE."
PRINT"DISPLAY CAN BE PRINTED IF THE APPROPRIATE DRIVER IS INSTALLED."
LIBRARY "SCLIB.TRC"
LIBRARY "SCRNDUMP.TRC"
!
DECLARE DEF accel
DIM A(1),B(1)
LET g=1.5 !Driving force strength
LET q=3.9 !Damping parameter
LET w=.666666666 !Forcing frequency
LET xint =0 !Initial angle
LET vint=0 !Initial angular velocity
LET tmin=0
LET tmax=4000
LET phi=0 !Phase of Poincaré section
LET xfix=1.538 !Fixed point angle
LET vfix=-.435 !Fixed point angular velocity
LET lambda=-6.03 !-7.38 !Unstable eigenvalue
INPUT prompt"Input max deviation from fixed pt; (try .3) :::maxdev
!INPUT prompt"Input components of unstable direction F-vector (.471, .853) :::Fx,Fv
LET fx=0.63 1.471 !Components of unstable F-vector
LET fv=1.00 1.853
LET gx=-.410 !Components of parameter (q) change vector
LET gv=-.294
LET tstart=1000 !Time of starting control
LET tstop=3000 !Time of stopping control
INPUT prompt"Dumpscreen to printer (y=1/n=0):::p
IF p=1 then
    INPUT prompt"Printer type (0)Epson (1)HP LaserJetII:::prntr
END IF
CALL SCREENDUMPDEVICE(PRNR)
!
```

```

CALL SETHMARGINS(60,60,0,0)
CALL SETXSCALE(TMIN,TMAX)
CALL SETYSCALE(-2,4)
CALL SETTAXES(0)
LET EPS=1E-6
LET TSTEP=.5
CALL SETTEXT("PENDULUM : POINCARÉ SECTION, CONTROL BY VARYING Q",
    "TIME-DIMENSIONLESS", "ANGULAR VELOCITY")
CALL RESERVELEGEND
!
DATA 0,0
CALL DATAGRAPH(A,B,1,0,"white")
LET qo=q
LET delq=0
LET dist=0
LET t=0
LET x=xint
LET v=vint
LET factor=lambda/(lambda-1)/(gx*Fx+gv+Fv)
CALL GOTOCANVAS
!
!CALCULATION AND GRAPHING BLOCK
LET phi=phi*2*pi

FOR i=1 to 10000000
    IF t>tstart and t<tstop THEN let switch$="on" ELSE let switch$="off"
    IF switch$="off" THEN
        LET q=qo
    END IF
    CALL rk4(x,v,tstep,xnew,vnew,t,w,g,q)      ! Take a step of size tstep
    LET tshalf=tstep/2
    CALL rk4(x,v,tshalf,xnh,vnh,t,w,g,q) !Take two half steps
    CALL rk4(xnh,vnh,tshalf,xn,vn,t+tshalf,w,g,q)
    LET d1=abs(xn-xnew)
    LET d2=abs(vn-vnew)
    LET delta=max(d1,d2)
    IF delta>eps then
        IF t>tmin then
            LET tnew=t+tstep
            LET w1=mod(phi-w*t,2*pi)      !Check for Poincaré section
            LET w2=mod(w*tnew-phi,2*pi)
            IF w1<w*tstep then
                IF w2<w*tstep then
                    LET ts=w1/w
                    CALL rk4(x,v,ts,xp,vp,t,w,g,q)      !CALCULATES POINT AT SECTION
                    IF abs(xp)>pi then LET xp=xp-2*pi*abs(xp)/xp
                    LET distx=xp-xfix
                    LET distv=vp-vfix
                    LET dist=aqr(distx^2+distv^2)
                    IF dist< maxdev AND switch$ = "on" then
                        LET delq=factor*(distx*Fx+distv*Fv)
                        CALL GRAPHPOINT(t, vp, 1)
                    ELSE
                        LET delq =0
                        CALL GRAPHPOINT(t, vp, 1)
                    END IF
                END IF
            END IF
        END IF
        LET q=q+delq
        END IF
    END IF
    LET t=t+tstep
    LET v=vnew
    LET t=t+tstep           !Expand step size
    LET tstep=tstep*.95*(eps/delta)^.25
    IF abs(x)>pi then      !bring theta back into range
        LET x=x-2*pi*abs(x)/x
    END IF
    ELSE                     !else reduce step size
        LET tstep=tstep*.95*(eps/delta)^.25
    END IF
    IF t>tmax then LET i=10000000
NEXT i
LET GS=STR$(G)
LET QS=STR$(Q)
CALL ADDLEGEND("      ,0,1,"WHITE")
CALL ADDLEGEND("G="&STR$(G)&"   Q="&STR$(Qo)&"   MaxDev="&str$(maxdev)&"   FixPt="&str$(xfix)&"&str$(vfix)&"&Date$,0,1,"WHITE")
CALL DRAWLEGEND
IF P=1 THEN CALL SCREENDUMP
GET KEY ANYTHING
CLEAR
END
!
SUB rk4(x,v,tstep,xnew,vnew,t,w,g,q)
    DECLARE DEF accel
    LET xk1=tstep*v
    LET vk1=tstep*accel(x,v,t,w,g,q)
    LET xk2=tstep*(v+vk1/2)
    LET vk2=tstep*accel(x+xk1/2,v+vk1/2,t+tstep/2,w,g,q)
    LET xk3=tstep*(v+vk2/2)
    LET vk3=tstep*accel(x+xk2/2,v+vk2/2,t+tstep/2,w,g,q)
    LET xk4=tstep*(v+vk3)
    LET vk4=tstep*accel(x+xk3,v+vk3,t+tstep,w,g,q)
    LET vnew=v+(vk1+2*vk2+2*vk3+vk4)/6
    LET xnew=x+(xk1+2*xk2+2*xk3+xk4)/6
END SUB
!
DEF accel(x,v,t,w,g,q)
    LET accel=-sin(x)-(1/q)*v+g*cos(w*t)
END DEF

```

# Solutions to selected problems

2.3 The right sides of the two first order equations are components of the vector  $\mathbf{F} = (v, g)$ . Since  $\nabla \cdot \mathbf{F} = \partial F_1/\partial x + \partial F_2/\partial v = 0$ , the phase area is conserved. If  $\mathbf{F}$  is modified to become  $(v, g - kv/m)$ , where  $m$  is the mass of the particle, then  $\nabla \cdot \mathbf{F} = -k/m$  and the phase area shrinks.

2.9 The critical points  $\theta = nm$  and  $\omega = 0$  are stable if  $n$  is zero or even, and unstable if  $n$  is odd. This can be seen using linear stability analysis or by noting that when  $n$  is even the pendulum bob is at the bottom of its motion whereas when  $n$  is odd the bob is at the top of its motion.

2.11 When the derivatives are set equal to zero for the Rossler system, the three equations, whose variables are the coordinates of the fixed points, have the two solutions

$$\begin{aligned} y &= [-c \pm (c^2 - 4ab)^{1/2}]/2a, \\ x &= -ay, \\ z &= -y. \end{aligned}$$

2.13 For the general set of differential equations

$$\begin{aligned} dx/dt &= F_1(x, y, z), \\ dy/dt &= F_2(x, y, z), \\ dz/dt &= F_3(x, y, z), \end{aligned}$$

the corresponding linearization is the set of differential equations

$$\begin{aligned} dx/dt &= (\partial F_1/\partial x)(x - x_0) + (\partial F_1/\partial y)(y - y_0) + (\partial F_1/\partial z)(z - z_0), \\ dy/dt &= (\partial F_2/\partial x)(x - x_0) + (\partial F_2/\partial y)(y - y_0) + (\partial F_2/\partial z)(z - z_0), \\ dz/dt &= (\partial F_3/\partial x)(x - x_0) + (\partial F_3/\partial y)(y - y_0) + (\partial F_3/\partial z)(z - z_0), \end{aligned}$$

where the partial derivatives are all calculated at the fixed point  $(x_0, y_0, z_0)$ . For the Rossler system these formulae lead to

$$dx/dt = -(y - y_0) - (z - z_0),$$

$$\begin{aligned} dy/dt &= (x - x_0) + a(y - y_0), \\ dz/dt &= z_0(x - x_0) + (x_0 - c)(z - z_0), \end{aligned}$$

where the values of  $x_0, y_0$ , and  $z_0$  are the solutions of Problem 2.10.

$$2.17 f(t) = t \text{ for } t \in (-T/2, T/2).$$

$$\begin{aligned} a_n &= \frac{\omega_0}{2\pi} \int_{-\pi/\omega_0}^{\pi/\omega_0} f(t) e^{-in\omega_0 t} dt \\ &= \frac{1}{T} \int_{-T/2}^{T/2} t e^{-in2\pi t/T} dt. \end{aligned}$$

Integration by parts leads to the appropriate result.

4.5 To maximize entropy, form the Lagrange function

$$J(M, p_i) = - \sum_{i=1}^N p_i \log_e p_i + M \sum_{i=1}^N p_i,$$

where the constraint is  $\sum_{i=1}^N p_i = 1$  and  $M$  is the Lagrange multiplier. Differentiation gives

$$\partial J / \partial p_i = -\log_e p_i - 1 + M;$$

this suggests that  $p_i = \text{constant}$ . But since  $\sum_{i=1}^N p_i = 1$ , we have the result  $p_i = 1/N$ .

4.8 Since  $e_{n+1} = e_n e^{\log_e 2 \beta} = e_n 2 \beta$ , then  $e_n = e(2\beta)^n$ . Setting  $e_n = 1$  and solving for  $n$  gives the result

$$n = \frac{\log_2(1/e)}{1 + \log_2 \beta}.$$

4.14 For the baker's transformation, the  $x$  and  $y$  directions may be treated independently. Therefore the formula

$$\lambda = \lim_{n \rightarrow \infty} \frac{1}{n} \sum_{i=0}^{n-1} \log_e |f'(x)|$$

may be used for each direction. In this case  $f'(x) = 2$ ,  $f'(y) = a$ , and therefore  $\lambda_x = \log_e 2$  and  $\lambda_y = \log_e a$ .

5.3 Following the approach indicated in Figure 5.3.

$N$	$e$	$d$
1	1	
4	1/3	$d = \lim_{n \rightarrow \infty} \frac{\log 2^{2^n}}{\log 3^n} = (2(\log 2/\log 3))$
16	1/9	
64	1/27	
$\vdots$	$\vdots$	

5.7 Use the formula

$$d_1 = \lim_{t \rightarrow \infty} \frac{\sum_{i=1}^n p_i \log p_i}{\log t}$$

for a few steps of the process shown in Figure 5.3. For example, with two pieces

$$d_1 \approx \frac{(1/3)\log(1/3) + (2/3)\log(2/3)}{\log(1/3)} = 1 - \frac{2 \log 2}{3 \log 3}.$$

With four pieces

$$\begin{aligned} d_1 &\approx \frac{(1/9)\log(1/9) + (4/9)\log(2/9) + (4/9)\log(4/9)}{\log(1/9)} = 1 - \frac{2 \log 2}{3 \log 3} \\ &= 0.579 \dots \end{aligned}$$

and so on for subsequent steps.

5.9 For  $q=0$  use the fact that  $\sum_{i=1}^n (p_i^0) = N$ .

For  $q=1$  consider the quantity  $[\log(\sum p_i^q)]/(q-1)$  which appears to tend toward  $0/0$  as  $q$  tends to 1. Use L'Hopital's rule – differentiate with respect to  $q$  in the numerator and denominator. Specifically, first express the above quantity as

$$\frac{\log(e^{q \log p_1} + e^{q \log p_2} + e^{q \log p_3} + \dots)}{q-1}$$

The appropriate differentiations lead to

$$\begin{aligned} &\frac{p_1^q \log p_1 + p_2^q \log p_2 + \dots}{p_1^q + p_2^q + \dots} \\ &= \frac{\sum p_i^q \log p_i}{\sum p_i^q} \end{aligned}$$

as  $q$  tends to 1. Since  $\sum p_i = 1$  the equivalence of  $d^{(1)}$  and  $d_1$  is evident.

5.12 To find  $\nabla \cdot \mathbf{F}$  first form the set of differential equations

$$\begin{aligned} d\theta/dt &= \omega, \\ d\omega/dt &= \theta - \omega/q. \end{aligned}$$

Then  $\mathbf{F} = (\omega, \theta - \omega/q)$  and  $\nabla \cdot \mathbf{F} = -1/q$ . It is obvious that  $\lambda_+ + \lambda_- = -1/q$  also.

The Kaplan-Yorke relation gives

$$d_L = \frac{2[(1/4)q^2 + 1]^{\frac{1}{2}}}{q/2 + [(1/4)q^2 + 1]^{\frac{1}{2}}},$$

which leads to the table

$q$	$d$
$\infty$	2
5	1.82
2	1.61
0	1.

These results may be compared to the data from problem 5.10, where  $d = 1.2$  for  $q = 2$  and  $d = 1.23$  for  $q = 5$ . It is evident that while the calculated values from the model described in this question change in the appropriate way as  $q$  increases, the calculated values are too large. Probably the major difficulty with this model is that it does not adequately represent the forcing term or the nonlinearity of the dynamics.

To find an effective value of  $q$  that will produce the numerically derived value of  $d$  (that matches the case for which the forced pendulum has  $q = 2$ , or  $q = 5$ ) one must solve for the effective  $q$  in the above expression using the following expression,

$$q_{\text{eff}} = [d_L^2 / (4\{2 - d_L\}^2 - 1/4)]^{\frac{1}{2}},$$

which yields  $q_{\text{eff}} = 0.56$  for  $d_L = 1.2$ , and  $q_{\text{eff}} = 0.62$  for  $d_L = 1.23$ .

6.1 In terms of the physical parameters the dimensionless quantities are

$$q = \omega_0 l/b, g = T/\omega_0^2 l, \text{ and } \omega_D = \omega_l/\omega_0.$$

# References

- Abarbanel, H.D.I., Brown, R., and Kadtke, J.B. (1990). Prediction in chaotic nonlinear systems: Methods for time series with broadband Fourier spectra, *Phys. Rev. A*, **41**, 1782–807.
- Abarbanel, H.D., Brown, R., Sidorowich, J.J., and Tsimring, L.S. (1993). The analysis of observed chaotic data in physical systems, *Rev. Mod. Phys.*, **65**, 1331–92.
- Abraham, N.B., Arimondo, E., and Boyd, R.W. (1988). Dynamics and chaos in nonlinear optical systems, in *Instabilities and chaos in quantum optics*. II, eds. N.B. Abraham, F.T. Arecchi, and L.A. Lugiato, Plenum Pub. Corp., NY, pp. 375–91.
- Abraham, N.B., Garmire, E.M., and Mandel, P. (Eds.) (1991). OSA Proceedings on Nonlinear Dynamics in Optical Systems, Optical Society of America, Washington, DC, Vol. 7.
- Abraham, R.H., and Shaw, C.D. (1984). *Dynamics: the geometry of behavior*, Part III, Ariel Press, Santa Cruz.
- Aihara, K., Takabe, T., and Toyoda, M. (1990). Chaotic neural networks, *Phys. Lett. A*, **144**, 333–40.
- Albano, A.M., Muench, J., Schwartz, C., Mees, A.I., and Rapp, P.E. (1988). Singular-value decomposition and the Grassberger–Procaccia algorithm, *Phys. Rev. A*, **38**, 3017–26.
- Aref, H. (1984). Stirring by chaotic advection, *J. Fluid Mech.*, **143**, 1–21.
- Argoul, F., Arneodo, A., Richetti, P., Roux, J.C., and Swinney, H.L. (1987). Chemical chaos: from hints to confirmation, *Acc. Chem. Res.*, **20**, 436–42.
- Arneodo, A., Grasseau, G., and Kostelich, E.J. (1987). Fractal dimensions and  $f(\alpha)$  spectrum of the Hénon attractor, *Phys. Lett. A*, **124**(8), 426–32.
- Arnold, V.I. (1965). Small denominators, I: mappings of the circumference into itself, *AMS Transl. Series 2*, **46**, 213.
- Atmanspacher, H. and Scheingraber, H. (1987). A fundamental link between system theory and statistical mechanics, *Found. Phys.*, **17**, 939–63.
- Atmanspacher, H., Scheingraber, H., and Voges, W. (1988). Global scaling properties of a chaotic attractor reconstructed from experimental data, *Phys. Rev. A*, **37**, 1314–22.
- Badii, G., Broggi, B., Derighetti, M., Ravani, S., Ciliberto, A., Politi, A., and Rubio, M.A. (1988). Dimension increase in filtered chaotic signals, *Phys. Rev. Lett.*, **60**, 979–82.
- Baierlein, R. (1971). *Atoms and information theory*, W.H. Freeman and Co., San Francisco, Chapter 3.
- Bak, P. (1986). The Devil's staircase, *Physics Today*, December, 38–45.
- Baker, G.L. (1986). A simple model of irreversibility, *Am. J. Phys.*, **54**, 704–8.
- Baker, G.L. (1995). Control of the chaotic driven pendulum, *Am. J. Phys.*, **63**, 832–8.
- Bergé, F., Pomeau, Y., and Vidal, Ch. (1984). *Order within chaos*, John Wiley and Sons, NY, p. 179.
- Berkooz, G., Holmes, P., and Lumley, J.L. (1992). Low dimensional models of the wall region in a turbulent boundary layer, *Physica D*, **58**, 402–6.
- Berkooz, G., Holmes, P., and Lumley, J.L. (1993). The proper orthogonal decomposition in the analysis of turbulent flows, *Ann. Rev. Fluid Mech.*, **25**, 539–75.
- Blackburn, J.A., Vik, S., Binruo, Wu, and Smith, H.J.T. (1989). Driven pendulum for studying chaos, *Rev. Sci. Instrum.*, **60**, 422–6.
- Bradley, E. (1992). A control algorithm for chaotic physical systems, in *Proceedings of the 1st Experimental Chaos Conference*, eds. Vohra, S., Spano, M., Shlesinger, M., Pecora, L., and Ditto, W., World Scientific, Singapore, pp. 152–8.
- Braiman, Y. and Goldhirsch, I. (1991). Taming chaotic dynamics with weak periodic perturbations, *Phys. Rev. Lett.*, **66**, 2545–8.
- Broomhead, D.S. and King, G.P. (1986). Extracting qualitative dynamics from experimental data, *Physica*, **20D**, 217–36.
- Brown, R. (1992). Using near neighbors to determine embedding dimensions for phase space reconstruction, in *Proceedings of the 1st Experimental Chaos Conference*, eds. Vohra, S., Spano, M., Shlesinger, M., Pecora, L., and Ditto, W., World Scientific, Singapore, pp. 24–30.
- Brown, R., Bryant, P., and Abarbanel, H.D.I. (1991). Computing the Lyapunov spectrum of a dynamical system from an observed time series, *Phys. Rev. A*, **43**, 2787–806.
- Carlson, J.M., Langer, J.S., and Shaw, B.E. (1994). Dynamics of earthquake faults, *Rev. Mod. Phys.*, **66**, 657–70.
- Casdagli, M., Des Jardins, D., Eubank, S., Farmer, J.D., Gibson, J., Hunter, N., and Theiler, J. (1992). Nonlinear modeling of chaotic time series: theory and applications, in *Applied Chaos*, eds. Kim, J.H., and Stringer, J., John Wiley and Sons, NY, pp. 335–80.
- Chang, A.M., Barantger, L.N., Pfeiffer, L.N., and West, K.W. (1994). Weak localization in chaotic versus nonchaotic cavities: a striking difference in the line shape, *Phys. Rev. Lett.*, **73**, 2111–14.
- Ciliberto, S., and Gollub, J.P. (1985). Phenomenological model of chaotic mode competition in surface waves, *Il Nuovo Cimento*, **6D**, 309–16.
- Coullet, P., and Iooss, G. (1990). Instabilities of one-dimensional cellular patterns, *Phys. Rev. Lett.*, **64**, 886–9.
- Cross, M.C., and Hohenberg, P.C. (1994). Pattern formation outside of equilibrium, *Rev. Mod. Phys.*, **65**, 851–1112.
- Davidson, A., Dueholm, B., and Beasley, M.R. (1986). Experiments on intrinsic and thermally induced chaos in an RF-driven Josephson junction, *Phys. Rev. B*, **33**, 5127–30.

- Decker, W., Pesch, W., and Weber, A. (1994). Spiral defect chaos in Rayleigh-Bénard convection, *Phys. Rev. Lett.*, **73**, 648–51.
- D'Humieres, D., Beasley, M.R., Huberman, B.A., and Libchaber, A. (1982). Chaotic states and routes to chaos in the forced pendulum, *Phys. Rev. A*, **26**, 3483–96.
- Ding, M., Grebogi, C., Ott, E., Sauer, T., and Yorke, J.A. (1993a). Plateau onset for correlation dimension: when does it occur? *Phys. Rev. Lett.*, **70**, 3872–5.
- Ding, M., Grebogi, C., Ott, E., Sauer, T., and Yorke, J.A. (1993b). Estimating correlation dimension from a chaotic time series: when does plateau onset occur? *Physica D*, **69**, 404–24.
- Ditto, W.L., Rauseo, S.N., and Spano, J.L. (1990). Experimental control of chaos, *Phys. Rev. Lett.*, **65**, 3211–14.
- Dougherty, A., Kaplan, P.D., and Gollub, J.P. (1987). Development of side branching in dendritic crystal growth, *Phys. Rev. Lett.*, **58**, 1652–5.
- Dugas, R. (1958). *Mechanics in the 17th century*, Central Book Co., NY, p. 76.
- Eckmann, J.P., and Ruelle, D. (1985). Ergodic theory of chaos and strange attractors, *Rev. Mod. Phys.*, **57**, 617–56.
- Farmer, J.D., and Sidorowich, J.J. (1987). Predicting chaotic time series, *Phys. Rev. Lett.*, **59**, 845–8.
- Farmer, J.D., Ott, E., and Yorke, J.A. (1983). The dimension of chaotic attractors, *Physica*, **7D**, 153–80.
- Feigenbaum, M.J. (1978). Quantitative universality for a class of nonlinear transformations, *J. Stat. Phys.*, **19**, 25–32.
- Firth, W.J. (1986). Instabilities and chaos in lasers and optical resonators, in *Chaos*, ed. A.V. Holden, Princeton University Press, Princeton, pp. 135–57.
- Fischer, I., Hess, O., Elsäßer, and Göbel (1994). High-dimensional chaotic dynamics of an external cavity semiconductor laser, *Phys. Rev. Lett.*, **73**, 2188–91.
- Fraser, A.M. (1989). Information and entropy in strange attractors, *IEEE Trans. on Information Theory*, **35**, 245–62.
- Fraser, A.M., and Swinney, H. (1986). Independent coordinates for strange attractors from mutual information, *Phys. Rev. A*, **33**, 1134–40.
- Fryksa, S.T., and Zohdy, M.A. (1992). Computer dynamics and shadowing of chaotic orbits, *Phys. Lett. A*, **166**, 340–6.
- Gills, Z., Iwata, C., Roy, R., Schwartz, I.R., and Triandaf, I. (1992). Tracking unstable steady states: extending the stability regime of a multimode laser system, *Phys. Rev. Lett.*, **69**, 3169–72.
- Gioggia, R.S., and Abraham, N.B. (1983). Routes to chaotic output from a single-mode dc-excited laser, *Phys. Rev. Lett.*, **51**, 6550–3.
- Glazier, J.A., and Libchaber, A. (1988). Quasiperiodicity and dynamical systems: an experimentalist's view, *IEEE Trans. on Circuits and Systems*, **35**, No. 7, 790–908.
- Gollub, J.P., and Benson, S.V. (1980). Many routes to turbulent convection, *J. Fluid Mech.*, **100**, 449–70.
- Grassberger, P., and Procaccia, I. (1983a). Measuring the strangeness of strange attractors, *Physica*, **9D**, 189–208.
- Grassberger, P., and Procaccia, I. (1983b). Characterization of strange attractors, *Phys. Rev. Lett.*, **50**, 346–9.
- Grassberger, P., and Procaccia, I. (1984). Dimensions and entropies of strange attractors from a fluctuating dynamics approach, *Physica*, **13D**, 34–54.

- Grebogi, C., Ott, E., and Yorke, J.A. (1987). Chaos, strange attractors and fractal basin boundaries in nonlinear dynamics, *Science*, **238**, 632–8.
- Grebogi, C., Hammel, S.M., Yorke, J.A., and Sauer, T. (1990). Shadowing of physical trajectories in chaotic dynamics: containment and refinement, *Phys. Rev. Lett.*, **65**, 1527–30.
- Gutzwiller, M.C. (1985). Mild chaos, in *Chaotic behavior in quantum systems*, ed. G. Casati, Plenum Press, NY, pp. 149–64.
- Gutzwiller, M.C. (1992). Quantum chaos, *Sci. Amer.*, January, 78–84.
- Gwinn, E.G., and Westervelt, R.M. (1985). Intermittent chaos and low-frequency noise in the driven damped pendulum, *Phys. Rev. Lett.*, **54**, 1613–16.
- Gwinn, E.G., and Westervelt, R.M. (1986). Fractal basin boundaries and intermittency in the driven damped pendulum, *Phys. Rev. A*, **33**, 4143–55.
- Halsey, T., Jensen, M.H., Kadanoff, L.P., Procaccia, I., and Shraiman, B.I. (1986). Fractal measures and their singularities: the characterization of strange sets, *Phys. Rev. A*, **33**, 1141–55.
- Harrison, R.G., and Biswas, D.J. (1986). Chaos in light, *Nature*, **321**, 394–401.
- Hayashi, C. (1964). *Nonlinear oscillations in physical systems*, McGraw Hill, NY, p. 35.
- Helleman, R.H.G. (1983). Self-generated chaotic behavior in nonlinear systems, in *Universality in chaos*, ed. P. Cvitanovic, Adam Hilger Publ., Bristol.
- Heller, E.J. (1984). Bound-state eigenfunctions of classically chaotic Hamiltonian systems: scars of periodic orbits, *Phys. Rev. Lett.*, **52**, 1515–18.
- Heslot, F., Castaing, B., and Libchaber, A. (1987). Transitions to turbulence in helium gas, *Phys. Rev. A*, **36**, 5870–3.
- Heutmaker, M.S., and Gollub, J.P. (1987). Wave vector field of convective flow patterns, *Phys. Rev. A*, **36**, 5870–3.
- Higgins, J.R. (1976). Fast Fourier transform: an introduction with some minicomputer experiments, *Am. J. Phys.*, **44**, 766–73.
- Hjelmfelt, A., and Ross, J. (1994). Pattern recognition, chaos, and multiplicity in neural networks of excitable systems, *Proc. Nat. Acad. Sci.*, **91**, 63–7.
- Hubinger, B., Doerner, R., and Martienssen, W. (1993). Local control of chaotic motion, *Z. Phys. B*, **90**, 103–6.
- Iansiti, M., Qing Hu, Westervelt, R.M., and Tinkam, M. (1985). Noise and chaos in a fractal basin boundary regime in a Josephson junction, *Phys. Rev. Lett.*, **55**, 746–9.
- Jensen, R.V. (1985). Stochastic ionization of bound electrons, in *Chaotic behavior in quantum systems*, ed. G. Casati, Plenum Press, NY, pp. 171–86.
- Jensen, R.V. (1987a). Chaos in atomic physics, *Atom Phys.*, **10**, 319–32.
- Jensen, R.V. (1987b). Classical chaos, *Am. Scientist*, **75**, 168–81.
- Jensen, R.V. (1992). Quantum chaos, *Nature*, **355**, 311–18.
- Jensen, M.H., Bak, P., and Bohr, R. (1984). Transition to chaos by interaction of resonances in dissipative systems. I. Circle maps, *Phys. Rev. A*, **30**, 1960–9.
- Kaplan, J.L., and Yorke, J.A. (1979). Chaotic behavior of multi-dimensional difference equations, in *Functional differential equations and the approximations of fixed points*, eds. H.O. Peitgen and H.O. Walther, Lecture notes in mathematics, Vol. 730, Springer-Verlag, Berlin, pp. 204–27.
- Kaplan, W. (1973). *Advanced calculus*, Addison-Wesley, Reading, MA, Chapter 7.
- Karma, A. (1993). Spiral breakup in model equations of action potential propagation in cardiac tissue, *Phys. Rev. Lett.*, **71**, 1103–6.

- Kessler, D.A., Koplik, J., and Levine, H. (1988). Pattern selection in fingered growth phenomena, *Adv. Phys.*, **37**, 255–339.
- Kostelich, E.J., and Lathrop, D.P. (1994). Time series prediction by using the method of analogues, in *Time series prediction: forecasting the future and understanding the past*, eds. A.S. Weigand and N.A. Gershenfeld, Addison-Wesley, Reading, Mass., pp. 283–95.
- Kostelich, E.J. and Schreiber, T. (1993). Noise reduction in chaotic time-series data: a survey of common methods, *Phys. Rev. E*, **48**, 1752–62.
- Lapedes, A.S. and Farber, R. (1987). Nonlinear signal processing using neural networks: prediction and systems modeling. Technical Report LA-UR-87-2662, Los Alamos National Laboratory.
- Lichtenberg, A.J., and Lieberman, M.A. (1992). *Regular and chaotic dynamics*, second edn, Springer-Verlag, NY.
- Lindberg, D., Turner, J.S., and Barkley, D. (1990). Chaos in the Showalter-Noyes-Bar-Eli model of the Belousov-Zhabotinskii reaction, *J. Chem. Phys.*, **92**, 3238–9.
- Lipsitz, L.A., and Goldberger, A.L. (1992). Loss of ‘complexity’ and aging, *JAMA*, **267**, 1806–9.
- Lorenz, E.N. (1963). Deterministic non-periodic flow, *J. Atmos. Sci.*, **20**, 130–41.
- Lorenz, E.N. (1991). Dimension of weather and climate attractors, *Nature*, **353**, 241–4.
- Mackey, M.C. (1992). *Time’s arrow: the origins of thermodynamic behavior*, Springer-Verlag, NY.
- Malmstadt, H.V., Enke, C.G., and Crouch, S.R. (1981). *Electronics and instrumentation for scientists*, Benjamin/Cummings Pub. Co., Reading, MA, p. 215.
- Malraison, B., Atten, P., Bergé, P., and Dubois, M. (1983). Dimension of strange attractors: an experimental determination for the chaotic regime of two chaotic systems, *J. Phys. Lett. (Paris)*, **44**, 897–902.
- Mané, R. (1981). On the dimension of the compact invariant sets of certain nonlinear maps, in *Dynamical Systems and Turbulence*, eds. D.A. Rand and L.S. Young, *Lecture Notes in Mathematics*, Vol. 898. Springer-Verlag, Berlin, 230–42.
- May, R.M. (1976). Simple mathematical models with very complicated dynamics, *Nature*, **26**, 459–67.
- Melo, F., and Douady, S. (1993). From solitary waves to static patterns via spatiotemporal intermittency, *Phys. Rev. Lett.*, **71**, 3283–6.
- Moon, F.C. (1987). *Chaotic Vibrations*, John Wiley and Sons, NY.
- Moon, F.C. (1992). *Chaotic and fractal dynamics, an introduction for applied scientists and engineers*, John Wiley and Sons, NY.
- Moon, F.C., and Li, G.-X. (1985). The fractal dimension of the two-well potential strange attractor, *Physica*, **17D**, 99–108.
- Morris, S.W., Bodenschatz, E., Cannell, D.S., and Ahlers, G. (1993). Spiral defect chaos in large aspect ratio Rayleigh-Bénard convection, *Phys. Rev. Lett.*, **71**, 2026–9.
- Nelkin, M. (1995). Universality and scaling in fully developed turbulence. To be published in *Adv. Phys.*
- Nitsche, G., and Dressler, U. (1992). Controlling chaotic dynamical systems using time delay coordinates, *Physica D*, **58**, 153–64.
- Orear, J. (1979). *Physics*, John Wiley and Sons, NY, Chapter 25.

- Ott, E. (1993). *Chaos in dynamical systems*, Cambridge University Press, Cambridge.
- Ott, E., Grebogi, C., and Yorke, J.A. (1990). Controlling chaos, *Phys. Rev. Lett.*, **64**, 1196–9.
- Ottino, J.M. (Jan. 1989). The mixing of fluids, *Scientific Am.*, **260**, 56–67.
- Ottino, J.M. (1990). Mixing, chaotic advection, and turbulence, *Ann. Rev. Fluid Mech.*, **22**, 207–53.
- Packard, N.H., Crutchfield, J.P., Farmer, J.D., and Shaw, R.S. (1980). Geometry from a time series, *Phys. Rev. Lett.*, **45**, 712–16.
- Poincaré, H. (1913). *The foundation of science: science and method*, English translation, 1946, The Science Press, Lancaster, PA, p. 397.
- Press, W.H., Flannery, B.P., Teukolsky, S.A., and Vetterling, W.T. (1986). *Numerical recipes: the art of scientific computing*, Cambridge University Press, Cambridge.
- Rapp, P.E. (1986). Oscillations and chaos in cellular metabolism and physiological systems, in *Chaos*, ed. A.V. Holden, Princeton University Press, Princeton, pp. 179–208.
- Robinson, H. (1921). *The mind in the making*, Harper and Brother, NY, p. 52.
- Rössler, O.E. (1976). An equation for continuous chaos, *Phys. Lett.*, **57A**, 397–8.
- Sinai, Y.G. (1970). Dynamical systems with elastic reflections, *Russ. Math. Surv.*, **25**, 137–89.
- Siggia, E.D. (1994) High Rayleigh number convection, *Ann. Rev. Fluid Mech.*, **26**, 137–68.
- Skinner, J.E. (1994). Low-dimensional chaos in biological systems. *Bio/technology*, **12**, 596–600.
- Smale, S. (1963). Diffeomorphisms with many periodic points, in *Differential and combinatorial topology*, ed. S.S. Cairns, Princeton University Press, Princeton, pp. 63–80.
- Sompolinsky, H., and Crisanti, A. (1988). Chaos in random neural networks, *Phys. Rev. Lett.*, **61**, 259–62.
- Spano, M.L., and Ditto, W.L. (1992). Taming chaos experimentally: A primer, in *Proceedings of the 1st Experimental Chaos Conference*, eds. Vohra, S., Spano, M., Shlesinger, M., Pecora, L., and Ditto, W., World Scientific, Singapore, p. 119.
- Sreenivasan, K.R. (1991). Fractals and multifractals in fluid turbulence, *Annual Rev. Fluid Mech.*, **23**, 539.
- Starrett, J., and Tagg, R. (1995). Control of a chaotic parametrically driven pendulum, *Phys. Rev. Lett.*, **74**, 1974–7.
- Sussman, G.J., and Wisdom, J. (1992). Chaotic evolution of the solar system, *Science*, **257**, 56–62.
- Swinney, H.L. (1983). Observations of order and chaos in nonlinear systems, *Physica*, **7D**, 3–15.
- Swinney, H.L., and Gollub, J.P. (1986). Characterization of hydrodynamic strange attractors, *Physica D*, **18**, 448–54.
- Takens, F. (1981). Detecting strange attractors in turbulence, in *Dynamical systems and turbulence*, eds. Rand, D.A., and Young, L.S., *Lecture Notes in Mathematics*, Vol. 898, Springer-Verlag, Berlin, 366–81.
- Thomas, G.B., and Finney, R.L. (1979). *Calculus and analytic geometry*, Addison-Wesley, Reading, MA, p. 718.
- Vallée, D., Edwards, W.S., and Gollub, J.P. (1994). Transition to spatiotemporal

- chaos via spatially subharmonic oscillations of a periodic front, *Phys. Rev. E*, **49**, R4738–86.
- Vicsek, T. (1989). *Fractal growth phenomena*, World Scientific, Singapore.
- Weigend, A.S., and Gershenfeld, N.A. (eds) (1994). *Time series prediction: forecasting the future and understanding the past*, Addison Wesley, Reading, MA.
- Wolf, A. (1986). Quantifying chaos with Lyapunov exponents, in *Chaos*, ed. A.V. Holden, Princeton University Press, Princeton, pp. 273–90.
- Wolf, A., Swift, J.B., Swinney, H.L., and Vastano, J.A. (1985). Determining Lyapunov exponents from a time series, *Physica*, **16D**, 285–317.
- Zhabotinskii, A.M. (1991). A history of chemical oscillations and waves, *Chaos*, **1**, 379–86.

# Index

- angle, 5, 7
- angular velocity, 4, 8, 10
- Arnold tongues, 92
- attractor, 5, 13, 17, 21
  - chaotic, 43
  - reconstructed, 137, 141, 143
  - strange, 45, 112, 170
- autonomous, 19
- BASINS (program listing), 216
- basins of attraction, 19, 59, 64, 103
- BIFURCATION (program listing), 203
- bifurcation, 66
  - diagram, 66, 71, 80, 82
  - pitchfork, 77
  - tangent, 82
- biological systems, 169, 189
- Burridge-Knopoff model, 184
- Cantor set, 109
- chaos, chaotic, 1, 2, 3, 5
  - control of, 159
  - route to, 81
  - spatio-temporal, 166; in earthquakes, 184; in fluids, 172; in thermal convection, 173; mixing fluids, 180; rotating fluid film, 176; spiral, 175
- characteristics equations, 18
- chemical reactions
  - Belousov-Zhabotinskii, 168
  - chaos in, 168
- CIRCLE MAP (program listing), 230
- conservative, 9, 12, 14
- CONTROL (program listing), 239
- convection, xi, 36
  - Rayleigh-Benard, 171
  - rolls, 174
- correlation function, 144
- crises, 82
- critical points, 17, 36
- damping, 4
- deterministic, 1, 183
- devil's staircase, 92
- difference equations, 74
- differential equations, 2
  - linearized, 17
- diffusion limited aggregation, 183
- dimension, 62, 110
  - capacity, 110
  - correlation, 114
  - generalized, 117
  - information, 116
  - Lyapunov, 123
  - properties of, 113
- dissipative, 5, 12, 14, 15, 41
- drive frequency (*see also* forcing), 4
- dynamical system, 2
- embedding 146
- entropy, 86
- experimental data, 133, 135
- EXPFFT (program listing), 203
- exponential divergence, 1, 84
- Feigenbaum number, 81, 106
- FFT, 33, 38, 73
- FFT (program listing), 211
- filtering, 134
- flow, 20, 74
- fluids
  - chaos in, 170
  - incompressible, 14
- focus, 18
- folding (and stretching), 41, 56, 88, 96
- forcing, 4
- Fourier analysis, x, 7
  - Fourier series, 27
  - Fourier transform, 28, 30

fractals, 5, 45, 109  
 Galileo, 4  
 Gaussian, 31  
 gravitation, 4  
 Hamiltonian systems, 14  
 harmonics, 5, 39  
 Hénon-Heiles, 35  
 HENON MAP (program listing), 226  
 heteroclinic (homoclinic) tangle, 100  
 information, 87, 127  
     Kolmogorov, 127  
     mutual, 145  
 interfacial growth, 180  
 intermittency, 180  
     in model equations, 178  
     type I, 84  
 invertible (*see* noninvertible)  
 irreversibility, 187  
 Josephson junction, 189  
 Koch curve, 112  
 Kolmogorov entropy, 126  
 lasers, chaos in, 166  
 limit cycle, 21  
 LOGISTIC MAP (program listing), 219  
 Lorentzian, 30  
 Lorenz equations, 36, 140  
 Lyapunov exponent, 5, 59, 84, 119, 150  
 manifold, 97, 100  
 mapping, 5  
 maps, 5, 74, 140  
     baker, 107  
     circle, 89  
     Hénon, 35, 108  
     horseshoe, 96, 102  
     logistic, 76  
     standard, 90  
     tent, 106  
 Maxwell-Bloch equations, 167  
 mode-locking *see* phase-locking  
 MOTION (program listing), 207  
 multifractals, 119, 180  
 neural networks, 158, 189  
 Newton's second law, 1, 4  
 noise, 1/f, 34  
 noncrossing, 9, 146  
 noninvertible, 75, 89, 92  
 nonlinear, xi, 1, 3, 188  
 numerical, 3, 193  
 PENDULUM (program listing), 199  
 pendulum, 2  
     animation, 40  
     damped, driven, 3

equation of, 4, 39  
 experimental, 137  
 linearized, 7, 10, 17  
 parameters, 5, 39, 136  
 time-delay coordinates, 141  
 undamped, 15  
 PENDLYAP (program listing), 227  
 period, 4  
 period doubling, 22, 67, 77, 100  
 periodic, 20, 81  
 phase locking, 89, 92, 102, 107  
 phase space, 7, 8, 19, 43  
     evolution of volume, 13, 122  
     periodic boundary conditions, 11, 20,  
         142  
     preservation of area, 9  
     trajectory, 3, 97  
 POINCARÉ (program listing), 201  
 Poincaré section, 5, 7, 21, 25, 43, 89, 173  
 power spectra (*see* Fourier), 7, 30, 32, 59,  
     61, 134, 172  
 PREDICT (program listing), 237  
 prediction xi, 127, 152  
     method of analogues, 153  
     method of least squares, 156  
     time, 128, 154  
 probability, 86, 106  
 problem solutions, selected, 242  
 quantum physics, 185  
 quasiperiodic, 90, 92  
 random, 126  
 RECDIM (program listing), 230  
 RECLYAP (program listing), 234  
 rimming flow, 176  
 Rossler equations, 36, 37  
 rotor, 10  
 routes to chaos, 81, 95  
 Runge-Kutta method, 193  
 saddle point, 18, 131  
 scars, 186  
 self-similarity, 44, 52, 92, 110  
 sensitivity to initial conditions, 1, 41, 84,  
     119, 128, 188  
 separatrix, 19, 59  
 shadowing, 129  
 snowflakes *see* interfacial growth  
 spatio-temporal chaos *see* chaos  
 spectral analysis, 27  
 statistical mechanics, 187  
 steady state, 41  
 stochastic, 1  
 stretching *see* folding  
 subharmonic cascade, 68, 82, 92

time delay  
     coordinates, 75, 139  
     choice of, 143  
 time series, 2, 27, 59, 134, 136, 172

transient, 3, 40  
 TrueBASIC, 253  
 turbulence  
     defect mediated, 179  
     strong, 179

uncertainty, 1, 188  
 universality, 81  
 winding number, 90, 102  
 window, 77, 81, 90

---

# Diskette order information

---

A new diskette that accompanies this second edition of the book may be purchased directly from one of the authors. The diskette has a menu-driven runtime program – CHAOS\_II – that accesses compiled programs. These can perform the simulations and data analysis discussed in this book. The revised diskette also includes a file of angular velocity data from an experimental pendulum and a variety of new programs for the analysis of that experimental data. CHAOS\_II is available in 3½ inch IBM format for AT and faster machines with 512K memory and Hercules, CGA, EGA, or VGA graphics. CHAOS\_II is executable without special language system diskettes, and is therefore inaccessible for modification. However, the TrueBASIC™ source code for the compiled programs is also provided on the diskette for those who wish to modify the programs or translate them into another language. (TrueBASIC is a trademark of True BASIC, Inc.)

The price of the diskette is \$15. Payment should be sent with the *order* in the form of (a) a check from US residents, or (b) a Postal Money Order or check drawn on a US dollar account in US funds, or US cash, from those living outside the United States. (Apologies for this necessary inconvenience.)

Make check or money order payable to: Gregory Baker.

Send orders with payment to: Gregory Baker

PO Box 707  
Bryn Athyn, PA  
USA, 19009

Mailing information should be clearly *printed* on a piece of paper which can be used as an address label.